CONSTITUTIVE MODELLING OF MUNICIPAL SOLID WASTE

BO ZHANG

Submitted for the Degree of Doctor of Philosophy from Loughborough University

Department of Civil and Building Engineering
Loughborough University
Loughborough, Leicestershire, LE11 3TU, UK

April 2007

Abstract

Design of landfills must consider both stability and integrity of the lining system. Therefore, stresses and strains in both mineral and geosynthetic lining materials must be controlled. Interaction between waste and barrier system is of particular importance for assessing the stability and structural integrity of steep non-self supporting barrier systems. The most appropriate approach to assess the interaction is the use of numerical modelling techniques, and therefore an appropriate constitutive model for waste material is required to represent its mechanical behaviour.

In a literature review the key aspects of mechanical behaviour of municipal solid waste (MSW) were investigated, including the influence of compressible and reinforcing particles on compression and shear behaviour of MSW were identified. Constitutive modelling of both MSW and soil material were reviewed, based on which the methodology for this study have been developed. In addition, requirements of an appropriate constitutive model for MSW have been suggested from the numerical modelling experience, and a framework to develop a constitutive model for MSW was produced.

A one-dimensional compression model was developed by including the influence of compressible particles on MSW compression behaviour. One-dimensional compression tests on both real and synthetic waste samples were modelled and the results have shown that the compression model can reproduce the measured behaviour. A fibre reinforcing model was developed by including the influence of reinforcing particles on MSW shear behaviour. A triaxial compression test on fibre reinforced sand was modelled and the results have shown that the reinforcing model can predict its shear strength.

A constitutive model for MSW has been developed by combining the Modified Cam-Clay with the one-dimensional compression and the fibre reinforcing models. Typical MSW triaxial compression tests have been modelled and the results have shown that the MSW model can reproduce the stress-strain behaviour in specific strain ranges. The constitutive model for MSW has been coded into a non-linear elasto-plastic finite element method program. Comparisons between the finite element analysis results and the analytical solutions have been performed and good agreements have been obtained.

Keywords: Municipal Solid Waste, Constitutive Model, Compression Behaviour, Shear Behaviour, Compressible Particles, Reinforcing Particles, Finite Element Method

Acknowledgments

The research project described herein was conducted at and funded by Department of Civil and Building Engineering, Loughborough University.

First of all I would like to thank my supervisors, Dr Neil Dixon and Dr Ashraf El-Hamalawi, for their continuous support during my PhD study. Neil always gave good advice and encouragement during my least inspired times. I have leant a lot from him, ranging from general research skills to specific knowledge in geotechnical engineering. Ashraf provided help and support particularly in using numerical modelling software and programming the finite element method. I experienced many fruitful discussion with him and have gained a lot of skills in this area.

I also gratefully appreciate help provided by researchers in the geotechnical landfill engineering research group within the department, namely Ulrich Langer, Anna Sia and Gary Fowmes. I had many discussions with Ulrich and Anna at the beginning of my research, which gave invaluable input into my research. Thank you to Gary for reading my thesis and providing constructive ideas.

Special thanks go to my friends and colleagues Huipeng Li and Jean-François Pinera. Although we were working on completely different research topics, they were always there to listen and give their opinions. Thank you to both of them for being with me over the last three and half years.

Furthermore, I would like to thank my parents, for giving me life, educating me, and encouraging me to pursue my interests, and my sister and brother in law who have always supported me unconditionally.

Finally, to my wife Hua Sha: thank you so much for your patience and support all the time, and for bringing us the greatest gift in our life three months ago, our son Yutong Zhang. I would like to dedicate this thesis to my wife and my son.

Table of Contents

List of Figures

List of Tables

List of Symbols

c	Cohesion intercept	2.2.2
c'	Effective cohesion intercept	2.2.2
e	Inter-void ratio	4.3
e_1	Inter-void ratio at unit mean effective stress	4.3
f	Yield function in elasto-plastic model	2.4.1
f	Intra-void ratio in the compression model	4.3
f_1	Intra-void ratio at unit mean effective stress	4.3
f_κ	Intra-void ratio at unit mean effective stress on swelling line	6.2.1
g	Plastic potential function	2.4.1
k	Arbitrary variable	2.4.2
l	Fibre length	2.3.1
n_e	Drainage porosity	4.2
p'	Effective mean stress	2.4.2
p'_0	Hardening parameter for the Modified Cam-Clay model	2.4.3
q	Deviator stress	2.4.2
v	Specific volume	2.4.3
v_1	Specific volume at unit mean effective stress	4.3
B	Strain-displacement matrix in the finite element method	7.2.3
C_C	Compression index	4.2
$C_{C\text{-}Inter}$	Inter-compression index	4.3
$C_{C\text{-}Intra}$	Intra-compression index	4.3
C_S	Swelling index	2.4.3
$C_{S\text{-}Inter}$	Inter-swelling index	4.3
$C_{S\text{-}Intra}$	Intra-swelling index	4.3
D	Elastic material matrix	2.4.1
D'	Effective material matrix	5.3
D^{ep}	Elasto-plastic material matrix	2.4.1
D_f	Material matrix for tensile stress	5.4

D_u	Material matrix for pore pressure	5.3
E	Effective Young's modulus	5.3
E	Local truncation error in the substepping algorithm	7.2.3
EP	Residual force used in modified Newton-Raphson method	7.2.2
F_H	Waste horizontal support	8.6
F_V	Waste downdrag force	8.6
G	Shear modulus	2.4.2
G_S	Secant shear modulus	2.2.2
H	Hardening quantity	2.4.1
K	Bulk modulus	2.4.2
K_0	Coefficient of earth pressure at rest	2.2.1
K_f	Fibre tensile stiffness	5.5.1
K_{fe}	Equivalent mobilised tensile stiffness	5.4
K_i	Incremental global stiffness matrix	7.2.2
K_W	Coefficient of pressure at rest for waste	2.2.1
K_w	Bulk modulus of water in undrained analysis	5.3
R	Triaxial sample radius in reinforcing model	5.5.1
R	Relative error in the substepping algorithm	7.2.3
R_0	Radius of the integration space	5.5.1
T	Total fibre force per unit volume in reinforcing model	5.5.1
T	Accumulate time step in the substepping algorithm	7.2.3
TOL	User defined tolerance	7.2.3
V_I	Total potential incompressible volume	4.3
V_S	Volume of waste particles	4.2
V_V	Volume of voids between waste particles	4.2
$V_{V\text{-}Inter}$	Inter voids volume	4.3
$V_{V\text{-}Intra}$	Intra voids volume	4.3
WC_{vol}	Water content at field capacity	4.2
α	Parameter for defining the elastic portion of the stress in the substepping stress point algorithm	7.2.3
β_i	Fibre effective factor	5.4
δ_{ij}	Kronecker delta	5.3

$\delta\varepsilon$	Incremental strain vector	2.4.1
$\delta\varepsilon^e$	Incremental elastic strain vector	2.4.1
$\delta\varepsilon^p$	Incremental plastic strain vector	2.4.1
$\delta\varepsilon^{vp}$	Visco-plastic strain in a time step	7.2.2
$\delta\varepsilon_p^e$	Incremental elastic volumetric strain	2.4.2
$\delta\varepsilon_p^p$	Incremental plastic volumetric strain	2.4.2
$\delta\varepsilon_q^e$	Incremental elastic deviator strain	2.4.2
$\delta\varepsilon_q^p$	Incremental plastic deviator strain	2.4.2
$\delta\sigma$	Incremental stress vector	2.4.1
ε_{ij}	Strain tensor	5.3
ε_z, ε_r, ε_θ	Direct strain components in cylindrical coordinates	5.3
θ_0	Critical angle to separate fibre under tension/compression	5.5.1
κ	Slope of swelling line in ***v-lnp'*** plane	2.4.3
κ_f	Slope of swelling line in ***f-lnp'*** plane	6.2.1
λ_f	Slope of virgin consolidation line in ***f-lnp'*** plane	6.2.1
μ	Poisson's ratio	2.4.3
ξ	Fibre tensile stiffness reduction factor	5.5.1
ρ	Volumetric content of fibre (or reinforcing particles)	2.3.1
σ_1	Maximum principal stress	2.3.1
σ_3	Minimum principal stress	2.3.1
σ_f	Equivalent tensile stress	5.4
σ_{ij}	Total stress tensor	5.3
σ'_{ij}	Effective stress tensor	5.3
σ_n	Normal stress on the failure plane	2.2.2
σ_v	Vertical stress in one-dimensional compression test	4.3
σ_z, σ_r, σ_θ	Direct stress components in cylindrical coordinates	5.4
τ_f	Shear stress at failure on the failure plane	2.2.2
ϕ	Friction angle	2.2.2
ϕ'	Effective friction angle	2.2.2
χ	Hardening parameter	2.4.1
ψ	Dilation angle	2.4.2

Δt	Time step used in visco-plastic method	7.2.2
Δu_i	Incremental nodal displacement vector	7.2.2
ΔP_i	Incremental nodal force vector	7.2.2
ΔT	Time step used in the substepping algorithm	7.2.3
$\Delta \varepsilon^{vp}$	Incremental visco-plastic strain	7.2.2
$\Delta \varepsilon^{e}$	Elastic portion of strain increment	7.2.3
$\Delta \varepsilon_{ss}$	Substep strain	7.2.3
$\Delta \sigma^{e}$	Elastic portion of stress increment	7.2.3
Λ	Scalar multiplier	2.4.1

CHAPTER

1

Introduction

1.1 Municipal Solid Waste and Landfill Lining System

Millions of tons of municipal solid waste (MSW) are being disposed of in the world everyday. Although small amounts of it is recycled or dealt with through other methods (e.g. incineration), most will be disposed in landfills. Increasing demand for landfill facilities leads to the usage of hard rock quarries as landfill sites in the UK. Due to the environmental contamination that might arise from the failure of landfill lining systems, consideration of lining system stability is a fundamental part of the landfill design and regulatory processes. In Europe, the European Community Landfill Directive (1999) has had a major impact on the level of lining system design required by the regulator. Jones and Dixon (2003) reported that incorrect or incomplete assessment of stability had led to a number of failures, both in the UK and overseas.

Hard rock quarries usually have steep side slopes and these must be lined. There are two approaches to the design of a steep slope lining system; self-supporting lining system and non self-supporting lining system. The essential difference between these two approaches lies in the support that the waste provides to the lining system. Self-supporting design assumes that the lining system can be constructed and is stable to full height without the support of waste but is seldom used in the UK due to its high cost. Most landfills built in quarries adopt non-self support lining system, the stability and integrity of which depend in part on the adjacent waste body for lateral support, as shown in Figure 1-1 (a) and (b). In addition, waste behaviour (including shearing and settlement) is also important for shallow slope lining systems because stresses and strain in liner elements can be induced by waste shearing and settlement, as shown in Figure 1-1 (c) and (d).

Design of landfills must consider stability both within and between elements of the lining system and within the waste to ensure that uncontrolled slippage does not occur. In addition, the design must also consider the long-term integrity of the lining system. Therefore, stresses and strains in

both mineral and geosynthetic lining materials must be controlled. Assessment of integrity requires consideration of interaction between the waste body and lining components. As mentioned above, this is of particular importance for assessing the stability and structural integrity of steep non-self supporting barrier systems. The most appropriate approach to assess the interaction between the waste and barrier system is the use of numerical modelling techniques (Dixon *et al.*, 2004).

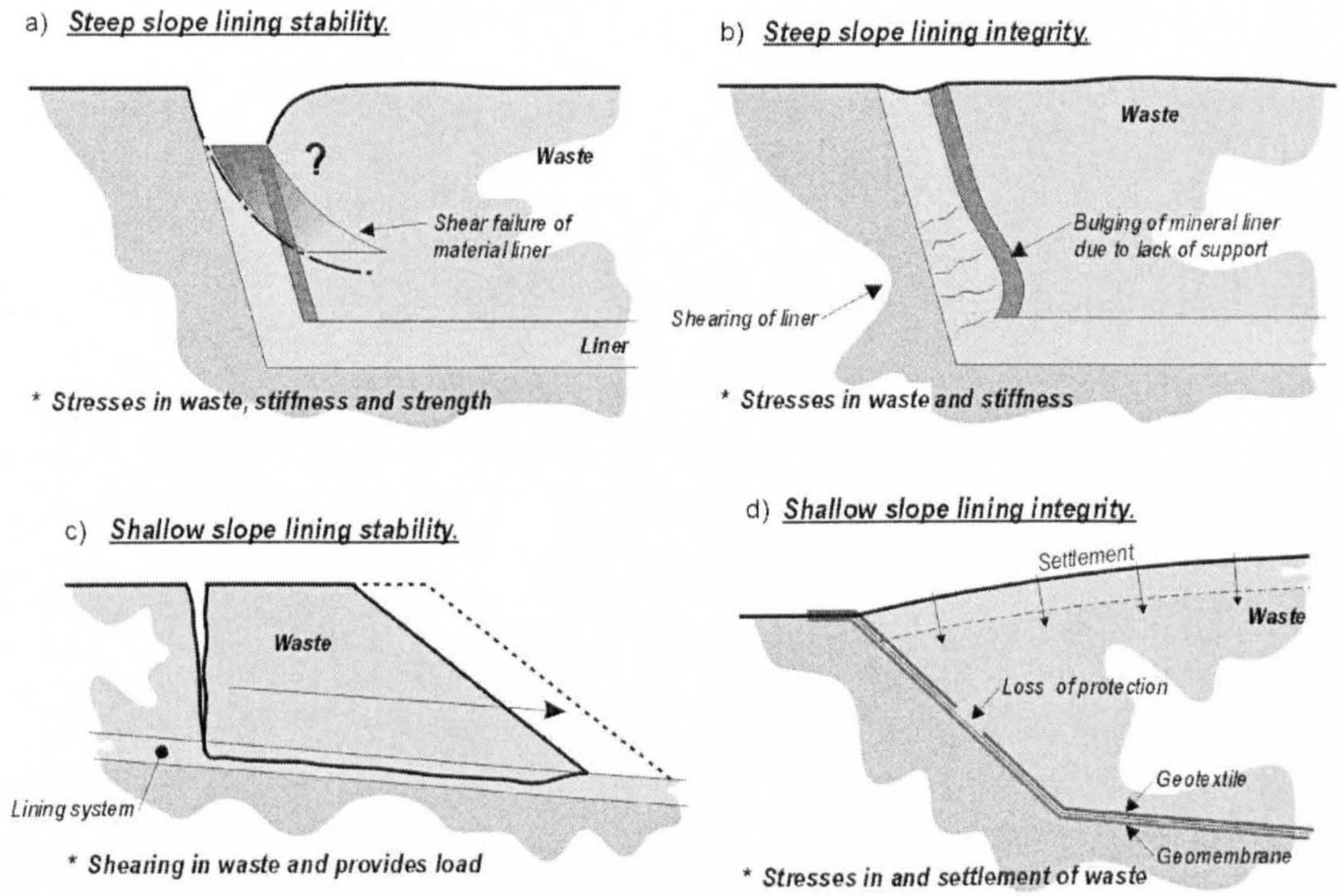

Figure 1-1 Waste support or load to landfill lining systems (Jones and Dixon, 2003)

Numerical modelling in geotechnical engineering comprise methods that attempt to satisfy all theoretical requirements, including realistic constitutive material models and satisfy boundary conditions that represent field conditions. Currently, soil models have been widely adopted to represent the waste behaviour in numerical analyses for landfills. Although some aspects of waste behaviour are similar to those of soils, a number of unique characteristics of waste (e.g. high compressibility, reinforcing nature, and biodegradation) cannot be accounted for by existing soil models. Therefore, an appropriate constitutive model for waste material is required urgently for numerical modelling of landfills, which has contributed to the proposal of this project– "Constitutive Modelling of Municipal Solid Waste".

1.2 Numerical Modelling and Constitutive Models

Numerical modelling techniques have been developed in geotechnical engineering for nearly half a century. Nowadays, with the accelerating development of computer technology and numerical

modelling techniques, a wide range of geotechnical engineering problems can be solved by this approach. A number of numerical modelling methods have been applied in the field of geotechnical engineering, such as the finite element method (FEM), finite difference method (FDM), discrete element method (DEM), and numerical manifold method (NMM), of which FEM and FDM are more commonly used. Regardless of which method is selected, a key part of modelling is the material constitutive model, which has to be capable of simulating the actual material response as accurately as possible.

Every kind of material has its own characteristic behaviour and/or reaction to external forces. A constitutive model is a mathematical model which is able to describe how the material reacts upon loading (i.e. the stress-strain relationship). It can also be called a constitutive law or constitutive relationship. The main advantage of establishing such a constitutive model is to enable the solution of complex events quantitatively. With the increase in computer power, more complicated constitutive models could be included in the numerical methods such as the finite element and finite difference methods.

Municipal solid waste exhibits extreme non-linear and complex mechanical behaviour compared to other engineering materials due to its heterogeneity. It can be considered that non-linear elasto-plastic and viscous behaviour of waste are similar to those of conventional soil, which already have a series of constitutive models accounting for these behaviours. Nevertheless, waste behaviour is more complicated than observed in soils, as waste comprises totally different particle types to soil particle, e.g. compressible, reinforcing and degradable particles. Therefore, soil models do not simulate MSW behaviour correctly. Constitutive models for MSW material need to be produced according to its behaviour, which is dominated by different waste components. Prior to producing an appropriate constitutive model for MSW, key aspects of MSW behaviour (e.g. compression and shear behaviour) have to be identified.

1.3 Aim and Objectives

The aim of this research is to produce an appropriate constitutive model for Municipal Solid Waste (MSW) which can be potentially applied in numerical analysis, to achieve this the following objectives need to be achieved:

1) To investigate the reported MSW compression and shear behaviour, and identify the factors controlling MSW behaviour, by reviewing the literature;

2) To identify the requirements of an appropriate constitutive model of MSW by investigating its application in numerical modelling of landfill engineering;

3) To develop a one-dimensional compression model for MSW considering compressible particles;

4) To develop a randomly distributed fibre reinforcing model for MSW considering reinforcing particles;

5) To produce an appropriate constitutive model for MSW by combining an elasto-plastic soil model with the compression and fibre reinforcing models, and to validate it against reported test results;

6) To implement the MSW model into a non-linear elasto-plastic finite element analysis computer code and to validate the coded program.

By achieving these objectives and producing clear conclusions, an advance in knowledge on constitutive modelling of MSW and implication of its application in numerical modelling are expected. It should be noted that long-term behaviour of waste would not be modelled in this study. Long-term waste behaviour, including creep and degradation, is important and should be included in an ideal constitutive model for MSW, however, this is beyond the scope of this thesis. The present study will focus on modelling the short-term behaviour of waste material, and the long-term behaviour should be considered in a future study.

1.4 Contribution to Knowledge

Successful accomplishment of the aim and objectives proposed above has meant a contribution to the general understanding of constitutive modelling of MSW. Key aspects of MSW mechanical behaviour have been identified and accordingly requirements of an appropriate constitutive model for MSW have been determined. A constitutive model for MSW has been developed by combining an elasto-plastic soil model with a compression model and a fibre reinforcing model. In addition, the proposed MSW model has been incorporated into the finite element method and a virtual model application has been carried out to demonstrate its advantages over soil constitutive models. Four conference papers have been published and two journal papers are in preparation, which are listed in 'List of Publications'.

In particular, the following contributions to knowledge have been achieved:

1) Both compressible and reinforcing particles have been identified as the controlling factors dominating MSW mechanical behaviour. Influence of compressible particles has been suggested not only on waste compression behaviour as traditionally thought, but also on its shear behaviour observed in triaxial compression tests;

2) An innovative phase relationship has been created for material containing compressible particles to model voids between and voids within particles separately. A compression model for MSW has been developed to include the influence of compressible particles on compression behaviour. By combining the compression model with the traditional elasto-plastic soil model, the influence of compressible particles on shear behaviour observed in triaxial compression tests can also be included;

3) A fibre reinforcing model was developed to include the influence of reinforcing particles on MSW shear behaviour. It has contributed to the knowledge of modelling the randomly distributed fibre reinforced soil. In addition, it has been shown that the model can be simply incorporated into the finite element method.

4) A constitutive model for MSW was developed and an elasto-plastic non-linear finite element program was coded and validated with the analytical solutions.

1.5 Outline of Chapters

Chapter 2 presents a literature reviews of MSW mechanical behaviour, constitutive modelling of MSW, and constitutive models for soils. Volume change behaviour (i.e. compression behaviour), strength and stress-strain behaviour (shear behaviour) of MSW material observed from a range of tests are reviewed and compared with those of soils. Methods to produce a constitutive model for MSW are reviewed and existing constitutive models for soil material are presented.

Chapter 3 demonstrates the methodology chosen for producing a constitutive model for MSW in this project. Requirements of an ideal constitutive model for MSW are identified through a review of the application of numerical modelling techniques in landfill engineering. Subsequently, a framework for producing a constitutive model for MSW is proposed and a methodology for implementing it in a numerical model is illustrated.

Chapter 4 presents the development of a one-dimensional compression model for MSW and its validation against MSW (and synthetic waste) compression test results.

Chapter 5 presents the development of a randomly distributed fibre reinforced material model and its validation against the fibre reinforced sand triaxial compression test results.

A constitutive model for MSW is produced in Chapter 6 following the model framework proposed in Chapter 3. A theoretical model is presented and analytical solutions for a particular boundary condition are derived and compared with soil model results. Model validation against MSW triaxial compression test results is performed.

Chapter 7 presents the program structure of the finite element method and the principles of non-linear elasto-plastic finite element analysis. Subsequently, the finite element method implementation of the fibre reinforced soil model and the MSW constitutive model are presented. Comparisons between the finite element analysis results and the analytical solutions are performed.

Chapter 8 includes the final discussion on the compression, fibre reinforced soil and MSW models proposed in previous chapters, covering modelling results and methods for determining parameters for the models. Finite element method implementation results are also discussed. Finally, the MSW model application in landfill modelling and its advantages over soil models are discussed.

Chapter 9 presents the conclusions of this project and recommend future work.

CHAPTER

2

Literature Review

2.1 Introduction

This chapter is a literature review about the reported mechanical behaviour and the methodology of constitutive modelling of MSW, which provides relevant information required for development of a constitutive model for MSW. Accordingly, a review of constitutive models for soils is also included.

2.2 MSW Mechanical Behaviour

The major task of constitutive modelling is to reflect real mechanical behaviour (stress-deformation-time relationship) of materials through mathematical equations in numerical modelling. Therefore, real MSW mechanical behaviour should be investigated prior to developing a constitutive model. Many research projects have been carried out on MSW mechanical behaviour in recent decades, most of which have concentrated on landfill settlement and shear strength of MSW. The major aim of settlement studies is to improve the efficiency of waste placement, predict final settlement profiles for the landfill cap and enable assessment of interaction between side slope barrier systems and the settling waste body. Therefore, most studies focused on the prediction of long-term settlement, i.e. long-term volume change behaviour at landfill scale. Studies on MSW shear strength have focused on obtaining the values of MSW shear strength parameters, i.e. cohesion and friction angle, which are necessary for limit equilibrium analyses in landfill design. Constitutive modelling of MSW needs more detailed information on how the material deforms due to certain changes in stress condition. Element tests on MSW samples, i.e. one-dimensional compression tests (e.g. Powrie and Beaven, 1999; Landva *et al.*, 2000; Machado *et al.*, 2002; and Langer, 2006), triaxial tests (e.g. Jessberger and Kockel, 1993, Grisolia *et al.*, 1995, and Machado *et al.*, 2002) and direct shear tests (e.g. Kölsch, 1993;

Kavazanjian, 2001; Gotteland *et al.*, 2000; and Langer, 2006) could provide such information. The literature review on mechanical behaviour of MSW is therefore carried out from two aspects; compression behaviour, which is based on the findings from one-dimensional compression tests; and shear strength and deformation behaviour, which is based on the findings from triaxial compression and direct shear tests.

2.2.1 Compression Behaviour

One-dimensional compression tests have been carried out on both real and artificial MSW samples to investigate volume change behaviour (Powrie and Beaven, 1999; Landva *et al.*, 2000; and Langer, 2006). Larger size samples than used in normal soil tests are necessary in MSW compression tests due to larger particle sizes and heterogeneity of MSW. Most of the compression test results show a relationship between instant volume change and effective stress, while there are a small number of tests for long-term volume change behaviour, i.e. secondary compression. Consolidation processes have not been considered for MSW in these tests due to the relative high permeability of MSW (an average of around 10^{-5} m/s, Qian *et al.*, 2002). However, Powrie and Beaven (1999) found that MSW permeability may change to very low values (between 10^{-7} to 10^{-8} m/s) under a high effective pressure (about 800 kPa). MSW behaviour without influence of increasing and dissipating of pore pressures will be investigated and modelled in this research as a starting point. In addition, for normal landfill (not bio-reactor) under consideration at present, MSW is not saturated except for the very bottom part.

➢ Instant Compression

Powrie and Beaven (1999) conducted one-dimensional compression tests on crude unprocessed UK household waste in a large compression cell, which was 2m in diameter and 3m high. Detailed test information and data were given in their paper for a specific waste sample DM3, e.g. tested void ratio values at each level of the effective vertical stresses and the test method used to obtain the void ratio values. Figure 2-1 and Figure 2-2 present the compression test results for sample DM3, showing curves of vertical strain versus logarithm of effective vertical stress, and void ratio versus logarithm of effective vertical stress. The curve of vertical strain versus logarithm of vertical stress has a almost linear relationship which is identical to observed soil compression behaviour, while the void ratio curve shows a very highly non-linear relationship. Powrie and Beaven (1999) suggested this is attributed to the existence of compressible particles in the MSW sample but no further study has been carried out. The non-linearity indicates that the traditional definition for void ratio in soil mechanics theory may no longer be applicable for waste

material and relevant amendments are required to include the influence of compressible particles on MSW compression behaviour.

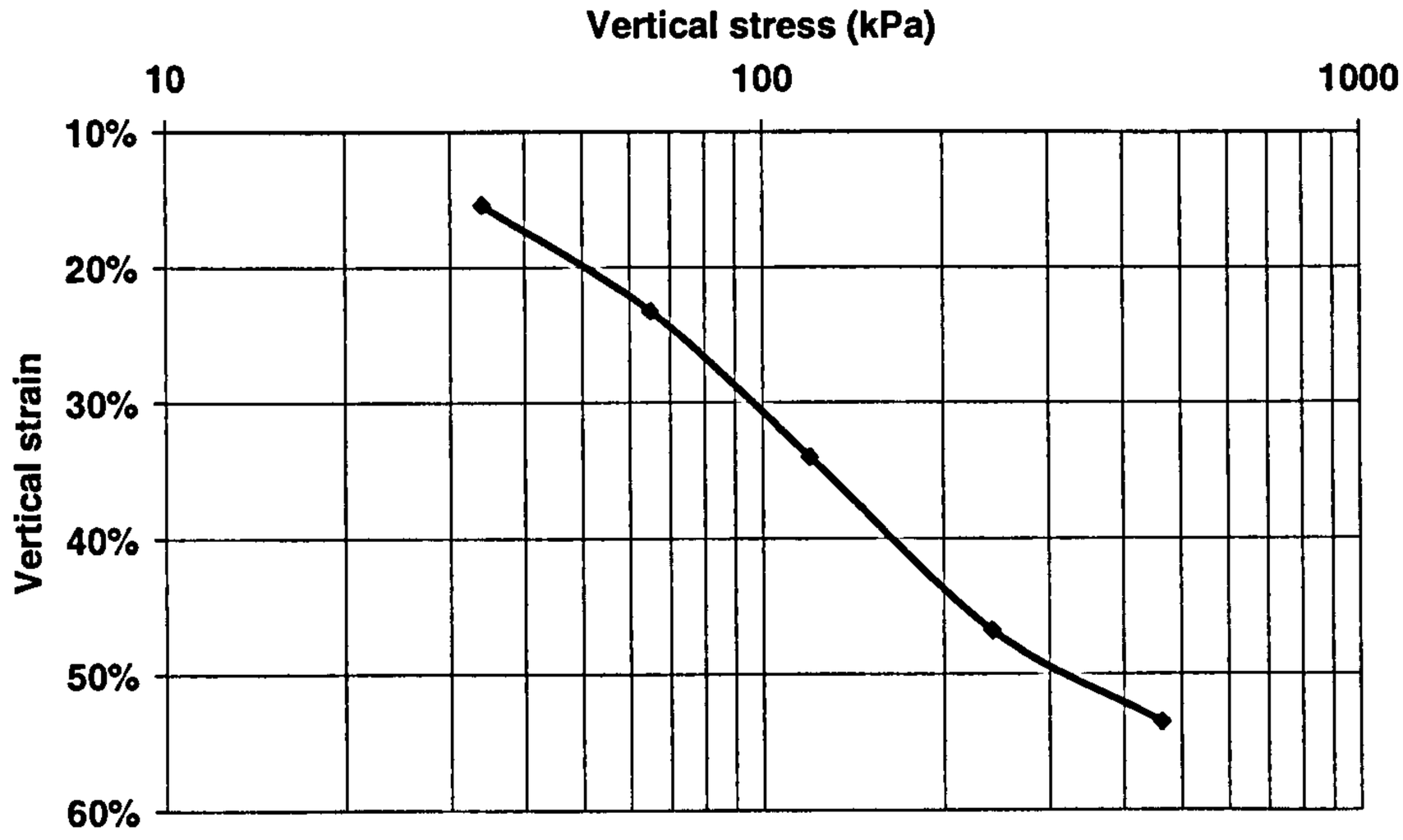

Figure 2-1 One-dimensional compression test curve for DM3: vertical strain vs. logarithm of vertical stress (Based on data from Powrie and Beaven, 1999)

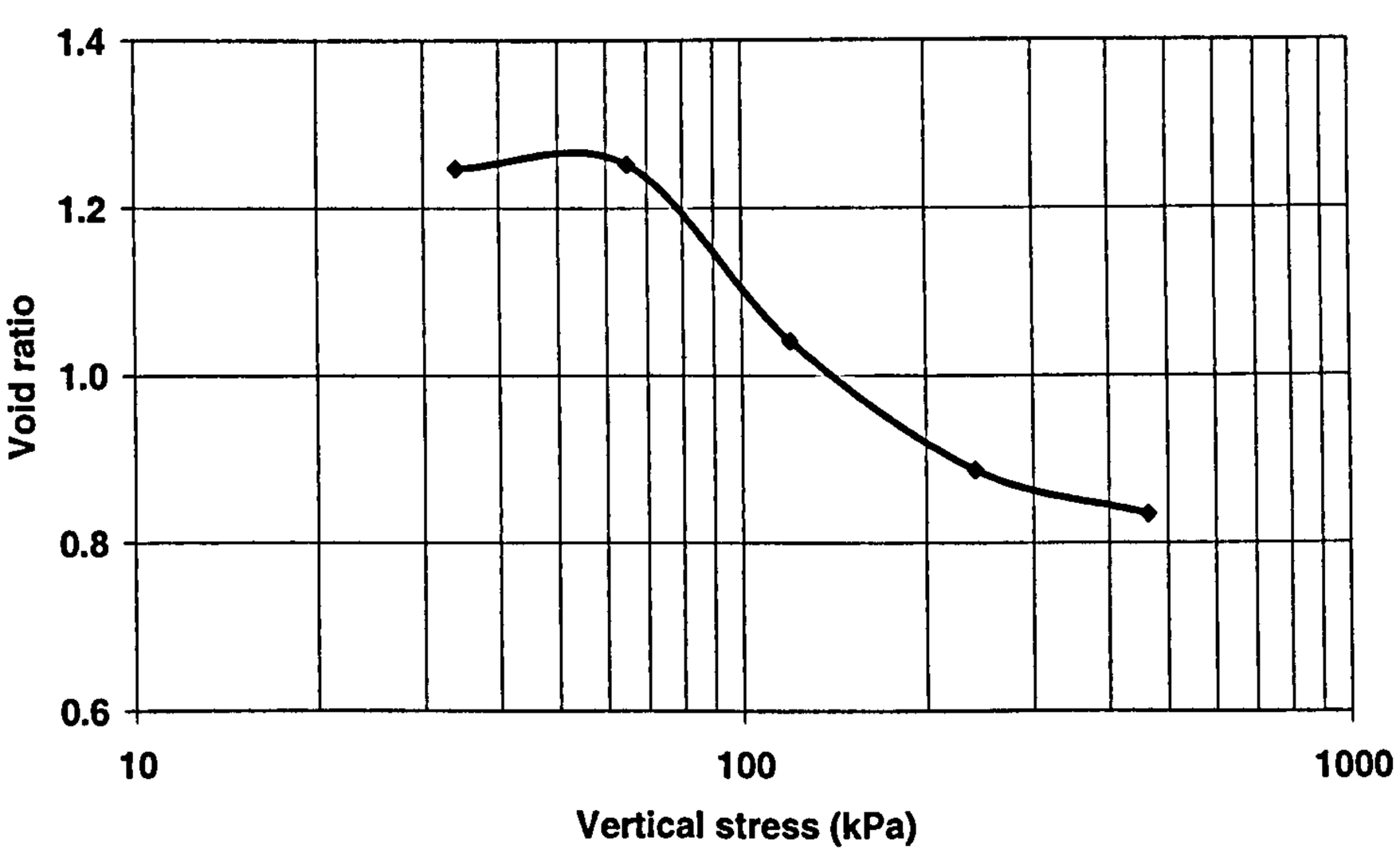

Figure 2-2 One-dimensional compression test curve for DM3: void ratio vs. logarithm of vertical stress (Based on data from Powrie and Beaven, 1999)

Landva *et al.* (2000) performed one-dimensional compression tests on both real MSW and artificial samples in a split-ring apparatus which was 0.6 m in diameter and 0.46 m high. Five different MSW samples were compressed. Two of the samples, SL1 (5 years old) and SL2 (2 years old), were obtained directly from a landfill in Canada. A third sample, AR1, was an

artificial sample, which was prepared by mixing constituents typically found in a domestic refuse. Two more samples, MA1 and MA2, were prepared by mixing sample SL2 and AR1. Prior to compressing the field samples, constituents larger than 150 mm in size were shredded. The compression test curves for all the samples were presented in Figure 2-3. It can be seen that the linear relationship can be simplified for all the compression curves as for soils (ignoring the shown creep behaviour which will be discussed in the following section), which means the coefficient of compression can be used to represent the waste compressibility. Landva *et al.* (2000) calculated the coefficient of compression for all the samples which range from 0.17 to 0.24, compared with 0.15 for DM3 (Powrie and Beaven, 1999) obtained from Figure 2-1. It appears that older waste is less compressible because sample SL1 (5 years old) has the lowest coefficient of compression of 0.17 in the data reported by Landva *et al.* (2000). Void ratio values were not measured in the test so that the relationship between void ratio and vertical stress can not be presented. Therefore, the influence of compressible particle on MSW compressive behaviour cannot be described from these tests. It is difficult to measure the void ratio values in MSW compression tests, as for soils, due to the much more complicated composition for MSW. Thus, the coefficient of compression rather than the compression index was normally used to represent the compressibility of MSW (e.g. Edil *et al.*, 1990).

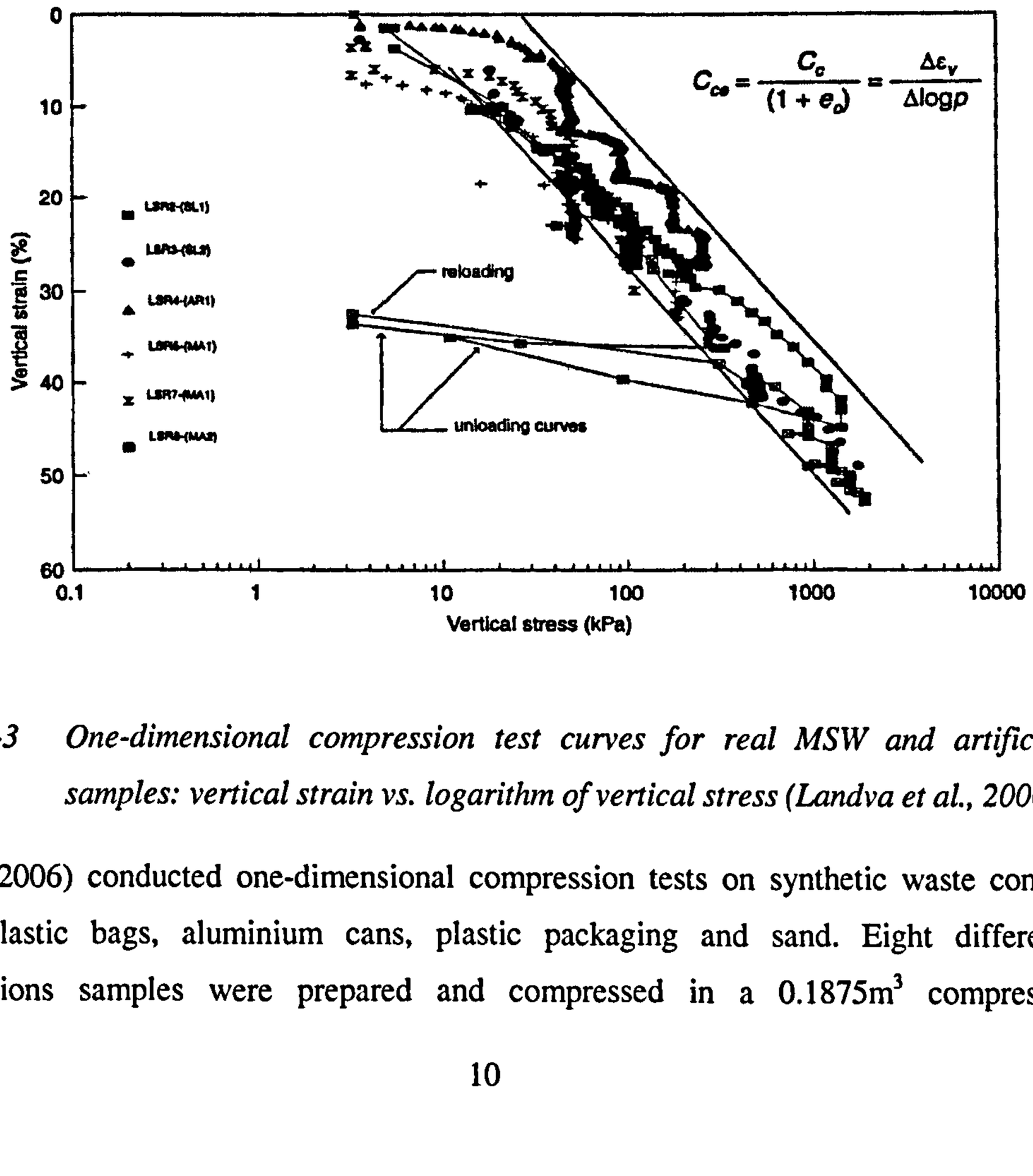

Figure 2-3 One-dimensional compression test curves for real MSW and artificial waste samples: vertical strain vs. logarithm of vertical stress (Landva et al., 2000)

Langer (2006) conducted one-dimensional compression tests on synthetic waste consisting of paper, plastic bags, aluminium cans, plastic packaging and sand. Eight different waste compositions samples were prepared and compressed in a 0.1875m^3 compression cell

(length×width×height=0.5m×0.5m×0.75m). Composition of all the samples are determined according to the waste classification system developed by Langer (2006), in which compressible particles are included. One of the main purposes of the compression test is to investigate the influence of compressible particles on MSW compression behaviour. It has been shown that with more compressible particles included in waste samples, higher compressibility would be obtained. One of the compression samples (SW09) aims to simulate a real waste composition including all the kinds of particles used in the study. The percentage of each kind of particle in SW09 was determined based on the findings from a real UK waste sample sorting analysis conducted by Langer (2006). Figure 2-4 shows the compression curve for SW09, in which both the virgin compression and unload/reload curves were presented. It can be seen that an almost linear relationship was obtained between the vertical strain and logarithm of the vertical stress for both virgin compression and unload/reload. Void ratio values were not measured in all the tests. The coefficient of compression for this sample can be estimated as 0.6, which is much higher than the values observed in real MSW samples by Powrie and Beaven (1999) and Landva *et al.* (2000) described above. However, a lower coefficient of compression (i.e. less steep curve) can be noticed when the vertical stress is over 30 kPa, which means the material become less compressible under higher stress level. It can be explained that some of the compressible particles had been compressed and hence the compressibility of the material was reduced. Real MSW samples obtained from landfills showed less compressibility because a large proportion of compressible particles were compressed during waste compaction and placement.

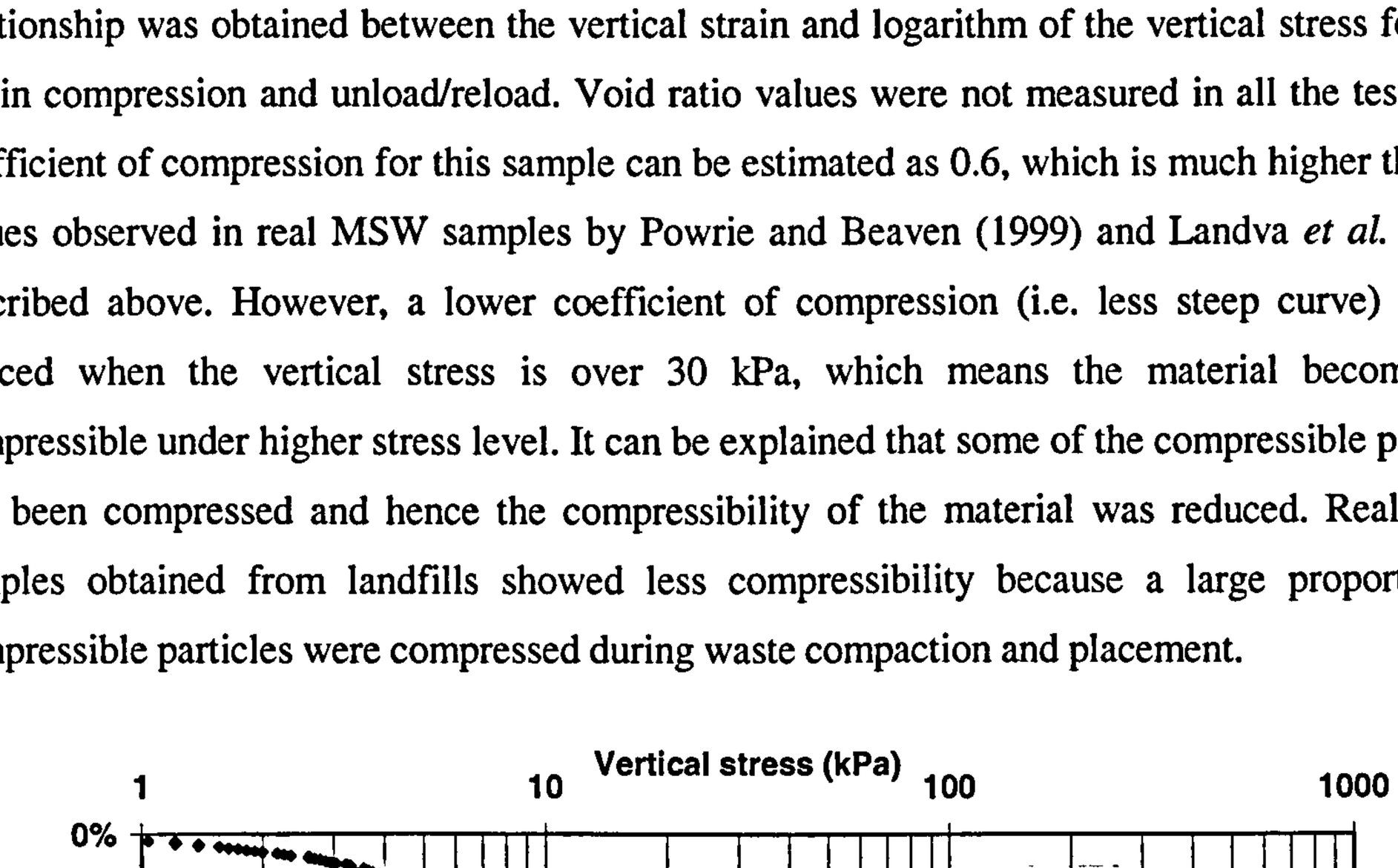

Figure 2-4 One-dimensional compression test curve for synthetic waste sample SM09: vertical strain vs. logarithm of vertical stress (Based on data from Langer, 2006)

1) Changes in organic levels through fibre decomposition will promote significant additional compression compared to those samples in nutrient-deficient conditions. In addition, the amount of additional strain increases with increasing organic content due to the higher percentages of decomposition at the higher organic levels (Wardwell and Nelson 1981).

2) Decomposition reduces the volume of organic solids permitting additional settlement in an organic soil under a constant effective overburden pressure. A large decrease in coefficient of consolidation was found as decomposition occurred (Al-Khafaji and Andersland 1981).

McDougall *et al.* (2004) pointed out that the laboratory tests performed by Wardwell and Nelson (1981), Al-Khafaji and Andersland (1981) suggested that decomposition can produce an increase in secondary settlement over and above that caused by simple creep and suggest that the increases are also influenced by the stress state. A degradation model for non-conservative soil has been proposed, which could be applied to predict the long-term compression of MSW due to degradation (McDougall and Pyrah, 2004).

Some important differences of MSW compression behaviour to soils, such as particle compression and degradation, have been identified in the review above. Constitutive modelling of MSW is necessary to simulate these special behaviour characteristics so that more accurate volume change of MSW can be obtained in numerical modelling.

➢ In Situ Horizontal Stress (K_0)

In soil mechanics, Terzaghi's one-dimensional consolidation theory considers compression only in one dimension. The soil model relates the vertical strain to the change in vertical stress, and this defines the volume change under zero horizontal displacement conditions. There is no need to consider the change in horizontal stress to calculate the deformation, even though the actual horizontal stress changes during loading and unloading. However, once soil deformation departs from the one-dimensional condition, it is necessary to consider the stage and changes of the stresses in the other directions and the associated volume change behaviour. The relationship between the horizontal effective stress and the vertical effective stress depends on the lateral deformation that accompanies changes in vertical stress. If the vertical stress and strain increase without any deformation in the horizontal directions (i.e. one-dimensional compression), the soil is said to be in an at-rest state, and the horizontal stress associated with this condition is termed as the at-rest pressure.

The ratio between the horizontal and vertical effective stresses during initial compression of a soil is a constant, defined by the coefficient of earth pressure at rest K_0. Values of K_0 for normally

➢ Long-term Compression

Long-term compression of soils, i.e. secondary compression is defined as compression which takes place after the primary consolidation is complete. The reason for secondary compression is that the soil structure is susceptible to a viscous or creep deformation under the action of sustained stress as the fabric elements adjust slowly to more stable arrangements. However, it has been widely acknowledged that long-term compression of MSW includes not only the creep deformation of the structure, similar to soils (secondary compression), but also the volume loss of chemical reaction, i.e. biodegradation (e.g. Sowers, 1968 and 1973; Edil *et al.*, 1990; Fassett *et al.*, 1994). Therefore, both creep and degradation behaviour should be considered for MSW long-term compression.

Creep reflects the compression behaviour while the waste is subjected to a constant load. Due to the porosity and highly compressive particles of MSW, creep must be an important aspect of long-term compression behaviour. Unfortunately, few studies have been carried out on creep effects in MSW, though some studies reflect the effect of creep on compression behaviour. Creep behaviour of MSW can be observed in pressuremeter tests conducted in MSW (Dixon *et al.* 2006). The MSW kept deforming while it was subjected to a constant load level during the interval (about ten minutes) between every loading and unloading step.

Landva *et al.* (2000) investigated the secondary MSW compression behaviour using oedometer tests on both real and artificial MSW samples. From the test results, it can be seen that the vertical strain beyond instant compression was linear with respect to the logarithm of time, which is the same as clay. It has been reconfirmed that the tested MSW material displayed the same type of creep behaviour (development of a reserve or plastic resistance) as that occurring in plastic clays of high water content.

Although a large amount of research on long-term landfill settlement can be found in the literature, most of these studies are not useful for constitutive modelling due to the fact that they do not separate the mechanisms of compression as mentioned above. There is also a lack of information of degradation effect on the mechanical behaviour of MSW. Therefore, it is necessary to refer to studies on organic soil.

A few laboratory studies have been carried out on fibre-kaolin mixtures to investigate the mechanical response to decomposition of fibre material in organic soils (Wardwell and Nelson, 1981; Al-Khafaji and Andersland, 1981; Andersland *et al.* 1981). Based upon these studies, it can be seen that fibre decomposition will have a significant effect on the compressibility characteristics of fibre-kaolin mixtures, which can be summarised as follows:

consolidated soils are generally in the range of 0.3 to 0.75 (Mitchell and Soga, 2005). Jaky (1944) has given a good estimate of K_0 for many soils:

$$K_0 = 1 - \sin\phi' \qquad \textit{Eq. 2-1}$$

in which ϕ' is the effective stress friction angle measured in triaxial compression tests.

Landva *et al.* (2000) measured K_0 during one-dimensional compression of MSW samples using a split-ring apparatus to study the influence of fibre content on the coefficient of earth pressure at rest in waste materials. Typical plots of K_0 versus the applied vertical stress are presented in Figure 2-5. It can be seen that the K_0 values remain approximately constant at different levels of vertical stress for each sample. The at-rest earth pressure coefficients determined from the split-ring test varied between 0.23 and 0.40. These values are plotted in Figure 2-6 against the percentage of elongated particles. As can be seen, the K_0 values decrease consistently with an increasing amount of fibrous constituents.

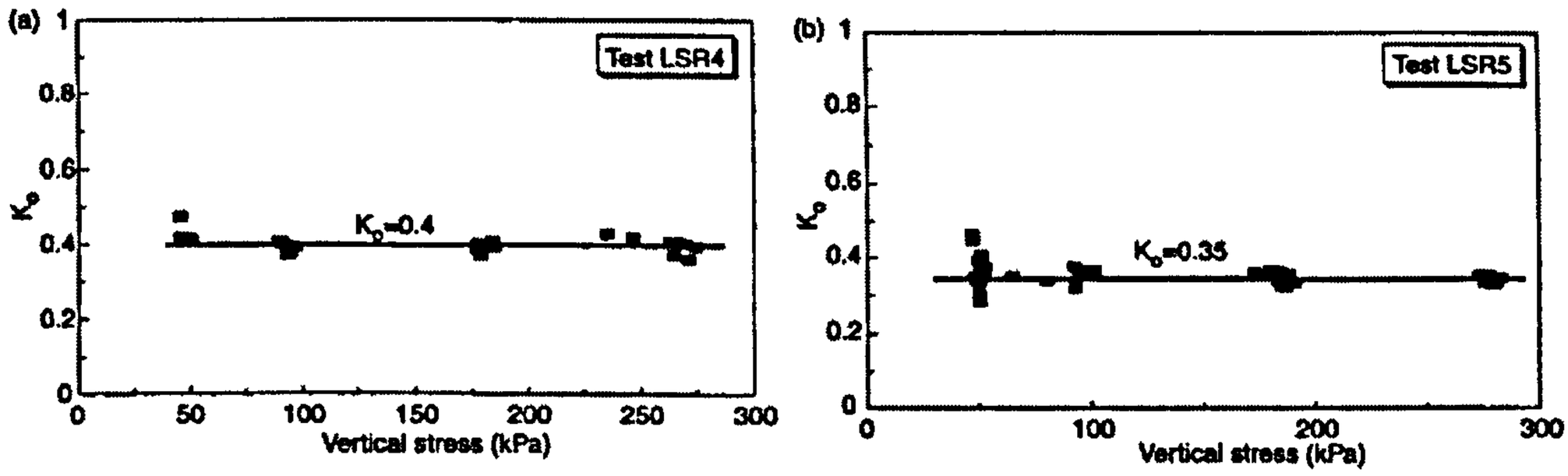

Figure 2-5 Typical plots of K_0 from split-ring testing (Landva et al. 2000)

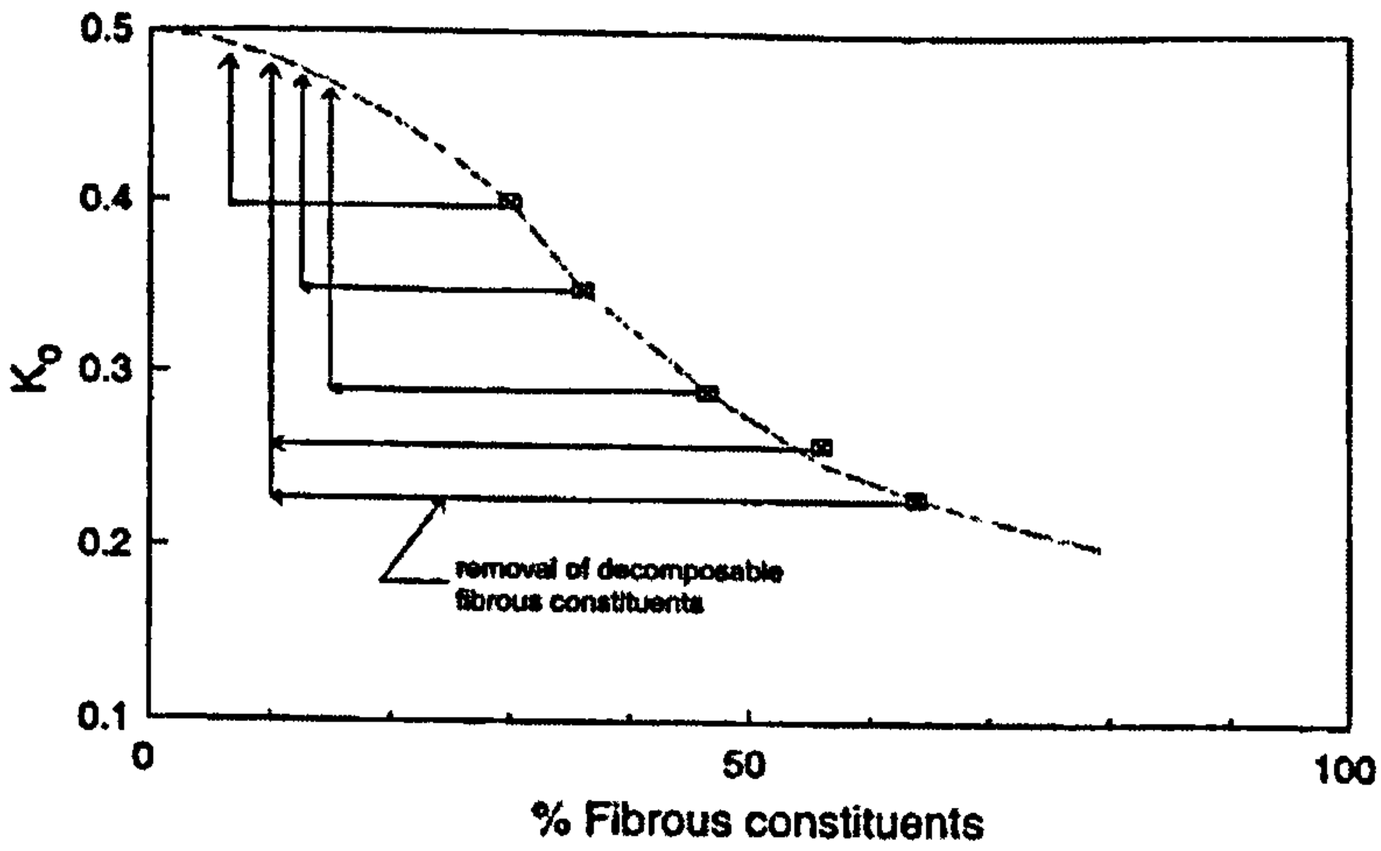

Figure 2-6 Effect of fibres content on K_0 (Landva et al. 2000)

Moreover, the authors pointed out that the total fibre content of MSW decreases with time, as many organic fibres will decompose over a long period of time. The critical condition for K_0 is

therefore the long-term state when decomposable fibres are no longer present. It was suggested that, the long-term values of the at rest earth pressure may be estimated roughly from a composite plot of K_0 versus content of fibrous constituents by finding the K_0 value that would correspond to the percentage content of non-decomposed constituents. Assuming the non-decomposed constituents to be plastic, glass, and metal in Figure 2-6, a long-term K_0 value of 0.47 to 0.49 can be estimated. Landva and La Rochelle (1983) found that the lateral resistance induced in triaxial samples of peat against bulging increased consistently with increasing fibre contents, which has the same trend as that shown in Figure 2-6.

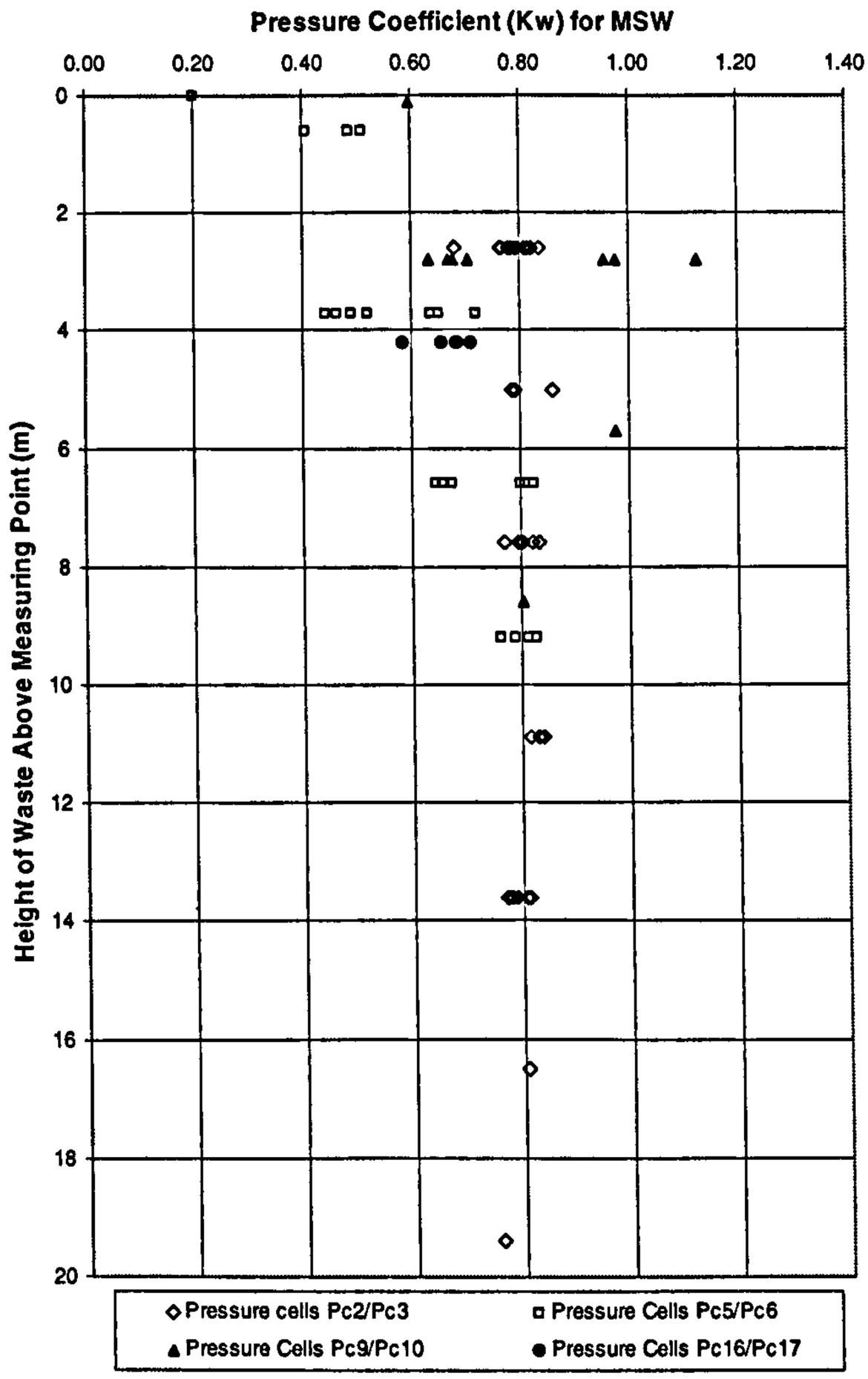

Figure 2-7 Measured ratios of horizontal to vertical stress in MSW (Dixon et al. 2004)

Dixon *et al.* (2004) measured horizontal and vertical stresses by pairs of pressure cells installed in four lifts of MSW in the Burntstump landfill in the UK. This data has provided unique in-situ measurements of the ratio between vertical and horizontal stresses. Effective stresses have been measured as all cells were located above the leachate level. Figure 2-7 shows the calculated

values of pressure coefficient K_w (which can be interpreted as K_0 values) for MSW versus measured vertical stress. It can be seen that, the large majority of K_w values produced by all four pairs of pressure cells are between 0.6 and 1.0. The values of K_w are relatively constant with vertical stress for the cells Pc2/Pc3 and Pc16/Pc17 while Pc5/Pc6 and Pc9/Pc10 show a trend of increasing K_w with depth. The reason for the trend of increasing K_w with vertical stress recorded by two of the pairs of cells is unclear. It may be reflecting a real phenomenon or a limitation of the instrumentation.

A significant difference between K_0 values obtained from in-situ measurements (Dixon *et al.*, 2004) and laboratory measurement (Landva *et al.*, 2000) has been noticed. Dixon *et al.* (2004) suggested that the large majority of K_0 values measured by pressure cells in the site are between 0.6 and 1.0, while Landva *et al.* (2000) determined the K_0 values from the split-ring test varied between 0.23 and 0.40 for fresh waste samples and 0.47 to 0.49 for decomposed waste samples. It is difficult to explain the reason why such significant differences were observed, but different test methods and different waste types should be counted.

2.2.2 Strength and Deformation Behaviour

All aspects of soil stability depend on soil strength, and the stress-deformation and stress-deformation-time behaviour of soils are important in any problem where ground movements are of interest, which are also applicable for MSW material. Shear behaviour of MSW will be reviewed from the following two aspects: shear strength and stress-strain behaviour, which are closely related to constitutive modelling of MSW. A more detailed and comprehensive review on MSW shear strength behaviour can be found in Langer (2006).

➢ Shear Strength

Most relationships for the characterisation of the stress-deformation and strength properties of soils are empirical and based on the phenomenological descriptions of soil behaviour, in which the Mohr-Coulomb equation is by far the most widely used for shear strength. It is expressed by

$$\tau_f = c + \sigma_n \tan\phi \qquad \textit{Eq. 2-2}$$

$$\tau_f = c' + \sigma_n' \tan\phi' \qquad \textit{Eq. 2-3}$$

where τ_f is shear stress at failure on the failure plane, c is a cohesion intercept, σ_n is the normal stress on the failure plane, and ϕ is a friction angle. Eq. 2-2 is defined for total stresses, and c and ϕ are referred to as total stress parameters. Eq. 2-3 applies to effective stresses, and c' and ϕ' are

effective stress parameters. As the shear resistance of soil originates mainly from actions at inter-particle contacts, the second equation is the more fundamental (Mitchell and Soga, 2005).

The Mohr-Coulomb equation has also been widely applied in waste mechanics to characterise the shear strength of MSW (e.g. Landva and Clark, 1990; Fassett *et al.*, 1994), i.e. c and ϕ are still the most widely used strength parameters for waste material. Intercept c can denote real cohesion between particles for soil, while it is common to define it as apparent cohesion for MSW due to the contribution from tensile strength of reinforcing particles. Shear strength of MSW can be measured through both field studies and laboratory tests. Dixon and Jones (2005) summarised the advantages and disadvantages associated with current available approaches for obtaining information on shear strength behaviour of MSW, as shown in Table 2-1.

Table 2-1 Review of methods for measuring shear strength behaviour of MSW (Dixon and Jones, 2005)

Location	Methods of Measurement	Comments	References
Field	Back analysis of slope failures	Adequate information seldom available (e.g. pore pressures, shape and position of shear surface)	Koerner and Soong (2000)
	Back analysis of cutting slope experiments	Large deformations observed but not shear failures	Singh and Murphy (1990), Cowland *et al.* (1993)
	Back analysis of existing stable slopes	Changing waste composition means past experience is not a guide to future performance	Gotteland *et al.* (2000)
	In situ direct shear tests	Difficult to perform and results related to low levels of stress	e.g. Jessberger and Kockel (1993)
	SPT, CPT and vane tests	No clear relationship between penetration resistance and MSW shear strength, could provide useful information in degraded more soil like materials	
Laboratory	Triaxial compression	Disturbed samples, peak shear strength not obtained due to compression and densification of sample	Jessberger and Kockel (1993), Grisolia *et al.* (1995)
	Direct shear	Large device required (e.g. 1×1×1m), disturbed samples, large displacements required to mobiles peak shear strength	Kolsch (1995), Gotteland *et al.* (2001)
	Simple shear	Large device required, disturbed samples, useful information on shear stiffness (used in seismic analyses)	Kavazanjian *et al.* (1999)

It was pointed out that back analysis of landfill slope failures, cut slope trials and existing stable slopes can provide information on the shear strength of a large mass of waste, but poor quality

input data makes such analyses problematic and often unreliable. In-situ techniques for measuring shear strength are presently inadequate and unreliable. Laboratory tests involve too much disturbance to the waste structure, and can not provide appropriate values of shear strength parameters for design levels of stress. However, to aid investigation of the shear strength mechanism of MSW, laboratory element tests (e.g. direct shear test and triaxial test) on both shredded waste samples and artificial samples are more appreciated for consideration than the field studies for this specific research. Some representative results of direct shear and triaxial test from the literature are discussed below.

Both direct shear and triaxial compression tests have been conducted on both shredded waste and artificial waste samples in previous studies to obtain the fresh waste shear strength parameters, in which deformation behaviour of MSW has also been investigated. Most of the tests were drained tests, i.e. there was no consideration of pore pressure increases or dissipation. The reason has already been explained above in the discussion of the one-dimensional compression tests. Therefore, in many applications there is no difference in using total strength or effective strength parameters for MSW.

Shear strength parameters apparent cohesion (c) and friction angle (ϕ) can be found directly from direct shear tests on MSW samples (e.g. Landva and Clark, 1990; Kölsch, 1993; Van Impe and Bouazza, 1996; Kavazanjian, 2001; Thomas *et al.*, 1999; Gotteland *et al.*, 2000; Langer, 2006). Normally, larger samples and devices are required for MSW than soil due to its larger particle sizes. Unlike direct shear tests on normal soil, peak value (i.e. shear failure) are seldom obtained in MSW direct shear test even at very large deformation (e.g. 20%) on the shear plane. The values of c and ϕ are usually determined corresponding to a mobilised shear stress at a certain shear strain value. Lack of failure is probably due to the deformability of many of the constituent particles in MSW samples. However, shear failure does exist in MSW material based on images of the waste slope failures in landfill (Jones and Dixon, 2003). The limited size of the currently used devices may partly result in failure not occurring in the test. In addition, mobilisation mechanism of tensile fibre in waste material is another possible reason. Reinforcing nature of MSW has already been recognised by many researches (e.g. Kölsh, 1995; Machado *et al.*, 2002; Langer, 2006). Besides it affects K_0 values of MSW as discussed above, it also can improve the MSW shear strength when fibre stresses are mobilised. However, it is apparent that not all the fibres can be mobilised under a certain strain level due to their uncertain initial orientation and condition. Since there is a lack of a standard test for MSW, including sample preparation, sample size, testing procedure and data analysis, the data on shear strength parameters from direct shear testing reported by researchers are widely spread, which also results from the variable nature of waste.

Conventional triaxial compression tests were also used to obtain the shear strength parameters for MSW samples (e.g. Jessberger and Kockel, 1993, Grisolia *et al.*, 1995). Similar to direct shear tests, no failure can be reached in the tests even if the sample experiences a large axial strain up to 40%. The values of shear strength parameters c and ϕ have to be obtained corresponding to a certain strain level. Detailed information about triaxial compression test results as present in the next section.

Dixon and Jones (2005) pointed out that inability to cause failure in the triaxial compression tests has led to shear strength test results being related to levels of strains (i.e. different shear strength parameters are given for each strain level). While this approach has some merit if used in design to try and control strains in the waste body, it can lead to confusion and great care should be taken in applying such values. Kavazanjian (2001) also provided a detailed assessment of triaxial tests on waste and concluded it is not an appropriate technique for measuring the shear strength parameter of MSW. However, it may still be a valid method to obtain the stress-strain behaviour of MSW that will be discussed in the following section. Dixon and Jones (2005) argued that the direct shear box is the most appropriate laboratory technique for determining the MSW shear strength. Large shear displacements are required to reach failure and volume changes should be recorded in order to enable the measured shear strength to be related to the sample density. Unfortunately, this kind of information is seldom provided in the literature, thus making interpretation of results difficult.

There is very limited reliable information about the influence of degradation on MSW shear strength, i.e. degraded waste shear strength, in the literature. Some evidence and arguments on change of stiffness and strength with degradation are presented as follows:

Landva and Clark (1990) found that the direct shear strength of refuse from an older landfill was lower after the refuse samples had been stored in the laboratory for a year and then soaked in leachate.

Kavazanjian *et al.* (2001) commented on the sparsity of quantitative information on the shear strength of degraded waste. However, from the little information that is available it would be indicated that the drained shear strength of degraded MSW is similar to that of fresh waste.

Al-Khafaji and Andersland (1981) suggested that decomposition of the organic (fibre) fraction produced a large decrease in vane shear strength at a given consolidation pressure. The strength reduction would result from fibre breakdown and formation of decomposition products.

➢ Stress-Strain Behaviour

Typical stress-strain behaviour of soils can be summarised in Figure 2-8 (a). It ranges from very brittle for some quick clays, cemented soils, heavily overconsolidated clays, and dense sands to ductile for insensitive and loose sands. An increase in confining pressure causes an increase in the deformation modulus as well as an increase in strength, as shown in Figure 2-8 (b). In addition, soil stress-strain relationships are usually non-linear. Soil stiffness (often expressed in terms of tangent or secant modulus) generally decreases with increasing shear strain or stress level up to a peak failure stress, as shown in Figure 2-9 (Mitchell and Soga, 2005).

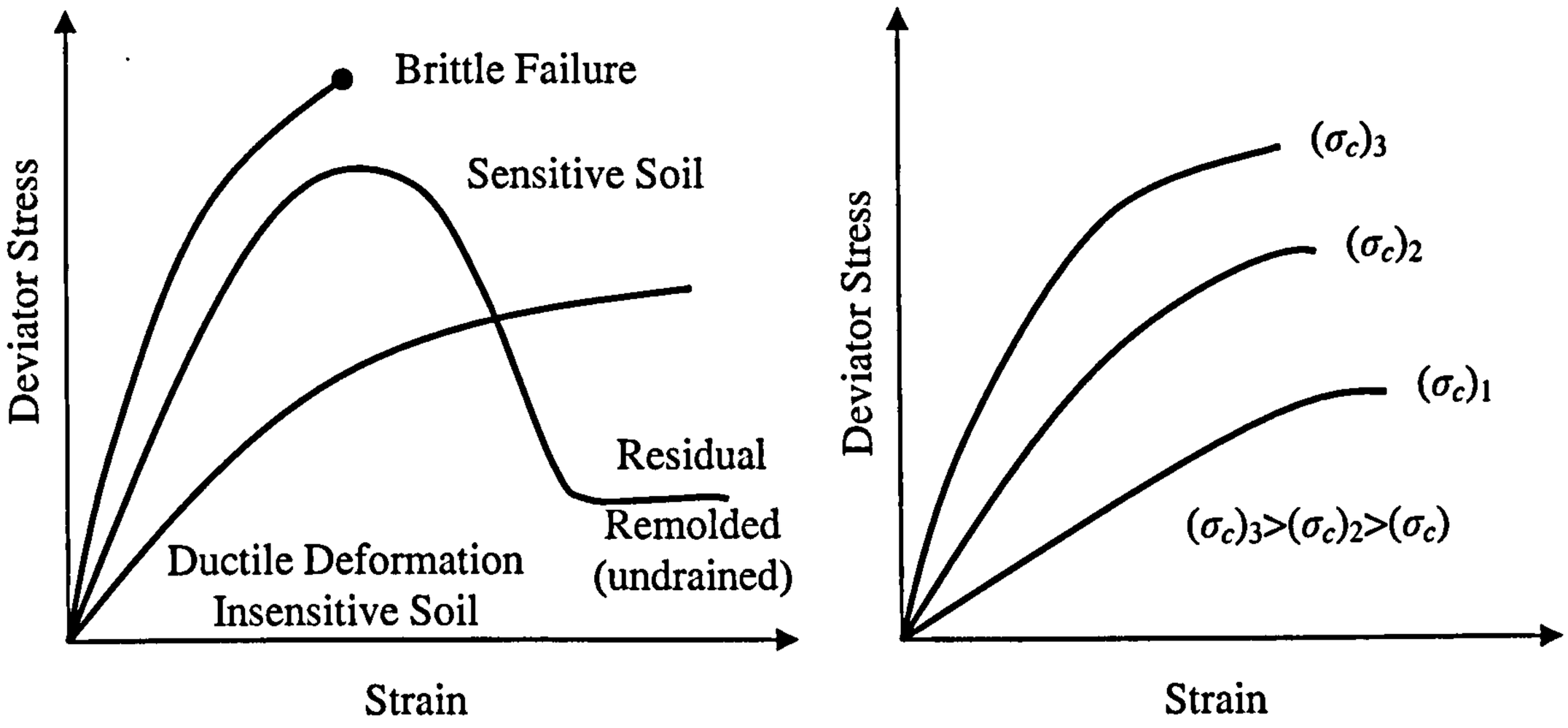

Figure 2-8 Stress-strain behaviour of soils. (a) Types of stress-strain behaviour and (b) Effect of confining pressure on the consolidated-drained stress-strain behaviour of soils (Mitchell and Soga, 2005)

Both triaxial compression and direct shear tests on MSW samples provide information on stress-strain behaviour of MSW. Since the direct shear test makes no pretence of imposing uniform stress conditions on the sample being tested (Muir Wood, 2005), the triaxial compression test is likely to remain the most appropriate laboratory test to investigate the MSW stress-strain behaviour, though it is probably not an appropriate device for measuring the MSW shear strength parameters argued by Kavazanjian (2001) and Dixon and Jones (2005). Triaxial compression test results reported by international researchers are described below.

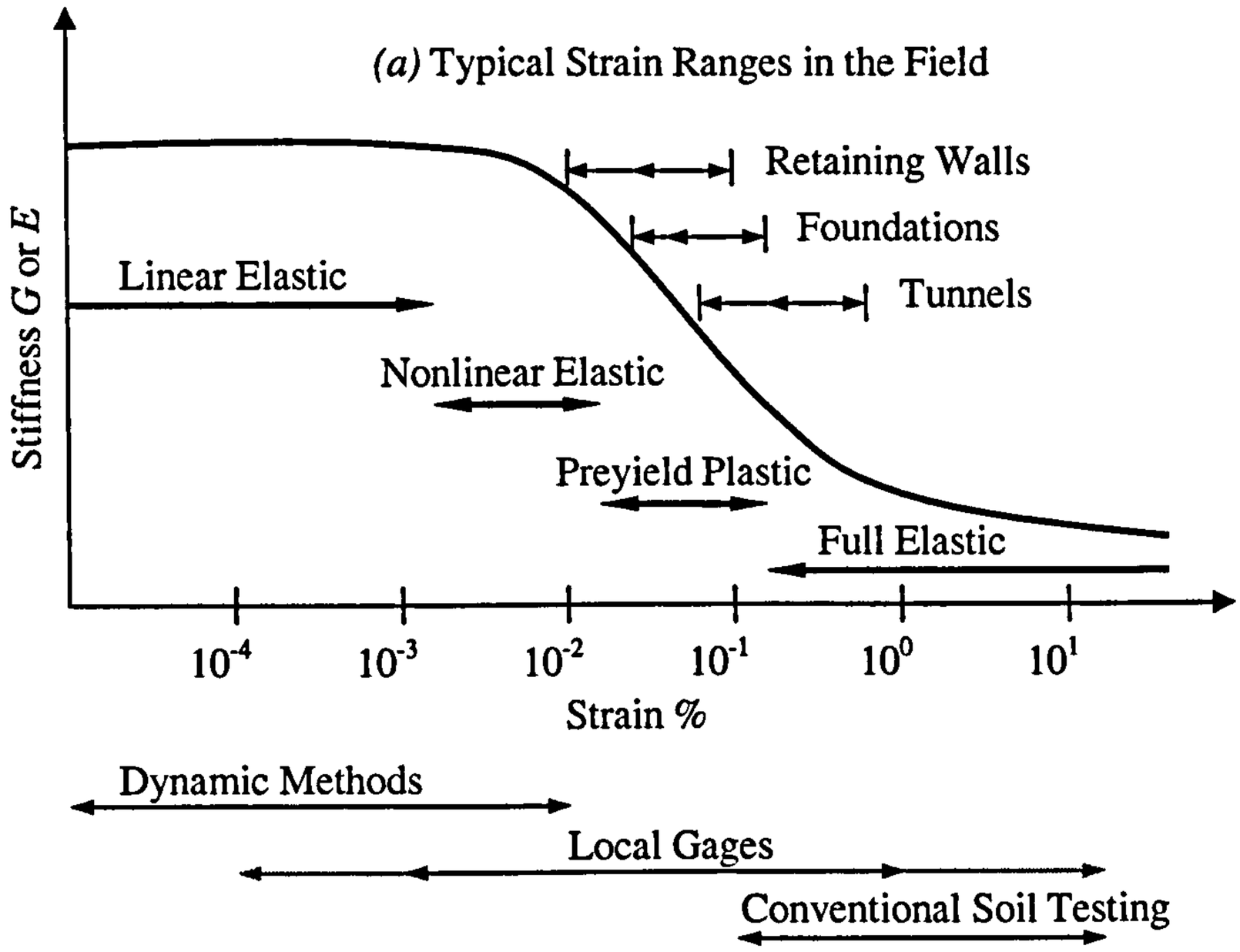

Figure 2-9 *Stiffness degradation curve: stiffness plotted against logarithm of strains. Also shown are (a) the strain levels observed during construction of typical geotechnical structure and (b) the strain levels that can be measure by various techniques (Mitchell and Soga, 2005)*

Jessberger and Kockel (1993) conducted triaxial compression tests on untreated and milled waste samples in a large (300 mm in diameter and 600 mm in height) and a small (100 mm in diameter and 200 mm in height) triaxial compression cells. Waste material (1 to 3 years old) was directly obtained from a landfill in Germany. Initially the material was processed by removing large constituents which was expected to falsify testing results. The untreated waste samples were prepared after the large constituents were separated, and milled waste samples were reconstructed after milling the waste material. Consolidated drained (CD) triaxial compression tests were then conducted on untreated and milled waste samples with different confining stresses (100 kPa, 200 kPa, 300 kPa and 400 kPa). Minor differences were noticed between the test results with untreated and milled samples. Therefore, only milled test results were presented (Figure 2-10) and discussed by Jessberger and Kockel (1993). Figure 2-10 also includes the triaxial compression test results on reconstructed waste samples reported by Grisolia *et al.* (1991). It can be seen that under different confining stresses, waste samples showed the same behaviour as soil material presented in Figure 2-8 (b), i.e. an increase in confining pressure causes an increase in the deformation modulus as well as an increase in strength.

Jessberger and Kockel (1993) summarised two aspects of observed MSW behaviour from triaxial compression tests which were different from soil triaxial compression test results as follows:

1) Failure cannot be observed even at very high sample compression greater than 40%, which was mentioned earlier in the previous section;

2) The waste material hardens with deformation, i.e. shear stiffness increases with deformation, while soil stiffness decreases with increasing shear strain as shown in Figure 2-8 and Figure 2-9.

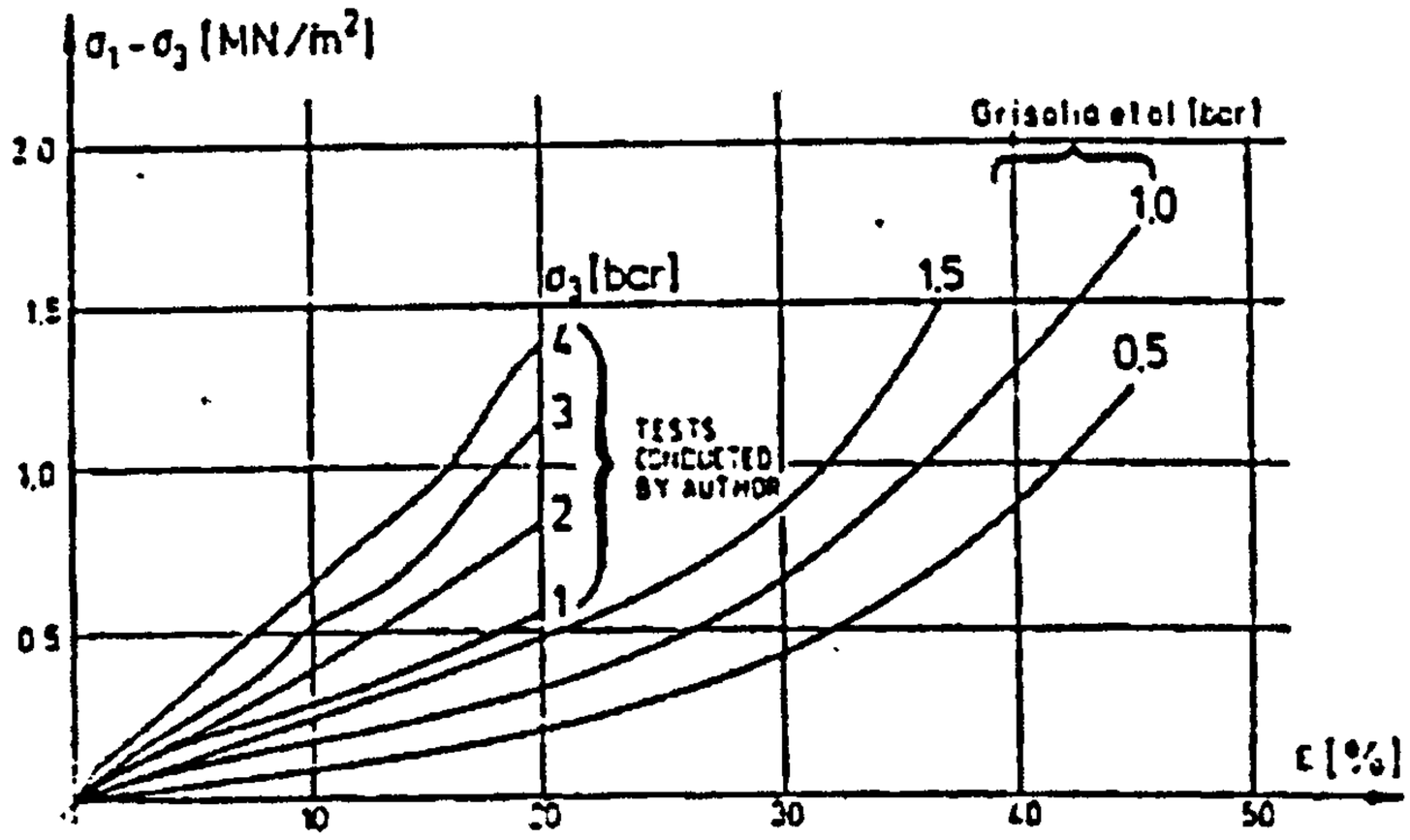

Figure 2-10 Stress-strain curves from triaxial compression tests on milled waste samples (Jessberger and Kockel, 1993)

Jessberger and Kockel (1993) argued that the high compressibility of MSW is responsible for the above observed behaviour It was explained that this high compressibility originated from a relatively large pore space in the waste sample. These pores included macro-pores between the waste particles and micro-pores representing the pore space within particles, which indicates particle compression may have an effect on the observed behaviour. In addition, reinforcing particles were not mentioned as having any contribution to the observed behaviour.

Jessberger *et al.* (1995) conducted more triaxial compression tests on different waste samples and acknowledged the influences of reinforcing particles on waste shear strength. It was argued that the reinforcement has no significant influence on the friction properties of the waste material, while it provided a significant cohesion intercept. The influences of reinforcing particles on waste stress-strain behaviour were not mentioned in the paper. However, a comparison between untreated and milled waste triaxial compression test results presented in the paper may indicated the influences of reinforcing particles. Figure 2-11 compared the triaxial compression test results

for untreated and milled waste samples that were prepared in the same way as those reported in Jessberger and Kockel (1993).

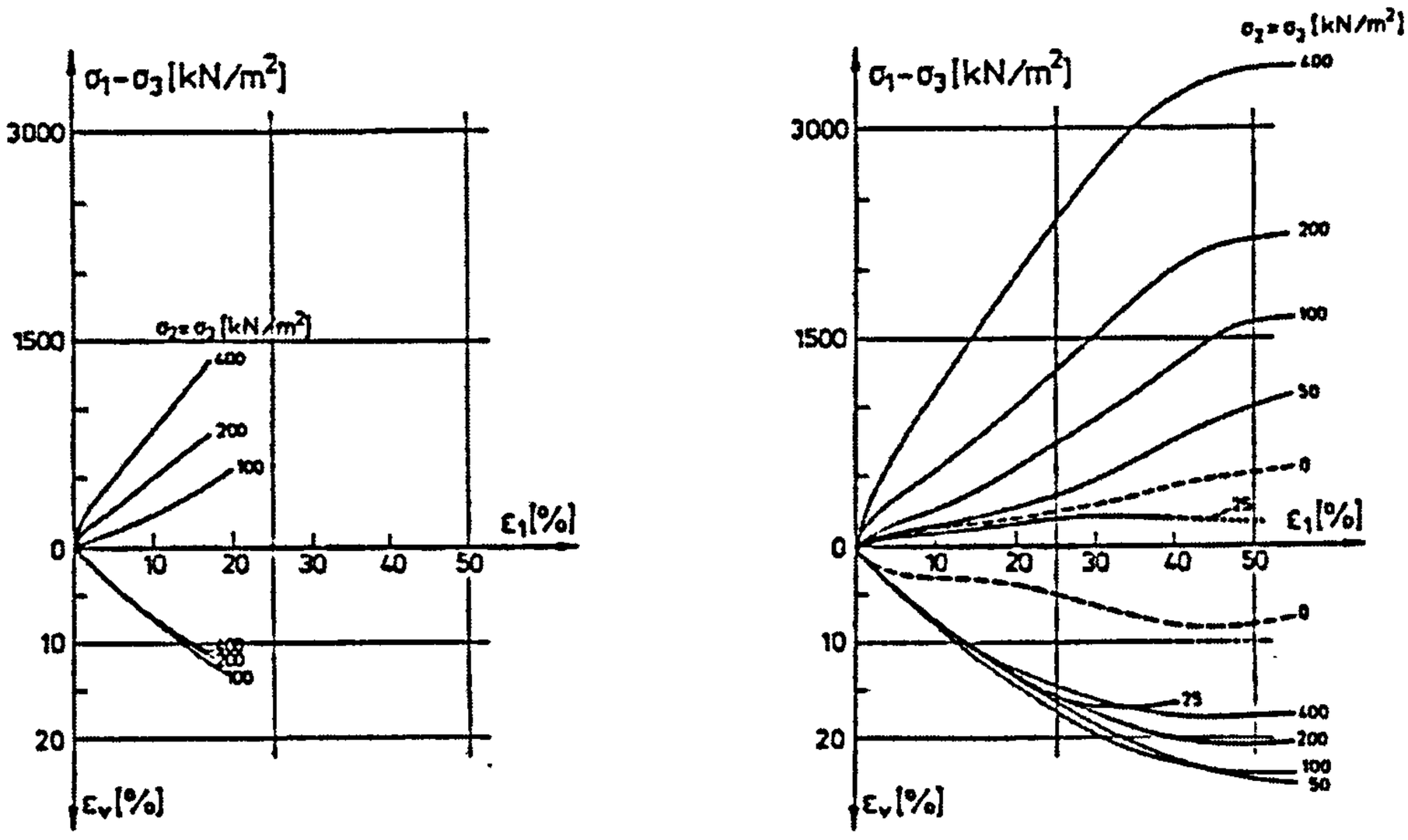

(a) *(b)*

Figure 2-11 Triaxial compression test results on untreated and milled waste samples: (a) Untreated waste, and (b) Milled waste (Jessberger et al., 1995)

The untreated waste test results are almost the same as the results presented in Figure 2-10, in which strain range is only up to 20%. However, the strain range for the milled waste test results were extended to more than 50% in Figure 2-11 (b). It can be seen that when the axial strain reached about 50%, a limit state which is similar to the critical state defined in soil mechanics was obtained in waste material. Whether this kind of limit state can be obtained in the untreated waste samples or not was not stated, but it was mentioned by Jessberger and Kockel (1993) that failure cannot be observed even at very large axial strain, which indicated that untreated waste had no similar limit state. Since reinforcing particles can be broken during the milling process, milled waste samples represented the non-reinforced waste material, while untreated waste samples represented the waste material with reinforcement. It can be concluded that waste material with reinforcement showed no failure and the shear stiffness kept increasing even when the axial strain reached 50% (date presented by Grisolia *et al.* (1991) in Figure 2-10), through which influences of reinforcing particles on MSW stress-strain behaviour can be confirmed.

Grisolia *et al.* (1995) performed triaxial compression tests on artificially reconstructed fresh waste samples whose composition was given in Table 2-2 (similar to the waste samples reported by Grisolia *et al.*, 1991, and results presented in Figure 2-10). The triaxial compression cell measured 650 mm in height and 250 in diameter. The water content of all the samples were maintained at

40% and the consolidation drained test was conduct at different confining stresses of 50 kPa, 100 kPa and 300 kPa. Figure 2-12 presents the typical stress-strain curves obtained from the drained triaxial compression tests, in which similar behaviour to those observed in Jessberger and Kockel (1993) can be noticed. It can again be noticed that the waste material showed higher strength and deformation modulus under higher confining stress, which is the same as for soils.

Table 2-2 Waste composition at 40% water content (Grisolia et al. 1995)

Organic matter	Paper	Plastic	Cloth & wood	Rubble d<20mm	Rubble d>20mm
[mass-%]					
22	32	8	6	12	20

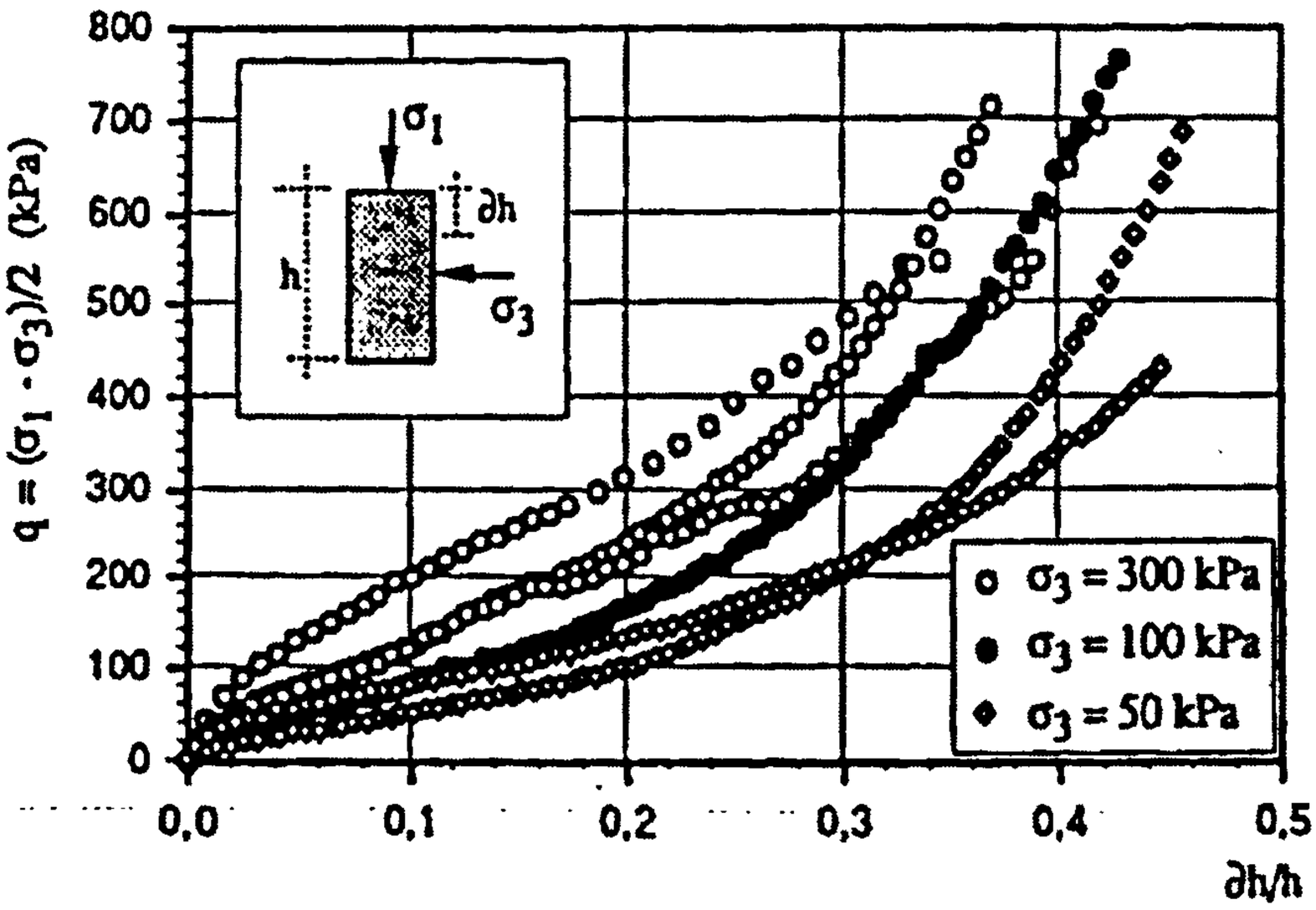

Figure 2-12 Stress-strain curves from triaxial compression tests on reconstructed waste samples (Grisolia et al. 1995)

Machado *et al.* (2002) carried out triaxial compression tests using statically compacted specimens (composition is given Table 2-3) with nominal unit weights of 10, 12, and 14kN/m^3, diameters of 150 and 200mm and heights of 300 and 400mm. The strain rate was 0.7mm/min and saturated specimens and specimens remoulded to the natural moisture content were tested. Effective confining pressures of 100, 200, and 400kPa were used. For preparing the sample waste from a borehole was thoroughly mixed and the largest particles were substituted by an equal amount of finer particles so the largest particle size would not surpass 30 or 40mm for the 150 and 200mm diameter specimens, respectively.

Test results on waste samples with different unit weight and water content showed almost the same trend, with only minor differences, and therefore typical results for one waste sample were presented in Figure 2-13. Typical stress-strain behaviour for MSW material can be noticed, as already observed by Jessberger and Kockel (1993) who tested untreated waste and Grisolia *et al.* (1995) who tested reconstructed waste. The soil-like behaviour of waste material, i.e. stronger and stiffer material under higher confining stress, is again confirmed in triaxial tests by Machado *et al.* (2002).

Table 2-3 Composition of waste samples of 15-years-old waste (Machado et al., 2002)

Stone	Rubber	Paper	Plastic	Textiles	Wood	Metal	Glass	Paste
[dry mass-%]								
10	2	2	17	3	4	5	2	55

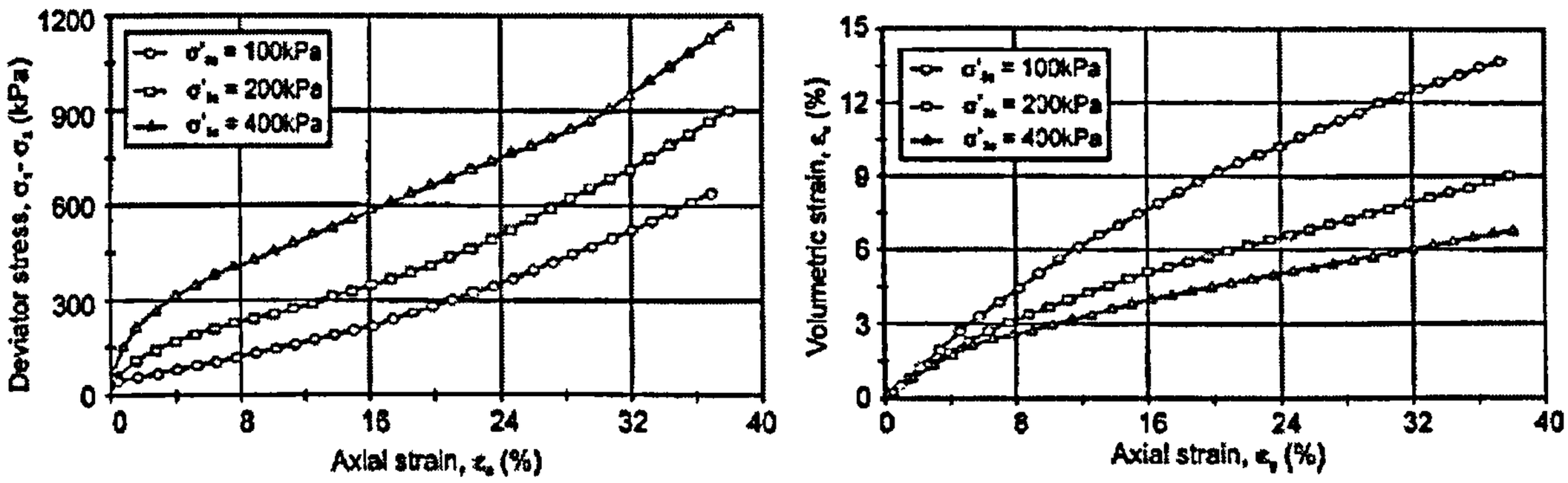

(a) *(b)*

Figure 2-13 Typical results from consolidated drained triaxial compression tests of MSW: (a) deviator stress vs. axial strain, and (b) volumetric strain vs. axial strain (Machado et al., 2002)

Volumetric behaviour of waste samples under triaxial compression is given in Figure 2-13 (b). It can be seen that under higher confining stresses less volumetric strains would be obtained with the axial strain increasing. This trend can also be noticed from the milled waste triaxial test results presented in Figure 2-11 (b). It is different to the typical normally consolidated soil volumetric behaviour which can be predicted by critical state soil models, in which the volumetric strains for different confining stresses are almost at the same level when the critical states are reached (Wood, 1990). This observed waste behaviour might be attributed to the influence of the compressible particles discussed in section 2.2.1, i.e. higher consolidation stresses would compress more compressible particles and harden the material.

In order to have a better understanding of the MSW stress-strain behaviour observed from triaxial tests, stress-strain curves obtained by Grisolia *et al.* (1995) (Figure 2-12) and Machado *et al.* (2002) (Figure 2-13 (a)) were re-plotted together for comparison in Figure 2-14. It confirms both test results have the same type of stress-strain curve except that Machado *et al.*'s MSW samples are stronger and also stiffer than the artificial waste samples. The observed stress-strain behaviour can be better described and summarised within the following three strain ranges:

1) Initial strain range: axial strain <10%;
2) Intermediate strain range: axial strain is between 10% and 20%; and
3) Large strain range: axial strain >20%.

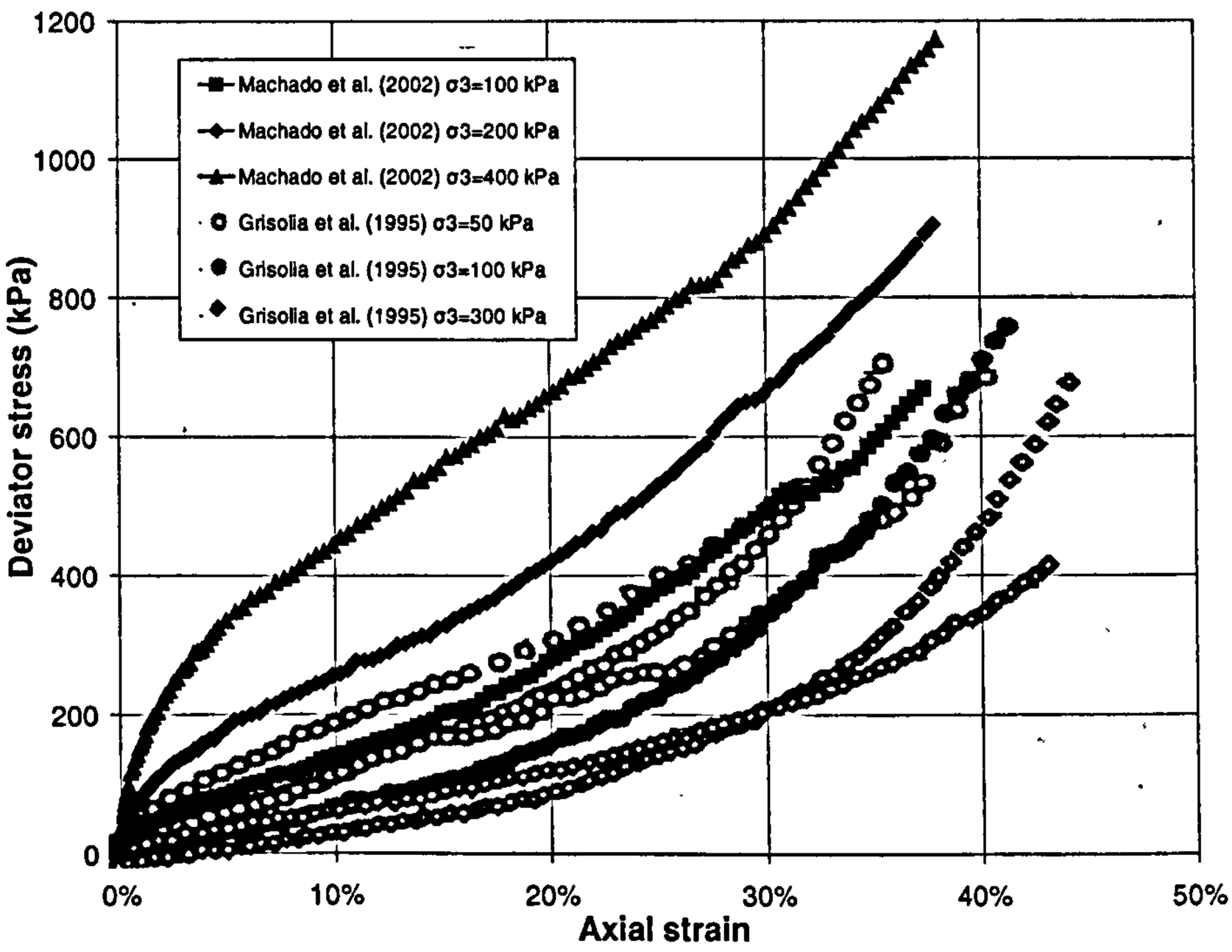

Figure 2-14 Comparison of stress-strain behaviour observed from triaxial tests

In the initial strain range, waste material shows a similar stress-strain behaviour observed in ductile deformation insensitive soil presented in Figure 2-8 a), starting with a low shear stiffness and decreasing subsequently. When it enters the intermediate strain range, the stress-strain curves show almost a linear line indicating a constant stiffness, with a small increase before it hits the large strain range. Normally in this intermediate strain range, soil material (normally consolidated) shows a large stiffness deterioration before it reaches the critical state. In the large strain range, an obvious trend of increasing stiffness can occur in waste material rather than a failure.

stiffness of MSW and shear strain level. It can be clearly seen from the test results that the secant shear stiffness of MSW decreases with the shear strain level.

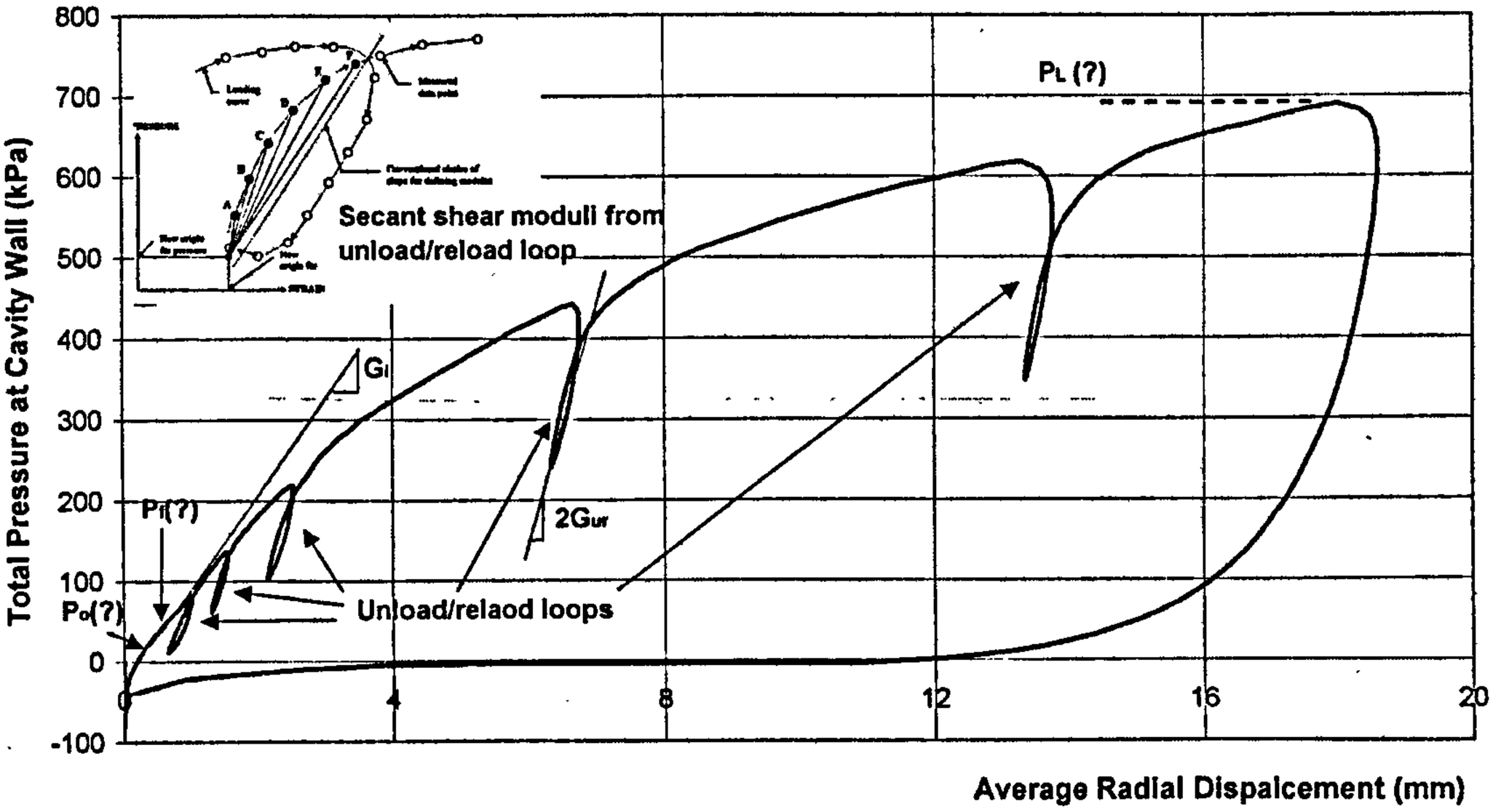

Figure 2-15 Pressure vs. cavity displacement plot from a pressuremeter test in fresh waste (Dixon et al. 2006)

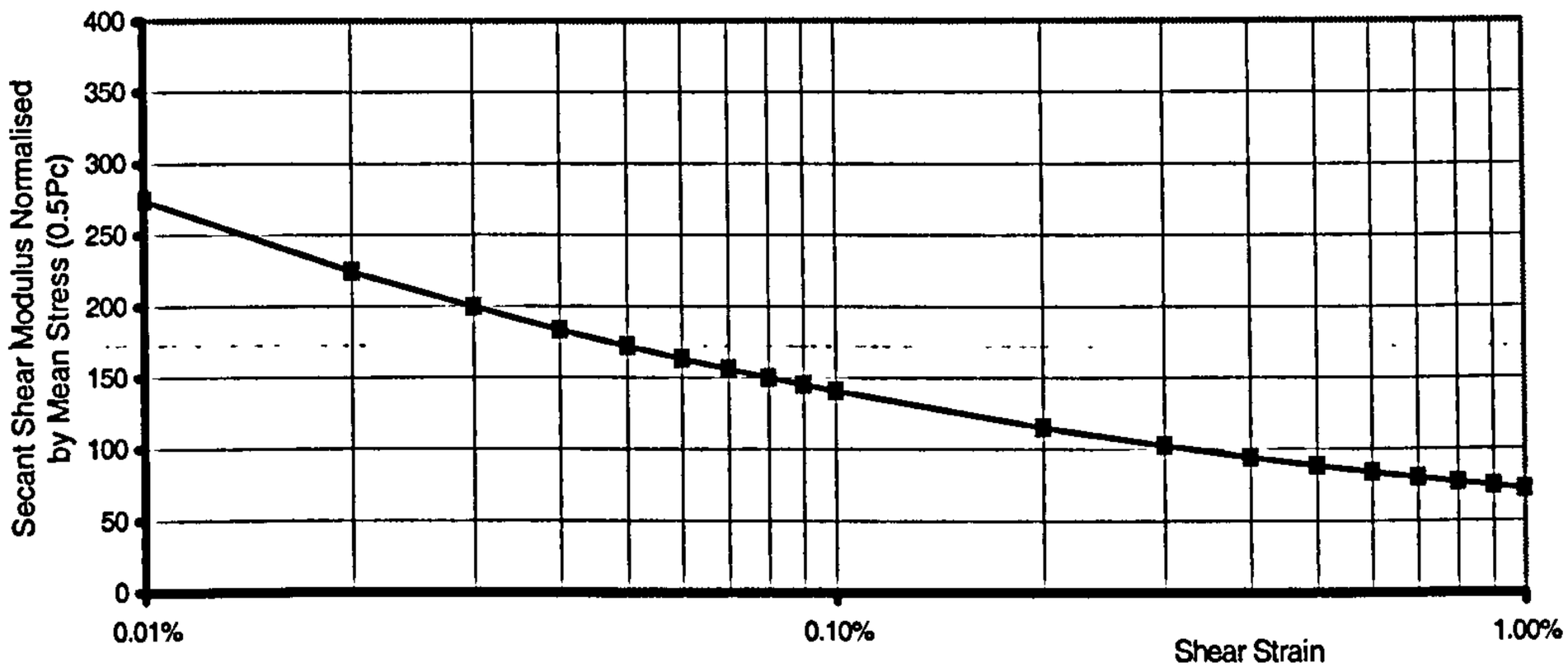

Figure 2-16 Normalised secant shear modulus varies with strain levels (after Dixon et al. 2006)

There is very little information about the stress-strain behaviour of degraded MSW in the literature. Dixon *et al.* (2006) found that older waste has a lower stiffness for a given horizontal stress from the pressuremeter test results. This may be due to the reduction of structural rigidity caused by MSW degradation.

2.3 Constitutive Modelling of MSW

A significant amount of research on mechanical behaviour of MSW has been carried out over the last few decades. However, modelling of mechanical behaviour, especially constitutive modelling,

Jessberger and Kockel (1993) and Grisolia *et al.* (1995) discussed the stress-strain behaviour observed from their tests and argued that the higher compressibility of the waste material were responsible for this behaviour, while Machado *et al.* (2002) indicated that the fibre reinforcing nature of MSW would dominate the behaviour. It must be considered however that both factors (i.e. high compressibility and reinforcing nature) play their significant roles respectively in different strain ranges on the waste stress-strain behaviour. In addition, the high compressibility of the waste material should be mainly attributed to its compressible particles which was noticed and discussed in section 2.2.1. The initial strain range behaviour should be dominated by compressible particles. Triaxial loading actually compresses the sample rather than shear it as particle compression occurs, therefore low stiffness is obtained in this strain range. In addition, the low strain range is insufficient to mobilise tensile stresses in reinforcing particles so that the reinforcing nature is very unlikely to have an effect on waste stress-strain behaviour. When the material enters the intermediate strain range, more compressible particles keep compressing and waste becomes denser. Meanwhile, some of the reinforcing particles begin to mobilise. Thus, waste stiffness remains almost constant and an increasing trend is noticed close to the large strain. Both the compressible and reinforcing particles are thought to have an effect on waste stress-strain behaviour in the intermediate strain range. When larger strain arrives, most of the compressible particles may have finished compression and more and more reinforcing particles are mobilised, therefore increasing shear stiffness can be obtained and no failure occurs. Peak strength was obtained from milled waste (without reinforcing particles) test reported by Jessberger *et al.* (1995) (Figure 2-11 (b)), which does confirm the effect of reinforcing particles on waste stress-strain behaviour at large strain range. Moreover, possible transformation from compressible particles to reinforcing particles (Langer, 2006) may additionally strengthen the material under high compressive stress condition.

In-situ pressuremeter tests also can provide information on stress-strain behaviour of MSW over a small strain range. Dixon *et al.* (2006) carried out a total of 43 pressuremeter tests in waste body in landfills, of which 33 were high pressure dilatometer (HPD) tests and 10 were self-boring pressuremeter (SBP) tests, to investigate the non-linear horizontal stiffness of MSW. Of these, 17 were in waste less than 1 year old, 15 in waste 3 to 5 year s old and 11in waste 12 to 15 years old. Figure 2-15 shows a typical plot of cavity pressure versus cavity strain obtained from a HPD pressuremeter test in MSW body. Unfortunately, shear strength information can not be obtained from the tests because cavity strains up to 30% were insufficient to mobilise limiting pressures in fresh waste. Secant shear moduli (G_s) values for shear strains in the range 0.01% to 1% were calculated by using the reload portion of unload/reload loops and applying the approach proposed by Whittle (1999). Figure 2-16 shows a typical relationship between the calculated secant

is rarely to be seen in the literature. This is because the importance of the MSW modelling has not been fully recognised, and some aspects of MSW mechanical behaviour have not yet been clarified, as discussed in section 2.2. It has been shown in section 2.2 that waste has similar behaviour as peat soil (e.g. high compressibility, fibre reinforcement), which means material model for peat might be used for waste material. Unfortunately, constitutive modelling study for peat soil is rarely seen in the literature.

2.3.1 Modelling Reinforcing Behaviour

To date only two technical papers have been found relating to constitutive modelling of mechanical behaviour of MSW (Machado *et al.*, 2002; Krase and Dinkler, 2005), in which they were trying to model the influence of reinforcing particles on MSW shear behaviour (i.e. reinforcing behaviour).

Machado *et al.* (2002) proposed a framework to model the MSW mechanical behaviour based on results from laboratory tests, i.e. triaxial compression and confined compression of large samples. It was suggested that two different effects command MSW mechanical behaviour: (1) a critical state framework for MSW paste and (2) an elastic perfectly plastic framework for waste fibres. The model was developed based upon a critical state soil model, by which soil-like behaviour of MSW could be represented. Soil models have been widely adopted for MSW in numerical analysis, which demonstrates some aspects of MSW behaviour are similar to those of soil behaviour. An important nature of MSW, i.e. reinforcing behaviour of its components has been specifically considered in Machado's model, by which a fibre model is introduced. In addition, a long-term settlement model is also proposed according to the site settlement investigation results, which will be discussed in section 2.3.2.

The idea of combining two separate models (matrix model and fibre model) together adopted by Machado *et al.* (2002) is not original. di Prisco and Nova (1993) applied this idea to produce a combined model for fibre reinforced soil. It is not difficult to select appropriate existing constitutive models for the two individual materials. The biggest challenge of this method is the way of combining the two individual constitutive models, which is defined as an integration strategy. di Prisco and Nova (1993) assumed strains were equal in the soil matrix and continuous threads, while the total normal stress were combined with stresses in soil and stresses in fibre multiplied with volume content of the threads according to total force equilibrium condition. It was also assumed that the shear stress components are only taken by soil, while the threads may take the compressive normal stress. However, it is widely acknowledged that fibres in reinforced soil can only make a contribution to tensile normal stress (Michalowski and Cermak, 2003). A

simple model combined linear elastic models for both material under axisymmetric loading was proposed. However, it could not model the experiment results well.

Machado *et al.* (2002) adopted more advanced constitutive models for both matrix and fibre material in MSW, especially for the matrix where a critical state soil model was applied. A linear elastic relationship with von Mises criterion was applied for the fibre material. Both the constitutive relationships were expressed in terms of effective mean stress p' and deviator stress q, i.e. axisymmetric stress condition is considered. A different integration strategy to di Prisco and Nova (1993) was adopted Machado *et al.* (2002), assuming both deviator stress and shear strain in MSW are obtained by adding the volume proportional contributions from both paste and fibre together. This solution has no physical or mechanical explanations, but it is surprising that the proposed model could reproduce the triaxial compression test curves on MSW samples reviewed in section 2.2.2, as presented in Figure 2-17.

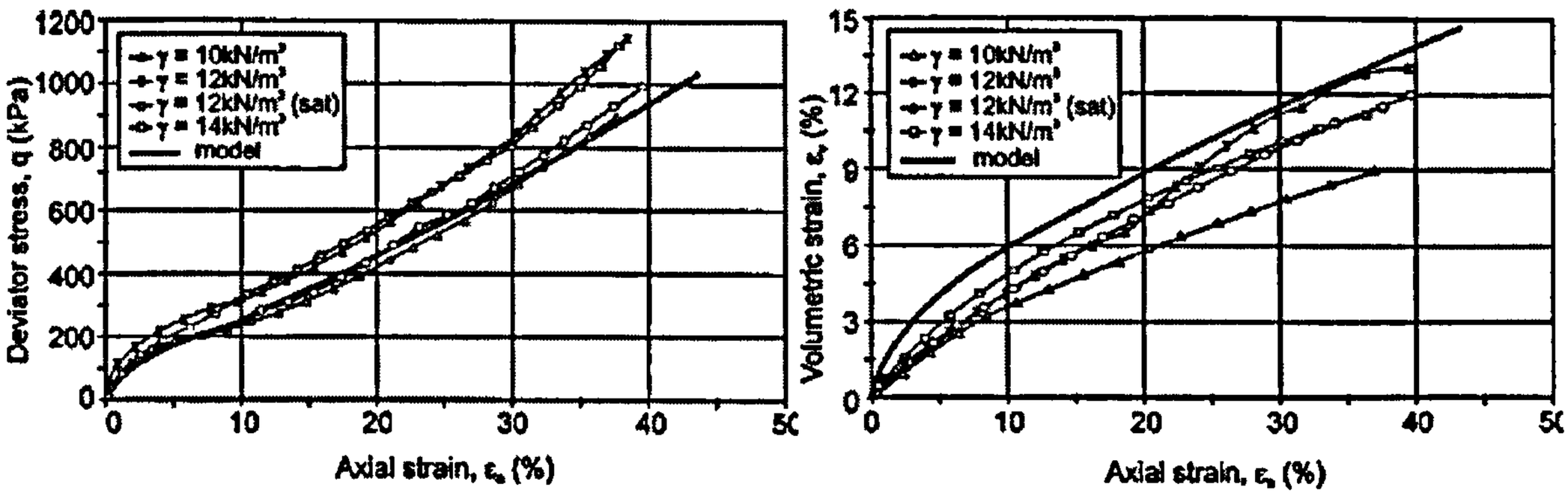

(a) *(b)*

Figure 2-17 Comparison between model and test results, confining stress is 200 kPa: (a) deviator stress vs. axial strain, and(b) volumetric strain vs. axial strain (Machado et al., 2002)

Krase and Dinkler (2005) used a different integration strategy, namely the mixture theory, to obtain a constitutive model for MSW. A linear elastic relationship with Mohr-Coulomb failure criterion was applied for matrix material, and a linear elastic model with normal stress dependant failure criterion was assumed for the fibre material. A constitutive model for MSW was proposed by combining matrix and fibre model through mixture theory. Finite element analysis was carried out to assess waste slope stability using the MSW constitutive model. Unfortunately, there is not much detailed information on mixture theory and an explanation of how it was applied into the model in their paper.

Mixture theory deals with the mechanics of mixtures or materials with two or more constituents interacting at a microscopic scale. Mixture theory appears to have originated from the work of Truesdell and Toupin (1960), and is now widely used in many fields. An excellent review article

on the different versions of mixture theory can be found in Bedford and Drumheller (1983). Mixture theory has been used in many fields including chemical engineering, materials science, biology and geosciences. In geotechnical engineering, mixture theory has been used mainly in consolidation-type problems. For instance, mixture theory has been used to reformulate and generalize Biot's theory (Biot, 1941) for three-dimensional consolidation (e.g., Coussy *et al.* 1988). In addition, it has also been applied in soil mixture modelling by Gutierrez (2003).

In mixture theory, each constituent of the mixture is assumed to simultaneously occupy the same region in space at a macroscopic scale. Thus, mixture theory approximates the macroscopic response of a heterogeneous material with a set of field equations for an equivalent homogenous material. This approximation is valid at scales much larger than the micro-scale at which the constituents can be individually distinguished. The approximation facilitates the development of tractable macroscopic models of complex systems of constituents, which interact at a microscopic level.

It appears that mixture theory would be a relevant solution to be applied to the modelling integration strategy of MSW. Nevertheless, not only are all the balance equations for each individual phase required, but also the additional equations for interaction between each phase are needed. This is the reason why a large number of parameters are needed in a model produced by this theory, e.g. the MSW model by Krase and Dinkler (2005). In addition, currently there is not a standard procedure for mixture theory to be incorporated into a numerical modelling method, e.g. finite element method or finite difference method. Therefore, it is difficult to apply mixture theory to constitutive modelling of MSW. Furthermore, with limited information on MSW mechanical behaviour at present, it may not be necessary to apply such a complete and complex theory to cover uncertain behaviour.

Both the MSW models explained above have acknowledged the reinforcing effect of fibre shaped material on MSW shear behaviour. They both attempted to produce a MSW model through combining individual models for two phases, i.e. matrix and fibre. The only difference between them is the integration strategy that they used for combining the two models. Machado *et al.* (2002) adopted a relatively simple method, which is similar to that of di Prisco and Nova (1993) for modelling of reinforced soil. The idea is easy to understand and it is also easy to apply, though physical and mechanical meanings have to be clarified through modifications. However, Karse and Dinkler (2005) applied a more complicated solution, mixture theory, as the integration strategy. Although it may be possible to produce a complete MSW model considering every aspect of behaviour, it is still on the theoretical level and it not easily applied at present. As a conclusion, an appropriate level of integration strategy, which should not only have its reasonable

physical and mechanical explanations, but also have a reasonable number of parameters, is required to model the MSW reinforcing behaviour.

Michalowski and Cermak (2003) proposed a failure criterion for randomly distributed fibre reinforced sand using an energy-based homogenisation technique rather than integrating two materials together. It was assumed that the work rate of the macroscopic stress is equated to the work dissipation rate in a deformation process under axisymmetric compression. Fibres are assumed to be distributed uniformly in all directions, then yielding of fibre-reinforced sand can be described with an isotropic model, and the principal directions of the macroscopic stress state are expected to coincide with the principal directions of the strain rate. To calculate the work dissipation in the entire specimen, the dissipation associated with a single fibre was described first as a function of the strain of the composite in the direction of this fibre. Then, the total work dissipation were integrated over all fibres. Since the fibres under compression do not contribute to the composite strength, integration of the dissipation should be performed only over the fibres subjected to tension. A critical angle was proposed to separate fibres subjected to tension and compression and can be calculated from the dilation angle of the matrix material.

When calculating the work dissipation rate associated with a single fibre, two fibre failure modes were considered, i.e. slip between the fibre/sand interface and rupture of the fibre. Since the rupture failure of fibres is possible only if the axial stress in the fibres is mobilised to the magnitude of the yield stress, there must exist a combination of stress and model parameters that determines when fibre sliding occurs and when fibre rupture occurs. A critical confining stress was derived from the requirement that the integrated shear stress on behalf of a fibre be equal to the tension limit force in the fibre. If the fibre reinforced sand is subjected to a confining stress less than the critical confining stress, the limit state of the composite is associated with a slip of fibres; otherwise plastic yielding of fibres will occur. Figure 2-18 presents the failure function for triaxial compression boundary condition, in which higher strength than pure sand (Mohr-Coulomb failure criterion) can be predicted for the fibre reinforced sand.

The model was applied to predict the failure stress of fibre reinforced sand in triaxial compression. The failure axial stress data points of fibre (polyamide) reinforced sand under different confining stresses with those of unreinforced sand by plotting them in a σ_1-σ_3 coordinate system, as shown in Figure 2-19. The predictions by their proposed model are very consistent with the test results, especially for the fibre content ρ=0.5%. For the case of fibre content ρ=2%, the model has slightly underestimated the strengths under lower confining stresses (50 kPa and 100 kPa), but over-predicted the strengths under the higher confining stresses (300 kPa and 400 kPa). The model can reproduce the shear strength behaviour of fibre reinforced sand observed in triaxial tests, but not the full stress-strain behaviour.

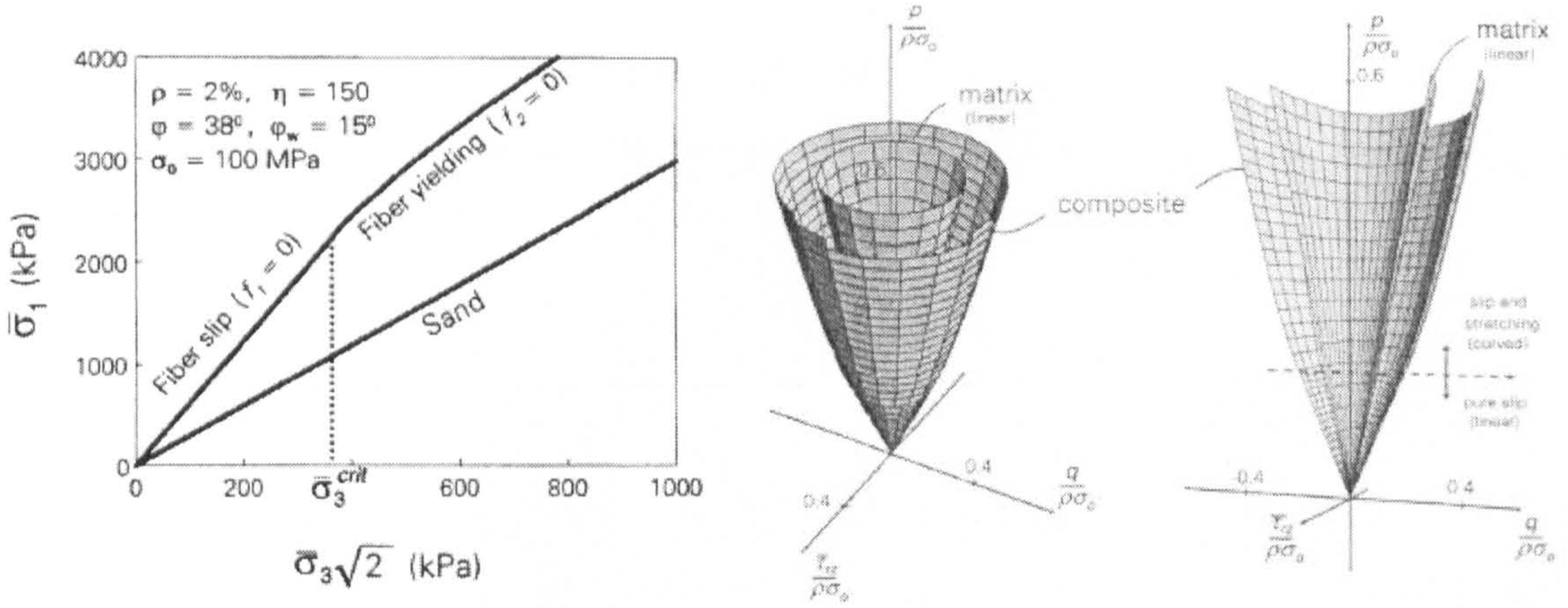

(a) *(b)*

Figure 2-18 Predicted failure function of fibre reinforced sand: (a) yield condition on triaxial compression plan, and (b) yield surface in stress space (Michalowski and Cermak, 2003)

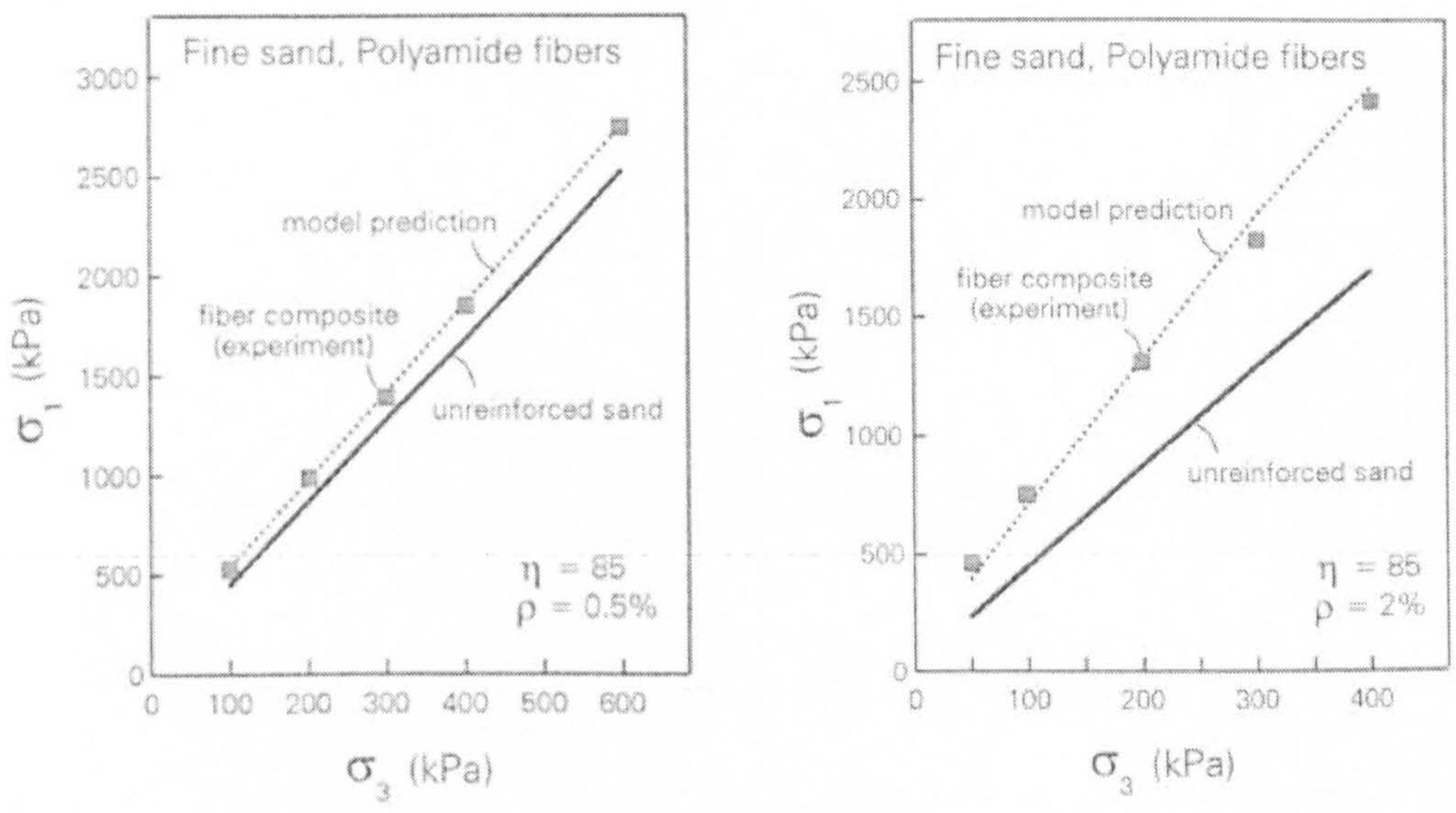

(a) *(b)*

Figure 2-19 Model prediction and experimental results for polyamide fibres (l=25.4 mm) in fine sand. (a) ρ=0.5% and (b) ρ=2.0% (Michalowski and Cermak, 2003)

2.3.2 Modelling Compression Behaviour

In addition to reinforcing behaviour, another important factor influencing MSW mechanical behaviour is the existence of compressible particles which was discussed in section 2.2. In soil constitutive models, it is preferable to link shear behaviour and volume change behaviour together (e.g. critical state soil models). It is expected that at a given stress level, the denser the soil the

higher the strength will be. When the soil is compressed to a denser state, the contact between particles is greater so that it is more difficult to cause relative displacement (shear). There is an assumption that the soil particles are incompressible or nearly incompressible. It is applicable for most soils under stress levels relevant for common problems, but it is not the case for MSW. As reviewed in section 2.2.1, particle compression may occur in MSW during compression and influence its compression behaviour, which can also influence the observed MSW stress-strain behaviour as discussed in section 2.2.2. Unfortunately at present, no study on modelling compressible particle behaviour has been found in the literature.

Long-term compression behaviour (creep and degradation) of MSW have been modelled by many researchers. Machado *et al.* (2002) applied an additional component in their constitutive model to calculate the secondary compression of MSW. A time-dependent function proposed by Ling et al. (1998) was adopted to calculate the long-term settlement of MSW in landfills. Krase and Dinkler (2005) also included a creep law in their constitutive modelling of MSW to calculate the long-term settlement of MSW due to creep and degradation. Neither of these models has considered the influence of compressible particles on the instant compression behaviour of MSW.

As for long-term settlement estimation methods, Edil *et al.* (1990); Ling *et al.* (1998) and Marques *et al.* (2003) suggested applying a simple time-dependent function to model the complicated MSW compressive mechanism including creep and degradation. Although these models can predict the settlement accurately at times (depending on the values of parameters), it can not be explained according to MSW compression behaviour. An appropriate model capable of reflecting the MSW compressive mechanism is required.

McDougall and Pyrah (2004) proposed a decomposition model for non-conservative soil through analysis of phase composition. It was postulated that decomposition of solid matter might initially enlarge the void space without significant overall volumetric reduction; however, the solid skeleton is progressively weakened until it can no longer support the current stress state and a collapse occurs. Densification due to collapse improves the soil skeleton's ability to resist further deformation, although the improvement is only temporary if continued, degradation produces further episodes of void enlargement and collapse. This model considered the effect of degradation from a creative and reasonable view. McDougall and Hay (2005) has also proposed a coupled model that relates the degradation process to changes in mechanical properties and hence behaviour. These types of approach could be incorporated into a waste constitutive modelling in the future.

2.4 Constitutive Model for Soils

It has been shown that the constitutive modelling of MSW has, to date, involved combination of soil and fibre models. To select an appropriate soil model for constitutive modelling of MSW, it is necessary to review existing constitutive models for soil.

There is a long history for the development of constitutive models for soil. Scott (1985) gave a detailed historical review and discussion of constitutive theories in the 19th Terzaghi Lecture: "Plasticity and Constitutive Relations in Soil Mechanics". He introduced the process of how the constitutive model evolved from initial isotropic elasticity to non-linear elasto-plasticity and emphasis on the plasticity of soil. In the last two decades, with the development of high-speed modern computer techniques, some more advanced and sophisticated models have been proposed, e.g. MIT-E3 model (Whittle, 1987), and bubble soil model (Stallebrass, 1997). Two representative constitutive models for soils, i.e. the elastic-perfectly plastic Mohr-Coulomb model and the Modified Cam-Clay model, which are widely used and could possibly be applied to the constitutive modelling of MSW will be introduced. Prior to this, basic equations of general elastic-perfectly plastic model and general elastic-hardening plastic model are explained.

2.4.1 General Elasto-Plastic Model Equations

The basic assumption of the elasto-plastic soil models that have been developed is the strain increments that accompany any changes in stress can be divided into elastic (^{e}) (recoverable) and plastic (^{p}) (irrecoverable) parts, which can be expressed as:

$$\delta\varepsilon = \delta\varepsilon^e + \delta\varepsilon^p \qquad \text{Eq. 2-4}$$

The elastic strain increment $\delta\varepsilon^e$ occurs whenever there is any change in stress $\delta\sigma$, and these two variables can be linked by:

$$\delta\sigma = D\delta\varepsilon^e \qquad \text{Eq. 2-5}$$

where D is the elastic material matrix. The first ingredient of the elasto-plastic model is therefore a description of the elastic behaviour. This elastic behaviour is the same for both non-hardening and hardening models. However, as soon as the material yields, different types of plastic behaviour will be defined for these two types of models, as shown in Figure 2-20. Therefore, the elastic-perfectly plastic model and the elastic-hardening plastic model need to be introduced separately as follows (Muir Wood, 2005):

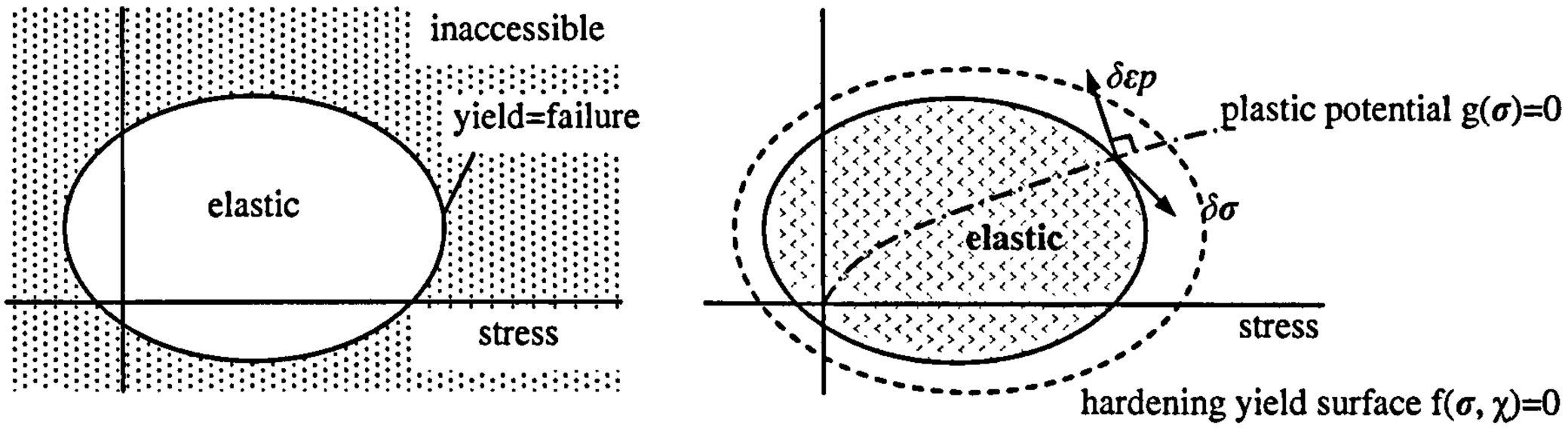

Figure 2-20 Difference between non-hardening and hardening model (a) elastic-perfectly plastic model, and (b) elastic-hardening plastic model (Muir Wood 2005)

➢ General Elastic-Perfectly Plastic Model

In the elastic-perfectly plastic model, i.e. non-hardening model, there is a region of stress space which can be reached elastically, without incurring any irrecoverable deformations, as shown in Figure 2-20 (a). However, as soon as the boundary of this elastic region is reached then the material yields (or fails) at constant stress level. The boundary of the elastic region is called a yield surface and is mathematically described by a yield function. The yield function is the second ingredient of the model which can be expressed as:

$$f(\sigma)=0 \qquad \textit{Eq. 2-6}$$

The plastic strain increment $\delta\varepsilon^p$ occurs only when the stress state lies on, and remains on, the yield surface during the load increment so that:

$$f(\sigma)=0;\ \delta f=\frac{\partial f}{\partial \sigma}^{T}\delta\sigma=0 \qquad \textit{Eq. 2-7}$$

where ^{T} indicates the transpose of the vector. This relationship is known as the consistency condition (Muir Wood, 2005).

A third ingredient of the model, flow rule, is needed to establish the link between stress state and plastic deformations. A plastic potential function $g(\sigma)$ is assumed such that the plastic strain increments is given by

$$\delta\varepsilon^{p}=\Lambda\frac{\partial g}{\partial \sigma} \qquad \textit{Eq. 2-8}$$

where Λ is a scalar multiplier which merely indicates the magnitude of the plastic strain increments. It is thus only the gradient of the plastic potential function $g(\sigma)$ that is required, the

actual value of the function is not relevant. It should be noted that the plastic strains are controlled by the current stresses at yield and not by the stress increment which brought the material to yield.

By combining Eq. 2-4, 2-5 and 2-8, the incremental stress can be obtained as:

$$\delta\sigma = D\delta\varepsilon - \Lambda D\frac{\partial g}{\partial \sigma} \qquad \textit{Eq. 2-9}$$

and it is not difficult to determine Λ by combining Eq. 2-7 and 2-9 as:

$$\Lambda = \frac{\frac{\partial f}{\partial \sigma}^{T} D\delta\varepsilon}{\frac{\partial f}{\partial \sigma}^{T} D\frac{\partial g}{\partial \sigma}} \qquad \textit{Eq. 2-10}$$

hence the elasto-plastic material matrix D^{ep} for elastic-perfectly plastic model can be obtained by:

$$\delta\sigma = \left[D - \frac{D\frac{\partial g}{\partial \sigma}\frac{\partial f}{\partial \sigma}^{T} D}{\frac{\partial f}{\partial \sigma}^{T} D\frac{\partial g}{\partial \sigma}} \right]\delta\varepsilon = D^{ep}\delta\varepsilon \qquad \textit{Eq. 2-11}$$

from which the stress increment can be calculated from any total strain increment that is causing yield.

➢ General Elastic-Hardening Plastic Model

Hardening models are natural extensions of the elastic-perfectly plastic models. The additional feature is that the yield function is no longer merely a function of the stress state. A hardening parameter is introduced to characterise the current size of the yield surface, as shown in Figure 2-20 (b). Non-hardening models reproduce the failure and the plasticity of material behaviour—the accumulation of the irrecoverable strains, while hardening plasticity enables to predict the pre-failure non-linear stress-strain relationship.

In addition to the three ingredients of the perfectly plastic models, an extra component of the model, the hardening rule, is required to define the way in which this hardening parameter changes as plastic strain occurs. The yield criterion and flow rule need rewriting due to the extra hardening parameter. For a hardening model the yield surface is not fixed but will depend on the history of the loading of the material, which is a function of a hardening parameter χ:

$$f(\sigma,\chi)=0 \qquad \textit{Eq. 2-12}$$

It is the same as the non-hardening models that the current stress state cannot lie outside the current yield surface. However, the size of the yield surface is no longer fixed as it was in the elastic-perfectly plastic model, i.e. it is able to expand in order to accommodate the imposed stress changes. The consistency condition shown in Eq. 2-7, which states that the stress stage must remain on the yield surface when plastic strains are being generated, now is expressed as:

$$f(\sigma,\chi)=0;\ \delta f=\frac{\partial f}{\partial \sigma}^{T}\delta\sigma+\frac{\partial f}{\partial \chi}\delta\chi=0 \qquad \textit{Eq. 2-13}$$

The same method as for the elastic-perfectly plastic model, i.e. defining a plastic potential, is used to indicate the ratio of the several incremental plastic strain components (Eq. 2-8). It may be convenient to assume that the yield criterion f and the plastic potential g are the same. This case is defined as associated flow (the flow is associated with the yield criterion) or normality (the strain increment vectors are normal to the yield surface at the current stress state) but this is certainly not a necessary assumption. Non-associated flow rule is applied if f and g are assumed to be different (Muir Wood, 2005).

The hardening rule links the change in size of the yield surface with the magnitude of the plastic strain, i.e. a link between hardening parameter χ and plastic multiplier Λ. For the elastic-hardening plastic model, the hardening parameter must be assumed as a function $\chi(\varepsilon^p)$ of the plastic strain so that the link can be established. Combining the consistency condition Eq. 2-13 and the flow rule Eq. 2-8, it results in:

$$\frac{\partial f}{\partial \sigma}^{T}\delta\sigma+\Lambda\frac{\partial f}{\partial \chi}\frac{\partial \chi}{\partial \varepsilon^{p}}^{T}\frac{\partial g}{\partial \sigma}=0 \qquad \textit{Eq. 2-14}$$

a procedure exactly the same as that used for the perfectly plastic model can be used to generate the stiffness relationship between stress increments and total strain increments:

$$\delta\sigma=\left[D-\frac{D\frac{\partial g}{\partial \sigma}\frac{\partial f}{\partial \sigma}^{T}D}{\frac{\partial f}{\partial \sigma}^{T}D\frac{\partial g}{\partial \sigma}+H}\right]\delta\varepsilon=D^{ep}\delta\varepsilon \qquad \textit{Eq. 2-15}$$

where H is the hardening quantity, expressed as:

$$H=-\frac{\partial f}{\partial \chi}\frac{\partial \chi}{\partial \varepsilon^{p}}^{T}\frac{\partial g}{\partial \sigma} \qquad \textit{Eq. 2-16}$$

2.4.2 Elastic-Perfectly Plastic Mohr-Coulomb Model

Elastic-perfectly plastic model states that there is not hardening or softening stiffness for the material, i.e. stiffness before failure is kept as a constant. As soon as the stress status reaches its yield criterion (or failure criterion), the material yields (or fails) at constant stress. Mohr-Coulomb failure criterion is familiar to all geotechnical engineers and the elastic-perfectly plastic Mohr-Coulomb model is generally available in most finite element programs. Muir Wood (2005) explained the model in terms of effective mean stress p' and deviator stress q for axisymmetric condition in detail as below:

Firstly, the elastic properties need to be defined as an isotropic elastic relationship:

$$\begin{Bmatrix} \delta p' \\ \delta q \end{Bmatrix} = \begin{bmatrix} K & 0 \\ 0 & 3G \end{bmatrix} \begin{Bmatrix} \delta \varepsilon_p^e \\ \delta \varepsilon_q^e \end{Bmatrix} \qquad \textit{Eq. 2-17}$$

where K is bulk modulus, G is shear modulus, $\delta \varepsilon_p^e$ is the incremental elastic volumetric strain, and $\delta \varepsilon_q^e$ is the incremental elastic distortional strain.

The yield function is then defined as:

$$f(\sigma) = f(p', q) = q - Mp' \qquad \textit{Eq. 2-18}$$

If $f<0$ the soil is behaving elastically; if $f>0$ the soil is yielding (failing) and generating plastic deformations. To have $f>0$ is impossible, which defines an inaccessible region in the stress plane. The value of the soil property M can be related to the angle of shearing resistance ϕ of the soil in triaxial compression (Muir Wood, 2005):

$$M = \frac{6 \sin \phi}{3 - \sin \phi} \qquad \textit{Eq. 2-19}$$

Finally, a flow rule is required to define the plastic deformation mechanism at the current stress state. A plastic potential function is given as:

$$g(\sigma) = g(p', q) = q - M^* p' + k = 0 \qquad \textit{Eq. 2-20}$$

where k is an arbitrary variable to allow the plastic potential function to be defined at the current state of stress and M^* is another soil property. This implies that the plastic strain increments are given by normality to the plastic potential function at the current state of stress:

$$\begin{Bmatrix} \delta\varepsilon_p^p \\ \delta\varepsilon_q^p \end{Bmatrix} = \Lambda \begin{Bmatrix} \partial g / \partial p' \\ \partial g / \partial q \end{Bmatrix} = \Lambda \begin{Bmatrix} -M^* \\ 1 \end{Bmatrix} \qquad \textit{Eq. 2-21}$$

where Λ is a scalar which has been defined in section 2.4.1. The ratio of the two components of plastic strain can be obtained as:

$$\frac{\delta\varepsilon_p^p}{\delta\varepsilon_q^p} = -M^* \qquad \textit{Eq. 2-22}$$

The link between M^* and angle of dilation is not as simple as the link between M and angle of shearing resistance because angle of dilation is essentially a plane strain concept. In plane strain the angle of dilation ψ has a geometrical meaning as the tangent to Mohr's circle of strain increment. Under conditions of triaxial compression a similar tangent angle ψ_c can be defined. The triaxial strain increment ratio can be expressed as (Muir Wood, 2005):

$$\frac{\delta\varepsilon_p^p}{\delta\varepsilon_q^p} = \frac{3}{4}(3\sin\psi_c - 1) \qquad \textit{Eq. 2-23}$$

in which $\sin\psi_c<1/3$ implies dilation. Then, if an angle of dilation ψ can be defined as a material property for use merely in analysis form:

$$M^* = \frac{6\sin\psi}{3-\sin\psi} \qquad \textit{Eq. 2-24}$$

for triaxial compression to be exactly similar to Eq. 2-20, the direct geometrical interpretation has been lost (Muir Wood, 2005). Angles ψ and ψ_c are linked through:

$$\sin\psi_c = \frac{1-3\sin\psi}{3-\sin\psi} \qquad \textit{Eq. 2-25}$$

A general expression for the elasto-perfectly plastic material matrix D^{ep} has already been given in Eq. 2-11. Therefore, the complete elastic-plastic material matrix for elastic-perfectly plastic Mohr-Coulomb model can now be generated (Muir Wood, 2005):

$$D^{ep} = \left[\begin{pmatrix} K & 0 \\ 0 & 3G \end{pmatrix} - \frac{1}{KMM^* + 3G} \begin{pmatrix} MM^*K^2 & -3M^*GK \\ -3MGK & 9G^2 \end{pmatrix} \right] \qquad \textit{Eq. 2-26}$$

The second term in the equation is only included if the soil is yielding. The elasto-plastic material matrix is in general asymmetric unless $M^*=M$ which is physically unreasonable. However, certain numerical analysis programs requires the material matrix to be symmetric for solution purposes

and it is for these programs that the assumption $M^*=M$ is often forced upon the user, otherwise some numerical modification is needed to overcome the limitation of the program (Muir Wood, 2005).

2.4.3 Modified Cam-Clay Model

By 1950, the mathematical basis of plasticity for metals was firmly established (Scott, 1985). Some elastic perfectly plastic models, from Tresca and von Mises models to Mohr-Coulomb and Drucker-Prager models had been applied to soil mechanics. Since that time, they have been extended by many investigators to account for the peculiarities of soil behaviour, such as strain work hardening rule and yielding under mean stresses. Drucker *et al.* (1957) proposed the work hardening theories and a cap yield surface controlled by volume change, i.e. soil would yield under mean stresses. Roscoe *et al.* (1958) developed the concepts of critical state and suggested the existence of a boundary state surface, which is usually called the Roscoe surface.

The developments mentioned above led to the construction of the critical state theory as well as the first and simplest modern elastic-hardening plastic soil constitutive model, named as Cam-Clay model, developed at the University of Cambridge, by Roscoe and his co-workers. The formulation of the original Cam-Clay model as an elastic-hardening plastic constitutive relationship is presented by Roscoe and Schofield (1963) and Schofield and Worth (1968). Afterwards, Roscoe and Burland (1968) proposed the Modified Cam-Clay (MCC) model. Over the last few decades, models of Cam-Clay form have been widely and successfully used for analysis of problems involving the loading of soft clays. It has been less successful in describing the behaviour of sands for which models which make use of distortional hardening and non-associated flow have generally been reckoned to be more satisfactory (Muir Wood 2005). Both the original Cam-Clay model and MCC model are available in many of the commercial soil mechanics numerical modelling software, e.g. Sage-CRISP, FLAC and PLAXIS. The only difference between these two forms is the shape of the yield surface. The original Cam-Clay yield surface plots as a logarithmic curve, whereas the MCC yield surface plots as an ellipse. The original Cam-Clay model is difficult to implement both theoretically and practically due to the discontinuity of its yield surface at the corner. Therefore, the MCC model has been more widely used in numerical modelling of geotechnical structures. Muir Wood (2005) explained the MCC model from the following four aspects, elastic properties, yield criterion, flow rule and hardening rule, which are the four essential components of a constitutive model to be included in a numerical model.

➢ Elastic Properties

It is assumed that the elastic behaviour of the soil is isotropic and defined by two elastic parameters, bulk modulus K and shear modulus G. It is well known that results of oedometer tests are typically presented in semi-logarithmic plots because it is found that the relationships between stress and volume change become almost linear—both during loading, unloading and reloading. It is logical then to use the average slope κ of an unload-reload line to characterise the elastic volumetric response, as shown in Figure 2-21(a).

It is assumed that κ is a soil constant for the MCC model:

$$v = v_\kappa - \kappa \ln p' \qquad \textit{Eq. 2-27}$$

where v_κ is an reference value of specific volume on a particular unloading-reloading relationship. The equation can be converted to an incremental relationship:

$$\delta\varepsilon_p^e = -\frac{\delta v}{v} = \frac{\kappa}{v}\cdot\frac{\delta p'}{p'} \qquad \textit{Eq. 2-28}$$

which implies that the bulk modulus K is not constant but is dependent on stress level:

$$K = \frac{\delta p'}{\delta\varepsilon_p^e} = \frac{v p'}{\kappa} \qquad \textit{Eq. 2-29}$$

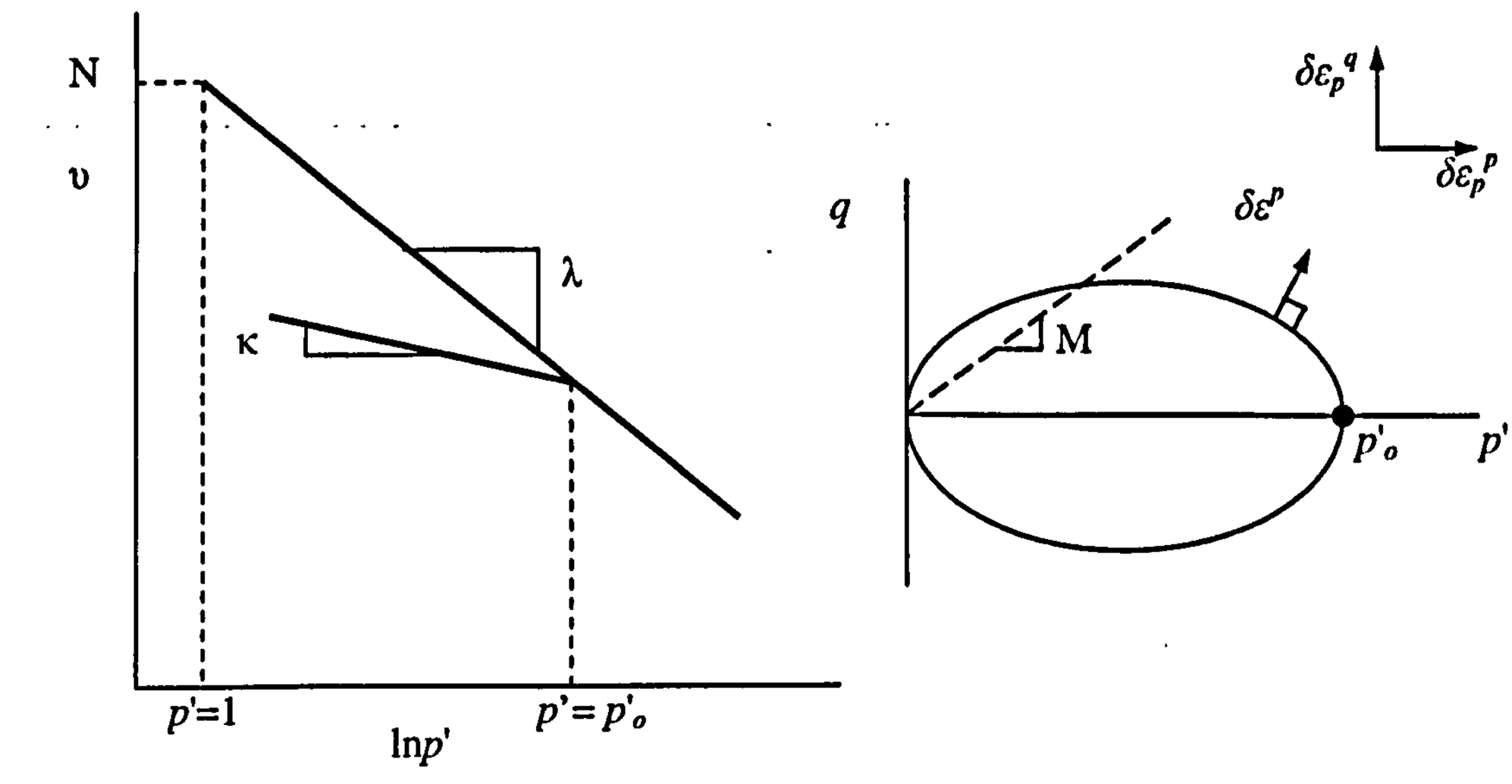

Figure 2-21 Modified Cam-Clay model. (a) linear normal compression and unloading-reloading in semi-logarithmic compression plane, and (b) elliptical yield locus (Muir Wood 2005)

In this form the value of κ is directly related to swelling index C_S:

$$\kappa = \frac{C_s}{\ln 10} \qquad \textit{Eq. 2-30}$$

In the original formulation for the MCC model, no elastic shear strains are considered. To avoid numerical problems and to achieve a better modelling inside the yield surface, elastic shear strains may often be computed from an elastic shear modulus G:

$$\delta\varepsilon_q^e = \frac{\delta q}{3G} \qquad \textit{Eq. 2-31}$$

An alternative will be to choose a constant value of Poisson's ratio μ, thus forcing a constant ratio of shear modulus and bulk modulus as below:

$$G = \frac{3(1-2\mu)}{2(1+\mu)}K \qquad \textit{Eq. 2-32}$$

Clearly if G is constant then the variation of bulk modulus K with stress level will lead to a varying Poisson's ratio μ. However, if Poisson's ratio μ is assumed to be constant then G changes together with the bulk modulus K or mean stress p', which leads to thermodynamic problems, i.e. it becomes possible to generate or dissipate energy on supposedly elastic cycles of stress change (Zytinski *et al.*, 1978). Woods and Rahim (2001) argued that, the use of a constant value of shear modulus, G, is preferable from a theoretical standpoint since the thermodynamic problems do not arise. However a constant value of Poisson's ratio is also often assumed (typically a value of about 0.3) for the following reasons:

1) The Cam-Clay and MCC models do not give very good results in situations where there are cyclic loads (whatever elastic properties are assumed). In practice a build up of pore pressure is often seen, whereas the models predict no change in pore pressures for stress cycles within the yield locus. If the effect of stress cycling is important in a problem, it is probably worthwhile considering the incorporation of a new constitutive model in the program.

2) Prediction of triaxial test results is usually better if a constant value of Poisson's ratio is used.

3) Attempts to measure G experimentally show that it is dependent on stress level (however it should be noted that the variation observed is not the same as for the bulk modulus—there is a strong correction with the size of yield locus, which is determined by p_0').

4) It is appropriate to assume that values of the critical state parameters are the same over the whole problem domain. In these circumstances a constant value of Poisson's ratio is to be preferred to a constant value of G bearing in mind the points made in 3).

In conclusion it is worth pointing out that the main strength of the Cam-Clay model is in the calculation of plastic strains during yielding as opposed to the elastic strains which are calculated for overconsolidated behaviour.

The elastic stiffness and compliance relationships can be written as:

$$\begin{Bmatrix} \delta p' \\ \delta q \end{Bmatrix} = \begin{bmatrix} vp'/\kappa & 0 \\ 0 & 3G \end{bmatrix} \begin{Bmatrix} \delta \varepsilon_p^e \\ \delta \varepsilon_q^e \end{Bmatrix} \qquad \textit{Eq. 2-33}$$

$$\begin{Bmatrix} \delta \varepsilon_p^e \\ \delta \varepsilon_q^e \end{Bmatrix} = \begin{bmatrix} \kappa/vp' & 0 \\ 0 & 1/3G \end{bmatrix} \begin{Bmatrix} \delta p' \\ \delta q \end{Bmatrix} \qquad \textit{Eq. 2-34}$$

➢ Yield Surface

Roscoe and Burland (1968) proposed an elliptical shape yield locus passing through the original of the stress plane (p', q) for the MCC model, as shown in Figure 2-21b). This introduces two variables: the aspect ratio of the ellipse M which controls the shape of the ellipse, the ratio of the vertical (q) axis to the horizontal (p') axis; and the size of the ellipse p'_0 which is the hardening parameters χ for the modified Cam-Clay model. The equation of the ellipse can be presented in various different ways. To fit in with the general presentation of hardening plastic models it can be written as:

$$f(\sigma, p'_0) = \frac{q^2}{M^2} - p'(p'_0 - p') = 0 \qquad \textit{Eq. 2-35}$$

so that, as discussed in section 2.4.1, $f>0$ indicates elastic behaviour, $f=0$ indicates that yielding is occurring and $f>0$ is not permitted.

For stress changes ($\delta p'$, δq) causing yield, the change in size of the yield locus can be written:

$$\delta p'_0 = (2p' - p'_0)\frac{\delta p'}{p'} + \frac{2q}{M^2}\frac{\delta q}{p'} \qquad \textit{Eq. 2-36}$$

from this expression the change in size of the yield locus required to accommodate any change in effective stress which causes yielding can be calculated.

➢ Flow Rule

It is assumed that the MCC model obeys the hypothesis of associated flow (normality) so that the plastic strain increment vector is assumed to be normal to the yield surface at the current stress

state, as shown in Figure 2-21 (b). The plastic potential function then has the same form as the yield criterion:

$$g(\sigma, p_0') = \frac{q^2}{M^2} - p'(p_0' - p') = 0 \qquad \textit{Eq. 2-37}$$

The plastic strain increments are given by:

$$\begin{Bmatrix} \delta\varepsilon_p^p \\ \delta\varepsilon_q^p \end{Bmatrix} = \Lambda \begin{Bmatrix} \partial g / \partial p' \\ \partial g / \partial q \end{Bmatrix} = \Lambda \begin{Bmatrix} 2p' - p_0' \\ 2q / M^2 \end{Bmatrix} \qquad \textit{Eq. 2-38}$$

➢ Hardening Rule

The hardening rule describes the dependence of the size of the yield locus p'_0 on the plastic strain. The MCC model is a volumetric hardening model in which it is assumed that the size of the yield locus depends only on the plastic volumetric strain through an expression:

$$\begin{Bmatrix} \partial p_0' / \partial \varepsilon_p^p \\ \partial p_0' / \partial \varepsilon_q^p \end{Bmatrix} = \begin{Bmatrix} v p_0' / (\lambda - \kappa) \\ 0 \end{Bmatrix} \qquad \textit{Eq. 2-39}$$

This hardening rule introduces one additional soil parameter λ. During isotropic normal compression, mean effective stress p' changes with distortional stress q kept constant at zero. There will be elastic volumetric strains given by Eq. 2-28 and, because the mean effective stress is always at the tip of the yield surface $p'=p'_0$, there will be plastic volumetric strains given by a rearrangement of Eq. 2-39:

$$\delta\varepsilon_p^p = \frac{\lambda - \kappa}{v} \frac{\delta p_0'}{p_0'} = \frac{\lambda - \kappa}{v} \frac{\delta p'}{p'} \qquad \textit{Eq. 2-40}$$

The total volumetric strain is then:

$$\delta\varepsilon_p = \delta\varepsilon_p^e + \delta\varepsilon_p^p = \frac{\kappa \delta p'}{v p'} + \frac{(\lambda - \kappa)\delta p'}{v p'} = \frac{\lambda}{v} \frac{\delta p'}{p'} \qquad \textit{Eq. 2-41}$$

Noting that the definition of the volumetric strain is:

$$\delta\varepsilon_p = \frac{\delta v}{v} \qquad \textit{Eq. 2-42}$$

Eq. 2-29 can be integrated to give the form of the normal compression relationship linking specific volume v and mean effective stress p':

$$v = N - \lambda \ln p' \qquad \textit{Eq. 2-43}$$

where N is a reference value of specific volume for unit value of mean effective stress. This is a linear normal compression relationship with slope λ in the semi-logarithmic plot, as shown in Figure 2-21 (b). It may be noted that

$$\lambda = \frac{C_c}{\ln 10} \qquad \textit{Eq. 2-44}$$

and the plastic compressibility λ can be directly related to the compression index C_c.

Now that all the ingredients of the model are in place, the full elasto-plastic material matrix D^{ep} linking the stress increments with the total strain increments can be obtained by substitution in Eq. 2-15 and 2-16, i.e. equations for the general elastic-hardening plastic constitutive model, which is not presented here due to its complexity. The hardening quantity H is given by:

$$H = -\frac{\partial f}{\partial p_0'}\frac{\partial p_0'}{\partial \varepsilon_p^p}\frac{\partial g}{\partial p'} = -(-p')\left(\frac{v p_0'}{\lambda - \kappa}\right)(2p' - p_0') \qquad \textit{Eq. 2-45}$$

2.5 Summary

Firstly, reported MSW mechanical behaviour, including compression behaviour and shear behaviour, have been reviewed. A number of special aspects of MSW behaviour, which are different to those of soil behaviour, have been identified for consideration in development of a constitutive model for MSW. These are as follows:

1) Particle compression occurs in compression of MSW, and it should be differentiated from volume change due to particle rearrangement so that traditional elasto-plastic material models can be used for MSW;

2) Long-term compression of MSW includes not only the creep deformation of the structure, the same as soils (secondary compression), but also volume loss due to chemical reaction-biodegradation;

3) K_0 values of MSW were observed from the laboratory test to be influenced by the content of reinforcing particles, i.e. they decrease consistently with an increasing amount of fibrous constituents.

4) Shear strength of MSW is influenced by the content of reinforcing particles. It seems that higher shear strength of a waste body can be reached when more fibre reinforcement is mobilised;

5) Triaxial compression tests on different kinds of waste samples have shown that MSW stress-strain behaviour appears to be dominated by compressible and reinforcing particles in different strain ranges.

6) Although there is little information on stiffness of degraded waste, pressuremeter test results showed that the older waste has a lower stiffness for a given meanstress.

Secondly, constitutive modelling of waste material has been reviewed, again through the two related aspects, modelling shear and compression behaviour. Difficulties with soil models have been recognised, and potential methods for constitutive modelling of MSW have been suggested as follow:

1) An appropriate compression model is required capable of reflecting the observed MSW instant compression behaviour, which should separate volume change due to particle compression and particle rearrangement rather than combining them;

2) An appropriate integration strategy is required to combine the two phases of waste material (i.e. matrix and fibre), which should not only have appropriate physical and mechanical explanations, but also have a reasonable number of parameters.

Finally, constitutive modelling of soils has been reviewed considering its potential application in constitutive modelling of MSW. Basic equations for general elasto-plastic soil models have been detailed for both perfectly plasticity and hardening plasticity. Essential components of a soil constitutive model have been identified. Two classic soil constitutive model, i.e. the Mohr-Coulomb perfectly plastic model and the Modified Cam-Clay model, have been presented at the level of numerical implementation.

CHAPTER

3

Methodology

3.1 Introduction

This chapter discusses the methodology which has been used to develop a constitutive model for MSW. Firstly, requirements of an appropriate constitutive model for MSW are determined through experience of numerical modelling in landfill engineering. Based upon these requirements, together with the reported MSW behaviour from the literature, which is found to be different than soil behaviour, gaps between MSW behaviour and existing constitutive models (both for soil and MSW) are investigated. Subsequently, a method for constitutive modelling of MSW is discussed from the two main aspects of modelling behaviour (i.e. compression and shear behaviour). In addition, methods for model implementation and validation are discussed.

3.2 MSW Constitutive Model Requirements

Based on studying the history of constitutive modelling of soils and existing constitutive models for soil, there is some experience applicable to the modelling of MSW. It is almost impossible to produce a perfect constitutive model for soil which could cover all aspects of soil mechanical behaviour, such as change of stiffness with stress and strain level, failure criterion, effect of stress path, contractant/dilatant behaviour, and anisotropic stiffness etc. Every existing soil model is designed to model one, or a limited number, specific aspects of soil behaviour. For example, the elastic-perfectly plastic Mohr-Coulomb model can only model the friction failure criterion of granular material, and Cam-Clay model covers the volumetric strain hardening behaviour and contractant/dilatant behaviour during shearing. Therefore, it is necessary to determine which aspects of MSW behaviour need to be included in the MSW constitutive model.

As discussed in Chapter 1, the motivation of constitutive modelling of MSW comes from the requirement of numerical modelling application to assess the interaction between the MSW body and lining systems (both steep and shallow slope lining systems), as well as the deformation and

stability of the MSW body itself. For different numerical modelling applications, the requirements of MSW constitutive model may differ. For example, according to the limited numerical modelling experience of landfill in the literature, most of them were designed to assess the stability of shallow lining systems, in which the horizontal support of MSW is of secondary importance. Therefore, the horizontal stress and deformation in MSW need not be considered, which is not the case for the steep wall lining system. This is a very simple and obvious example and more detailed information will be explained in the following sections.

3.2.1 Modelling Horizontal MSW Support

The importance of MSW horizontal support to the stability of steep slope wall lining systems has been demonstrated though numerical modelling by Fowmes *et al.* (2005). It has shown that, in the absence of the waste, failure occurs through the toe of the lining system, however, with waste support, strains are much lower. The deformation of the lining system is also shown to be dependent on the stiffness of MSW material. The stiffness issue is of concern because support is currently considered in the limit equilibrium method design but not stiffness of MSW. This is exactly the reason why numerical modelling techniques are needed.

According to the numerical modelling experience, two aspects of MSW mechanical behaviour are required to be emphasised for constitutive modelling of MSW, that is, in-situ horizontal stress and non-linear horizontal stiffness. In numerical modelling, a relevant K_0 value is essential to generate the initial horizontal support from the MSW body for the steep side slope lining system. During the construction stages, when the lining system has the tendency to move towards the waste body and compress the waste, non-linear stiffness changes of the waste body needs to be modelled in order to predict the displacement of the lining system. Compared to the limit equilibrium method, interaction between waste and barrier is considered by modelling the stiffness change of the waste body.

In addition, if the long-term integrity of the lining system needs to be evaluated through numerical modelling, the MSW stiffness and K_0 values may change with time due to stress relaxation and degradation of MSW. Unfortunately, there is a lack of information about this time-dependent MSW behaviour as mentioned in the literature review. For simplification, it could be modelled by inputting parameters dependent on time rather than modelling the full degradation process.

3.2.2 Modelling MSW Settlement

Long-term MSW settlement in landfills appears to be of more concern than the instant volume change behaviour of MSW in the literature, in which the final settlement is predicted to improve

the efficiency of waste placement. However, recent numerical analysis studies (Jones and Dixon, 2005; Fowmes *et al.*, 2006; Sia, 2007) have shown that instant waste settlement (i.e. primary drained compression under waste self-weight) can result in local failure of lining components on the side slope (including both shallow and steep slopes) even if the global factor of safety for stability is adequate. It should be noted that for shallow slope lining systems, horizontal waste deformation and shearing may exert loadings on the liner, of which the mechanism is completely different to the horizontal support for the steep slope lining system discussed in section 3.2.1.

It seems that the prediction of the instant volume change of MSW under self weight is as important as the long-term behaviour if the step by step construction of landfills is modelled to assess the strain in the lining components. When the long-term integrity of the lining system needs to be evaluated, long-term MSW settlement including creep and degradation mechanism should be considered in the analysis. Jones and Dixon (2005) stated the need for a MSW constitutive model that can more closely represent both short-term and degradation controlled long-term behaviour including heterogeneous properties.

3.2.3 Modelling MSW Slope Stability

Failures of temporary waste slopes have been reported in the literature, e.g. Jones and Dixon (2003). To evaluate the waste slope stability, limit equilibrium methods applied in soil slope stability analysis can be adopted, provided that physical properties and shear strength parameters are known for MSW. Strength parameters based on Mohr-Coulomb failure criterion (c and ϕ) are again the most widely applied in this type of analysis. Numerical modelling techniques are also applicable for waste slope stability analysis. Not only can the safety factor of the slope be assessed using the limit equilibrium method, numerical modelling can also predict the stress and deformation of the slope. To predict the failure of a waste slope, a failure criterion is required for waste material, and to predict stresses and deformations, stress-strain behaviour is required for waste material.

3.3 MSW Behaviour to Model

Requirements of an appropriate MSW constitutive model have been identified through numerical modelling experience from the literature, which can be summarised in the following five aspects: instant compression, creep and degradation, in situ horizontal stress, shear strength and non-linear stress-strain behaviour. By comparison with the reported MSW behaviour from the literature in Chapter 2, problems that need to be solved in constitutive modelling of MSW are discussed below.

3.3.1 Instant Compression

Similar instant compressive behaviour to that of soils has been found for waste material through one-dimensional compression tests, provided that only the relationship between compressive strain and effective vertical stress is investigated, as discussed in section 2.2.1. Non-linear behaviour was noticed when the void ratio change was investigated according to the limited test data reviewed in section 2.2.1. Compressible particles are considered to have an effect on observed instant compression behaviour of MSW and need to be modelled.

3.3.2 Creep and Degradation

It has been concluded that most of the long-term settlement prediction methods mix both creep and degradation mechanisms together, to produce just one settlement function for waste material. Separated modelling of creep and degradation contributions to settlement has been suggested in constitutive modelling of MSW. Creep behaviour of MSW could be simulated by soil creep models. Degradation settlement should be considered in the total long-term waste settlement once degradation occurs in the landfill. According to the degradation settlement model proposed by McDougall and Pyrah (2004), not only would a loss of volume occur due to degradation, but also collapse of the waste structure in response to volume loss would cause waste settlement. This settlement model can be included in a MSW constitutive modelling framework to predict long-term settlement due to degradation.

3.3.3 In-Situ Horizontal Stress (K_0)

A significant difference between K_0 values obtained from in-situ measurements (Dixon *et al.*, 2005) and laboratory measurement (Landva *et al.*, 2000) has been noticed in section 2.2.1. Different test methods and waste types should have an effect on the results. Since the in-situ horizontal stress is induced in the one-dimensional compression boundary condition, it is mainly dominated by the MSW compressive behaviour. In addition, it is partly influenced by the fibre reinforcing particles which has been observed by Landva *et al.* (2000). Therefore, development of a constitutive model for MSW which can reproduce its compression behaviour and the influence of reinforcing particles on its deformation behaviour could lead to prediction of accurate K_0 values using the MSW model in numerical modelling.

3.3.4 Shear Strength

It has been confirmed that MSW shear strength is increased by the presence of reinforcing particles. This reinforcing mechanism has been applied in the assessment of other reinforcing

materials, e.g. fibre reinforced soil, with higher shear strength obtained compared to pure soil. Shear strength dependent on reinforcing particles should be included in the MSW constitutive model. Time-dependent shear strength due to degradation also can be predicted by reducing the fibre content. The initial attempt to model the degradation effects might be through setting different parameter values for different stages of degradation, instead of modelling the degradation process.

3.3.5 Stress-Strain Behaviour

Not only the shear strength, but also the non-linear stress-strain behaviour has been found to be influenced by the fibre reinforcing nature of MSW. Stress-strain curves of triaxial tests on MSW samples have shown a different deformation behaviour compared to soil behaviour, as shown in section 2.2.2. It has been suggested that, both reinforcing nature and compressible particles have contribution to the observed behaviour, which should be included in the constitutive modelling.

3.4 Constitutive Modelling of MSW

Developing a constitutive model for MSW that covers the five aspects of its mechanical behaviour discussed in section 3.3 is the main task of this project. Generally, an elasto-plastic soil material model has potential in modelling four aspects of them (but only for soil behaviour), that is, instant compression, in-situ horizontal stress, shear strength and non-linear stress-strain relationship. An additional creep function and degradation model are required to predict the long-term settlement. Therefore, in order to carry out the constitutive modelling of MSW, an elasto-plastic constitutive model for MSW is required. Constitutive modelling of MSW material can be performed by incorporating the influence of compressible and reinforcing particles (which are believed to dominate the MSW mechanical behaviour as reviewed in section 2.2) into an elasto-plastic soil constitutive model. The structure of constitutive modelling of MSW will be explained in detail as follows.

3.4.1 An Elasto-Plastic Soil Constitutive Model

Many soil models, from the simplest linear elastic model to the most complicated MIT-E3 model (Whittle, 1987), are available for constitutive modelling of MSW. However, an appropriate level of soil model suitable for MSW modelling needs to be determined. Firstly, the model should be capable of modelling the basic elasto-plastic behaviour. In addition, since the additional modification needs to consider the influence of compressible and reinforcing particles, the soil model should not be so complicated that too many parameters are required. Based on these

principles, two soil models, i.e. the elastic-perfectly plastic Mohr-Coulomb model and the modified Cam-Clay model have been selected for further MSW modelling in this research.

Mohr-Coulomb failure criterion is familiar to all geotechnical engineers and the elastic-perfectly plastic Mohr-Coulomb model is widely used in stability analysis of geotechnical structures. The advantages of Mohr-Coulomb model are that it is very simple, and has an appropriate friction failure criterion for granular material. The main disadvantage of this model is that it is not capable of modelling the non-linear stress-strain relationship, and only a linear relationship is available until the failure is reached. It has been mentioned that, generally speaking, an elastic-plastic soil material model has potential to model four of the five aspects of MSW behaviour, that is, instant compression, in-situ horizontal stress, shear strength and non-linear stiffness, but only shear strength is included in the Mohr-Coulomb model. The main purpose to adopt the Mohr-Coulomb model is to simply demonstrate the improvement of shear strength that can occur due to the presence of reinforcing particles in the material.

The Modified Cam-Clay model is the simplest modern elastic-hardening plastic soil constitutive model. Conventionally, the compression and shear behaviour of soils are considered separately. The Modified Cam-Clay model is able to integrate both aspects of soil behaviour and as such provide a significant advance in soil modelling over the simpler Mohr-Coulomb model. Therefore, the four aspects of MSW behaviour mentioned above can be possibly covered by selecting the Modified Cam-Clay as the elasto-plastic model for MSW.

3.4.2 A Compression Model

A compression model is required to represent the influence of compressible particles on MSW behaviour. The traditional definition of void ratio needs to be amended in the compression model to consider the presence of compressible particles as discussed in section 2.2.1. In addition, the compression model should be able to separate the compression due to particle rearrangement (i.e. soil-like behaviour) and particle compression. A flow rule is usually assumed for an elasto-plastic soil model, and it is of great importance in soil constitutive modelling because it governs dilatancy effects which in turn have a significant influence on volume changes and on strength. In summary, the flow rule specifies the direction of plastic straining at every stress state. It defines the relationship between incremental plastic volumetric strain and plastic shear strain once the material is yielding. This incremental plastic volumetric strain should not include the compression of compressible particles themselves if they exist. Otherwise, modelling results of both volume change and shear strength would mislead. Therefore, it is necessary to remove the volume change due to compression of particles when the traditional soil constitutive model is adopted. Therefore, the MSW instant compression can be calculated from two parts, i.e. compression of compressible

particles, and compression due to particles rearrangement by elasto-plastic material models. The compression model will be developed to cover three aspects of MSW behaviour, i.e. instant compression, in situ horizontal stress, and non-linear stress-strain behaviour.

3.4.3 A Fibre Reinforcing Model

A fibre reinforcing model is required to represent the influence of reinforcing particles on MSW behaviour. As reviewed in section 2.3.1, different levels of integration strategy were used by researchers to obtained the constitutive models for MSW by combining two models (soil model and fibre model) together. An appropriate level of integration strategy, which should not only have its reasonable physical and mechanical explanations, but also have a reasonable number of input parameters, is required to model the MSW reinforcing behaviour. The reinforcing model will be developed to cover three aspects of MSW behaviour, i.e. shear strength, non-linear stress-strain behaviour, and in situ horizontal stress.

3.4.4 Long-Term Settlement Model

If the long-term settlement of MSW needs to be evaluated, volume change due to both creep and degradation should be included. The coefficient of secondary compression $C_{\alpha\varepsilon}$ from soil mechanics can be applied in the calculation of MSW creep settlement. The degradation model proposed by McDougall and Pyrah (2004) can be used to calculate the degradation settlement, but is not implemented in this current study.

3.4.5 Framework of Constitutive Modelling of MSW

According to the discussion above, the framework for developing a constitutive model for MSW can be described in Figure 3-1. A constitutive model for MSW can be obtained by combining four sub-models together, i.e. an elasto-plastic soil model (Modified Cam-Clay), a compression model (modelling compressible particles), a fibre reinforcing model (modelling reinforcing particles), and a long-term settlement model (modelling creep and degradation). Each sub-model can cover a number of aspects of MSW behaviour as discussed in section 3.3. Generally the Modified Cam-Clay can potentially simulate four aspects of the required behaviour but needs modification considering compressible and reinforcing particles, as shown in Figure 3-1. The compression model considers the influences of compressible particles on MSW behaviour, including instant compression, in-situ horizontal stress and nonlinear stress-strain behaviour. The fibre reinforcing model includes the influences of reinforcing particles on MSW behaviour, which are shear strength, stress-strain behaviour and in-situ horizontal stress. The long-term settlement model

should cover the creep and degradation behaviour, which is beyond the scope of this study but should be considered for future work.

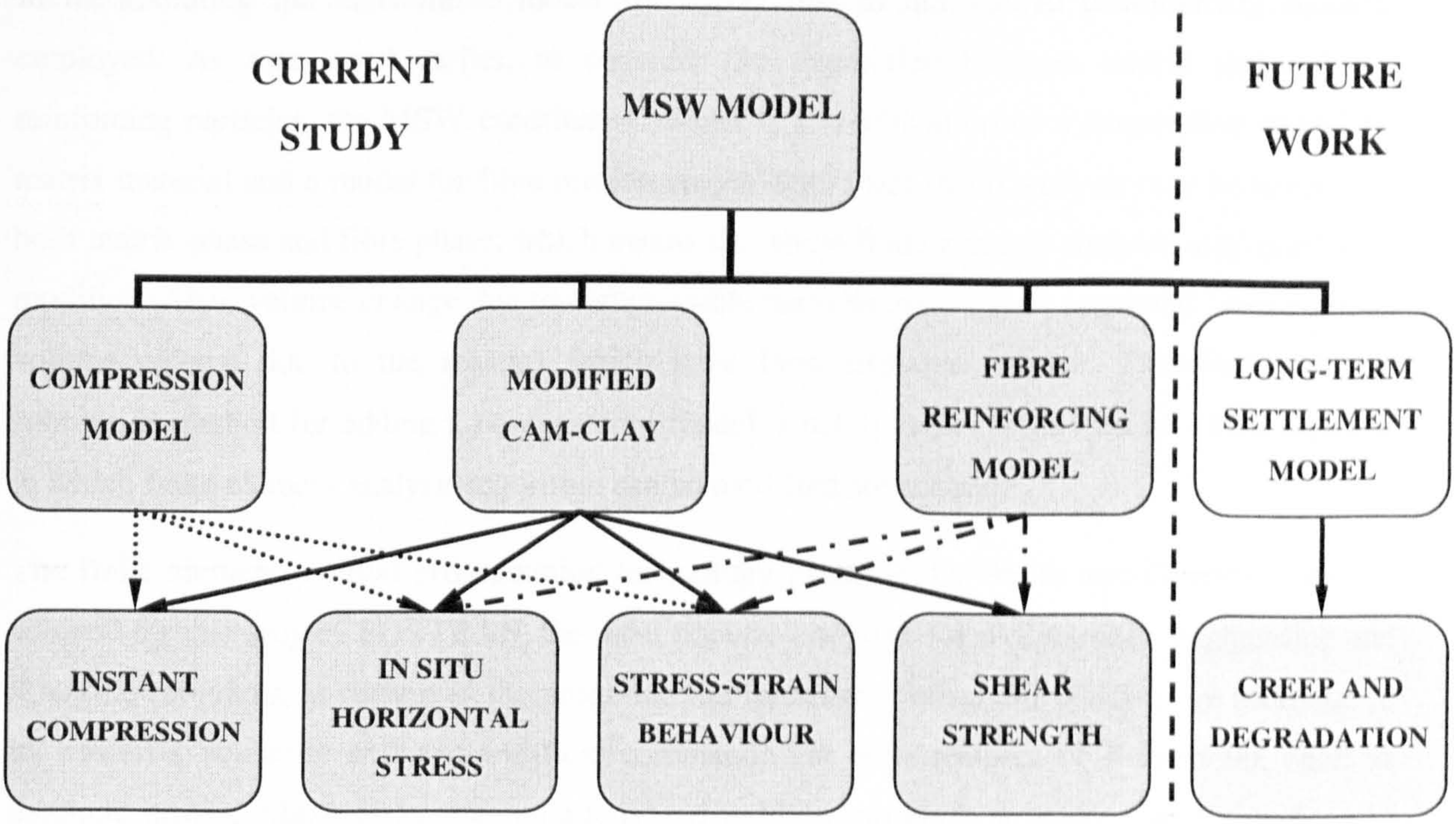

Figure 3-1 Framework of constitutive modelling of MSW

3.5 Model Implementation

An elasto-plastic constitutive model for MSW will be developed by modifying an elasto-plastic soil model as discussed above. Since the main purpose of developing a constitutive model for MSW is to carry out numerical analysis to evaluate stability and integrity of landfill structures related to MSW behaviour, it is necessary to program the proposed model to ensure its availability in numerical analysis. Therefore, the proposed constitutive model needs to be incorporated into a numerical analysis method, e.g. either finite element method (FEM) or finite difference method (FDM).

The finite element method has been selected to incorporate the constitutive model for MSW. This is because the finite element method meets most of the requirements of numerical modelling in landfill engineering, and modelling of the element tests for validation in this study. In addition, finite element method is the most widely used numerical analysis method in engineering, including geotechnical engineering. A great deal of finite element method software or programs have been developed to solve non-linear elasto-plastic problems in geotechnical engineering, and these are available for this project to incorporate a new constitutive model.

Generally, finite element method software allows users to add their own material model through adding an additional subroutine related to the new constitutive model, e.g. Sage-CRISP, PLAXIS

and ABAQUS. The main advantage of this method is that the subroutine does not interfere with the general FEM algorithm so that the user need not consider it. However, there is a disadvantage in incorporating the constitutive model for MSW due to the special development methods employed. As mentioned earlier, to consider the interaction between matrix material and reinforcing particles, the MSW constitutive model is a combination of a constitutive model for matrix material and a model for fibre reinforcement. Stress and strain analysis may be needed for both matrix phase and fibre phase, which means the whole finite element analysis may need to be modified. Also, volume change due to compressible particles needs to be separated from the total volume change due to the reasons which have been explained above. Therefore, the one subroutine method for adding a new material model is not suitable for this study. Other methods in which finite element analysis algorithm can be modified are needed.

The finite element method programming technology proposed by Smith and Griffith (1998) is adopted for this project. FORTRAN, the most popular language for writing large engineering and scientific programs, is chosen as the programming language. Fortran 90 will also be used due to its powerful scientific and mathematical command. The new features of Fortran 90, such as dynamic arrays, whole array manipulations and modular program structure, have significantly improved the efficiency of finite element method programming. Using Fortran 90, a library of subroutines can be created which is held in compiled form and each subroutine can be called at any time. Also, a nested programming structure is adopted, and structure charts rather than flow charts are used to describe the actions, which will be seen in Chapter 7.

Smith and Griffith (1998) has assembled a library of over 100 subroutines, together with some 50 example programs which access the library. The finite element analysis applications range from structural analysis, solid analysis to soil stress-strain analysis, in which material non-linearity has also been considered. Unfortunately, only elastic-perfectly plastic material models have been included, e.g. the elastic-perfectly plastic Von Mises model and the elastic-perfectly plastic Mohr-Coulomb model, rather than elastic-hardening plastic material models. In addition, the tangent stiffness method and the visco-plastic method have been adopted to carry out the non-linear finite element analysis rather than the modified Newton-Raphson method which is the most accurate method (Potts and Zdravkovic, 1999). Thus, firstly, the modified Cam-Clay model needs to be coded into the finite element analysis with the modified Newton-Raphson method for this project. After that, it can then be modified to accommodate the proposed constitutive model for MSW.

To solve a specific boundary value problem (e.g. triaxial compression test) by the FEM using the above described program method, a main program is needed to define the geometry, finite element mesh, material properties, constitutive relations and non-linear elasto-plastic analysis algorithm. Therefore, all the main programs in this study need to be re-coded, while some

subroutines (e.g. shape function, matrix calculation etc.) provided by Smith and Griffith (1998) can be called by the main programs. In order to validate the programs, the finite element analysis results obtained from program will be compared with the analytical solutions for both the Modified Cam-Clay model and the MSW constitutive model, which will be carried out in Chapter 7.

It should be noted that, a disadvantage of applying this method is not having a graphical pre-processor and post-processor system like standard commercial finite element software. Data files are normally used to carry out the task of input and output, which needs additional transformation to display the graphical results. This is acceptable for simple boundary conditions such as element tests which will be modelled in this project, while powerful pre-processor and post-processor are needed for further modelling of landfill structures.

3.6 Model Validation

The compression model will be validated by the one-dimensional MSW compression tests reported by Powrie and Beaven (1999) and Langer (2006), and the fibre reinforcing model will be validated by the triaxial compression tests on fibre reinforced sand reported by Michalowshi and Cermak (2003). The triaxial compression tests reported by Machado *et al.* (2002) will be used to validate the constitutive model for MSW.

CHAPTER

4

A One-Dimensional Compression Model

4.1 Introduction

A waste may be considered to be a skeleton of solid particles (including incompressible granular components, compressible granular components and fibre reinforcing components, according to the classification system proposed by Langer (2006)) enclosing voids which may be filled with gas, with liquid, or with a combination of gas and liquid. Similar to soils (Taylor, 1948), if a waste sample is placed under stress in such a way that its volume is decreased, there are three possible factors to which this decrease might be contributed:

1) A compression of the solid matter;

2) A compression of water and air within the voids;

3) An escape of water and air from the voids.

In soil mechanics, the solid matter and the pore water are assumed to be incompressible, which means the soil volume change is only due to the volume change of voids. This indicates that the compressibility of a soil is not governed to any appreciable degree by the compressibility of the mineral grains of which it is composed. It is rather a function of the extent to which grains can shift positions by rolling and sliding. More specifically, the compressibility of a soil mass depends only on the rigidity of the soil skeleton. The rigidity, in turn, is dependent on the structural arrangement of particles and, in fine-grained soils, on the degree to which adjacent particles are bonded together. (Taylor 1948)

However, for waste material, the situation seems much more complex. Since a large proportion of the solid particles are compressible in a waste, compression due to compressible particles cannot be ignored considering their contribution to the total volume change. Therefore, the compressibility of waste depends not only on the rigidity of the structure, but also on the rigidity of the individual particles. A compression model is required to separate the two contributions of

the waste compression, which is one of the essential components of constitutive modelling of MSW as discussed in section 3.4. A one-dimensional compression model will be proposed and validated by the MSW one-dimensional compression tests from the literature.

4.2 A Case Study

A clear picture of waste volume change behaviour could be observed from one-dimensional compression tests on waste samples. Powrie and Beaven (1999) presented the one-dimensional compression test results on a MSW sample taken from a landfill in detail, summarised as follows:

1) **Sample source and composition**–Sample DM3 was called crude domestic refuse obtained direct from the tipping face of a landfill. The waste composition was analysed though a breakdown by weight into 11 categories, as shown in Table 4-1.

2) **Sample size**–The compression cell is 2 m in diameter and 3 m high, which is large enough for original waste samples considering the particle sizes comprising the waste.

3) **Detailed data**–A series of data under different vertical stresses have been presented in the paper, including dry density, drainable porosity, water content at field capacity and saturated hydraulic conductivity.

Table 4-1 Material classification of sample DM3 (Powrie and Beaven, 1999)

Waste component	Dry density of component (Mg/m^3)	Saturated density of component (Mg/m^3)	% of total mass
Paper/card	0.4*	1.2*	39.9
Plastic film	1.0*	1.0*	4.4
Dense plastics	1.1*	1.1*	6.4
Textiles	0.3*	0.6*	5.5
Misc. combustibles	1.0†	1.2†	11.8
Misc. non-combustibles	1.8*	2.0*	2.4
Glass	2.9*	2.9*	7.0
Putrescibles	1.0*	1.2†	13.3
Ferrous metals	6.0*	6.0*	3.2
Non-ferrous	6.0†	6.0†	1.2
Fines (<10 mm)	1.8†	2.0†	4.9
Total	—	—	100.0

* From Landva and Clark (1990); † Assumed values.

A case study is carried out based upon this one-dimensional compression test to investigate the possibility of separating the different compression mechanisms of waste, that is, inter and intra-void compression. The terms of inter and intra-void were firstly seen in Landva and Clark (1990), in which inter-void was defined as void between waste particles, while intra-void was defined as void within waste particles.

The method of obtaining the void ratio value of waste samples should be investigated in advance to understand the real meaning of void ratio in the test. In the experiment, before every loading step, the waste sample in the cell was flushed by water from the bottom then left to freely drain. The water content at field capacity WC_{vol} (i.e. after free drainage) and drainage porosity n_e can then be measured using the relevant amount of water. The specific volume v can be determined from the expression below:

$$v = \frac{V_S + V_V}{V_S} = \frac{1}{1-(WC_{vol} + n_e)} \qquad \textit{Eq. 4-1}$$

where V_S is the volume of waste particles and V_V is the volume of voids between particles. It was deduced that the void ratio value calculated from this specific volume expression was affected by the volume change of waste particles if some of the particles were compressible. This is the reason why the relationship between void ratio and effective stress (logarithm) from the test shows a highly non-linear trend (Figure 2-2). If the solid particles in the waste sample are assumed to be incompressible, i.e. the change of void ratio is calculated from vertical strain of the sample, the curve changes to an almost linear relationship (calculated data dash line), as shown in Figure 4-1.

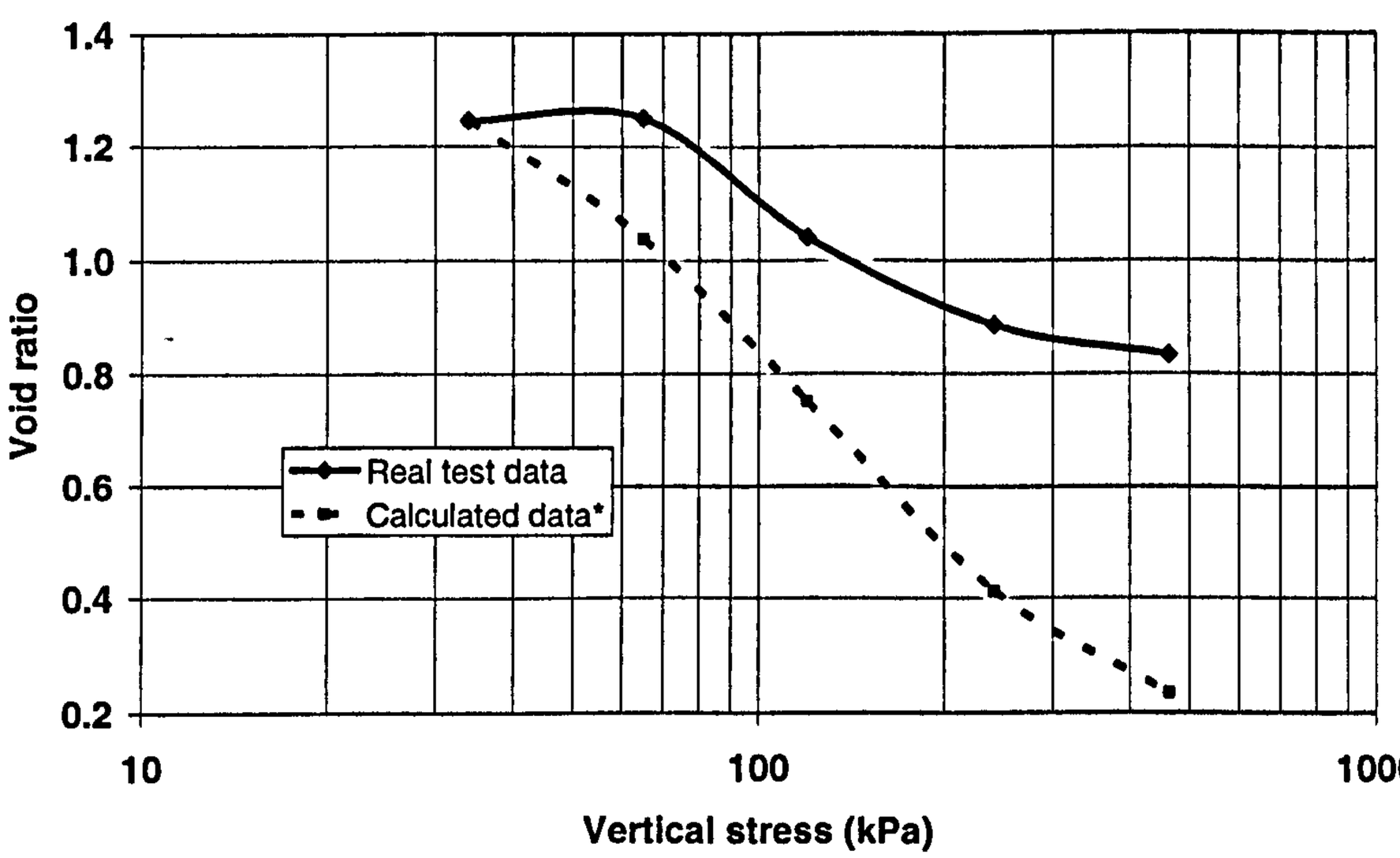

* Calculated from the real test data assuming no particle compression in the MSW sample

Figure 4-1 Amended void ratio vs. logarithm of vertical stress for compression sample DM3 reported by Powrie and Beaven (1999)

The detailed calculation has been shown in Table 4-2. It can be seen that the calculated void ratio value under the first stress level is set as the same as the tested void ratio value (e=1.247), and the

assumed solids volume is kept the same as this level for the following loading steps. Thereafter, the void ratio assuming no compressible particles at each step can be calculated from the assumed voids volume and the constant assumed solids volume. It can be seen through this simple calculation that the concept of void ratio used in soil mechanics may not be appropriate to represent MSW volume change behaviour.

Table 4-2 Calculation of void ratio assuming no intra-voids compression based on the data from Powrie and Beaven (1999)

Vertical stress (kPa)	Cell volume (m3)	Voids volume percentage	Voids volume (m3)	Solid volume (m3)	Tested void ratio	Assumed voids volume (m3)	Assumed solids volumes (m3)	Calculated void ratio
34	6.851	55.5%	3.802	3.049	1.247	3.802	3.049	1.247
65	6.214	55.6%	3.455	2.759	1.252	3.165	3.049	1.038
120	5.344	51.0%	2.725	2.619	1.041	2.295	3.049	0.753
241	4.310	47.0%	2.026	2.284	0.887	1.261	3.049	0.414
463	3.763	45.5%	1.712	2.051	0.835	0.714	3.049	0.234

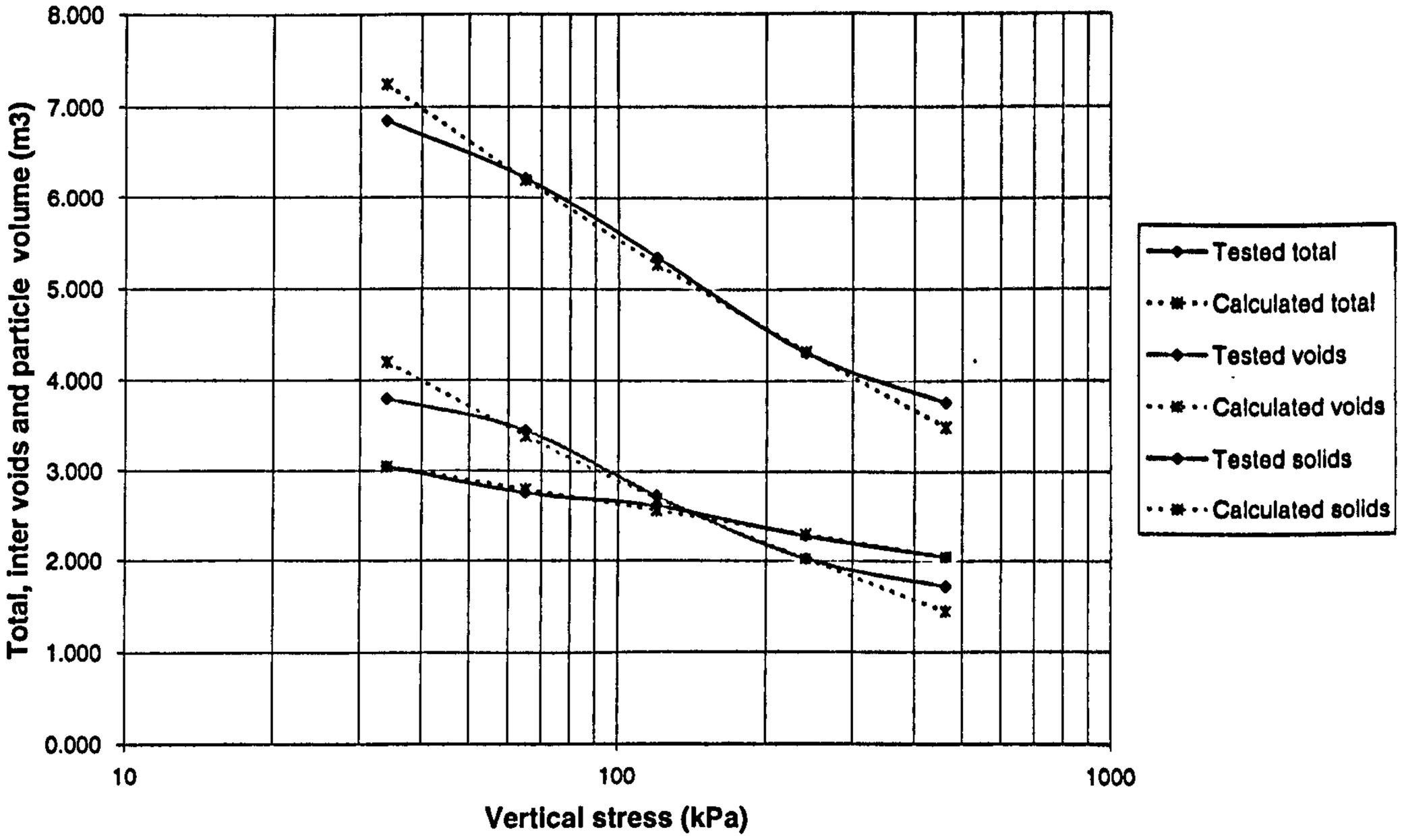

Figure 4-2 Total volume change, inter voids volume change and particle volume change under different stress level (Based on data from Powrie and Beaven, 1999)

Interesting findings can be noticed if the volumetric change due to particle compression (intra-voids compression) is separated from that due to particle re-arrangement (inter voids compression). In Figure 4-2, the volume change of compressible particles (solids volume) and

inter-voids have been separated based upon the test data shown in Table 4-2, plotting together with the total volume change (solid lines). It can be seen from the figure that the volume change trends for both compressible particles and inter voids are mostly linear against the logarithm of stress, which show the same trend as that of the total volume change. It should be noted that under the lower and higher stress level (less than 60 kPa or more than 110 kPa), inter voids volume change and total volume change show more non-linear relationship than the other parts.

In order to model the volumetric behaviour observed in the test, a simple method based on phase relation analysis has been adopted. Figure 4-3 shows the waste phase relationship, which assumes two phases for waste, which are waste particles and inter-voids between particles (water is not considered).

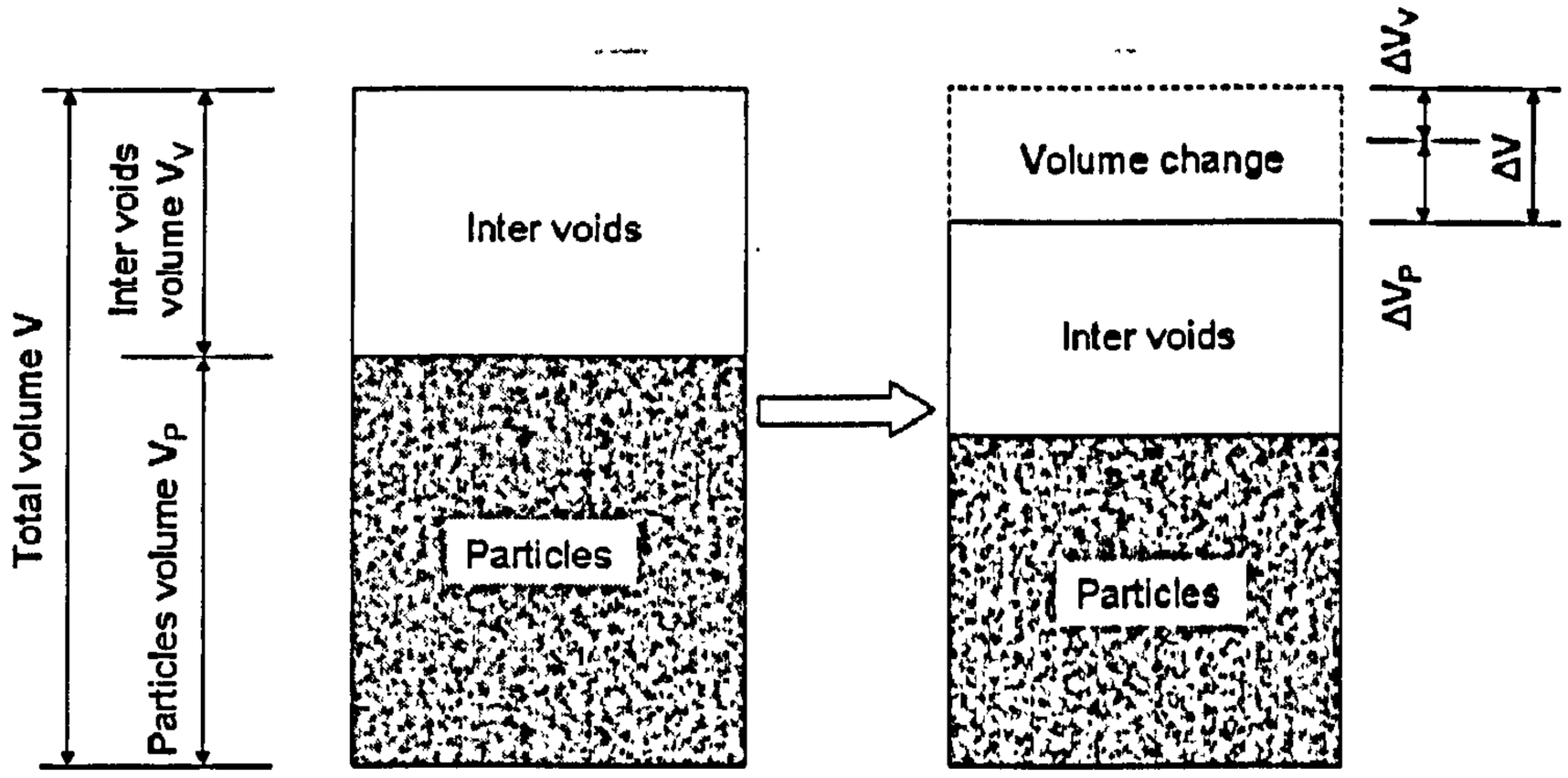

Figure 4-3 Waste phase relation for case study

Particles could be classified as compressible solid particles and incompressible solid particles. As soon as the vertical stress increment is exerted on the waste sample, both of the particle types (in reality only the compressible components) and voids volumes are compressed to a certain amount, which contributes to the total volume change:

$$dV = dV_P + dV_V \qquad \textit{Eq. 4-2}$$

where dV_P is the volume change of waste particles (normally dV_S is used in soil mechanics), and dV_V is the volume change of voids between the particles.

Based on the findings (linear relationship) in the test data of DM3 (Figure 4-2), particle volume change could be expressed as:

$$dV_P = C_P \log \frac{\sigma_{v0} + d\sigma_v}{\sigma_{v0}} \qquad \textit{Eq. 4-3}$$

where C_P is a new parameter which describes the compressibility of waste particles (more accurately, compressibility of the proportion formed of compressible particles) in waste, σ_{v0} is the initial vertical stress before loading and $d\sigma_v$ is the vertical stress increment.

As for the inter voids volume change, the application of void ratio e is kept so that soil models are still applicable and it is easier to compare soil and waste models and parameters with each other. The expression of inter-void ratio e is:

$$e = \frac{V_V}{V_P} \qquad \textit{Eq. 4-4}$$

In soil mechanics, it is simple to obtain total volume change from the void ratio change. For waste material with compressible components, the void volume change is not only determined by the void ratio, it is also affected by the volume change of compressible components themselves, which could be expressed in the following equation:

$$dV_V = d(e \cdot V_P) = V_P \cdot de + e \cdot dV_P \qquad \textit{Eq. 4-5}$$

The change rate of void ratio can be expressed as in soil mechanics:

$$de = C_C \cdot \log \frac{\sigma_{v0} + d\sigma_v}{\sigma_{v0}} \qquad \textit{Eq. 4-6}$$

where C_c is the compression index which describes the compressibility of waste (soil) skeleton. Therefore, the total volume change has the following expression by combining Eq. 4-2, 4-3, 4-5 and 4-6:

$$dV = [C_C \cdot V_P + (1+e) \cdot C_P] \cdot \log \frac{\sigma_{v0} + d\sigma_v}{\sigma_{v0}} \qquad \textit{Eq. 4-7}$$

It could be inferred from the above equations that the particle volume change (Eq. 4-3) and void ratio changes (Eq. 4-6) are assumed to be linear against the logarithm of stress, while inter-voids volume between particles (Eq. 4-5) and total volume (Eq. 4-7) are not linear due to the variation of particle volume. If the particles are not compressible (C_P=0), Eq. 4-7 could be simplified as:

$$dV = C_C \cdot V_P \cdot \log \frac{\sigma_{v0} + d\sigma_v}{\sigma_{v0}} \qquad \textit{Eq. 4-8}$$

which has the same formulation as that in soil mechanics.

In soil mechanics, only one specific volume value at the unit stress level (normally σ_v=1 kPa) is needed to define the initial condition. Applying this idea into waste material, two other parameters

might be needed to define the initial condition, which are initial total volume and initial particles volume.

This simple method is assessed by modelling the one-dimensional compression test results of sample DM3 presented by Powrie and Beaven (1999). The initial particle volume (under the first level vertical stress 34 kPa) could be obtained directly from the test results. However, the initial total volume cannot be determined from the test directly because the waste sample might have experienced a higher stress history than the first stress level. Back analysis is needed to determine the correct value.

The values of parameter C_C and C_P could be determined from the slopes of respective curves. Figure 4-1 shows the relationship between void ratio and average vertical stress. Compression index C_C can be obtained from the slope of this curve. The first point of this curve should be excluded for obtaining the compression index because its value is even less than that of the second point. The value of C_C can be worked out as 0.641 by linear regression from the last four data points. Parameter C_P is 0.880 calculated from the respective curve in Figure 4-2.

The modelling results have been plotted in Figure 4-2 using dashed lines. It is not surprising that the calculated particle volumes are almost the same as those from the test because the parameter C_P was directly obtained from the test curve. The other two curves for modelling results show a good fit to the test results except the initial recompression part of the curves. It is demonstrated that the simple method is capable of modelling waste volumetric behaviour in the case study.

4.3 A Compression Model

An obvious drawback of the simple method proposed in the case study is that the waste initial condition is not as well defined as it is for soil. In the above case study, the waste conditions were known under a certain vertical stress level. However, a general initial condition (e.g. the specific volume under unit stress for soils) is required for the waste compression model. In soil mechanics, particle volume is constant so that it can be set as unity in the phase relationship analysis. Therefore, the specific volume can be expressed as:

$$v = 1 + e \qquad \textit{Eq. 4-9}$$

For waste material, it may be feasible to fix the incompressible particles volume as constant in the analysis. However, as compressible particles can be converted into incompressible particles under a threshold stress, it is more reasonable to define the total potential incompressible volume (including the final volume of compressible particles and volume of incompressible particles at the maximum stress) as constant. This volume could be simply considered as the material volume

and calculated through material density of the particles. However, it is more reasonable to link this volume value with the maximum stress the waste will experience.

An additional parameter, intra-void ratio, is used to describe the ratio of voids volume within waste particles to the total potential incompressible volume:

$$f = \frac{V_{V-Intra}}{V_I} \qquad \textit{Eq. 4-10}$$

where V_I is the total potential incompressible volume and $V_{V\text{-}Intra}$ is the volume of intra-voids.

Inter-void ratio (ratio of voids volume between waste particles to the total potential incompressible volume) is similar to the normal soil void ratio:

$$e = \frac{V_{V-Inter}}{V_I} \qquad \textit{Eq. 4-11}$$

where $V_{V\text{-}Inter}$ is the volume of inter-void. e and f are defined as ***inter-void ratio*** and ***intra-void ratio***, respectively. An innovative phase relation for waste is proposed according to the above equations, as shown in Figure 4-4. Thereafter, the waste specific volume could be defined as:

$$v = 1 + e + f \qquad \textit{Eq. 4-12}$$

The volume change could be obtained by differentiating the equation:

$$dv = de + df \qquad \textit{Eq. 4-13}$$

which means the waste volume change comes from both inter-void ratio change and intra-void ratio change. The inter void ratio change has the same expression as Eq. 4-6, except the compression index needs to be modified to inter-compression index $C_{C\text{-}Inter}$. The intra-void ratio change df is defined in the same way as below:

$$df = C_{C-Intra} \log \frac{\sigma_{v0} + d\sigma_v}{\sigma_{v0}} \qquad \textit{Eq. 4-14}$$

in which $C_{C\text{-}Intra}$ is the intra compression index for waste. Therefore, the total volume change under pressure has the expression:

$$dv = (C_{C-Inter} + C_{C-Intra}) \log \frac{\sigma_{v0} + d\sigma_v}{\sigma_{vo}} \qquad \textit{Eq. 4-15}$$

For the unloading and swelling curves, the volume change under reloading is expressed as:

$$dv = (C_{S-Inter} + C_{S-Intra}) \log \frac{\sigma_{v0} + d\sigma_v}{\sigma_{vo}} \qquad \text{Eq. 4-16}$$

in which $C_{C\text{-}Inter}$ and $C_{S\text{-}Intra}$ are the inter and intra swelling index for waste, respectively.

These expressions have simpler formulas than the method proposed in the case study, but more significantly has a clearer physical meaning, which is more appropriate for waste compression with compressible components. Moreover, both inter and intra void ratio changes are assumed to be linear with logarithm stress level so that the total volume change trend is also linear.

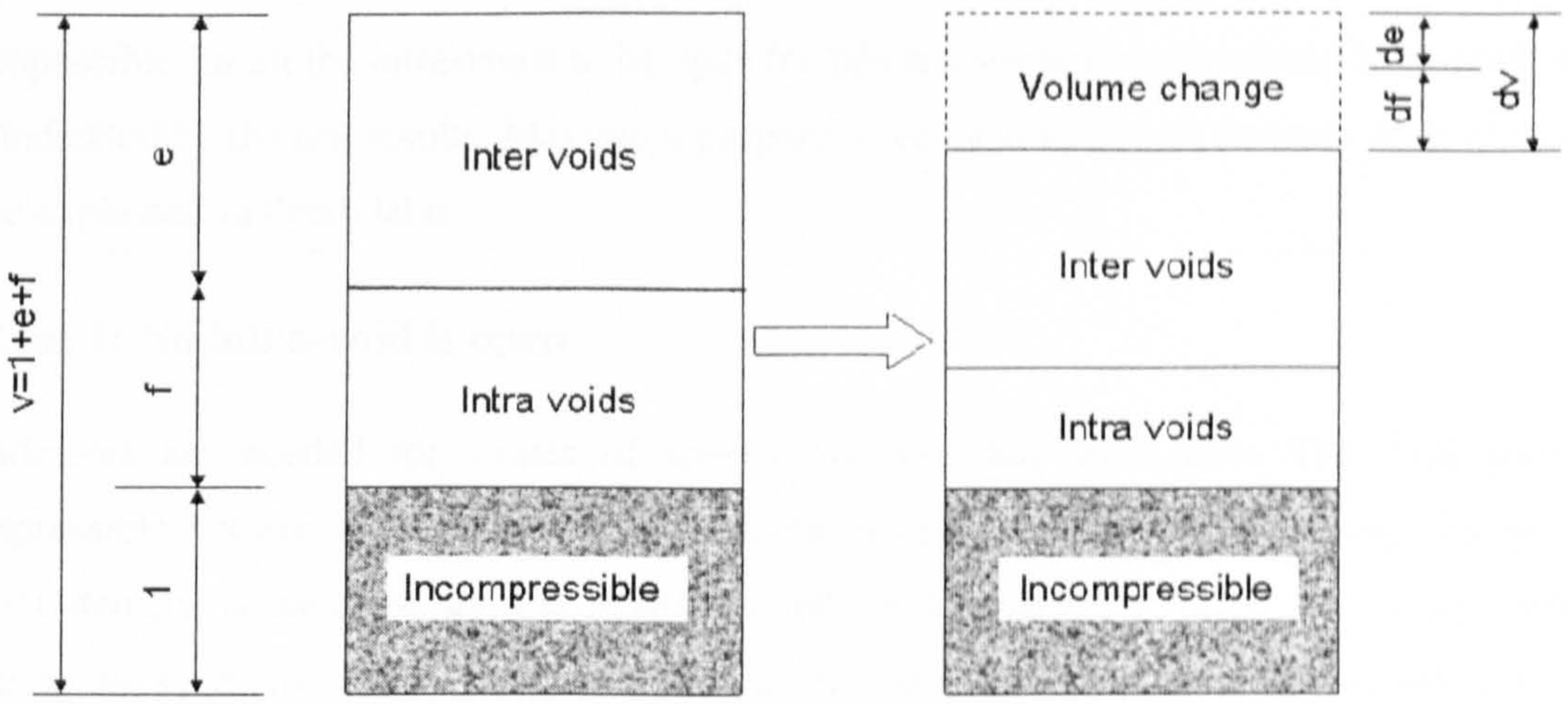

Figure 4-4 Waste phase relation for the compression model

4.4 Model Validation

Due to very limited test data on compression contribution of compressible particles in MSW, Powrie and Beaven's compression data is again used to validate the compression model. In addition, compression test results on synthetic waste from Langer (2006) are also simulated by the compression model.

4.4.1 Compression Data Reported by Powrie and Beaven (1999)

The compression model is validated using the one-dimensional compression test reported by Powrie and Beaven (1999), which has been used in the case study in section 4.2. The void ratios obtained in the experiment include the inter-void ratio, and perhaps part of the intra-void ratio, depending on the waste composition, as discussed in section 4.2. If all the intra particle voids are closed, the calculated void ratio is only the inter-void ratio; if all the intra-particle voids are open, the calculated void ratio includes both parts; if part of the intra particle voids are open, the calculated void ratio includes the inter-void ratio and part of the intra-void ratio. It is hard to distinguish what is the proportion of intra-void ratio from this limited test information. Three

cases according to different proportions of open intra voids discussed above, including two ultimate status and one intermediate status, are considered as follows:

1) Case 1: No intra-void is open, which means the calculated void ratio is the inter-void ratio;

2) Case 2: 30% intra-voids are open, the calculated void ratio is consisted of partly inter and partly intra void ratio, which is the middle case;

3) Case 3: Assuming all voids are intra-voids, without inter voids (not realistic but can be modelled), which means 73.4% intra-voids are open.

It is impossible for all the intra-voids to be open for this test because some closed intra-voids have been indicated by the test results. Maximum proportion of intra-voids can be open is 73.4% which will be explained in detail later.

➢ Case 1: No intra-void is open

Amendments are needed for values of specific volume and void ratio. The total potential incompressible volume needs to be assumed if the compression model is applied. The average material density is assumed as 1.6 Mg/m3 which is a reasonable value for waste material according to synthetic waste study carried out by Langer (2006). In addition, since it only indicates the total voids volume, it is not a sensitive variable influencing the results. The amended values of void ratio assuming no intra-void is open according to different stress levels have been calculated in Table 4-3.

Table 4-3 Amended void ratio values from test for Case 1 (after Powrie and Beaven 1999)

Vertical stress (kPa)	Dry density (Mg/m^3)	Specific volume v	Percentage of voids volume (%)	Inter void ratio e	Intra void ratio f	Calculated conventional void ratio	Conventional void ratio from test
1	0.33	4.848					
34	0.39	4.103	55.5%	2.277	0.826	1.247	1.247
65	0.43	3.721	55.6%	2.069	0.652	1.252	1.252
120	0.5	3.200	51.0%	1.632	0.568	1.041	1.041
241	0.62	2.581	47.0%	1.213	0.368	0.887	0.887
463	0.71	2.254	45.5%	1.025	0.228	0.835	0.835

It is rather simple to calculate the void ratio for this case. The percentage voids volume obtained directly from the test are considered only as the percentage of the inter voids. After determining the inter-void ratio, the intra-void ratio can be easily calculated from Eq. 4-12. Calculated conventional void ratios are the same as those values directly taken from the test, which confirms

the calculation method. Specific volume, inter void ratio and intra void ratio for this case have been plotted together in Figure 4-5 (continuous line) under different vertical stress levels, in which the nearly linear relationship can be recognised.

The compression model has been applied to calculate the void ratio, void and particle volumes, and vertical strain. Four parameters are needed in this case, that is, specific volume under unit stress v_1=7, inter void ratio under unit stress e_1=4.2 (which means intra void ratio under unit stress $f_1=v_1-e_1-1$=1.8), inter compression index C_C=1.2 and intra compression index A=0.6. The values of these parameters have been listed in Table 4-4, together with the values for the other two cases. These values of parameters are the best-fit values, which are estimated from the test curves shown in Figure 4-5.

Table 4-4 Model parameters for three cases

Parameters	v_1	e_1	f_1	$C_{C\text{-}Inter}$	$C_{C\text{-}Intra}$
Case 1	7	4.2	1.8	1.2	0.6
Case 2	7	3.3	2.7	0.9	0.9
Case 3	7	0	6	0	1.8

The specific volume, inter void ratio and intra void ratio predicted by the compression model have been plotted in Figure 4-5, together with the calculated values from the test (Table 4-5). It can be seen from the figure that, the compression model can predict the trend of all the three values. In addition, comparisons between test and model prediction have also been conducted for particle and void volume, and vertical strain under different stress level, which can be seen in Figure 4-6 and Figure 4-7. They have shown the model has the capability to reproduce test results.

Table 4-5 Void ratios, volumes and strain predicted by the compression model for Case 1

Vertical stress (kPa)	*v* from model	*e* from model	*f* from model	Total volume (m3)	Inter voids volume (m3)	Intra voids volume (m3)	Solids volume (m3)	Vertical strain
1	7.000	4.200	1.800					
34	4.243	2.362	0.881	6.851	3.814	1.423	3.037	0.154
65	3.737	2.025	0.712	6.033	3.269	1.150	2.764	0.255
120	3.257	1.705	0.552	5.259	2.753	0.892	2.507	0.350
241	2.712	1.342	0.371	4.379	2.166	0.599	2.213	0.459
463	2.202	1.001	0.201	3.555	1.617	0.324	1.938	0.561

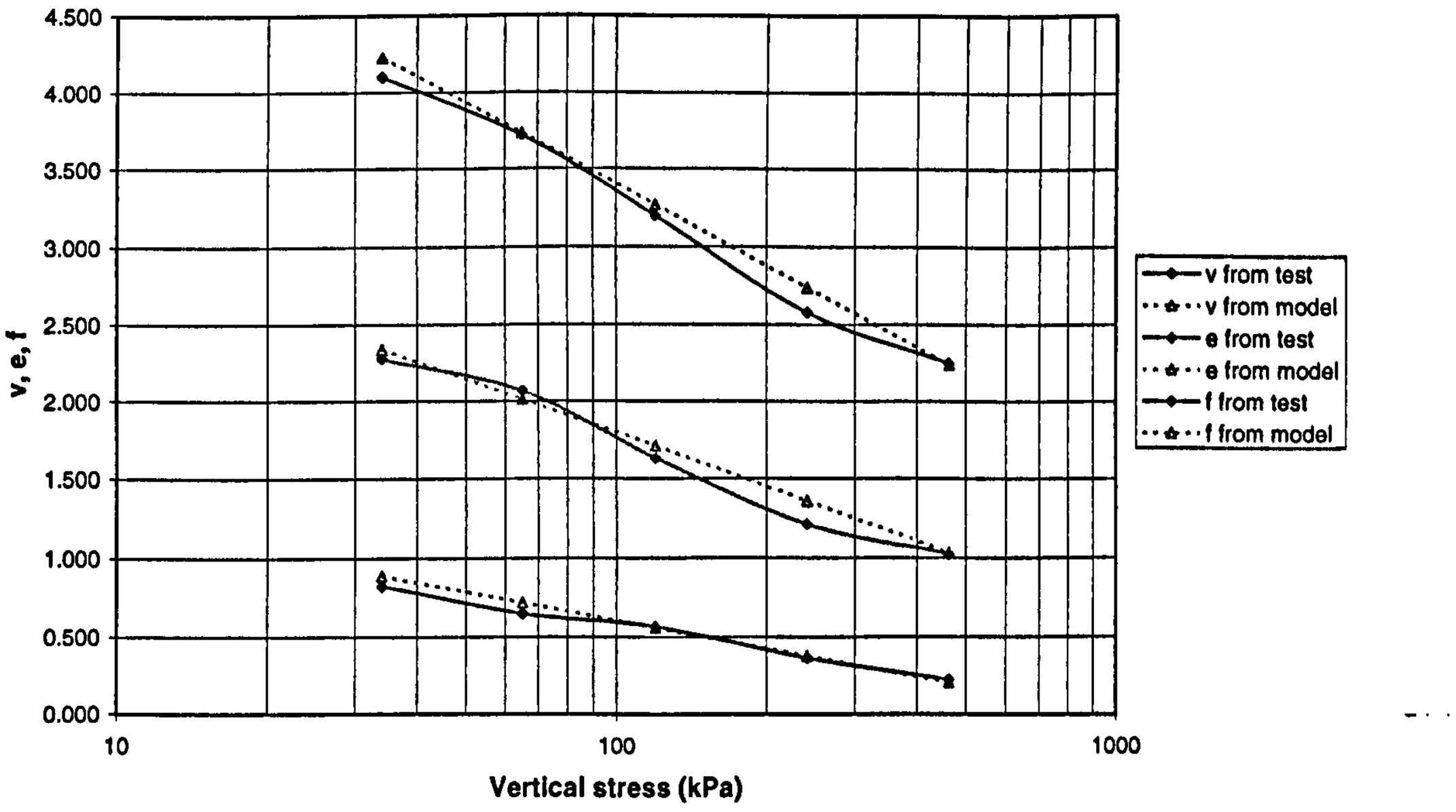

Figure 4-5 Specific volume, inter void ratio, intra void ratio at different stress levels obtained from the test and predicted by the compression model for Case 1

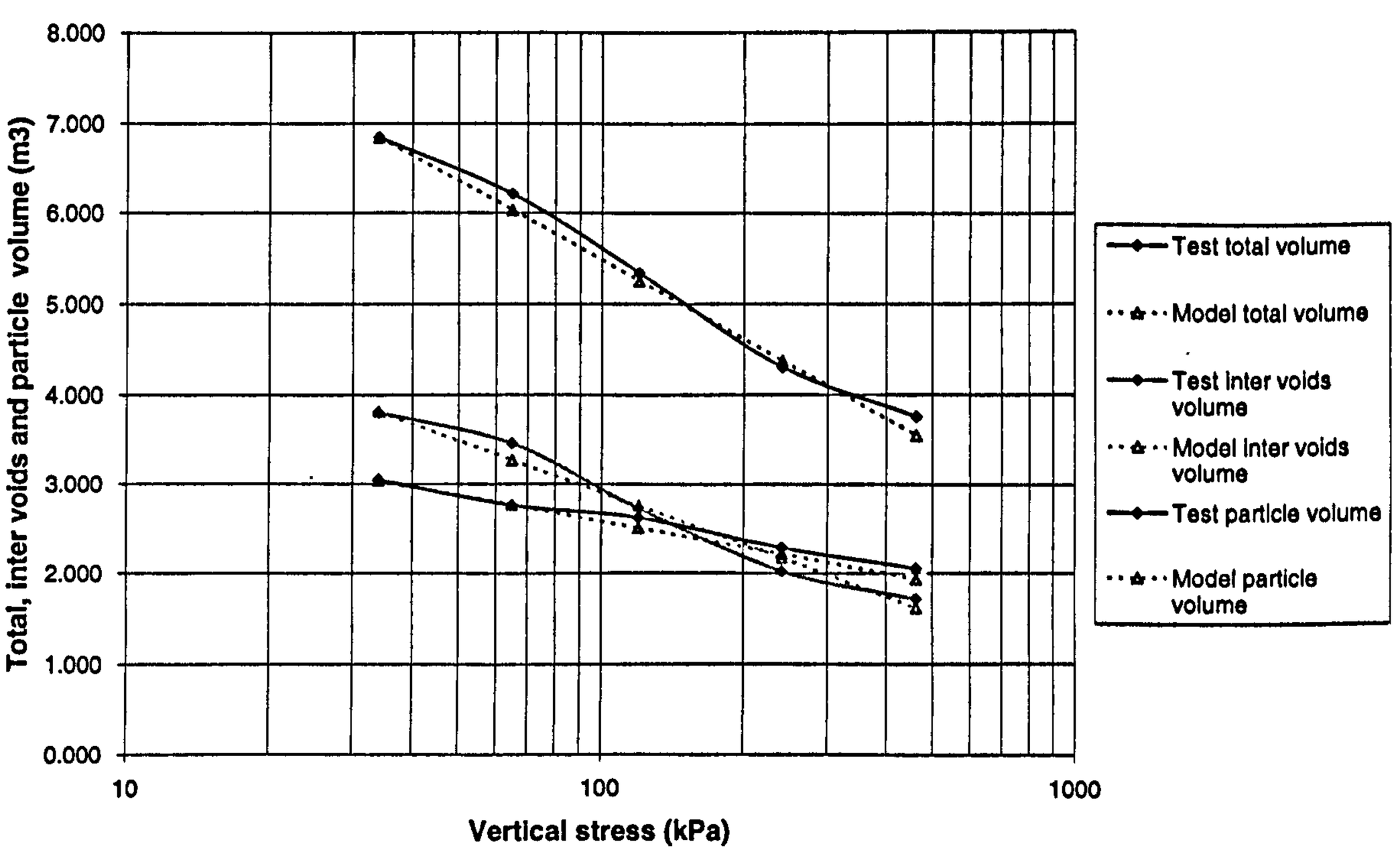

Figure 4-6 Total volume, inter voids volume and particles volume at different stress levels obtained from test and predicted by the compression model for Case 1

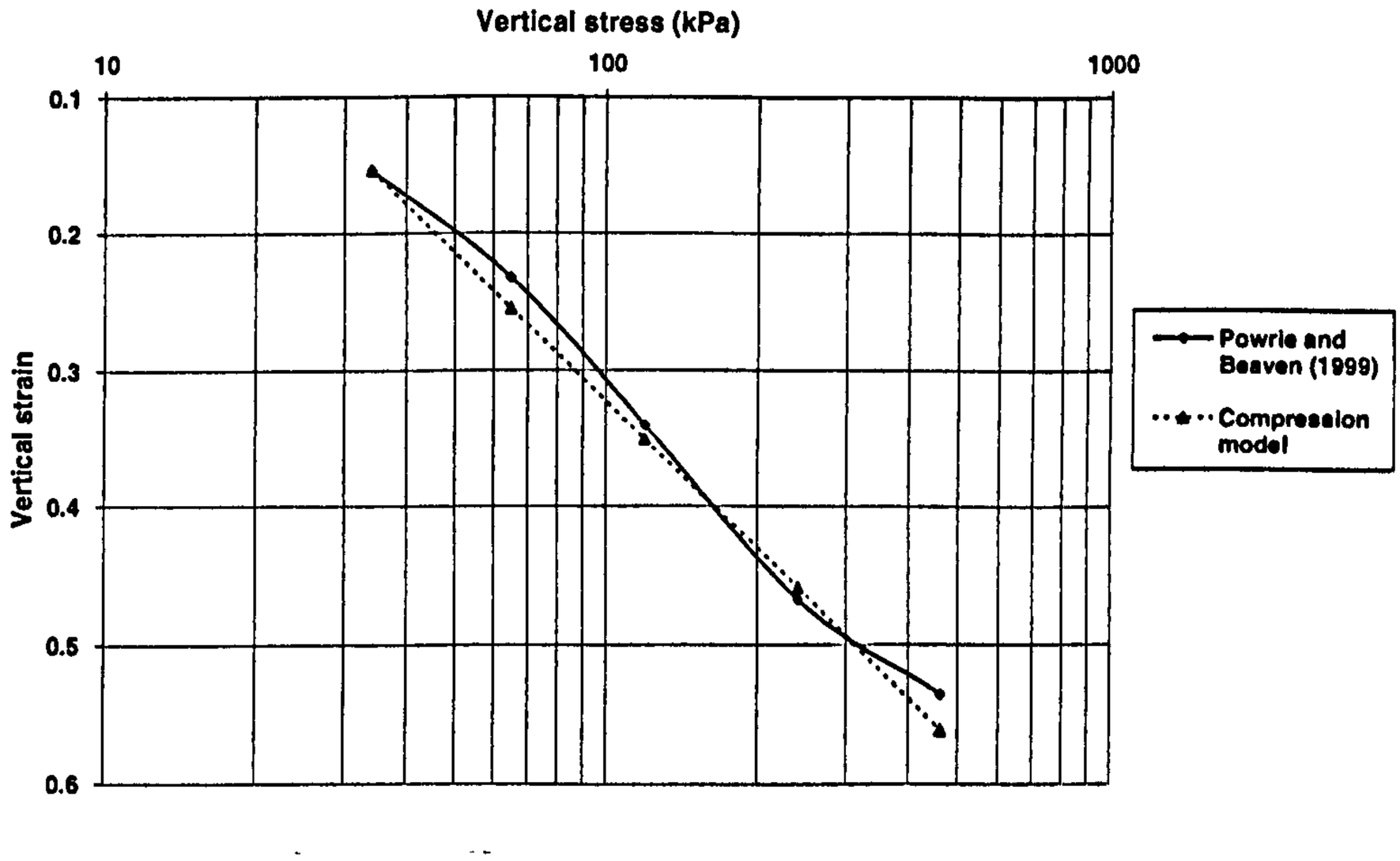

Figure 4-7 Vertical strain at different stress levels obtained from test and predicted by the compression model for Case 1

➢ Case 2: 30% intra-voids are open

The amended values of void ratio assuming 30% intra-voids are open according to different stress levels have been calculated and presented in Table 4-6, and have also been plotted in Figure 4-8 (solid lines). The compression model is then applied to this case, which is shown in Table 4-7. Values of parameters needed have already been given in Table 4-4. For this case, the closed intra-void ratio can be determined firstly, as it has to be the same as the intra-void ratio in Case 1. Since it is assumed that 30% of the intra-voids are open, the proportion of the closed part is 70%. Therefore, the total and open intra-void ratios can be calculated. Finally the inter-void ratio can also be obtained simply.

Table 4-6 Amended void ratio values from test for Case 2 (after Powrie and Beaven 1999)

Vertical stress (kPa)	Dry density (Mg/m3)	Specific volume *v*	Percentage of inter-voids plus open intra-voids (%)	Open intra void ratio	Closed intra void ratio	Intra void ratio *f*	Inter void ratio *e*
1	0.33	4.848					
34	0.39	4.103	55.5%	0.354	0.826	1.180	1.923
65	0.43	3.721	55.6%	0.279	0.652	0.931	1.790
120	0.5	3.200	51.0%	0.243	0.568	0.811	1.389
241	0.62	2.581	47.0%	0.158	0.368	0.526	1.055
463	0.71	2.254	45.5%	0.098	0.228	0.326	0.928

Table 4-7 Void ratios, volumes and strain predicted by the compression model for Case 2

Vertical stress (kPa)	*v* from model	*e* from model	*f* from model	Total volume	Inter voids volume	Intra voids volume	Solids volume	Vertical strain
1	7.000	3.300	2.700	8.097				
34	4.243	1.922	1.322	6.851	3.103	2.134	3.748	0.154
65	3.737	1.668	1.068	6.033	2.694	1.725	3.339	0.255
120	3.257	1.429	0.829	5.259	2.307	1.338	2.953	0.350
241	2.712	1.156	0.556	4.379	1.867	0.898	2.513	0.459
463	2.202	0.901	0.301	3.555	1.455	0.486	2.100	0.561

Figure 4-8 combines the modelling results with test results for Case 2. The compression model can predict the trend of all the three value changes. Comparisons between test and model prediction for particle and void volume, and vertical strain under different stress level would be almost the same as that of Case 1, which are not repeated here.

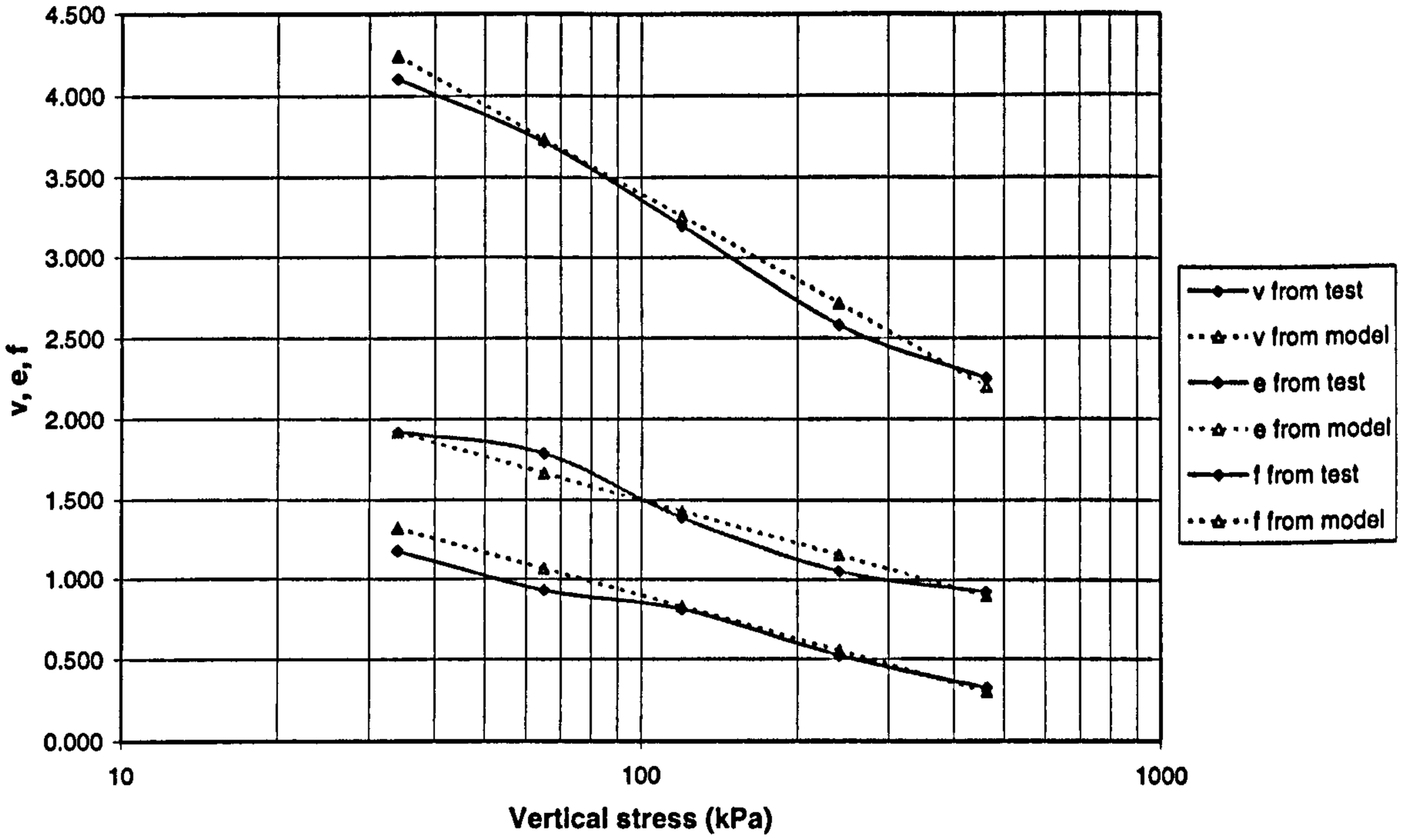

Figure 4-8 Specific volume, inter void ratio, intra void ratio at different stress levels obtained from the test and predicted by the compression model for Case 2

➢ Case 3: All voids are intra-voids

It has been mentioned that this case is impossible in reality because the inter-void ratio for particular material cannot be zero. It is included in the calibration for the purpose to demonstrate

the compression model. According to the assumption, all the calculated void ratio from the test should be intra-void ratio, and the closed intra-void ratio remains the same. The proportion of the open intra-voids can be calculated as 73.4%. Accordingly, the total intra void ratio can be obtained, as shown in Table 4-8. The compression model is then applied to this case, which is shown in Table 4-9. Values of parameters needed have already been given in Table 4-4.

Table 4-8 Amended void ratio values from test for Case 3 (after Powrie and Beaven 1999)

Vertical stress (kPa)	Dry density (Mg/m3)	Specific volume v	Percentage of inter-voids plus open intra-voids (%)	Open intra void ratio	Closed intra void ratio	Intra void ratio f	Inter void ratio e
1	0.33	4.848					
34	0.39	4.103	55.5%	2.277	0.826	3.103	0
65	0.43	3.721	55.6%	2.069	0.652	2.721	0
120	0.5	3.200	51.0%	1.632	0.568	2.200	0
241	0.62	2.581	47.0%	1.213	0.368	1.581	0
463	0.71	2.254	45.5%	1.025	0.228	1.254	0

Table 4-9 Void ratios, volumes and strain predicted by the compression model for Case 3

Vertical stress (kPa)	v from model	e from model	f from model	Total volume	Inter voids volume	Intra voids volume	Solids volume	Vertical strain
1	7.000	0	6.000	8.097				
34	4.243	0	3.243	6.851	0	5.236	6.851	0.154
65	3.737	0	2.737	6.033	0	4.419	6.033	0.255
120	3.257	0	2.257	5.259	0	3.645	5.259	0.350
241	2.712	0	1.712	4.379	0	2.765	4.379	0.459
463	2.202	0	1.202	3.555	0	1.941	3.555	0.561

Figure 4-9 combines the modelling results with test results for Case 3. Again the compression model can predict the trend of all the three values change. Comparisons between test and model prediction for particle and void volume, and vertical strain under different stress level would be almost the same as that of Case 1 and 2, which need not repeat here.

By applying the waste compression model to Powrie and Beaven's compression data, it can be seen that the model results match the test results very well for all the three cases assuming different proportion of intra-voids are open. Although Case 3 is not the realistic situation, the model can reproduce the results just like the other two cases. It implies that the model is able to predict the total volume loss for any proportion of inter and intra voids. Unfortunately, little

information is available for the proportion of inter or intra voids in a MSW sample. An additional parameter is required to represent the ratio between inter and intra voids volume. Sensitivity analysis needs to carry out for this additional parameter in further study of connecting the volumetric behaviour with shear behaviour of MSW.

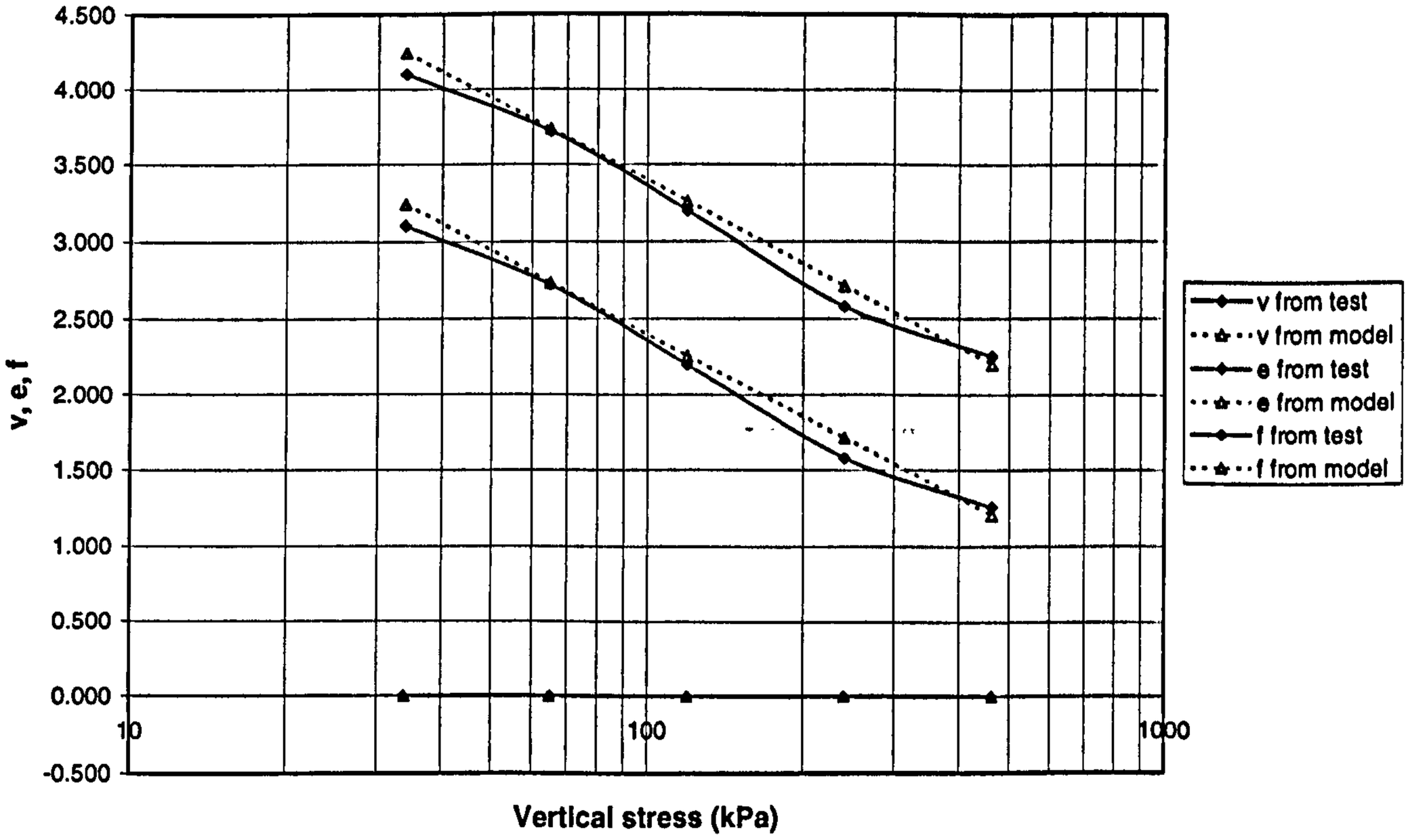

Figure 4-9 Specific volume, inter void ratio, intra void ratio at different stress levels obtained from the test and predicted by the compression model for Case 3

4.4.2 Synthetic Waste Compression Behaviour

Langer (2006) conducted one-dimensional compression tests on synthetic waste. Due to the expected characteristic of the compositions and their components, as shown in Table 4-10, the results of the compression tests have been split into four different sub-categories, that is, incompressible composition, compressible composition, mono-component composition, and a simulation of a real waste composition (Langer, 2006).

Samples SW01 and SW07 have a greater proportion (more than 90% by mass) of Leighton-Buzzard sand and a small proportion of compressible particles, such as paper, plastic bags, aluminium cans and plastic packaging. These two samples have been classified as an incompressible composition.

SW02_1, SW02_2 are two repeatability samples and SW02_3 was the sample which came from SW02_1 and SW02_2 after compression and having approximate double the unit weight. This composition was expected to be very compressible as a large amount of compressible and

lightweight particles (aluminium cans, paper, textiles and plastic packaging) were involved. SW03 seems to be an incompressible composition with approximate 60% incompressible, heavy components (tyre-chunks and brick) according to its mass ratio in Table 4-10. However, the compressible particles still dominated its compressive behaviour because they represented the largest volume in this composition. Therefore, these four samples were classified as compressible composition in Langer (2006).

SW04 was dominated by a single component, aluminium cans, not only in terms of its mass ratio, but also in volumetric terms. This sample was defined as mono-component composition in Langer (2006). It can be noticed that SW03 and SW04 have the similar proportion of incompressible particles (i.e. tyre chunks and brick), with SW03 containing three different compressible particles while SW04 mainly having only the aluminium cans. Therefore, these two samples are considered as one group in this study and their results will be compared together.

SW09 aimed to simulate real MSW including all the kinds of components listed in Table 4-10, which was based on the findings from a real UK waste sample sorting analysis conducted by Langer (2006).

Table 4-10 Composition of synthetic waste by mass ratio for compressive samples (Langer 2006)

Composition	Incompressible		Compressible				Mono	Real
Samples	SW01	SW07	SW02_1	SW02_2	SW02_3	SW03	SW04	SW09
Aluminium cans		2.6%	22.7%	22.7%	23.3%	15.1%	50.0%	5.2%
Paper	1.1%		32.3%	32.3%	30.4%	15.0%		21.4%
Textiles			16.0%	16.0%	16.5%	10.0%		2.4%
Flexible plastic bags	0.1%		8.7%	8.7%	9.0%			16.9%
Rigid plastic packaging		2.6%	11.5%	11.5%	11.8%		5.0%	3.3%
Rigid plastic bottles			8.7%	8.7%	9.0%			3.2%
Tyre chunks						30.1%	25.0%	1.2%
Brick						29.8%	20.0%	1.9%
Leighton-Buzzard Sand	98.8%	94.9%						7.6%
Clay								37.0%
Sum	100%	100%	100%	100%	100%	100%	100%	100%
Estimated material density (Mg/m3)	1.637	1.63	1.27	1.265	1.275	2.02	2.45	1.34

The relationship between sample volumes and effective vertical stress can be obtained directly from the test data. In order to compare with the compression model results, it is necessary to have

the relationship between specific volumes (or void ratios) and effective vertical stress. Material density of the combined solid components are therefore required to calculate the specific volumes. It is not difficult to calculate the material density for each sample by considering the contribution of each component according to its known mass ratio. It should be noted that the material density for each component is estimated from the material properties, in which intra-void ratio has been excluded. All these values have been given in Table 4-11. Since the mass of each component in the sample is known, all particle volumes (excluding intra voids) can be calculated from the mass and material density values. The total potential incompressible volume defined in the compression model can be calculated by adding all particle volumes together:

$$V_I = \sum V_I^i = \sum \frac{m^i}{\rho_m^i} \qquad \textit{Eq. 4-17}$$

where m^i and ρ^i_m are the mass and material density of the i^{th} component, respectively.

The material density for the whole sample can be obtained from the total mass divided by the total potential incompressible volume:

$$\rho_m = \frac{\sum m^i}{V_I} \qquad \textit{Eq. 4-18}$$

The values of material density of each sample are shown in Table 4-10. Once the material density for the whole sample is obtained, the specific volume can be calculated using:

$$v = \frac{\rho_d}{\rho_m} \qquad \textit{Eq. 4-19}$$

in which ρ_d is the dry density of the whole waste sample.

Table 4-11 Estimated density of material comprising each component (Mg/m^3)

Aluminium cans	Paper	Textiles	Flexible plastic bags	Rigid plastic packaging
2.72	1.00	1.54	0.96	0.94
Rigid plastic bottles	Tyre chunks	Brick	Leighton-Buzzard Sand	Clay
1.32	2.65	2.19	1.65	1.9

In the following sections, the compression test results for each sample will be presented and modelled according to different compositions proposed by Langer (2006). Results of SW03 will be compared with the mono-component composition SW04 as mentioned earlier.

➢ Incompressible Composition SW01 and SW07

SW01 and SW07 are composed of a significant proportion of sand (98.8% and 94.9% respectively), with 1.1% paper and 0.1% plastic bags for SW01, 2.6% aluminium cans and 2.6% plastic packaging for SW07. Figure 4-10 shows the relationships between sample volumes and vertical stresses for both the samples, with unload/reload loops.

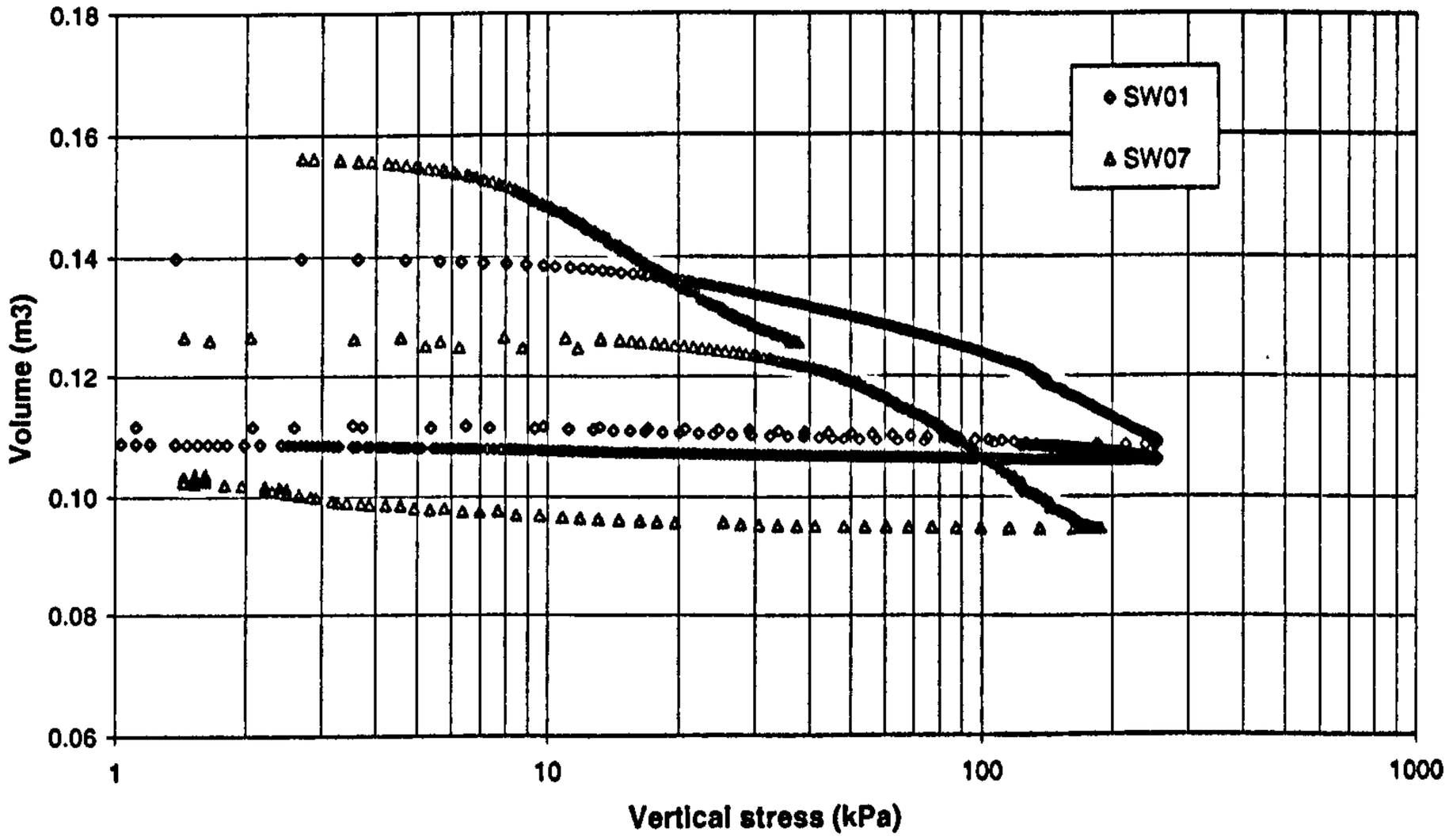

Figure 4-10 Waste volume vs. vertical stress for samples SW01 and SW07

Relationships between specific volumes and vertical stresses have been calculated and plotted in Figure 4-11, in which the following behaviour can be noticed:

1) SW07 (C_C=0.61) has a steeper slope compression line than SW01 (C_C=0.4), which means it has a higher value of compression index. Due to both the samples having a high proportion of incompressible components, the observed behaviour should be dominated by the compressible particles in the samples. Aluminium cans and plastic packaging have high intra-void ratios, and the voids are hardly open to sand (with small entrance), which means the sand cannot easily move into these intra voids during compression. However, although screwed paper and plastic bags can have high intra-void ratio, most of these voids are open, which means they can be filled with the sand in this case. Therefore, more intra voids volume change (compression of compressible particles) in SW07 than in SW01 occurs, which can explain the experimental results.

2) Slopes of the unload/reload lines for the two samples are more or less the same, which are very small. The swelling index value C_S are 0.022 and 0.027 for SW01 and SW07, respectively. Considering again the sample compositions, this behaviour should be dominated

by the incompressible components (sand in this case) in this type of composition. It can be deduced that most of the swelling results from the inter-voids volume change (compression of the waste skeleton), which means most of the intra-voids volume change (compression of compressible particles) are plastic, fitting observed compressed particles at the end of the test.

It can be summarised that the big difference in compression indices for the two samples comes from the compressible particles, while the similarity of swelling index results from the incompressible particles and plastic deformation of the compressible particles.

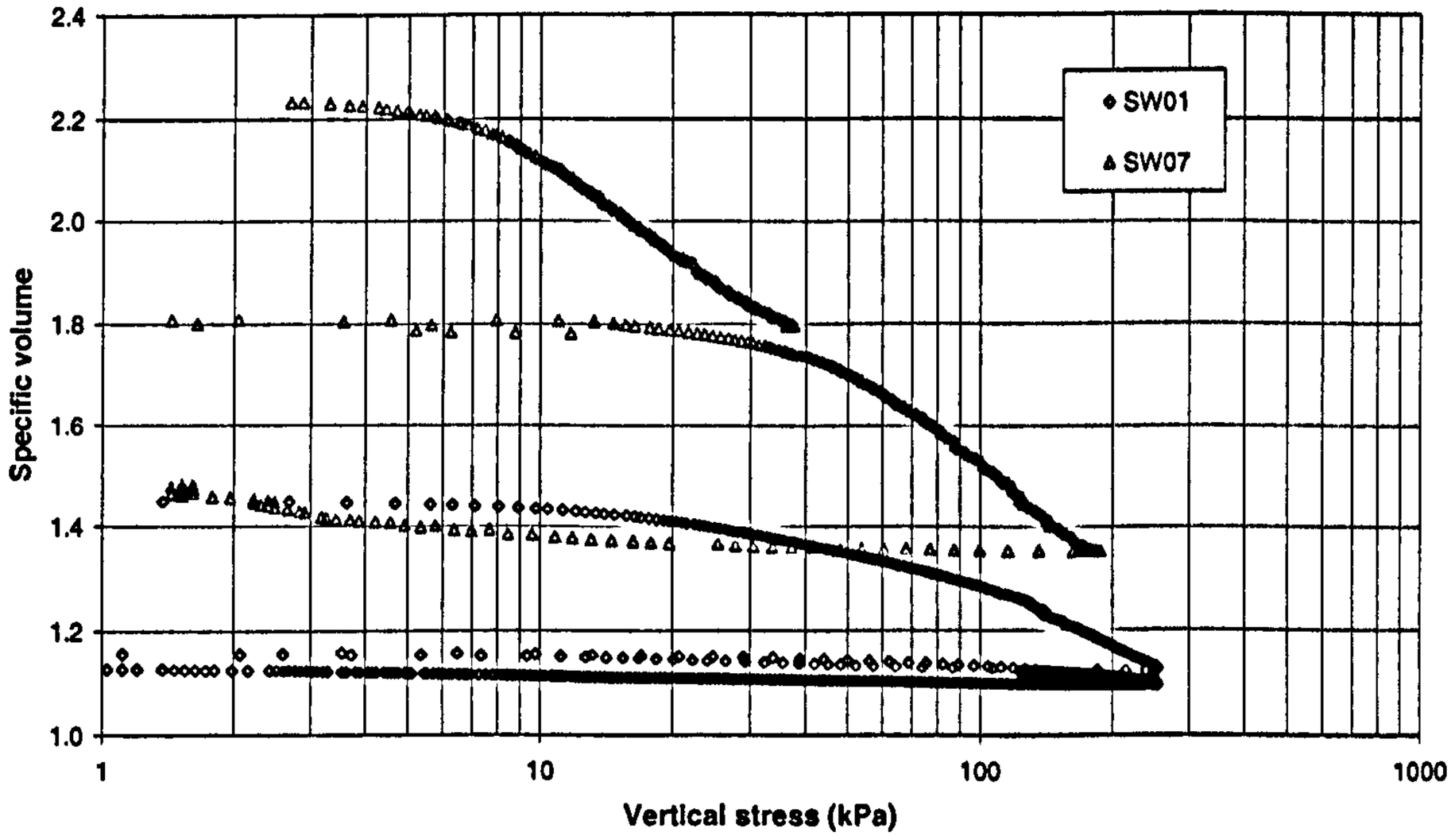

Figure 4-11 Specific volume vs. vertical stress for sample SW01 and SW07

In order to apply the compression model to these two tests, parameters for the two compression parts (inter void volume change and intra void volume change) are required. Parameters for inter void volume change can be obtained from pure sand compression, but this has not been done. According to the above analysis, SW01 can be considered as pure sand, neglecting the influence of paper and plastic bags. Thus, parameters for intra voids volume change, intra void ratio under unit pressure f_1, intra compression index $C_{C\text{-}Intra}$ and intra swelling index $C_{S\text{-}Intra}$ are all zero for SW01 assuming no compressible particles in the sample. The inter void volume change parameters, inter void ratio under unit pressure e_0, inter compression index $C_{C\text{-}Inter}$ and inter swelling index $C_{S\text{-}Inter}$ can be obtained by curve-fitting for SW01, shown in Figure 4-12. Values of the back-analysed parameters have been listed in Table 4-12. It should be noted that the compression index C_C and swelling index C_S of the samples are the addition of the inter and intra index.

Table 4-12 Modelling parameters for SW01 and SW07

Sample	e_1	f_1	$C_{C\text{-Inter}}$	$C_{C\text{-Intra}}$	$C_{S\text{-Inter}}$	$C_{S\text{-Intra}}$
SW01	1.07	0	0.4	0	0.022	0
SW07	1.07	0.68	0.4	0.21	0.022	0.005

It can be seen from Figure 4-12 that the model can reproduce the test data except the initial part of the curve, which shows a non-linear behaviour. Before loading, the sample has experienced a high stress level due to its pre-compression, which leads to the non-linear behaviour at the beginning (Langer, 2006).

Having determined the parameters for SW01, they can be adopted by SW07 as parameters for inter voids volume change. The remaining parameters can be obtained by curve-fitting of the total compression behaviour, as can be seen in Figure 4-13. Values of the parameters have also been listed in Table 4-12. It can be seen that an initial intra-void ratio and an intra compression index are required for this sample. Although it has been discussed above that the two samples have almost the same slope of reload/unload lines, a very small intra swelling index (0.005) is still needed to reproduce the test data, which means a slight recoverable swelling occurs in compressible particles.

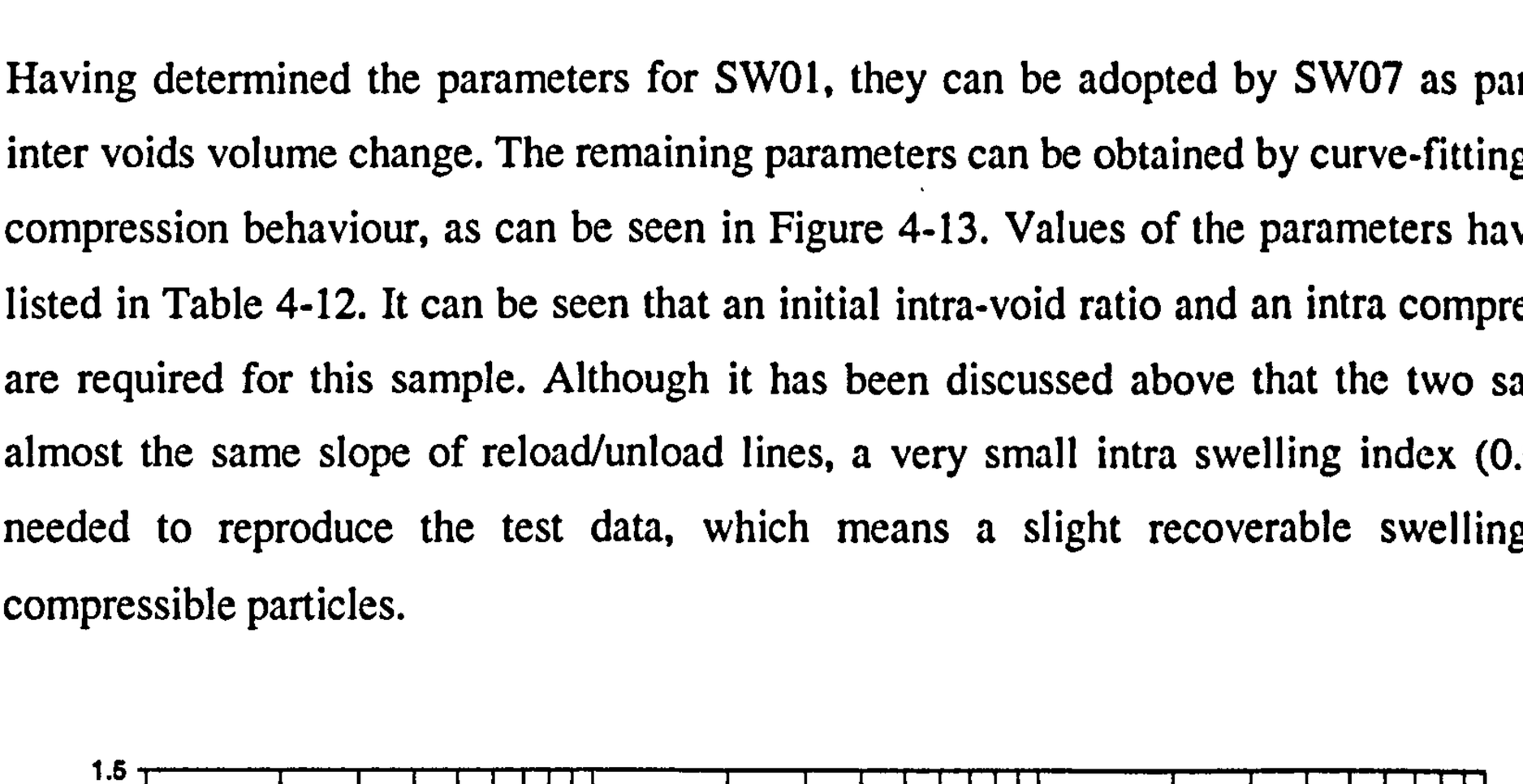

Figure 4-12 Specific volume vs. vertical stress from test and modelling for sample SW01

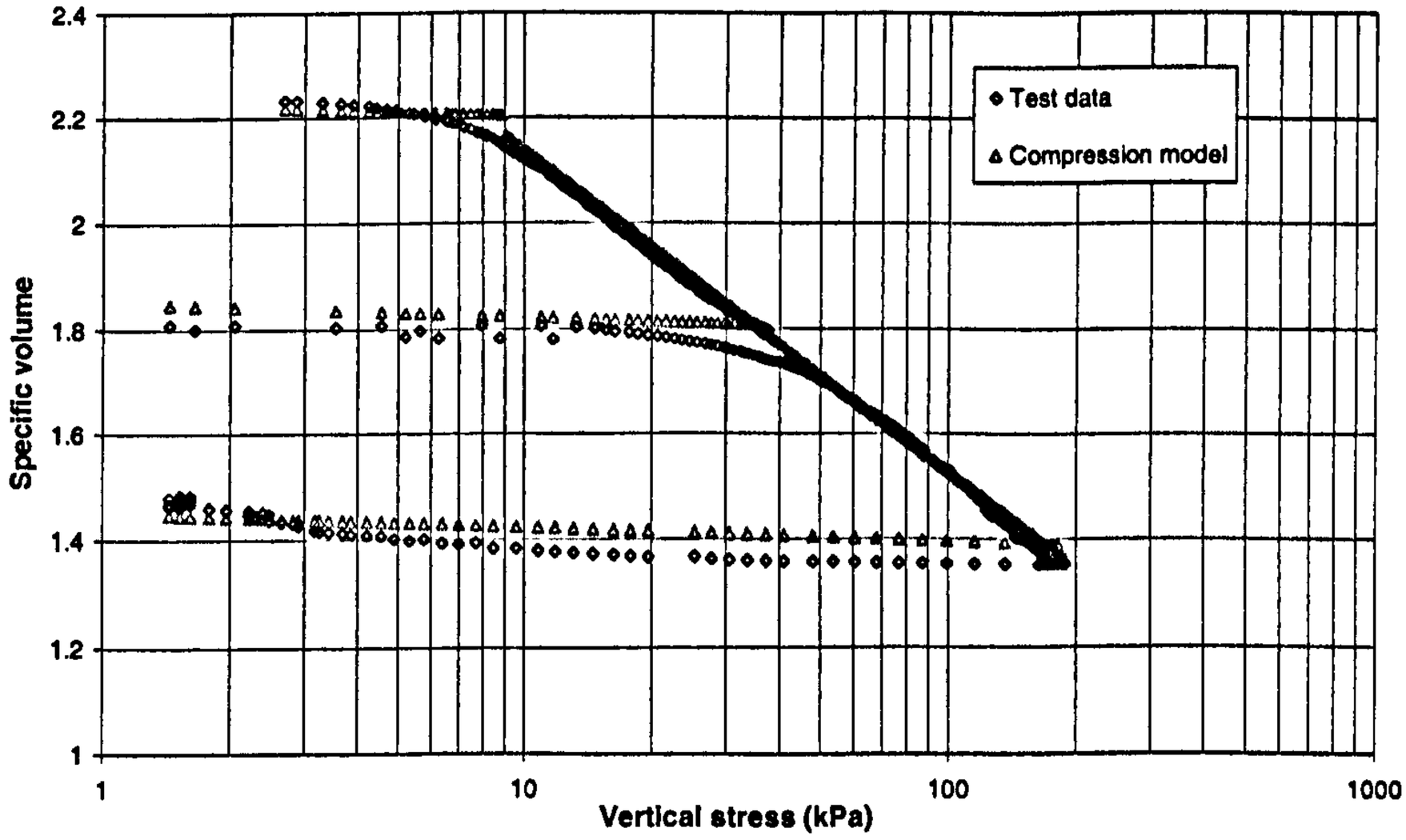

Figure 4-13 Specific volume vs. vertical stress from test and modelling for sample SW07

It should be noted that during the above modelling process, the parameters were obtained for incompressible and compressible components separately and added their effects on total volume change simply, which means the inter-phase compression behaviour between different kinds of particles (e.g. sand/paper, sand/cans) have been ignored in the compression model.

➢ Compressible Composition SW02

SW02_1, SW02_2 and SW02_3 have the same composition, in which the components of SW02_3 came from those of SW02_1 and SW02_2 after compression and having approximately double the unit weight . Figure 4-14 shows the relationship between the sample volumes and the effective vertical stresses for the three samples, in which similar slopes of compression and swelling for each sample can be noticed. Figure 4-15 shows the relationship between the specific volumes and the effective vertical stresses. It has been shown clearly in the figure that, SW02_3 could be seen as the same sample as SW02_1 and SW02_2 which were compressed at higher vertical stress levels. This is consistent with that of the three samples having the same composition. It is proposed that only one set of parameters is required to model all three tests.

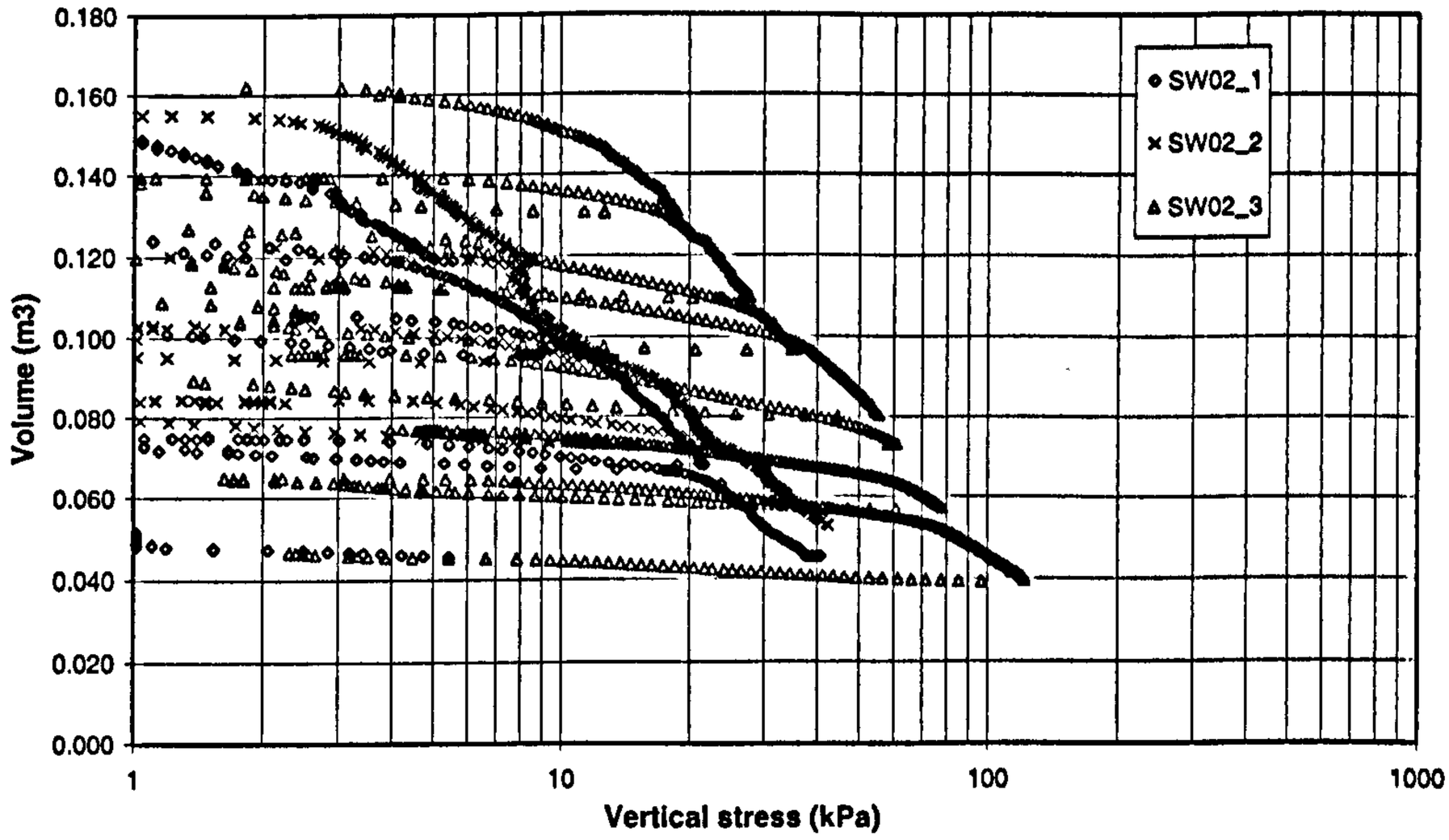

Figure 4-14 Waste volume vs. vertical stress for sample SW02_1, SW02_2 and SW_02_3

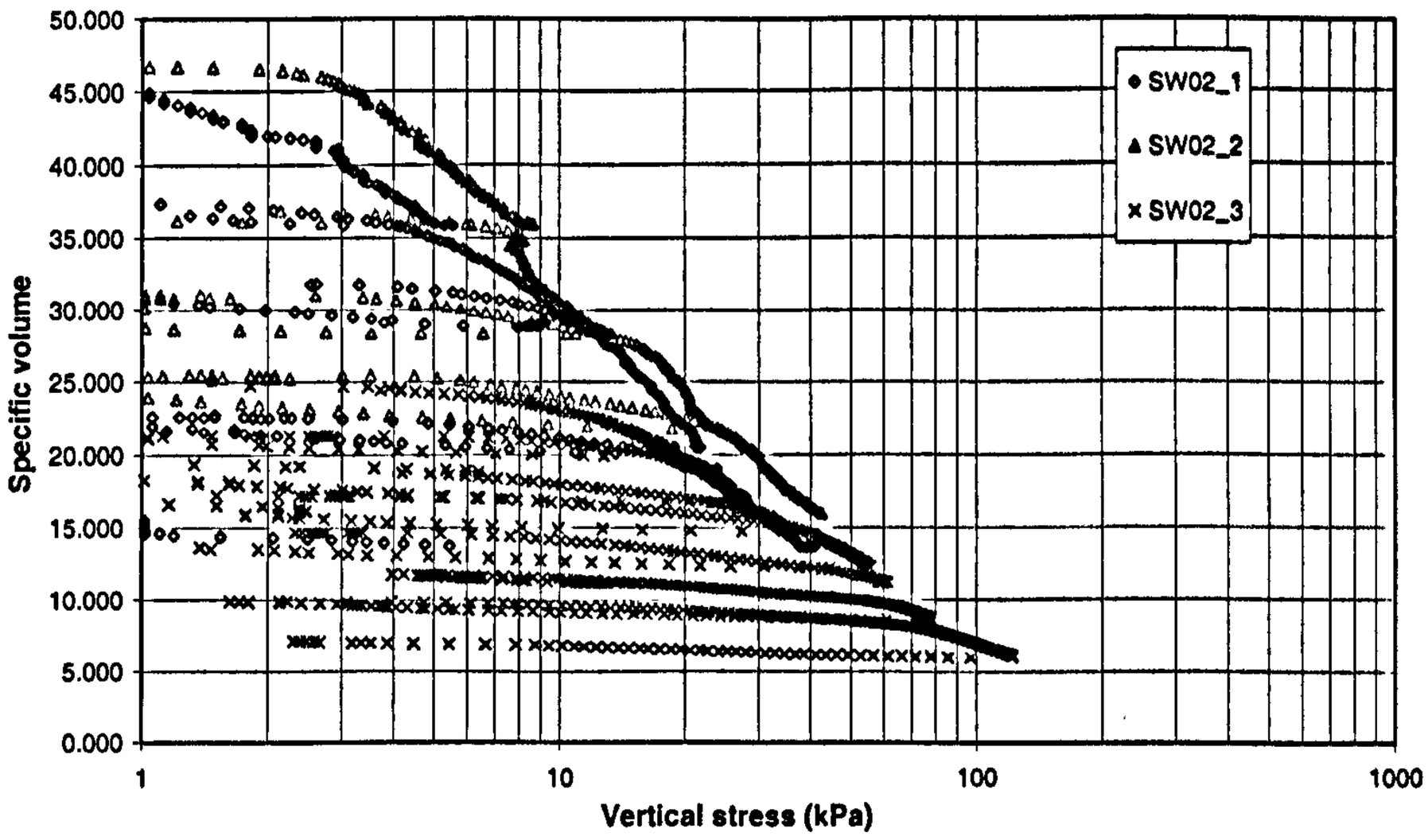

Figure 4-15 Specific volume vs. vertical stress for sample SW02_1, SW02_2 and SW02_3

Firstly, total compression index and swelling index are determined by averaging the values of samples SW02_1 and SW02_2, that is, C_C=22 and C_S=2. It should be noted that, it is difficult to separate the inter and intra voids volume change in this case. An assumption of the same contributions from inter and intra-voids has been made, which means relevant parameters for both mechanism have the same values, as shown in Table 4-13. Figure 4-16 and Figure 4-17 show the modelling results in comparison with the test data for SW02_1 and SW02_2. There is a good

agreement between the model prediction and test results for sample SW02_1 and SW02_2 by using the same parameters.

Table 4-13 Modelling parameters for SW02_1, SW02_2 and SW02_3

Sample	e_1	f_1	$C_{C\text{-Inter}}$	$C_{C\text{-Intra}}$	$C_{S\text{-Inter}}$	$C_{S\text{-Intra}}$
SW02_01	27	27	12	12	1	1
SW02_2	27	27	12	12	1	1
SW02_3	27	16	12	6	1	0.2

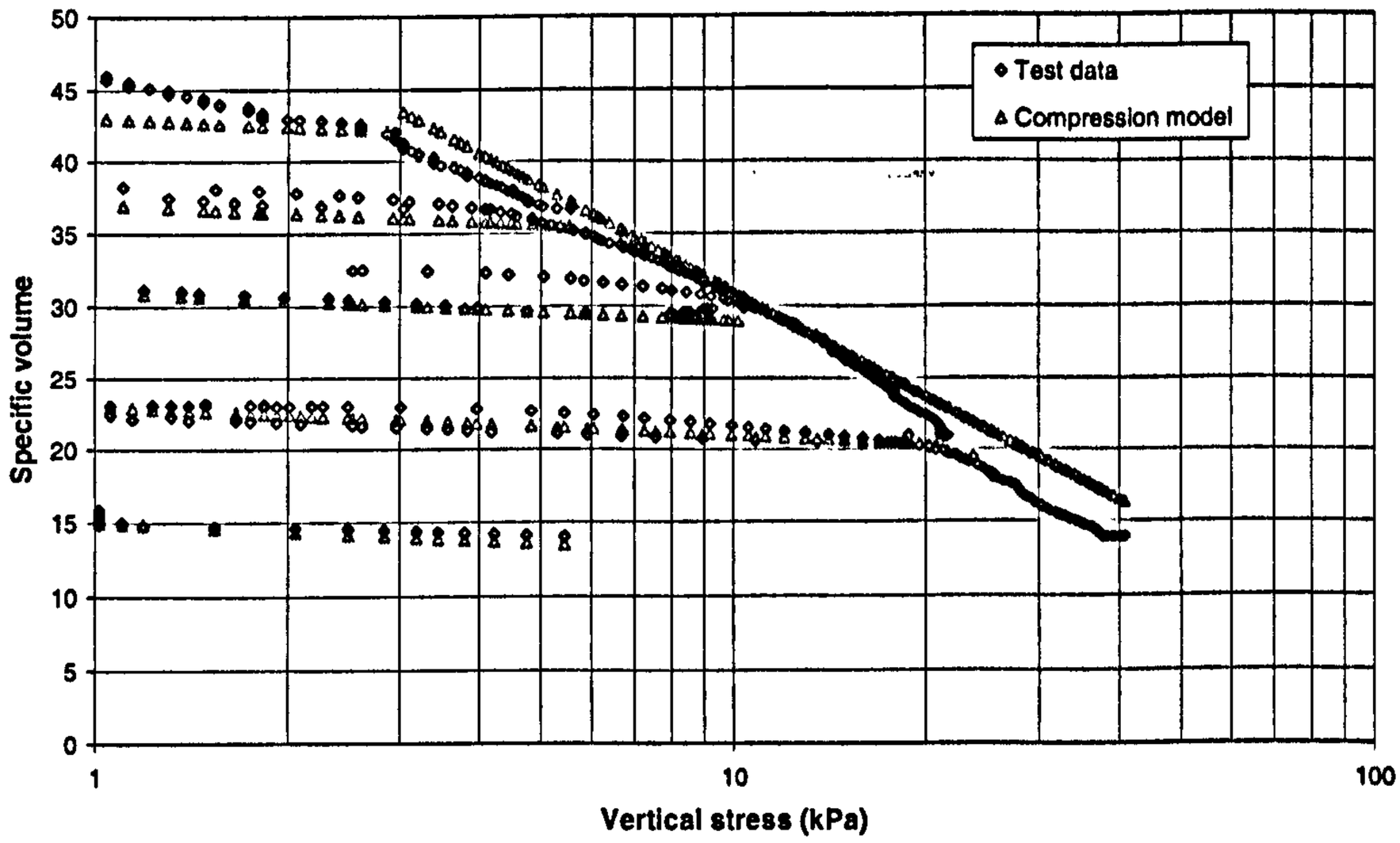

Figure 4-16 Specific volume vs. vertical stress from test and modelling for sample SW02_1

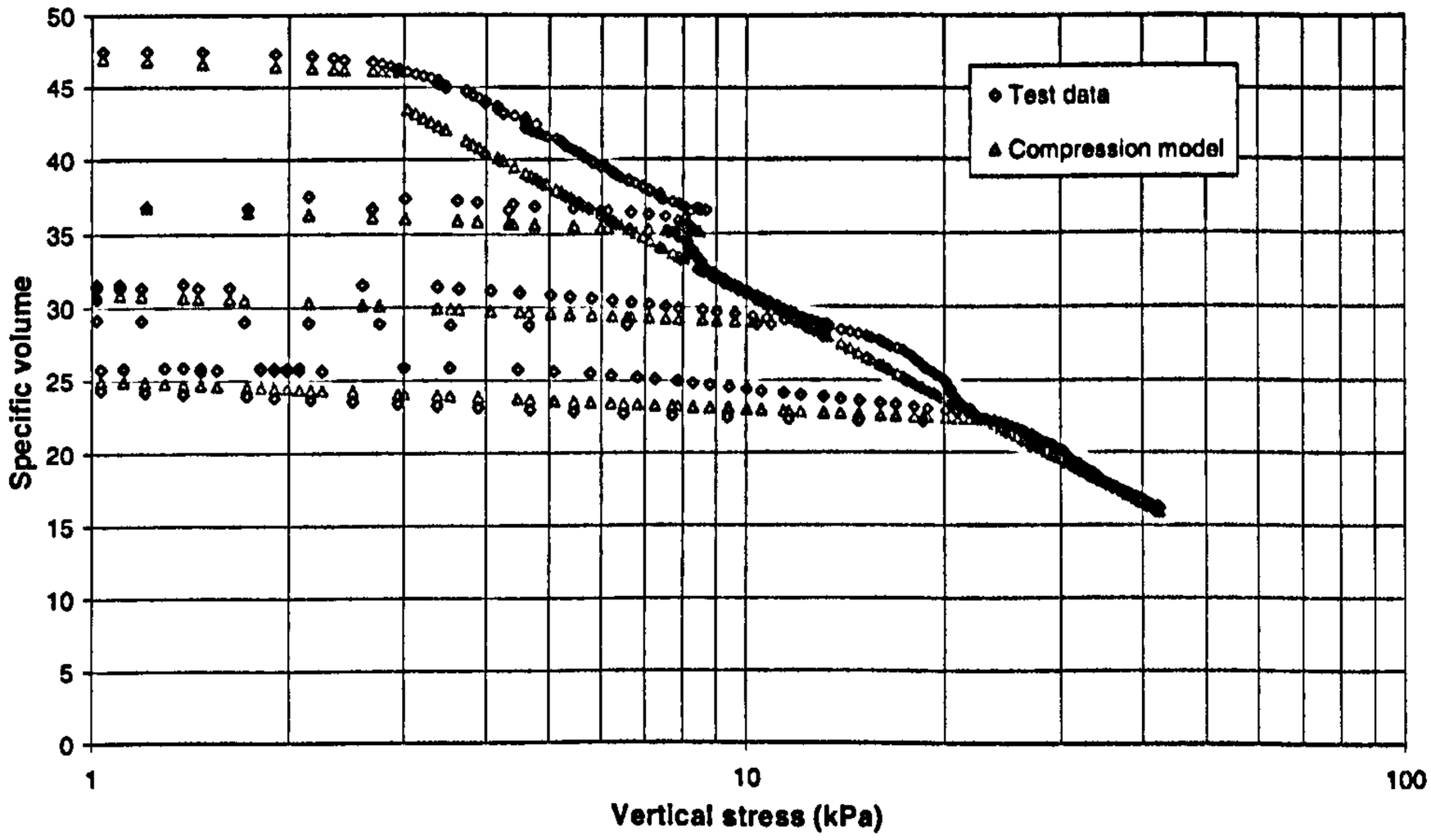

Figure 4-17 Specific volume vs. vertical stress from test and modelling for sample SW02_2

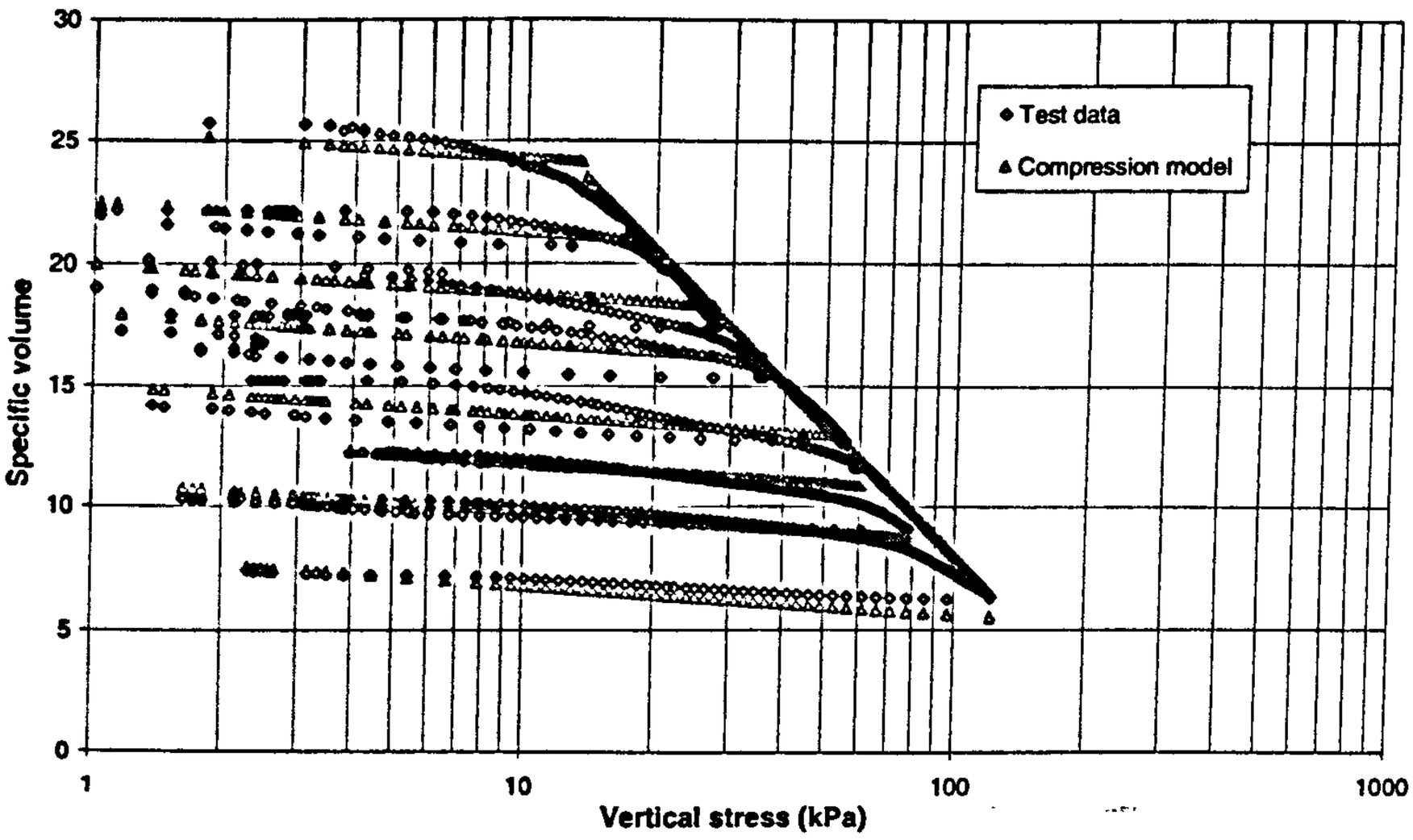

Figure 4-19 Specific volume vs. vertical stress from test and modelling for sample SW02_3 using improved parameters

➢ Mono-Component Composition SW04 together with SW03

SW03 and SW04 were mixtures of approximately half weight incompressible particles (tyre-chunks and brick) and half weight compressible particles (aluminium cans, paper, textiles and plastic packaging). The difference between these two samples is, SW04 has 50% (in mass ratio) aluminium cans dominating its behaviour (this is why it is defined as mono-component composition), while SW03 has a mixture of compressible particles including cans, paper and textiles.

The volume changes and specific volume changes under compression have been given in Figure 4-20 and Figure 4-21. It can be seen from the figures that, the two test results show similar compression and swelling behaviour, while SW04 has a much higher specific volume compared to SW03 at the same stress level. The compression index C_C is 12 and 14 for SW03 and SW04, respectively, and the swelling index C_S is 0.8 for both samples. This difference should be due to the high intra-void ratio of aluminium cans, which was discussed in the incompressible composition. Another interesting finding is that, slope of the compression line remains almost constant for SW04, while non-linear relationship is noticeable for SW03 at higher stress level. It is obvious that SW03 becomes stiffer under higher vertical stresses, which is the same behaviour as SW02. It confirms that the compressible composition (SW02 and SW03) has this behaviour, while the mono-component composition (SW04) does not have. It might implicate that some of the compressible particles, such as paper and textiles, dominate the behaviour at lower stresses and become stiffer at higher stresses.

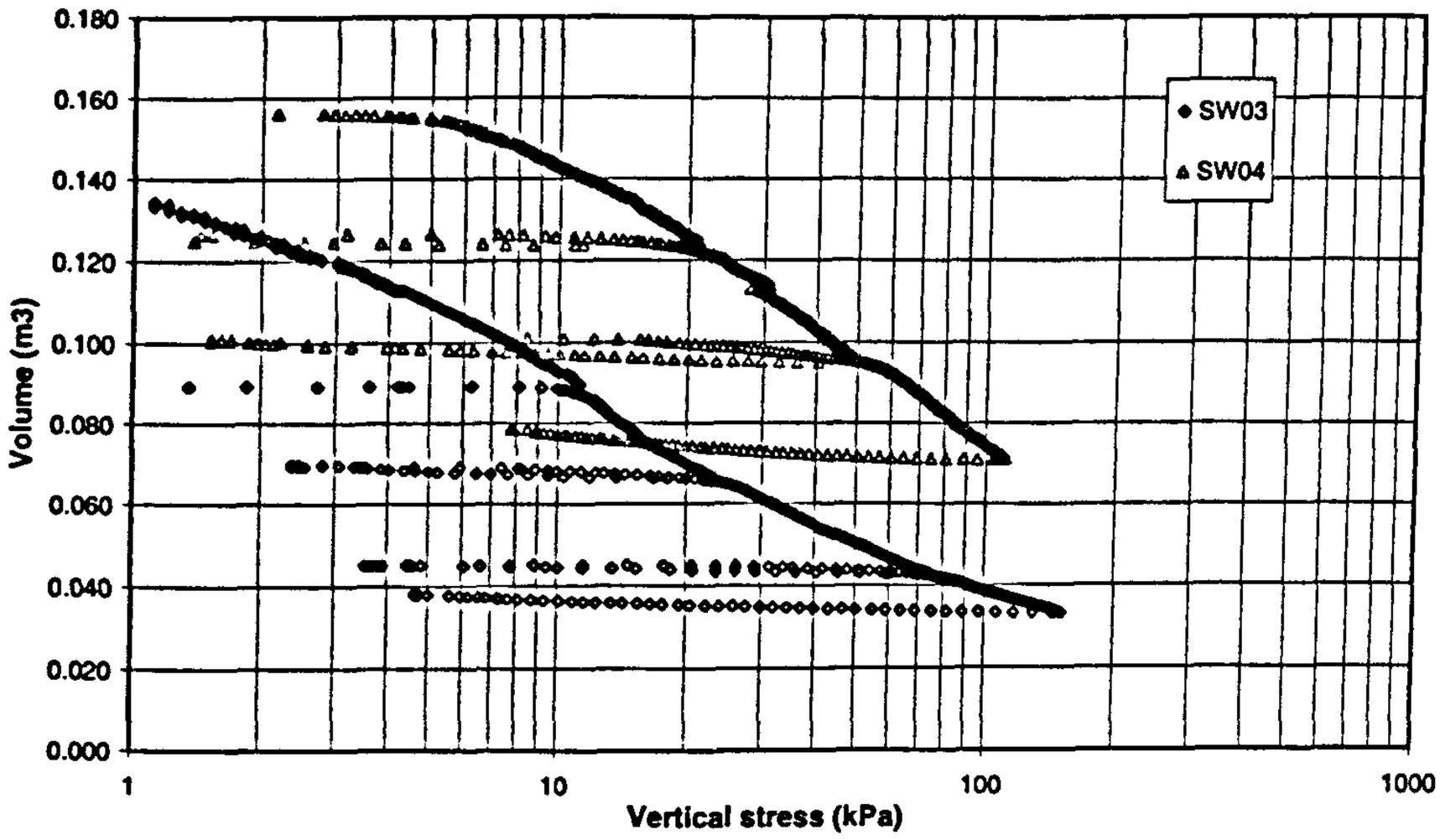

Figure 4-20 Waste volume change under compression for sample SW03 and SW04

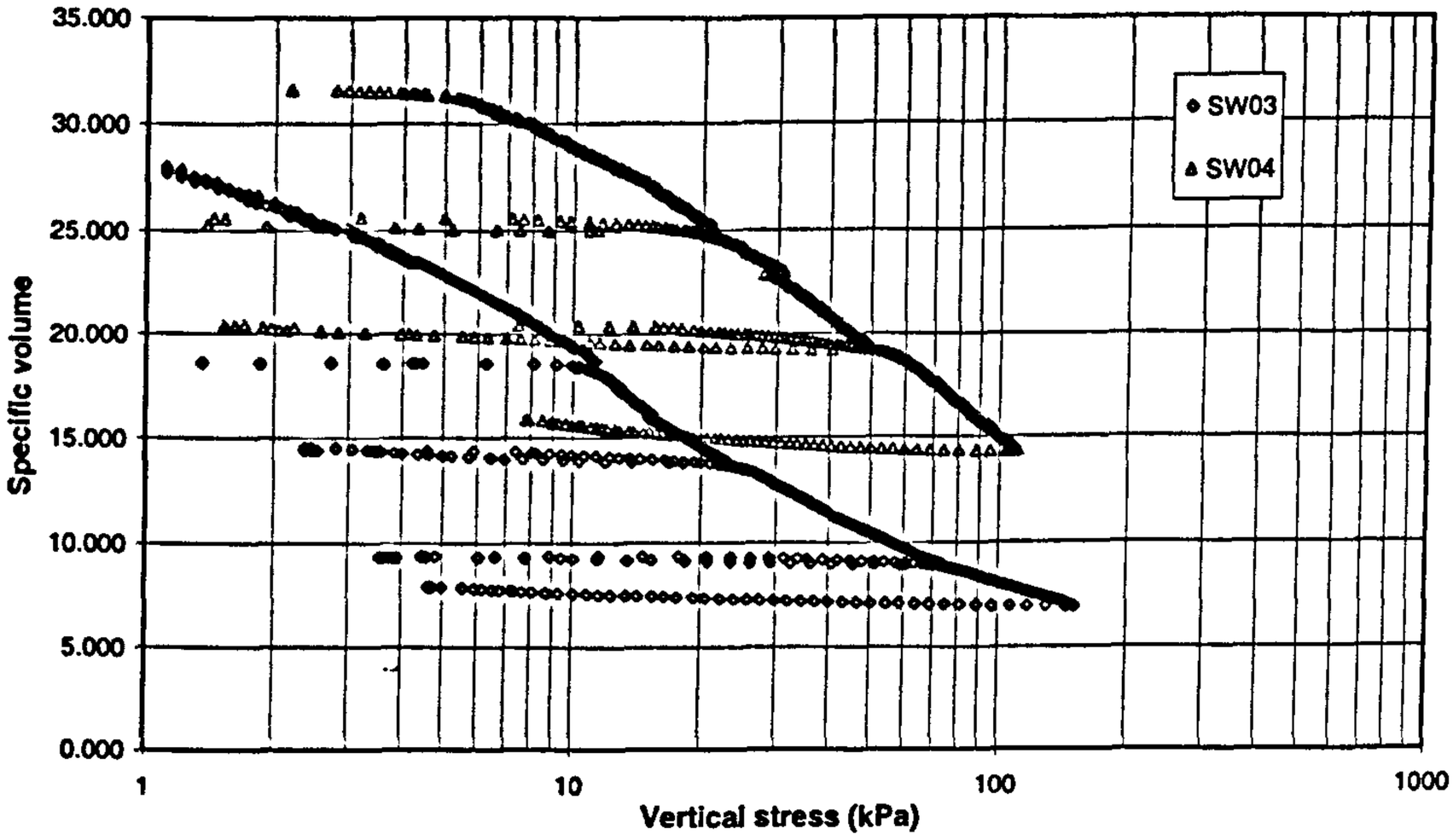

Figure 4-21 Specific volume vs. vertical stress for sample SW03 and SW04

Curve-fitting parameters for modelling these two samples have been given in Table 4-14. Again, since the information to separate inter and intra voids volume change cannot be easily collected from the test, the same contributions from both mechanisms are assumed for both samples. It can be seen that, both samples have almost the same values for the compression index, the same values for the swelling index, while higher specific volume under unit pressure for SW04. Comparison between modelling and test results for the two samples can be seen in Figure 4-22 and Figure 4-23. There are good agreements between modelling and test for both the samples,

except for the high pressure (more than 50 kPa) part of SW03 that has already been discussed as being non-linear. An improved intra compression index seems needed to model the compression behaviour under high stresses.

Table 4-14 Modelling parameters for SW03 and SW04

Sample	e_1	f_1	$C_{C\text{-Inter}}$	$C_{C\text{-Intra}}$	$C_{S\text{-Inter}}$	$C_{S\text{-Intra}}$
SW03	15	15	6	6	0.4	0.4
SW04	21	21	7	7	0.4	0.4

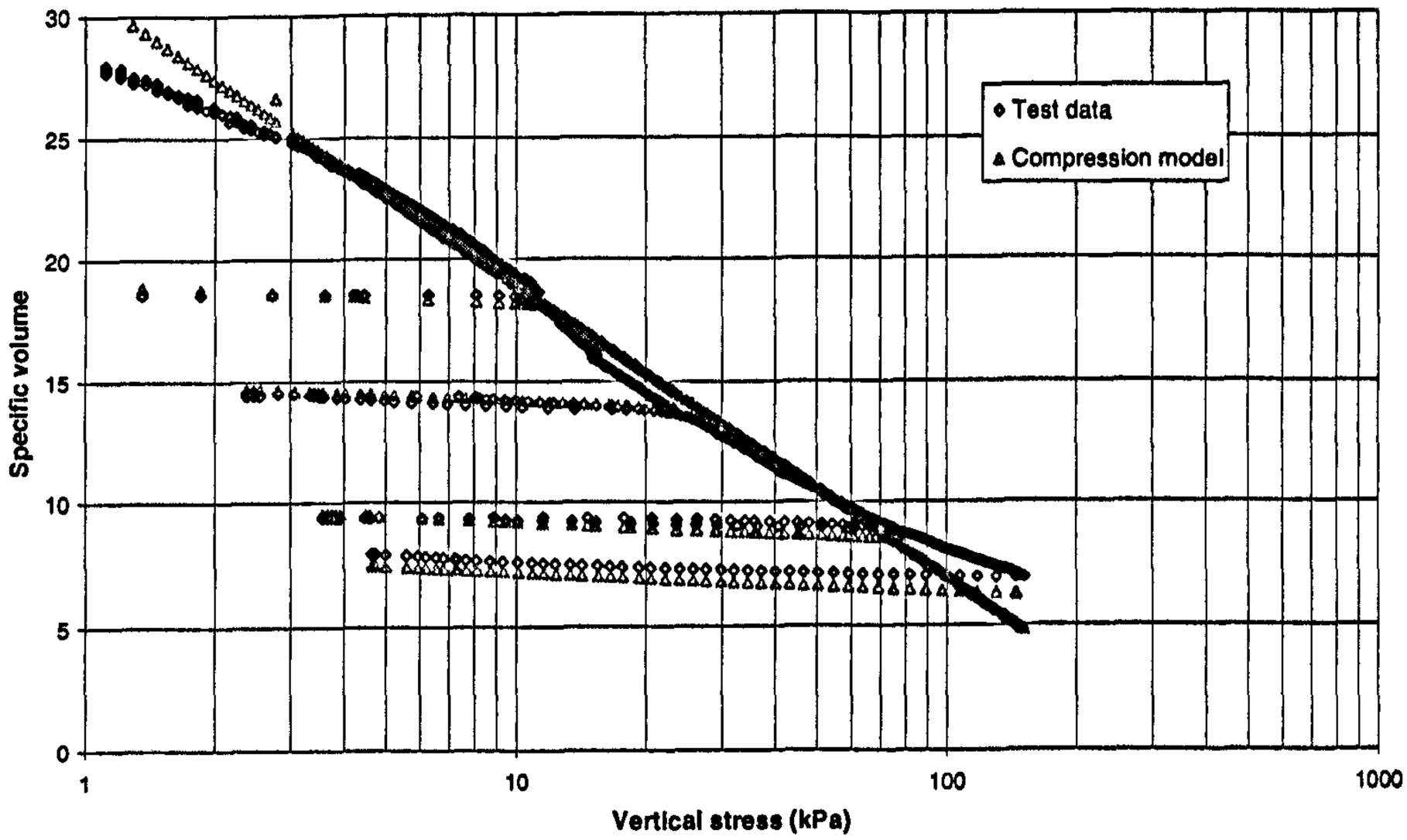

Figure 4-22 volume vs. vertical stress from test and modelling for sample SW03

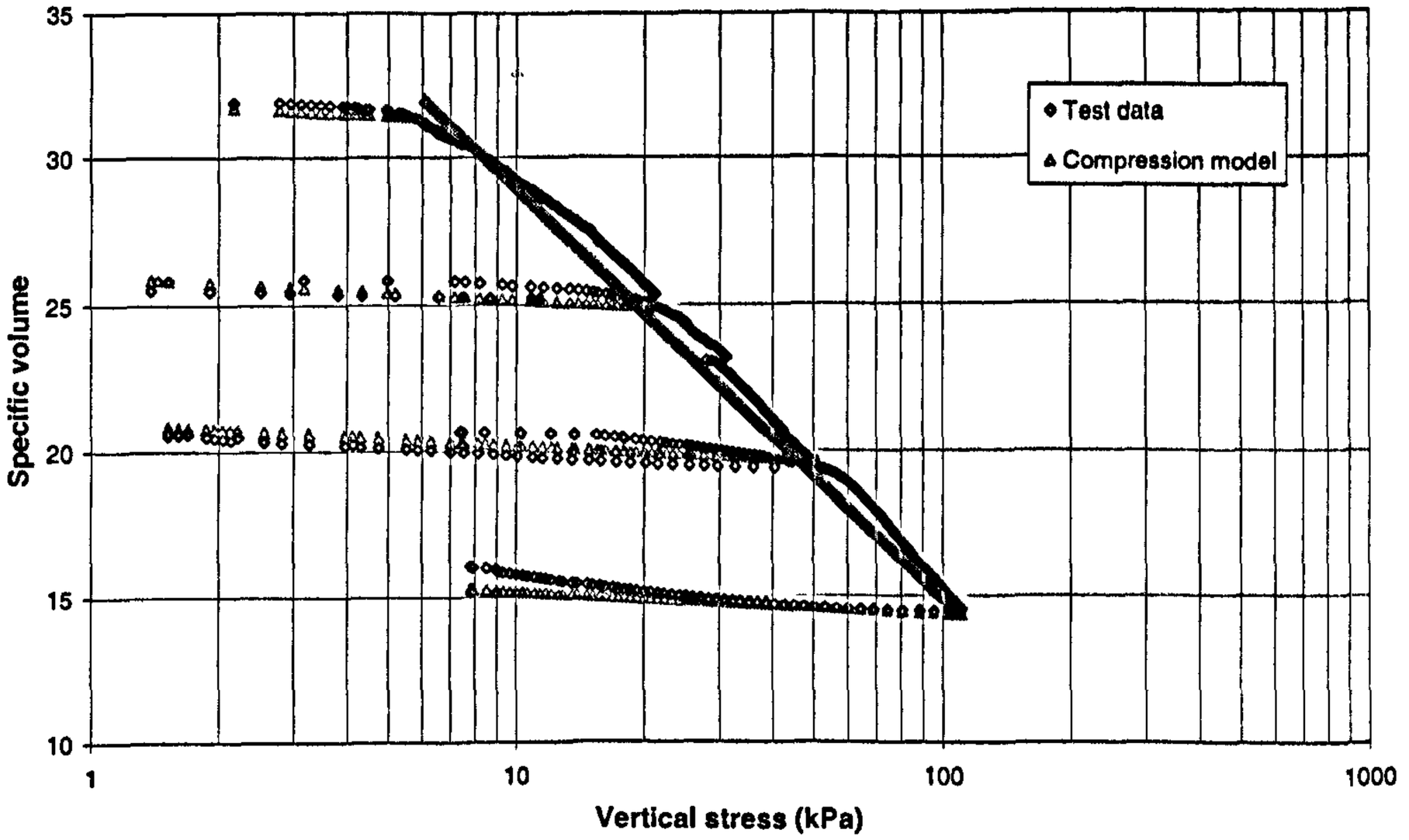

Figure 4-23 Specific volume vs. vertical stress from test and modelling for sample SW04

➢ Simulation of A Real Waste Composition SW09

SW_09 was based on the findings from a waste sorting analysis conducted on Narborough Landfill (Langer 2006).The compression curve has been presented in Figure 2-4. It can be seen that this composition showed similar characteristics to the compressible compositions SW_02_1, SW_02_2 and SW_03. A non-linear trend is observed under high stress levels, which could be modelled by different compression index values for different parts of the compression curve, i.e. a stress dependent compression index value.

Values of modelling parameters for SW09 have been given in Table 4-15, in which inter and intra parameters are assumed to be the same again. Relationships between specific volume and effective vertical stress from both test and modelling have been plotted in Figure 4-24, in which the unload/reload curves are modelled well but the compression line is not reproduced using only one total compression index value. It seems two total compression index values are required to model the compression curve under different stress levels. It is obvious that a smaller compression index is needed when the effective vertical stress is more than 40 kPa in this case. It is simple to reproduce the test results with a better agreement through this method, which is the same as the compressible composition SW02 discussed above.

Table 4-15 Modelling parameters for SW09

Sample	e_1	f_1	$C_{C\text{-}Inter}$	$C_{C\text{-}Intra}$	$C_{S\text{-}Inter}$	$C_{S\text{-}Intra}$
SW09	9	9	4	4	0.3	0.3

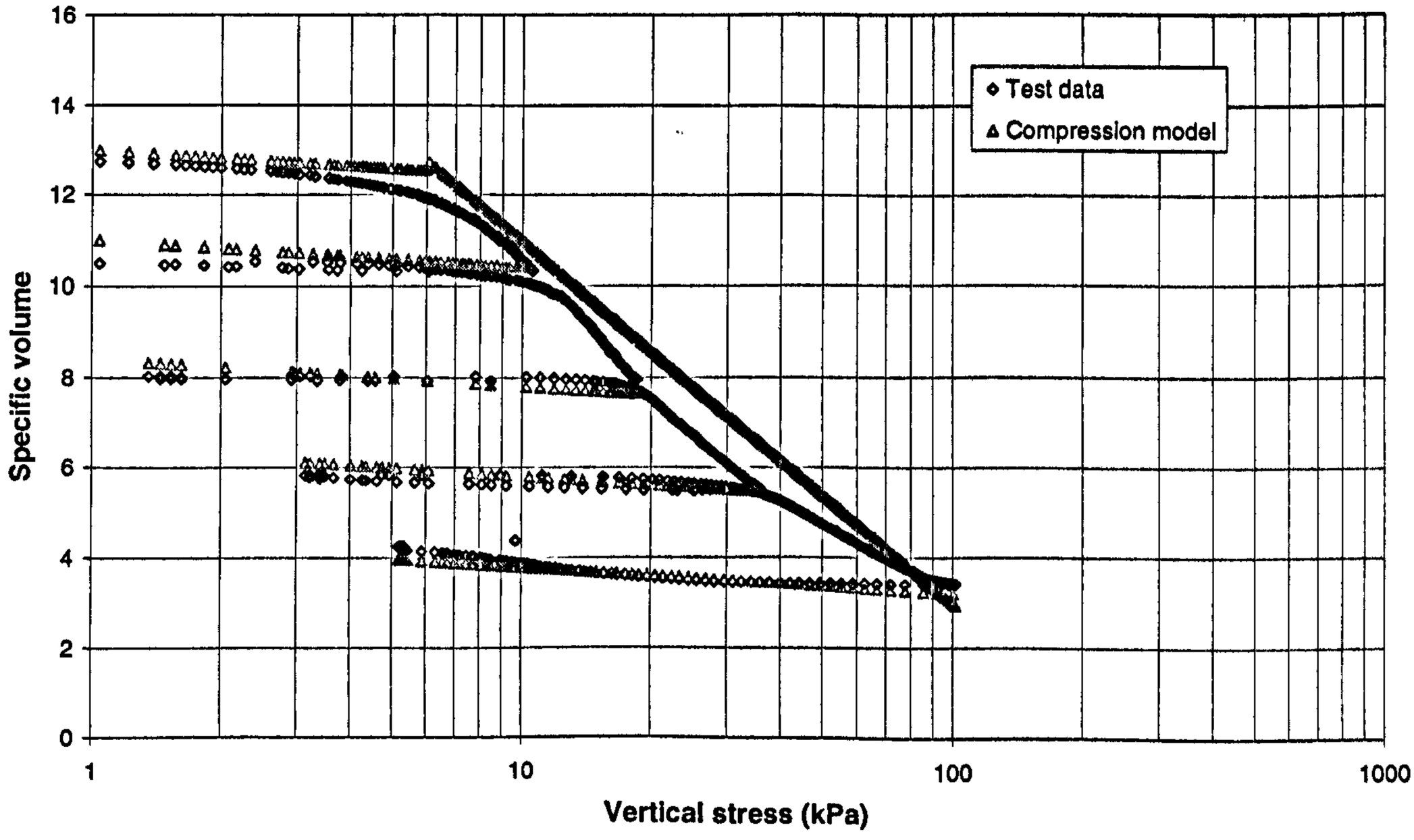

Figure 4-24 Specific volume vs. vertical stress from test and modelling for Sample SW09

4.5 Discussion and Summary

Firstly, a case study from a MSW one-dimensional compression test reported by Powrie and Beaven (1999) was carried out to demonstrate the contribution of compressible particles in waste material. A basic compression model based on this case study was proposed using the traditional soil phase relationship, and its efficacy was demonstrated by modelling the same test.

Following that, a main drawback of the above compression model was noticed, which restricts its application for wastes in general cases. A one-dimensional compression model for MSW was proposed using an innovative phase relationship that consider inter and intra voids in waste material. The model has very simple formulas, and a clear physical meaning, which is more appropriate for waste material than the model from the first case study. In this improved model, both inter and intra void ratio changes are assumed to be linear with a logarithmic stress change so that the total volume change trend is also linear.

Finally, the compression model was validated using one-dimensional compression test data. The compression model was firstly validated using one-dimensional compression tests reported by Powrie and Beaven (1999). An additional assumption is required to determine the inter and intra void ratios from the test. Three different conditions were assumed, that is, no intra void is open, 30% intra-voids are open and all voids are intra-voids. The modelling results showed that the compression model can reproduce the test results well for all the three cases.

One-dimensional compression tests on synthetic waste samples reported by Langer (2006) were also modelled by the compression model, which further demonstrated the efficacy of the compression model. In order to better reflect the compressive behaviour of the synthetic waste, relationships between specific volume and effective vertical stress for each sample have been obtained by assuming material density for each component in the sample. Meanwhile, modelling parameters can be easily determined from this relationship. The results have shown good agreements between test data and modelling curves, except for the higher stress part for some samples. It seems variable compression index values are required for different stress levels due to the existence of some specific compressible particles in synthetic waste (perhaps also for real waste). It is also demonstrated that the model can be used by changing one aspect of the parameters (e.g. intra voids change parameters) if the other aspect of compression mechanism (e.g. inter voids compression) is the same for different samples, e.g. modelling the incompressible composition and compressible composition.

It should be noted that the compression model was developed in one-dimension compression boundary condition framework so that further assumptions are required when it is further incorporated into the constitutive model for MSW considering more general stress conditions in

this project. A compression model developed for isotropic compression boundary condition is required in future work.

In addition, some interesting findings on compression mechanisms of synthetic waste have been identified through modelling different waste compositions, which are summarised as follows:

1) For the incompressible compositions (SW01 and SW07), the value of compression index is dominated by compressible particles, while the value of swelling index is dominated by incompressible particles. With more closed intra void (aluminium cans and plastic packaging), the sample showed a much higher volume change in virgin compression. The unload/reload behaviour seems almost the same for both samples, which means most of the intra voids compression are plastic volume changes.

2) For the compressible composition (SW02 and SW03), both values of compression index and swelling index are dominated by compressible components. The compression index has a tendency to increase with higher stress levels for both samples. However, the swelling index for SW02 has a tendency to decrease under higher stresses, which confirms that most of the intra voids compression are plastic.

3) The increasing compression index under higher stresses found in the compressible composition seems to be dependent on the type of the compressible particles, which is observed from the comparison study between the compressible composition (SW03) and the mono-component composition (SW04). Compressible particles, such as paper and textiles, seem to dominate this behaviour rather than aluminium cans and plastic packaging, which has been further confirmed in the test of real waste composition SW09. The non-linear behaviour under higher stresses seems to be controlled by some specific compressible particles in the waste, which could be due to the compression of compressible particles themselves. It could also be due to the interaction between incompressible particles and compressible particles, which is beyond the capability of the proposed compression model for MSW.

CHAPTER

5

A Fibre Reinforcing Model

5.1 Introduction

Reinforcing nature of MSW has been recognised by many researches (e.g. Kölsh, 1995; Langer, 2006), and is readily observed in waste bodies. Fibre-matrix nature of waste has been observed from videos taken in boreholes through a landfill and it can also be seen in the back scarp of waste slope failures. Fibre reinforcing components in MSW are usually composed of plastic, paper, textile etc. Existence of the fibre reinforcing components in MSW affects its mechanical response, e.g. improving its shear strength and changing its stress-strain behaviour, as reviewed in section 2.2.2.

It is well known that soil (and other materials such as metal, rubber, concrete etc.) strength can be improved by adding a proportion of fibre material (e.g. synthetic fibre, metal fibre, even roots), provided that tensile strength of the fibres are mobilised. Studies on this kind of reinforcing material could be applied to model the shearing behaviour of MSW dominated by the fibre reinforcing particles. However, a major difference between those purpose-reinforcing materials and MSW is that, the former reinforcement is often orientated in one or more known directions (or positions) to improve the strength in certain directions (except the randomly distributed fibre reinforced soils), while fibre reinforcing components of MSW are mostly randomly distributed throughout the MSW body. MSW reinforcing components in landfills seems to have a tendency to be distributed horizontally or sub-horizontally due to pre-treatment and compaction, which would result in the anisotropic (e.g. orthotropic) shear behaviour. It is apparent that layer fibres in waste material result in different shear strength behaviour in different directions, which is dependent on the mobilised tensile stresses of fibres. For instance, if fibres are distributed horizontally, horizontal shear strength of the material would be the lowest since no tensile stress can be mobilised in fibres. However, it is decided that waste will be modelled as the randomly distributed fibre reinforced material due to the following reasons:

1) The randomly distributed fibre reinforcing material is the most general and complex situation in all of the reinforcing materials, compared with the situation that fibres are orientated in one or more known directions. Once a model for the randomly distributed fibre reinforced material is produced, it should be not difficult to modify the model for the situation of fibre with a known distribution by changing the orientation of the mobilised tensile stresses;

2) Currently, there is no quantification of reinforcing fibre orientation in a waste body resulting from compaction in landfills. It is not wise to produce a model for the unconfirmed information. Moreover, the model for randomly distributed fibre reinforced material can be modified to be applicable for special cases as mentioned above.

To model shear behaviour of the randomly distributed fibre reinforced material, such as randomly distributed fibre reinforced soil and waste material, an approach (called mobilised tensile stress analysis) originated from the effective stress theory in soil mechanics, will be developed in this chapter. A randomly distributed fibre reinforcing model will be produced by combining the mobilised tensile stress analysis with a constitutive model for fibres, as well as a model for soil (e.g. the elastic-perfectly plastic Mohr-Coulomb model, the Modified Cam-Clay model). Firstly, the basic principal and a framework of the mobilised tensile stress analysis will be introduced. Subsequently, the undrained analysis process for saturated soils will be investigated. Based on the idea of the undrained analysis, the linear mobilised tensile stress analysis will be fully presented, in which two sub-analyses will be explained in detail and parametric studies will be carried out. The fibre reinforcing model will be validated by the triaxial compression tests on fibre reinforced sand reported by Michalowski and Cermak (2003).

5.2 Model Framework

It is assumed in soil mechanics that only the effective stress (stresses in the soil skeleton) induce strain in the soil skeleton. The effective stress can be calculated as the difference between total stress and pore pressure for saturated soil, which means the fluid distributed in the voids of soil takes part of the responsibility to resist the compressive loading. This idea will be borrowed to model the randomly distributed fibre reinforced material. The randomly distributed fibres can be considered as distributed uniformly in a MSW body, like the fluid in soil. Fibres are assumed to be mobilised to sustain only the tensile stress, which can provide an extra confining stress (horizontal support) for the material in certain directions (i.e. the directions that matrix material expands). The approach is named Mobilised Tensile Stress Analysis (MTSA). Two levels of the analysis can be conducted comparable to pore pressure analysis in soil mechanics:

1) Linear mobilised tensile stress analysis (LMTSA)—This analysis corresponds to the undrained analysis of saturated soil which could be simply conducted by the finite element

method. In the undrained condition, pore pressure is calculated through the fluid bulk stiffness and the total volumetric strain, which is linear. Similarly, the mobilised tensile stress in fibres is calculated through an equivalent modulus for all the fibres and the tensile strain, which is also linear.

2) Non-linear mobilised tensile stress analysis (NMTSA)—This analysis corresponds to the consolidation analysis of saturated soil which has to be a coupled analysis in finite element analysis. In reality, fibres must be mobilised at different strain levels due to their initial position and orientation, and bond failure between fibres and particles or tensile failure of fibres must occur with the development of shear strain. Therefore, non-linear mobilised tensile stress analysis should be considered for a more advanced model. This could be carried out similarly to the consolidation analysis of saturated soil coupled with seepage (non-linear pore pressure) in finite elements analysis. A relationship between non-linear mobilised tensile stress and shear strain should be proposed similar to the equation of continuity in the consolidation analysis.

More classifications for the above analysis are required considering fibre tensile failure or interface failure between fibre and matrix material. Moreover, different randomly distributed fibre reinforcing models will be obtained if a certain analysis is combined with different soil constitutive models. Figure 5-1 shows the hierarchical structure of the MTSA and the different randomly distributed fibre reinforced material models.

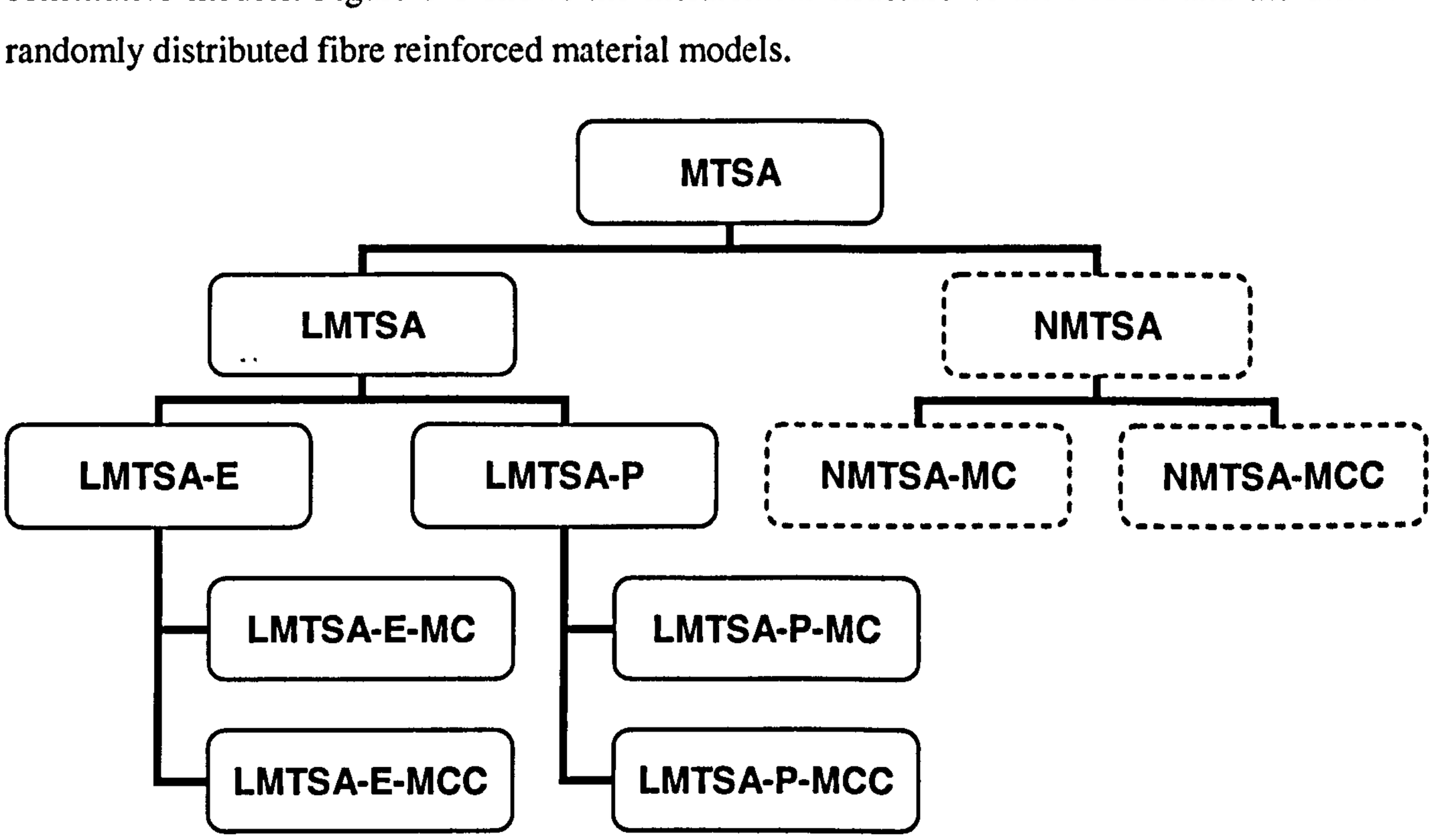

Figure 5-1 Hierarchical structure of MTSA and different randomly distributed fibre reinforcing models

For LMTSA, two sub-analyses, i.e. LMTSA-E and LMTSA-P, are required according to material model for fibres and whether failure occurs in either fibre material itself or between fibre and

matrix material. LMTSA-E stands for the LMTSA with a linear ***elastic*** constitutive model for fibre material without failure, which means the mobilised tensile stress will increase linearly with the tensile strain of the whole material without an ultimate strength. LMTSA-P stands for the LMTSA with an elastic-perfectly ***plastic*** constitutive model for fibre material, which means a plastic mobilised tensile stress will be reached under a certain tensile strain level. A randomly distributed fibre reinforced material model can be produced by integrating a soil constitutive model with either of the analyses, i.e. LMTSA-E or LMTSA-P. A perfect elastic-plastic Mohr-Coulomb model (MC) and a critical state soil model, the modified Cam-Clay model (MCC) will be considered to combine with both analyses. Four different material models will be produced, i.e. LMTSA-E-MC, LMTSA-E-MCC, LMTSA-P-MC and LMTSA-P-MCC, as shown in Figure 5-1. Both linear analyses, LMTSM-E and LMTSM-P will be fully presented in this chapter, as well as combination with the Mohr-Coulomb models for matrix, while the combination with the Modified Cam-Cam model will be included Chapter 6 and implemented in the finite element method in Chapter 7.

For NMTSA, since the non-linear behaviour of the mobilised tensile stress and its failure criterion would be considered in an extra equation, there may be no need to include any constitutive model for the fibres or interfaces. Therefore, it can be combined with a soil constitutive model directly as shown in the figure, e.g. NMTSA-MC and NMTSA-MCC. The NMTSA is only regarded as future work and will not be included in this research, which is the reason why the dashed boxes are used in the model structure.

5.3 Undrained Analysis

Saturated soils are two-phase particulate materials in which the voids between the particles are full of fluid (i.e. water). In addition, the permeability of the material may be sufficiently low or the loads applied so quickly that generated excess pore pressures have no time to dissipate during the time-scale of the analysis. The conventional undrained triaxial compression test on soil samples is capable of simulating this situation. Figure 5-2 shows the boundary condition of an undrained compression test. The total stresses (axial stress σ_z and radial stress σ_r) on the soil sample can be separated into effective stresses (σ_z' and σ_r') on solid particles and pore pressure (u) from water. This means the water in soil takes partial responsibility to sustain normal compressive stresses in any direction, while only effective stresses on solid particles contribute to deformation of the soil skeleton and failure of the sample.

Naylor (1974) described a method of separating the stresses to pore pressures and effective stresses. The method is based on the concept of effective stress in matrix notation, thus:

$$\sigma_{ij} = \sigma'_{ij} + u\delta_{ij} \qquad \textit{Eq. 5-1}$$

in which σ_{ij} is the total stress tensor, σ'_{ij} is the effective stress tensor, and δ_{ij} is the Kronecker delta which can be expressed as:

$$\delta_{ij} = 1,\ i = j;\ \ \delta_{ij} = 0,\ i \neq j \qquad \textit{Eq. 5-2}$$

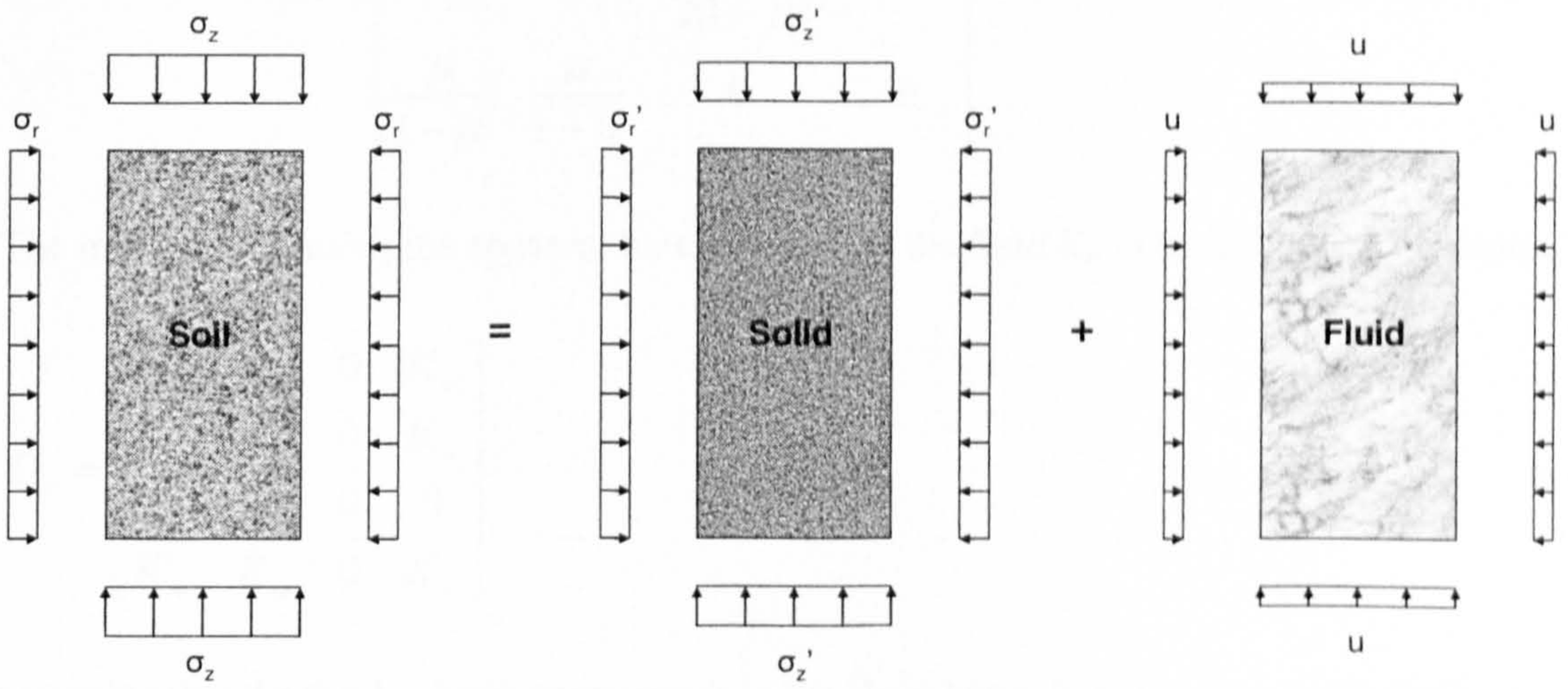

Figure 5-2 Boundary condition of the conventional undrained triaxial compression test on a saturated soil sample

The stress-strain relationship for the soil skeleton can be written in incremental form as:

$$\delta\sigma'_{ij} = D'\delta\varepsilon_{ij} \qquad \textit{Eq. 5-3}$$

in which ε_{ij} is the strain tensor, $\boldsymbol{D'}$ is the effective constitutive matrix, and the stress-strain relationship for pore pressure is:

$$\delta u = D_u \delta\varepsilon_{ij} \qquad \textit{Eq. 5-4}$$

where $\boldsymbol{D_u}$ is the constitutive matrix for water pressure. Combining Eq. 5-1, Eq. 5-3 and Eq. 5-4, the total stress-strain relationship can be obtained as:

$$\delta\sigma_{ij} = D\delta\varepsilon_{ij} \qquad \textit{Eq. 5-5}$$

where $\boldsymbol{D}$ is the constitutive matrix in terms of total stress:

$$D = D' + D_u \qquad \textit{Eq. 5-6}$$

For the axisymmetric condition in a triaxial test, the matrix $\boldsymbol{D'}$ is a 4×4 elastic stress-strain matrix in terms of effective Young's modulus ($\boldsymbol{E}$) and Poisson's ratio ($\boldsymbol{\mu}$)

$$D' = \frac{E(1-\mu)}{(1+\mu)(1-2\mu)} \begin{bmatrix} 1 & \frac{\mu}{1-\mu} & 0 & \frac{\mu}{1-\mu} \\ \frac{\mu}{1-\mu} & 1 & 0 & \frac{\mu}{1-\mu} \\ 0 & 0 & \frac{1-2\mu}{2(1-\mu)} & 0 \\ \frac{\mu}{1-\mu} & \frac{\mu}{1-\mu} & 0 & 1 \end{bmatrix} \qquad \textit{Eq. 5-7}$$

The matrix D_u contains the apparent bulk modulus of the fluid K_w in the following locations.

$$D_u = \begin{bmatrix} K_w & K_w & 0 & K_w \\ K_w & K_w & 0 & K_w \\ 0 & 0 & 0 & 0 \\ K_w & K_w & 0 & K_w \end{bmatrix} \qquad \textit{Eq. 5-8}$$

assuming that the third column corresponds to the shear terms in the axisymmetric analysis.

To implement this method in the finite element program, it is necessary to form the global stiffness matrix using the total stress-strain matrix D, while effective stresses for use in the failure function are computed from total strains using the effective stress-strain matrix D'. Pore pressure are simply computed from

$$u = K_w(\varepsilon_r + \varepsilon_z + \varepsilon_\theta) \qquad \textit{Eq. 5-9}$$

The method has been widely applied in finite element method to simulate the undrained analysis for soil materials and satisfactory results have been obtained. Different soil models can be adopted in the undrained analysis, e.g. the elastic-perfectly plastic Mohr-Coulomb model and the modified Cam-Clay model. Smith and Griffiths (1998) produced an example of undrained analysis combined with the Mohr-Coulomb model in their finite element program, which will be discussed in detail in Chapter 7.

5.4 Linear Mobilised Tensile Stress Analysis (LMTSA)

As in the undrained analysis for saturated soils discussed above, the randomly distributed fibre reinforced material (e.g. randomly distributed fibre reinforced soil, waste material) can also be separated to a two-phase particulate material in which fibres are distributed randomly and uniformly in the matrix. It should be noted that only the dry material (i.e. drained condition) is considered in this study. Strains are assumed to be compatible between the two phases as in the undrained analysis for saturated soils. Fibre reinforcing components are only capable of sustaining tensile stress, which means they are effective only when the normal strains are tensile. Figure 5-3

presents the boundary condition of a randomly distributed fibre reinforced material sample under axisymmetric compressive loading. Fibres are only effective horizontally rather than vertically because the horizontal strain is tensile but vertical strain is compressive in this boundary condition. Therefore, fibre reinforcing particles provide an extra support (σ_f) to the matrix material horizontally. A same amount of stress with reversed direction ($-\sigma_f$) is sustained by fibres horizontally.

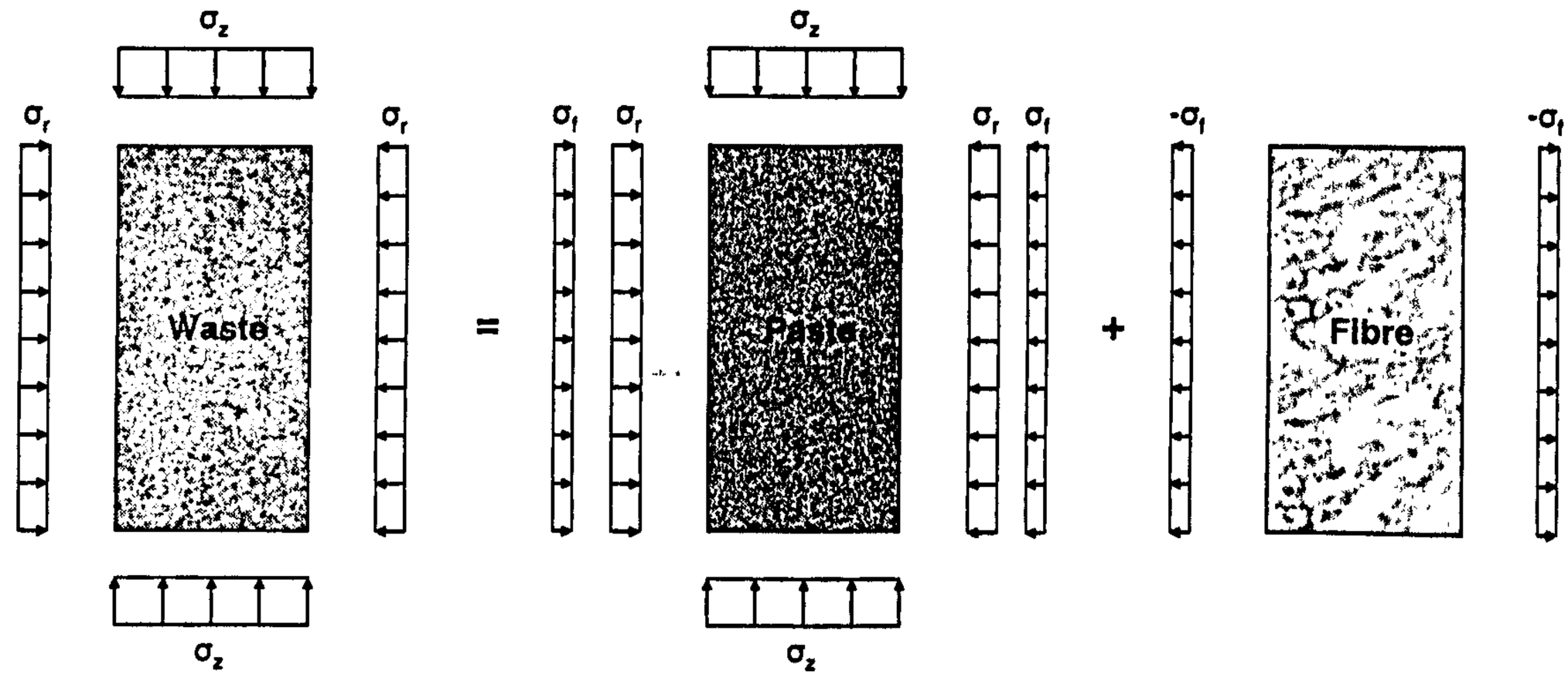

Figure 5-3 Boundary conditions of the conventional triaxial compression test on a randomly distributed fibre reinforced material sample

Based upon the analysis above, the effective stresses on matrix material in this situation can be expressed as:

$$\sigma'_r = \sigma_r + \sigma_f \qquad \textit{Eq. 5-10}$$

$$\sigma'_a = \sigma_a \qquad \textit{Eq. 5-11}$$

$$\tau'_{rz} = \tau_{rz} \qquad \textit{Eq. 5-12}$$

$$\sigma'_\theta = \sigma_\theta + \sigma_f \qquad \textit{Eq. 5-13}$$

which can be presented in matrix notation as follows:

$$\sigma'_{ij} = \sigma_{ij} + \delta_{ij}\beta_i\sigma_f \qquad \textit{Eq. 5-14}$$

where δ_{ij} is the Kronecker delta which is the same as that in the undrained analysis, and β_i is the fibre effective factor, which can be expressed as:

$$\beta_i = 1,\ \varepsilon_{ij} > 0;\ \beta_i = 0,\ \varepsilon_{ij} \le 0 \qquad \textit{Eq. 5-15}$$

The fibre effective factor β_i ensures that fibres are only effective in the directions where the macroscopic strains are tensile.

The effective (for the matrix) and total stress-strain relationships are the same as those in the undrained analysis for saturated soils, which have been shown in Eq. 5-3 and 5-5. The stress-strain relationship for the fibre reinforcing components is:

$$\delta\sigma_f = -D_f \delta\varepsilon_{ij} \qquad \textit{Eq. 5-16}$$

Therefore, the total stress-strain matrix $\boldsymbol{D}$ is:

$$D = D' + D_f \qquad \textit{Eq. 5-17}$$

The matrix $\boldsymbol{D_f}$ can be expressed as follows for the axisymmetric boundary condition:

$$D_f = \begin{bmatrix} \beta_1 K_{fe} & 0 & 0 & 0 \\ 0 & \beta_2 K_{fe} & 0 & 0 \\ 0 & 0 & 0 & 0 \\ 0 & 0 & 0 & \beta_4 K_{fe} \end{bmatrix} \qquad \textit{Eq. 5-18}$$

For the conventional triaxial compression test shown in the figure, the effective fibre factor can be more specific as:

$$\beta_1 = \beta_4 = 1,\ \beta_2 = 0 \qquad \textit{Eq. 5-19}$$

K_{fe} is the equivalent mobilised tensile stiffness of all the fibre contribution to the composite material. Generally, its value is dependent on both the properties of fibres themselves and the fibre/matrix interaction. In the following section, a method to obtain the equivalent mobilised tensile stiffness will be proposed.

5.5 Equivalent Mobilised Tensile Stiffness K_{fe}

Based on the principle of undrained analysis for saturated soils, the linear mobilised tensile stress analysis (LMTSA) has been produced to model the influences of the fibre reinforcing components. A critical parameter for the LMTSA is the equivalent mobilised tensile stiffness K_{fe}, which can be obtained through integrating the contribution of every single effective fibre together. In this section, the relationship between the equivalent mobilised tensile stiffness and the single fibre stiffness will be established for the two sub-analyses, i.e. LMTSA-E and LMTSA-P, according to different assumptions for the mobilised tensile stress-strain relationship in fibre reinforcing components.

5.5.1 Equivalent Tensile Stiffness for LMTSM-E

In order to determine the equivalent mobilised tensile stiffness, initially the contribution of a single fibre should be considered so that the total contribution could be calculated by integration of the contribution from each single fibre. A single fibre with a certain orientation will be investigated as shown in Figure 5-4. Assuming the tensile stiffness of this fibre is K_f, then the tensile stress in the mobilised fibre is:

$$\delta\sigma_t = K_f \delta\varepsilon_t \qquad \textit{Eq. 5-20}$$

where $\delta\varepsilon_t$ is the incremental tensile strain of the fibre. In fact, it presents a linear elastic constitutive relationship for a single fibre. For the LMTSA, the fibre strain is assumed to be equal to the matrix strain in the direction of the fibre orientation. Another reasonable assumption is made here that the matrix strain in the direction of a single fibre inclined at θ to the horizontal is equal to the macroscopic strain in the direction ε_θ for the whole sample, therefore

$$\delta\sigma_t = K_f \delta\varepsilon_\theta \qquad \textit{Eq. 5-21}$$

which is the stress contribution from a single fibre. It can then be integrated across the whole sample to calculate the equivalent mobilised tensile stiffness.

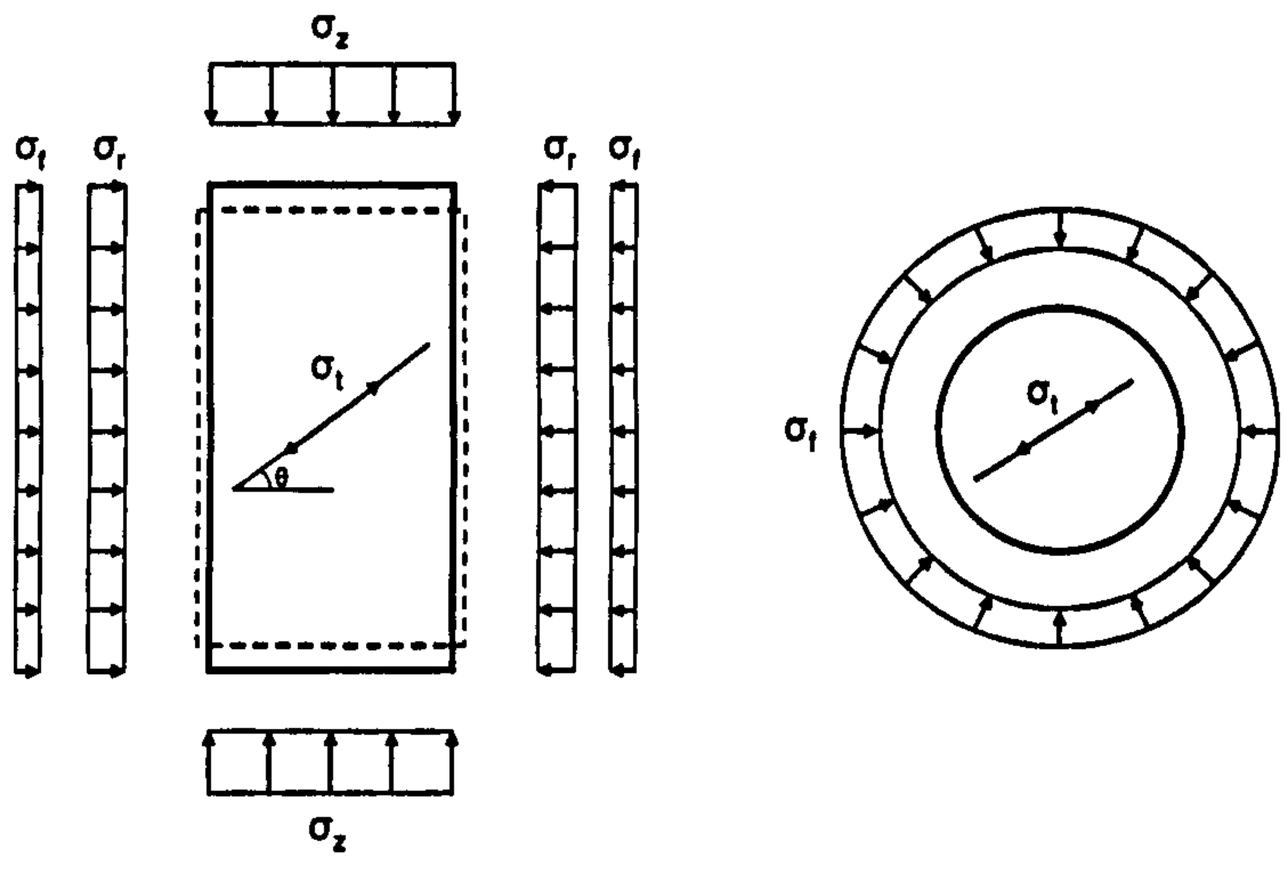

Figure 5-4 A single fibre stress analysis

Before the integration, it is noticed that not all the fibres in the sample are in tension under the conventional triaxial compression loading. Therefore, the integration should be performed only over the fibres subjected to tension. The method proposed by Michalowski and Cermak (2003) is adopted to separate fibres subjected to tension and compression in order to perform the integration only over the fibres subjected to tension. To perform this integration in a uniformly deforming cylindrical specimen, an integration space is introduced where all fibres are moved to the origin in

a parallel manner as shown in Figure 5-5 (c). Michalowski and Cermak (2003) pointed out that such a transformation does not affect the work dissipation rate, because in the uniform deformation field dissipation depends only on the orientation of the fibres and not their location in the specimen (and it is also independent of the shape of the specimen). These assumptions are also applicable for the integration of fibre stress contribution.

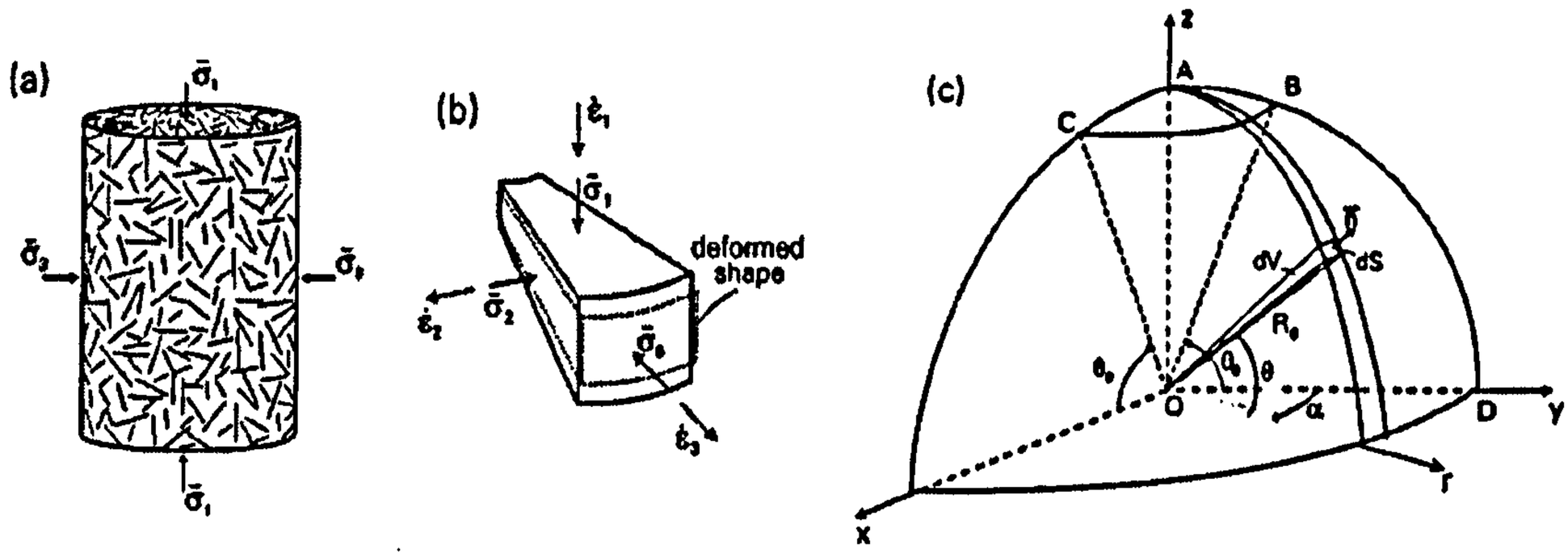

Figure 5-5 Axisymmetric compression: (a) specimen; (b) deformation element; and (c) integration space (Michalowski and Cermak, 2003)

The conical surface ***OCB*** separates all fibres under compression (above the surface) from those under tension, which is shown in Figure 5-5 (c). The inclination angle θ_0 of this surface to the horizontal was calculated from the requirement that strain in the direction of fibres coinciding with this surface is equal to zero. The incremental strain in any direction can be expressed by axial and radial strains as:

$$\delta\varepsilon_\theta = \delta\varepsilon_1 \sin^2\theta + \delta\varepsilon_3 \cos^2\theta \qquad \textit{Eq. 5-22}$$

In the direction where $\theta=\theta_0$, strain becomes zero, so it can be deduced that:

$$\tan^2\theta_0 = -\frac{\delta\varepsilon_3}{\delta\varepsilon_1} \qquad \textit{Eq. 5-23}$$

According to the stress dilatancy relationship for the Mohr-Coulomb yield condition, the relationship between axial and radial incremental strain for triaxial compression can be expressed as:

$$\frac{\delta\varepsilon_3}{\delta\varepsilon_1} = -\frac{1}{2}K_\psi \qquad \textit{Eq. 5-24}$$

Combining these two equations, the inclination angle was obtained by Michalowski and Cermak (2003):

$$\theta_0 = \tan^{-1}\sqrt{K_\psi / 2} \qquad \textit{Eq. 5-25}$$

in which

$$K_\psi = \frac{1+\sin\psi}{1-\sin\psi} \qquad \textit{Eq. 5-26}$$

where ψ is the dilation angle of the paste material.

As soon as the critical angle θ_0 is obtained, horizontal stress contributed by all the fibres can be integrated from the contribution of a single fibre (Eq. 5-21). The number of fibres in volume V of the composite can be written as $\rho V / \pi r^2 l$, where ρ is the fibre volumetric concentration, r is the radius of the fibre and l is the length of the fibre. A general form for the total fibre force horizontally in axisymmetric compression per unit volume can be expressed as:

$$T = \frac{1}{(1/6)\pi R_0^3}\int_V \frac{K_f \rho \varepsilon_\theta \cos\theta}{l} dV \qquad \textit{Eq. 5-27}$$

where R_0 is the radius of the integration space. In the equation, only $\int_V \varepsilon_\theta \cos\theta dV$ needs to be evaluated for axisymmetric compression. A closed-form solution to the integral has been found:

$$\int_V \delta\varepsilon_\theta \cos\theta dV = \frac{1}{6}\pi R_0^3 \cdot \frac{1}{8K_\psi}\left[(3K_\psi + 2)\sin\theta_0 \cos\theta_0 + (3K_\psi - 2)\theta_0\right] \qquad \textit{Eq. 5-28}$$

then the total fibre force per unit volume in Eq. 5-27 becomes:

$$T = -\frac{K_f \rho N_0}{l}\varepsilon_r \qquad \textit{Eq. 5-29}$$

where N_0 is a factor expressed as:

$$N_0 = \frac{1}{8K_\psi}\left[(3K_\psi + 2)\sin\theta_0 \cos\theta_0 + (3K_\psi - 2)\theta_0)\right] \qquad \textit{Eq. 5-30}$$

Considering the balance condition for a triaxial compression sample shown in Figure 5-3, the total fibre force per unit volume can be expressed by the total mobilised tensile stress σ_f as:

$$T = \frac{\sigma_f A_s}{V_s} = \frac{2\sigma_f}{R} \qquad \textit{Eq. 5-31}$$

where A_s is the side surface area of the cylindrical sample, V_s is the volume of the sample and R is the radius of the sample. Combining Eq. 5-29 and Eq. 5-31, the equivalent horizontal support can be obtained as:

$$\sigma_f = \frac{R\rho N_0}{2l} K_f \varepsilon_r \qquad \textit{Eq. 5-32}$$

Therefore, the equivalent tensile stiffness can be calculated from the stiffness of a single fibre:

$$K_{fe} = \frac{R\rho N_0}{2l} K_f \qquad \textit{Eq. 5-33}$$

The ratio of K_e to K_{fe} can be identified by a reduction factor ξ:

$$\xi = \frac{R\rho N_0}{2l} \qquad \textit{Eq. 5-34}$$

This factor characterises the reduction of a single fibre tensile stiffness to the tensile stiffness for the whole specimen under axisymmetric loading, assuming a linear elastic stress-strain relationship for fibres. It appears the reduction factor ξ depends on three parameters; the fibre volume content ρ, the ratio of the specimen radius to the fibre length R/l, and the critical angle to separate fibres under tension/compression θ_0. It is not surprising that the reduction factor is bigger with higher fibre content and larger critical angle. It seems a little difficult to understand the influence of the ratio R/l on the reduction factor ξ at the first glance. With larger ratio of R/l, i.e. larger sample size or shorter fibre length, the fibre amount becomes more so that the total fibre force can be increased. It can be deduced that, with shorter fibres without any limitation, the fibre reinforcing components are more effective, which is not true. There should be a lowest bound limitation for the length of a fibre that provides the necessary anchorage of the fibre ends, which depends on the interface between the fibre and the surround material (e.g. sand in fibre reinforced sand). Since the interaction between fibres and paste is not considered in the LMTSA, the anchorage information cannot be included in the equations. Moreover, the equivalent mobilised tensile stiffness is not influenced by the radius of the fibre due to the same reason. The contact area between a fibre and paste is obviously dependent on both length and radius of the fibre, which should be considered in a future study.

Triaxial tests on fibre reinforced sand (Michalowski and Cermak, 2003) are used to justify the calculation of the equivalent mobilised tensile stiffness K_{fe} for the LMTSM-E. A typical group of parameters for fine sand with polyamide fibres has been selected, ρ=0.5%, R=47.25mm, l=25.4mm and the internal friction angle ϕ=38°, then θ_0 can be calculated as 55.4°. The reduction factor ξ is calculated by Eq. 5-34 as 2.36×10^{-3}. It should be noted that, Michalowski and Cermak

(2003) assumed the normality rule for the sand, which means the dilation angle ψ and the internal friction angle ϕ have the same values. The relationship between ξ and ψ(or ϕ), ξ and θ_0 have been plotted in Figure 5-6, in which the factor increases with both angles. It can be seen that the reduction factor is not sensitive to the friction angle within its typical range, the value is 2.25×10^{-3} for 30° and 2.61×10^{-3} for 60°. It is not necessary to plot the relationship of the factor ξ with fibre content ρ and the ratio R/l because they are obviously linear.

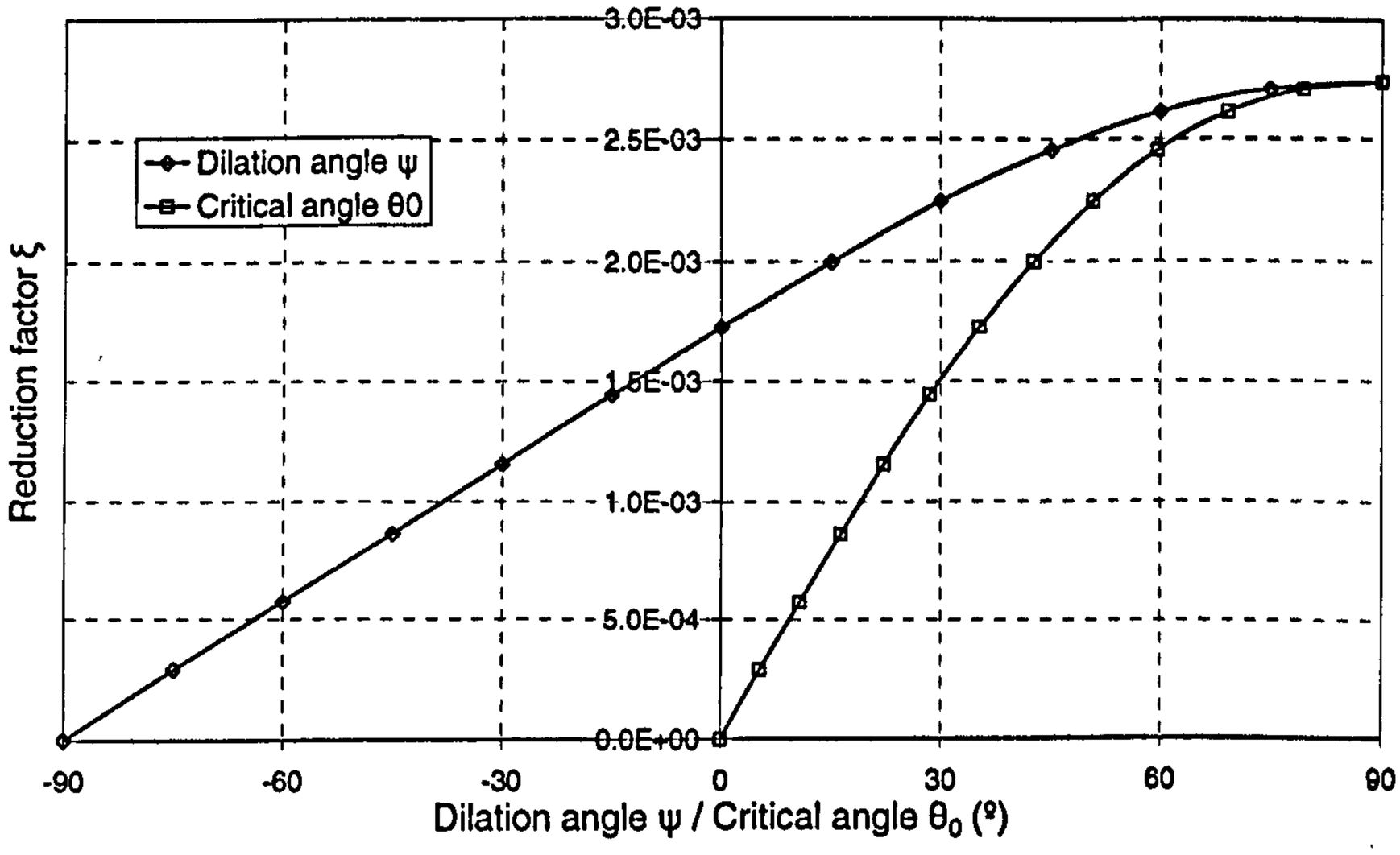

Figure 5-6 Relationship between the reduction factor ξ and the dilation angle/critical angle

Once the reduction factor is determined, the equivalent fibre tensile stiffness K_{fe} can be obtained from the single fibre tensile stiffness K_f. Three types of fibres were used by Michalowski and Cermak (2003) in reinforced sand: polyamide monofilament, steel galvanized wire, and polypropylene fibrillated fibres. However, there is no information on the tensile stiffness of any fibre material mentioned in the paper. Young's modulus for steel material is about 2×10^8 kPa. Therefore, the equivalent tensile stiffness for the steel fibre sand can be calculated as 5×10^5 kPa using Eq. 5-33. If Young's modulus of the sand is assumed to be 2.5×10^3 kPa, the equivalent tensile stiffness seems too large to provide a sensible fibre effect. It is not surprising since the big difference between stiffness of fibres and sand particles leads to strain incompatibility between the two phases, while strain compatibility was assumed for this linear analysis. Therefore, it is impossible to directly obtain the equivalent tensile for the steel fibre sand. While for the polyamide fibre sand, if the Young's modulus for polyamide material is assumed as 1×10^5 kPa, the equivalent tensile stiffness can be calculated as 236 kPa, which is within a more reasonable range (it is very close to the back analysis results shown in section 5.6). It is suggested that for the polyamide fibre reinforced sand the equivalent tensile stiffness can be calculated using Eq. 5-33 assuming strain compatibility between fibres and sand.

5.5.2 Equivalent Tensile Stiffness for LMTSA-P

A failure criterion for fibre reinforcing components, or between fibre and matrix (i.e. fibre failure criterion) is required for the LMTSA-P. A single fibre will be considered firstly as in the LMTSA-E. Linear elastic properties (Eq. 5-20) have been assumed for a single fibre, and strain compatibility between fibre and matrix (Eq. 5-21) has been also assumed. An elastic-perfectly plastic constitutive relationship has been assumed for a single fibre under one-dimensional tension, which is shown in Figure 5-7 (a). σ_{fu} and ε_{fu} are the ultimate stress and strain for a single fibre, respectively. The stress-strain relationship can be expressed by

$$\sigma_t = \begin{cases} K_f \varepsilon_\theta, & \varepsilon_\theta < \varepsilon_{\theta u} \\ K_f \varepsilon_{\theta u}, & \varepsilon_\theta \geq \varepsilon_{\theta u} \end{cases} \qquad \textit{Eq. 5-35}$$

As mentioned in section 5.5.1, fibres with inclined angles to the horizontal plane less than the critical angle θ_0 are in tension and their tensile stress can provide extra horizontal support to the triaxial sample. Since the sample expands horizontally and compresses vertically, it is obvious that fibres with lower critical angles reach their yield stress earlier than those with higher critical angles. Consequently, fibres distributed horizontally yield at the first, and fibres with inclined angles yield consecutively as the angle increases. A maximal horizontal support from fibres can be integrated from every single fibre with its yield stress.

Through the above analysis, it is possible to obtain the equivalent tensile stress-strain relationship for the whole sample. This relationship would not be as linear as a single fibre because fibres in different directions would reach yield under different strain levels. However, in the LMTSA-E, the equivalent tensile stiffness has been assumed to be a constant, which represents a linear elasticity relationship. This is because only a total force balance, assuming no yield occurs in any fibre, has been considered to establish the relationship between K_f and K_e (Eq. 5-25 and Eq. 5-26). Therefore, if every single fibre is assumed to reach a yield stress, this yield stress level is the maximum possible contribution to confine the sample horizontally. The equivalent tensile stress provided by fibres needs to be amended accordingly. Three stages need to be considered according to the failure of a single fibre, which is shown in Figure 5-7 (b):

I No fibre reaches the yield stress;

II Part of the fibres reach the yield stress;

III All of the fibres in tension reach the yield stress.

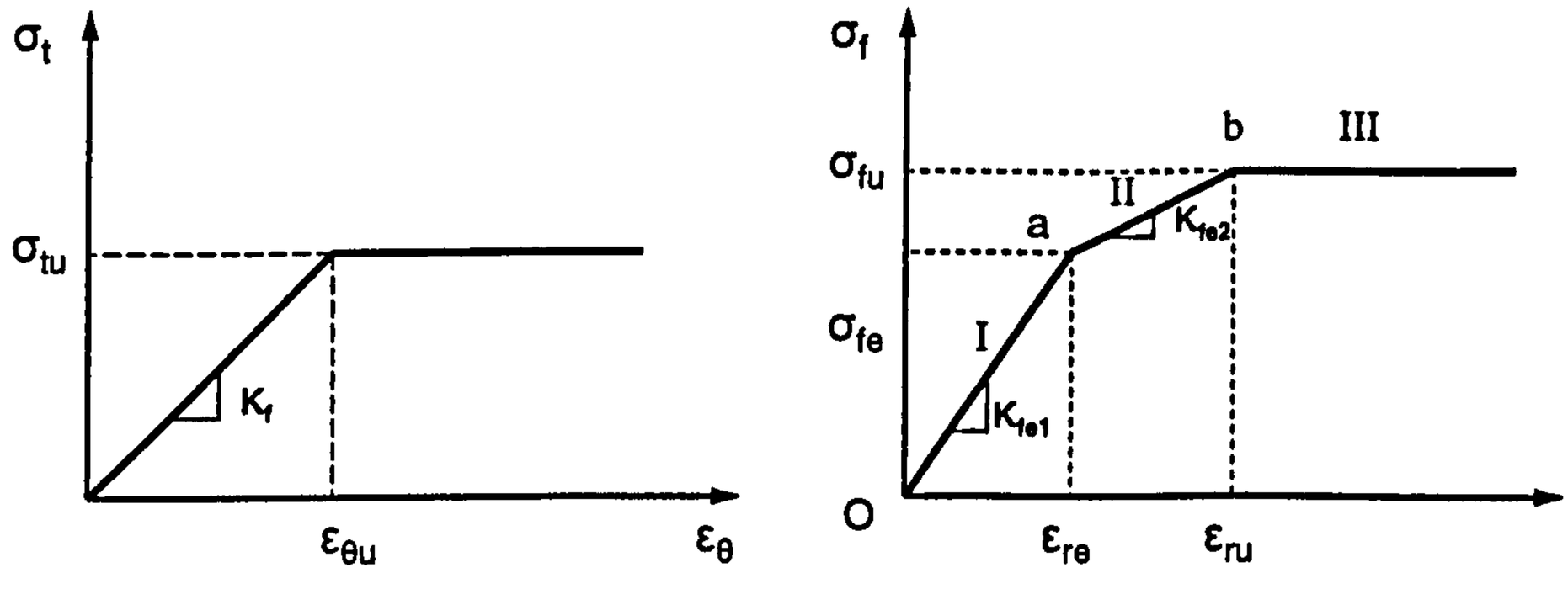

(a) *(b)*

Figure 5-7 Fibre failure criterion (a) single fibre; (b) fibre contribution

The stiffness for stage I and II are assumed to be constant as a start point, which is not true. Two critical states, point a and b in the figure, need to be investigated to separate the three stages. At point ***a***, fibres in the horizontal plane are reaching their yield stress, the horizontal support fibres can provide is reaching its ultimate elastic value σ_{fe}. At point ***b***, fibres with critical angel θ_0 are reaching their yield stress, all the fibres giving horizontal support are entering their plastic status, and the support fibres can provide is reaching its maximal value σ_{fu}. These two ultimate stress values could be calculated by integrating stresses of the individual fibre for the respective integration space (Figure 5-5). The equivalent stiffnesses for stages I and II can be obtained by assuming linear stress-strain relationship for simplification.

From Eq. 5-28, the expression of support stress provided by fibres is:

$$\sigma_f = \frac{R\rho N_0}{2l} K_f \varepsilon_r \qquad \textit{Eq. 5-36}$$

At point a:

$$\sigma_{fe} = \frac{R\rho N_0}{2l} K_f \varepsilon_{re} \qquad \textit{Eq. 5-37}$$

in which ε_{re} is the horizontal (radial) strain of the sample at point ***a***. It is equal to the ultimate elastic strain of a single fibre because horizontal fibres are reaching yield stress at this point:

$$\varepsilon_{re} = \varepsilon_{\theta u} \qquad \textit{Eq. 5-38}$$

Therefore, the equivalent tensile stiffness for stage I is:

$$K_{fe1} = \frac{\sigma_{fe}}{\varepsilon_{fe}} = \xi K_f \qquad \textit{Eq. 5-39}$$

which is equal to that of the linear model.

At point ***b***, all fibres under tension are in a plastic state:

$$\sigma_{fu} = \frac{RK_f\rho}{2l}\frac{1}{(1/6)\pi R_0^3}\int_V \varepsilon_{\theta u}\cos\theta \cdot dV = \frac{RK_f\rho(\sin\theta_0\cos\theta_0+\theta_0)}{3l}\varepsilon_{\theta u} \qquad \textit{Eq. 5-40}$$

in which $\varepsilon_{\theta u}$ is the ultimate elastic strain for a single fibre. When fibres with critical angle θ_0 reach their ultimate elastic strain, the horizontal (radial) strain of the sample can be expressed as:

$$\varepsilon_{ru} = \frac{K_\psi}{K_\psi\cos^2\theta_0 - 2\sin^2\theta_0}\varepsilon_{\theta u} \qquad \textit{Eq. 5-41}$$

Therefore, combining the above two equations, the equivalent tensile stiffness for stage II is:

$$K_{fe2} = \frac{\sigma_{fu}-\sigma_{fe}}{\varepsilon_{ru}-\varepsilon_{re}} = \varsigma K_f \qquad \textit{Eq. 5-42}$$

in which

$$\varsigma = \frac{[3R\rho N_0 - 2R\rho(\sin\theta_0\cos\theta_0+\theta_0)](K_p\cos^2\theta_0 - 2\sin^2\theta_0)}{6l(K_p - K_p\cos^2\theta_0 - 2\sin^2\theta_0)} \qquad \textit{Eq. 5-43}$$

It has been noticed that ς is a very small value (e.g. 10^{-19}) for the case studied in the LMTSA-E section. This is due to the radial strain (Equation 36) that causes the yield of fibres with critical angle being nearly infinity, which leads the average stiffness to be a rather small value nearly zero. If we consider a general situation that fibres with angle θ ($0<\theta<\theta_0$) reach the yield stress, total fibre tensile stress horizontally is:

$$\sigma_f = \frac{RK_f\rho}{2l}\frac{1}{(1/6)\pi R_0^3}\left(\int_{V1}\varepsilon_{\theta u}\cos\theta\cdot dV + \int_{V2}\varepsilon_\theta\cos\theta\cdot dV\right) \qquad \textit{Eq. 5-44}$$

in which V_1 is the partial volume of the integration space (Figure 5-5) from horizontal to θ, and V_2 is the volume of the space from θ to θ_0. Through integration, the stress can be expressed as:

$$\sigma_f = \frac{R\rho K_f}{2l}(N_0+N_1+N_2)\varepsilon_r \qquad \textit{Eq. 5-45}$$

in which

$$N_1 = \frac{1}{8K_\psi}(12K_\psi\cos^2\theta - 24\sin^2\theta - 9K_\psi - 6)\sin\theta\cos\theta \qquad \textit{Eq. 5-46}$$

$$N_2 = \frac{1}{8K_\psi}\left(12K_\psi \cos^2\theta - 24\sin^2\theta - 9K_\psi + 6\right)\theta \qquad \textit{Eq. 5-47}$$

For the LMTSA-E without a failure criterion, the factor N_0 is always a constant, which means a linear relationship between tensile stress and radical strain. However, the factor $N_0+N_1+N_2$ describing the stress-strain relationship after fibres yield is not a constant, and it is a function of the yield angle θ. Figure 5-8 shows the relationship between the factor and the yield angle for the same case that has been studied. It can be seen from the figure that the factor increases from θ=0 to θ=15° and decrease steadily to zero at the critical angle θ_0. This means the tensile stiffness increases slightly at the beginning of fibre yielding, but falls steadily after the peak value. When θ reaches its critical value θ_0, the stiffness goes to zero.

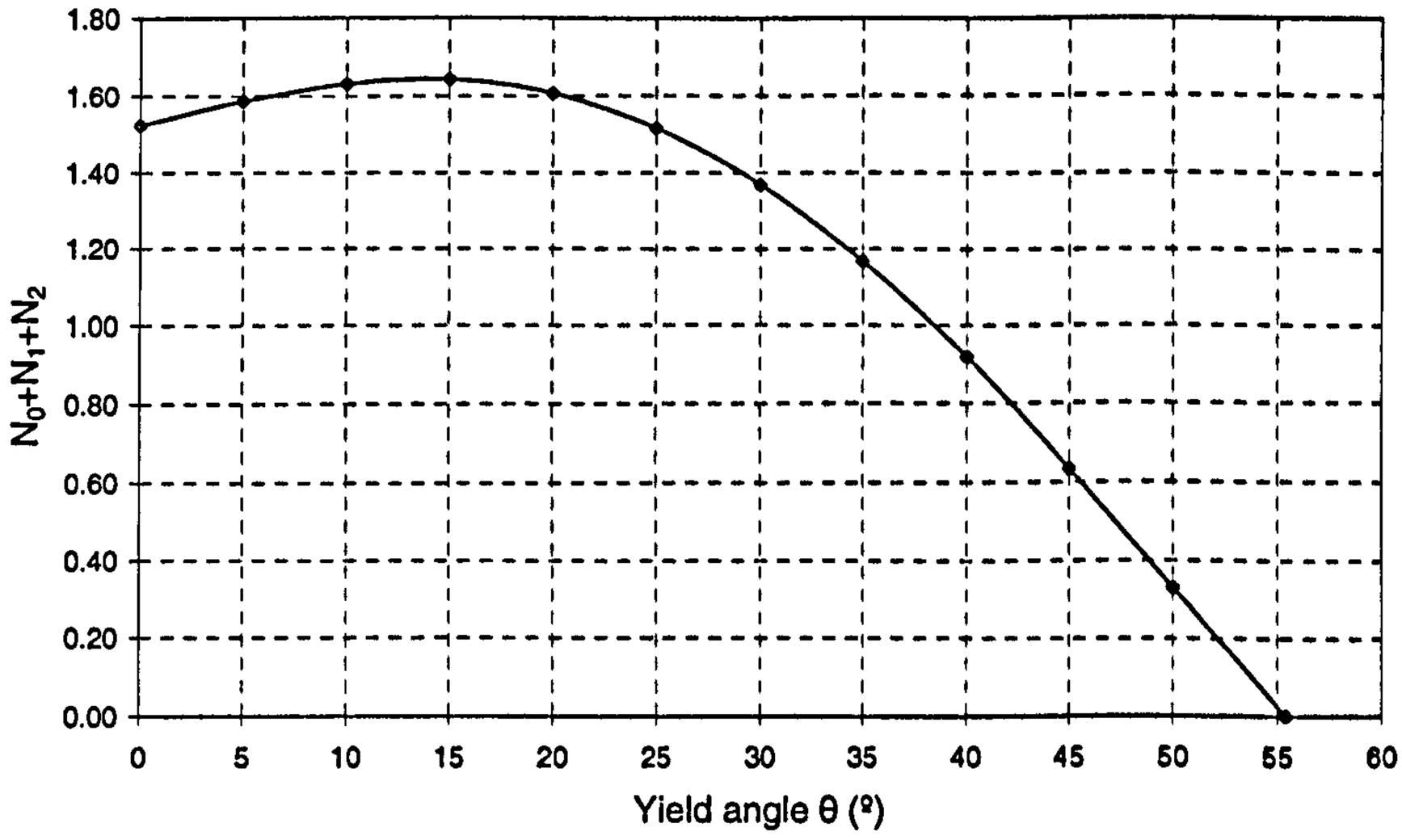

Figure 5-8 Relationship between factor $N_0+N_1+N_2$ and yield angle 0

Figure 5-9 shows the relationship between tensile stress provided by fibres and the radical strain, assuming the ultimate strain of each of the single fibre is 1%. It can be seen that, when the radial strain is less than the ultimate strain of the single fibre, the stress-strain relationship is linear as in the LMTSA-E described in section 5.5.1. As soon as the fibres start yielding, it produces a non-linear relationship, in which the stiffness increases at the beginning, but falls quickly afterwards, until the tensile stress reaches its ultimate value.

Assuming an elastic-perfectly plastic material model for all the fibres, a non-linear mobilised tensile stress-strain relationship has been obtained for the whole fibre reinforced material, as shown in Figure 5-9. It is more difficult to include this non-linear behaviour into LMTSA-P than including the constant equivalent mobilised tensile stiffness in LMTSA-E. To simplify the

analysis, an assumption has been made, that is, a constant equivalent mobilised tensile stiffness is assumed before the maximum total tensile stress has been reached, in which the non-linear behaviour is ignored but the failure is included. It can be seen from Figure 5-9 that the stress-strain curve can be modelled using a linear elastic-perfectly plastic like relationship.

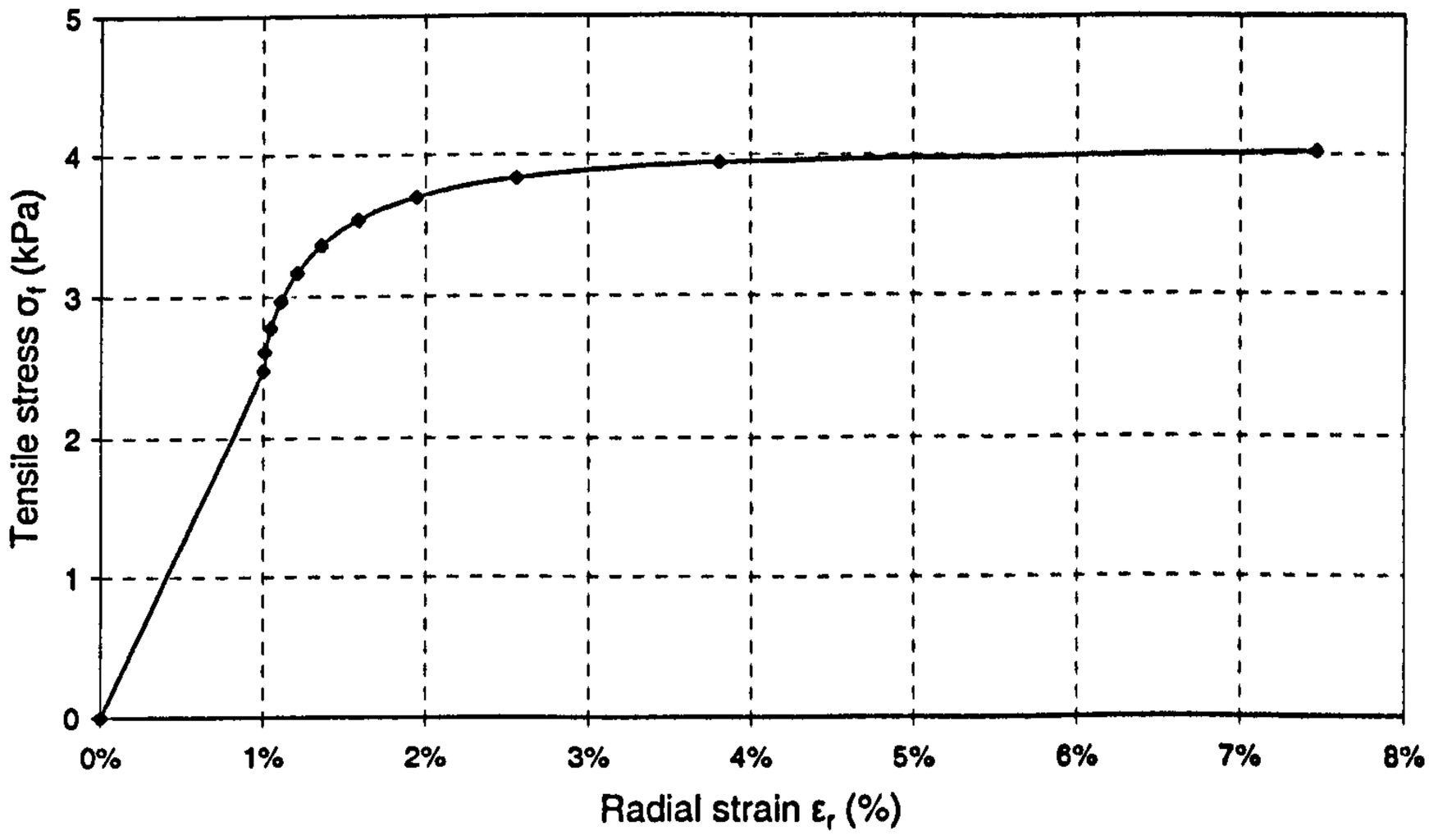

Figure 5-9 Relationship between tensile stress and radial strain

5.6 Validation of LMTSA-E-MC

Until now, the linear mobilised tensile analysis (LMTSA) has been presented, and the methods of calculating the equivalent mobilised tensile stiffness for the linear elastic and the elastic-perfectly plastic fibre material (LMTSA-E and LMTSA-P) have been proposed. To produce a constitutive model for a randomly distributed fibre reinforced material, a material model for the matrix is needed in which to incorporate the LMTSA-E or LMTSA-P analyses. In order to simply demonstrate the efficacy of the methodology, the elastic-perfectly plastic Mohr-Coulomb matrix material model has been combined with LMTSA-E, i.e. LMTSA-E-MC, through the finite element formulation and validated with the fibre reinforced sand triaxial data from Michalowski and Cermak (2003). The detailed finite element implementation process will be presented in Chapter 7.

Results from the Mohr-Coulomb model for pure sand and the Michalowski's model for reinforced sand, have been reproduced in Table 5-1. In order to obtain an appropriate value for K_f, a back analysis has been performed through the finite element analysis (LMTSA-E-MC) at the first experimental data point (σ_3=50 kPa) for the sample with fibre volumetric content ρ=0.5%. The back analysis result is K_f=275 kPa, which is very close to the estimated value from polyamide fibre stiffness, which is 236 kPa as discussed in section 5.5.1 (it confirms the estimated value in

this case is in a reasonable range). Finite element analyses have been carried out for different confining stresses and the results have been given in Table 5-1 for comparison. The LMTSA-E-MC modelling results for fibre content ρ=0.5% have also been plotted in Figure 5-10 (a), compared with the Michalowski's model prediction and experimental results presented in Figure 2-19 (a). It can be seen from Figure 2-19 (a) that the LMTSA-E-MC results are very close to those of the Michalowski's model, in which the two curves are almost overlapped, and certainly they fit the experimental data well.

Table 5-1 Failure axial stresses (kPa) under different confining stresses predicted by different models

Confining stress	Mohr-Coulomb (kPa)	Fibre content	Michalowski's (kPa)	LMTSA-E-MC (kPa)
σ_3=50 kPa	210.2	ρ=0.5%	228.5	229.8*
		ρ=2%	302.9	295.8
σ_3=100 kPa	420.4	ρ=0.5%	457.0	458.9
		ρ=2%	605.8	591.6
σ_3=200 kPa	840.8	ρ=0.5%	913.9	917.2
		ρ=2%	1211.6	1182.5
σ_3=300 kPa	1261.1	ρ=0.5%	1370.9	1376.2
		ρ=2%	1817.4	1773.5
σ_3=400 kPa	1681.5	ρ=0.5%	1827.8	1833.9
		ρ=2%	2423.2	2365.0
σ_3=600 kPa	2522.2	ρ=0.5%	2741.7	2751.8
		ρ=2%	3634.8	3546.7

*Value from a back analysis.

Modelling results for a fibre content of ρ=2% are also give in Table 5-1 and plotted in Figure 5-10 (b), together with the Michalowski's model prediction and experimental results. Since only the fibre content is changed to be four times as high as the first case, the equivalent tensile stiffness is also four times higher than in the first case according to Eq. 5-33, i.e. K_f=1.1×10^3 kPa. It can be seen from the modelling curves of ρ=2% in Figure 5-10 (b) that, the LMTSA-E-MC modelling strengths are slightly lower than those of the Michalowski's model under higher confining stresses, which is closer to the experimental data.

The LMTSA-E-MC modelling appears to be able to accurately predict the strength of polyamide fibre reinforced fine sand samples under different confining stresses. It indicates that most of the fibres in these tests did not fail, either the fibres in tension or interfaces between fibres and sand, which is the primary assumption of the LMTSA-E-MC model. The LMTSA-P-MC model is required in cases where slippage between fibres and sand, or tensile failure happens in fibres as in

an elastic-perfectly plastic material. Further tests on fibre reinforce sand are required to validate the LMTSA-P-MC.

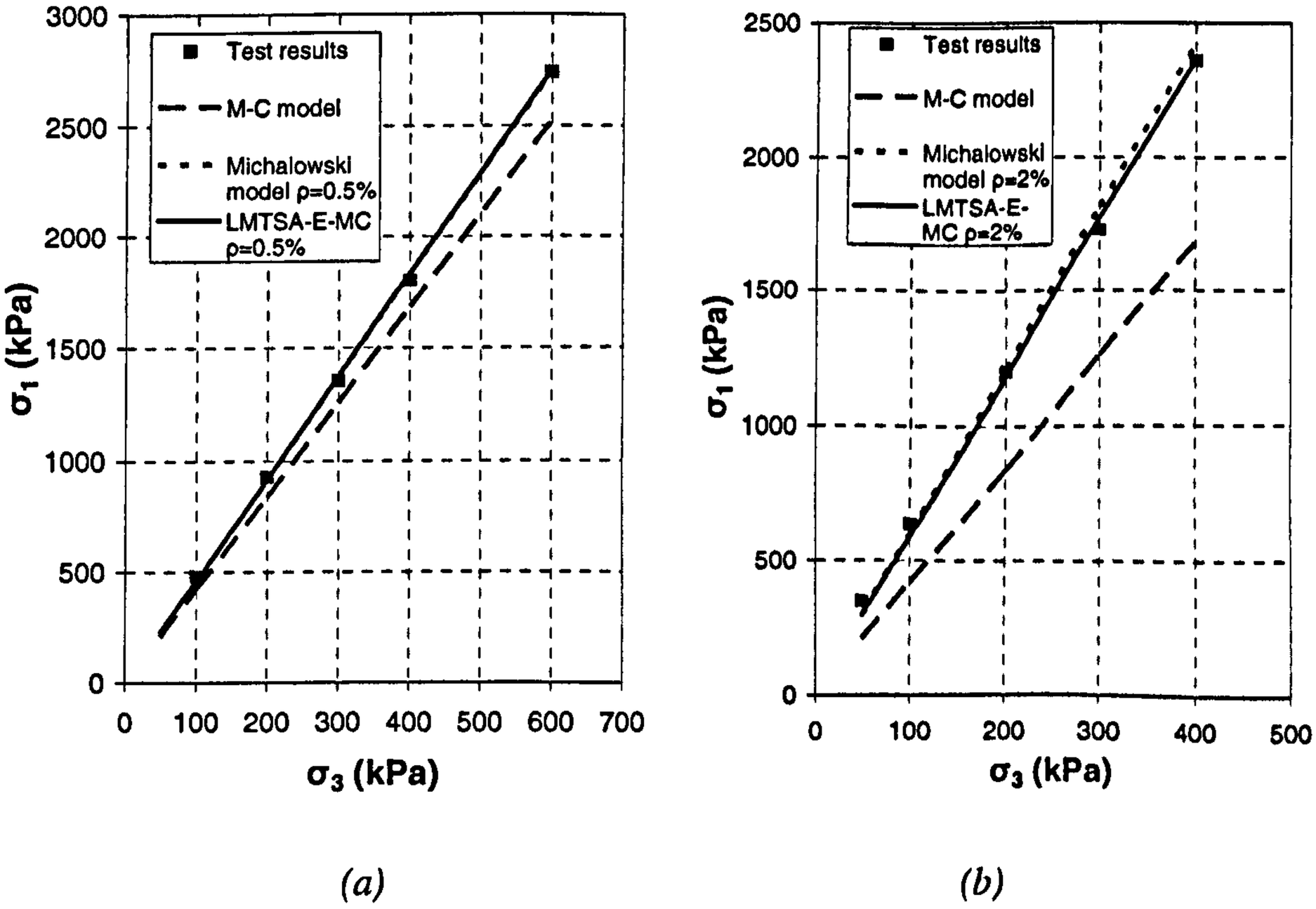

Figure 5-10 LMTSA-E-MC model prediction compared with Michalowski's model prediction and experimental results for fibre reinforced sand (a) ρ=0.5% and (b) ρ=2.0%

Although a complete sensitivity analysis has not been done here, it can be seen from both the test and modelling results that the fibre volumetric content ρ has a substantial influence on failure strength of the fibre reinforced material. Therefore, the fibre volumetric content can be considered as the most critical parameter of the fibre reinforcing model.

5.7 Discussion and Summary

Based on the idea of the effective stress theory in soil mechanics, a concept of mobilised tensile stress analysis to model fibre reinforced material has been proposed. Two types of the mobilised tensile stress analysis have been identified; the linear mobilised tensile stress analysis (LMTSA) and the non-linear mobilised tensile stress analysis (NMTSA). The LMTSA assumes strain compatibility between fibres and paste material, while the NMTSA does not. Only the LMTSA is included in the thesis, and the NMTSA is regarded as a future development.

A general framework to produce a randomly distributed fibre reinforced material model has been introduced. A fibre reinforcing model consists of a fibre material model and a matrix material model through a mobilised tensile stress analysis run in a finite element method program. For

example, the LMTSA-E-MC model combines the elastic fibre model (E) with the elastic-perfectly plastic Mohr-Coulomb model (MC) through the linear mobilised tensile stress analysis (LMTSA).

In order to develop the LMTSA, the principle of undrained analysis implemented in the finite element method for saturated soils was introduced. Saturated soil in an undrained analysis is considered as a two-phase material including soil skeleton and fluid, in which the fluid takes partial responsibility to sustain normal compressive stresses in any direction, while only effective stresses on solid particles can cause deformation of the soil skeleton and failure of the combined material. Similarly, the randomly distributed fibre reinforced material can also be considered as a two-phase material including paste and fibres, in which the fibres take partial responsibility to sustain tensile stresses in the direction that the combined material expands, for example the horizontal direction in the boundary condition of the conventional triaxial compression test. In other words, the fibres contribute an additional confining stress for the paste material, by which the combined material strength can be improved and the stress-strain relationship will be changed. In the undrained analysis, the pore pressure changes linearly with the total volume strain change, while in the LMTSA the fibre reinforcing confining stress changes linearly with the macroscopic tensile strain change in the specific direction.

Formulas of the LMTSA have been derived and presented following the route of the undrained analysis. A critical parameter, the equivalent mobilised tensile stiffness K_{fe}, is required to determine for the LMTSA. Methods of determining the equivalent mobilised tensile stiffness for two sub-analyses, i.e. LMTSA-E and LMTSA-P, have been presented. Different fibre material models have been appointed for the two sub-analysis, i.e. the linear elastic fibre model for LMTSA-E and the elastic-perfectly plastic fibre model for LMTSA-P. The equivalent mobilised tensile stiffness can be calculated from a single fibre stiffness by integrating every fibre's contribution through the whole sample.

A randomly distributed fibre reinforcing model LMTSA-E-MC has been proposed by combining the LMTSA-E with the elastic-perfectly plastic Mohr-Coulomb model for the matrix phase. It has been implemented in the finite element method program and validated using fibre sand triaxial compression test results from the literature. The model is able to predict the strength of fibre reinforced fine sand sample accurately. The advantages of the proposed model, as well as the method to produce the model can be summarised as follows:

1) An innovative method has been adopted to produce a constitutive model for the randomly distributed reinforced material. A constitutive model consists of a fibre phase model and a matrix phase model through mobilised tensile stress analysis, which can be executed in the finite element method program. Reviewing the literature on modelling shear behaviour of MSW, the model was presented in a clearer way with more reasonable physical and

mechanical meanings compared with the method proposed by Machado *et al.* (2002), and meanwhile the model has much less parameters compared with the mixture theory method proposed by Krase and Dinkler (2005);

2) The approach can be executed through the finite element method in a simple way similar to the undrained analysis for saturated soils. The finite element method is one of the most popular numerical methods in geotechnical engineering so that the model has a great prospect to be applied in real world problems;

3) The model and the approach are applicable for all kinds of fibre reinforced material, especially fibre reinforced soil and MSW, in which fibres are distributed randomly. Eventually, fibre reinforcing effects of this type of fibre reinforced material (an additional confining stress) can be modelled using this approach;

4) A method of obtaining the equivalent mobilised tensile stiffness for a randomly distributed fibre reinforce material has been proposed for the LMTSA, in which only the contribution of fibres in tension are counted. Both the linear elastic model and the elastic-perfectly plastic model for fibre material have been included.

Although the approach has the above advantages, it still needs to be improved in the following aspects, which should be covered in the following chapters or future development:

1) Interaction between fibres and paste—The LMTSA assumes strain compatibility (i.e. without interaction) between the two phases in the fibre reinforced material, which is not true (especially under the low normal stress condition when bond failure occurs). The NMTSA considering the interaction is recommended for future study;

2) Boundary condition—Only the axisymmetric stress condition (strictly speaking, the conventional triaxial compression condition) has been considered in this study. Further developments on extending the approach to the more general boundary conditions, e.g. plane strain and three dimensional cases are required;

3) Anisotropic behaviour—As mentioned earlier, horizontally layered fibres are likely to occur in waste placement, which results in waste anisotropic behaviour. Waste anisotropic behaviour study can be carried out through changing fibre orientations in the proposed model by integrating mobilised tensile stresses from different directions. More experimental work on anisotropy is suggested in the future to validate the anisotropic reinforcing model.

4) Stress-strain relationship—Although the LMTSA-E-MC has been validated with the experiment results on improved strength of fibre reinforced sand samples and these is a good agreement, the full stress-strain relationship (i.e. fibre reinforcing effects on shearing

behaviour) has not been modelled. In the following chapters, a more advanced material model for paste, i.e. the Modified Cam-Clay will be included in the approach to model the non-linear stiffness behaviour of reinforcing particles;

5) Waste material—The final model in this project will serve for the waste material rather than for fibre reinforced sand. Thus, some special considerations have to be included during producing a constitutive model for MSW, which will be discussed in Chapter 6.

CHAPTER

6

A Constitutive Model for MSW

6.1 Introduction

A one-dimensional compression model and a randomly distributed fibre reinforcing model have been developed in Chapter 4 and Chapter 5 respectively, to model the volumetric and shear behaviour of waste material. A constitutive model for MSW will be proposed in this chapter through combining the two models with a classic elasto-plastic soil constitutive model—the Modified Cam-Clay model (MCC). The analytical solution of the proposed model will be assessed using triaxial compression test results reported in the literature.

6.2 General Development of the MSW Constitutive Model

The MCC model (or the Cam-Clay model) is one of the first hardening plastic models that has become generally adopted for soils, as reviewed in section 2.4.3. It predicts the plastic volumetric change under isotropic compression, and couple volumetric strain with shear distortion. Moreover, it has a simple formulation and only five parameters are needed, which can be easily obtained from conventional laboratory tests. Developed half a century ago, the MCC model is still widely adopted to simulate soil behaviour in numerical modelling today.

The MCC model has been reviewed in section 2.4.3, in which the four essential components of the model, elastic properties, yield surface, flow rule and hardening rule are presented in detail. The one-dimensional compression model (CM) modifies the volumetric behaviour of the MCC, and the randomly distributed fibre reinforcing model (RM) alters the shear behaviour of the MCC according to waste behaviour reported in the literature. Using the MCC model as a base, the modified formulas for the MSW constitutive model are given below according to modification of CM and RM.

6.2.1 Volumetric Behaviour

Under isotropic compression, the virgin consolidation line and the swelling lines of the MCC model (Figure 2-21 (a)) are assumed to be both straight in v-lnp' space and have been described by the following equations in section 2.4.3:

$$v = N - \lambda \ln p' \qquad \textit{Eq. 6-1}$$

$$v = v_\kappa - \kappa \ln p' \qquad \textit{Eq. 6-2}$$

The values of κ, λ and N are characteristics of the particular type of soil, whereas the value of v_κ is different for each swelling line. Volume change along the virgin consolidation line is mainly irreversible or plastic, while volume change along a swelling line is reversible or elastic.

According to the CM proposed in Chapter 4, voids in waste are separated into inter-void (between particles) and intra-void (inside particles). Inter-void ratio e and intra-void ratio f were defined in Eq. 4-11 and Eq 4-10, assuming the total potential incompressible volume of waste particles is equal to unit. Therefore, when the volumetric strain is calculated in MSW model, both the inter and intra-void ratio change should be included. Volumetric strain due to inter-void ratio change can still be obtained by Eq. 6-1 and Eq. 6-2, in which all the parameters are only related to the inter-void ratio as they are in soil mechanics. The additional compression due to intra-void ratio change can be calculated from the following equations:

$$f = f_1 - \lambda_f \ln p' \qquad \textit{Eq. 6-3}$$

$$f = f_\kappa - \kappa_f \ln p' \qquad \textit{Eq. 6-4}$$

in which f_1 is the intra-void ratio value under unit pressure on the virgin consolidation line, and f_κ is the value on the swelling lines. λ_f and κ_f are the slopes of intra-void ratio change lines (virgin consolidation and swelling respectively) in v-lnp' plane, which can be calculated from the values of intra compression index $C_{C\text{-}Intra}$ and intra swelling index $C_{C\text{-}Intra}$ defined in section 4.3:

$$\lambda_f = \frac{C_{C-Intra}}{\ln 10} \qquad \textit{Eq. 6-5}$$

$$\kappa_f = \frac{C_{S-Intra}}{\ln 10} \qquad \textit{Eq. 6-6}$$

6.2.2 Shear Behaviour

Critical state soil models (including the MCC model) are coupled models between volumetric and shear strain, in which a flow rule is defined to characterise the ratio between incremental plastic volumetric strain and plastic shear strain, as shown in Chapter 2. Since waste shear behaviour is only coupled with the component of volumetric strain due to inter-voids change, as it is for soils, it is obvious that the volumetric strain caused by intra-voids compression should be excluded. This is the reason why the inter and intra-void ratio should be defined separately when the volumetric strain is calculated as described in section 6.2.1.

In addition, waste shear behaviour is affected by reinforcing particles comparable to randomly distributed fibre reinforced materials as described in Chapter 5. The RM proposed in Chapter 5 will be adopted for the waste constitutive model by combining it with the MCC model. At present, the RM can only be applied for the triaxial compression boundary value problem. The principle of the RM is that fibres can contribute a confining stress in the direction that particulate material (i.e. paste) expands. The effective shear stress in the paste, or the deviator stress q for the particular boundary condition can be reduced due to the fibre confining stress in one of the principal stress directions. This can result in the shear strength of the mixed material being increased, and meanwhile the stress-strain behaviour being altered. Since the current RM is restricted to the axisymmetric boundary condition, the combined waste model will also be restricted to the same boundary condition. More detailed model development under the triaxial compression boundary condition will be present in the following section.

6.3 MSW Constitutive Model under Triaxial Compression

The constitutive model for MSW will be developed under the triaxial compression boundary condition due to the reasons explained above. Firstly, analytical solutions for the MCC model under triaxial compression are derived. Subsequently, the compression and reinforcing models are combined with the MCC model respectively to demonstrate their efficacies in modelling the influences of compressible and reinforcing particles on MSW behaviour. Finally, the MSW model is produced and validated by the typical MSW triaxial compression test results.

6.3.1 Analytical Solutions for MCC

Analytical solutions for the MCC model under simple boundary conditions, e.g. drained triaxial compression and undrained triaxial compression, have been derived by Potts and Zdravkovic (1999), in which J-p' stress plane was adopted rather than q-p' plane. J is another form of the deviator stress expressed as:

$$J = \frac{1}{\sqrt{6}}\sqrt{(\sigma_1' - \sigma_2')^2 + (\sigma_2' - \sigma_3')^2 + (\sigma_3' - \sigma_1')^2} \qquad \textit{Eq. 6-7}$$

The MCC model will be combined with the compression and reinforcing model later in this chapter to develop a constitutive model for MSW. The MSW model will be validated by the drained triaxial compression test results on MSW samples reported by Machado *et al.* (2000). Therefore, only the drained triaxial compression boundary condition need to be considered in this chapter. In this section, the analytical solutions for the MCC model under drained triaxial compression are derived in the ***q-p'*** stress plane. The four essential components of the MCC model, namely elastic properties, yield criterion, flow rule and hardening rule, have been outlined in section 2.4.3.

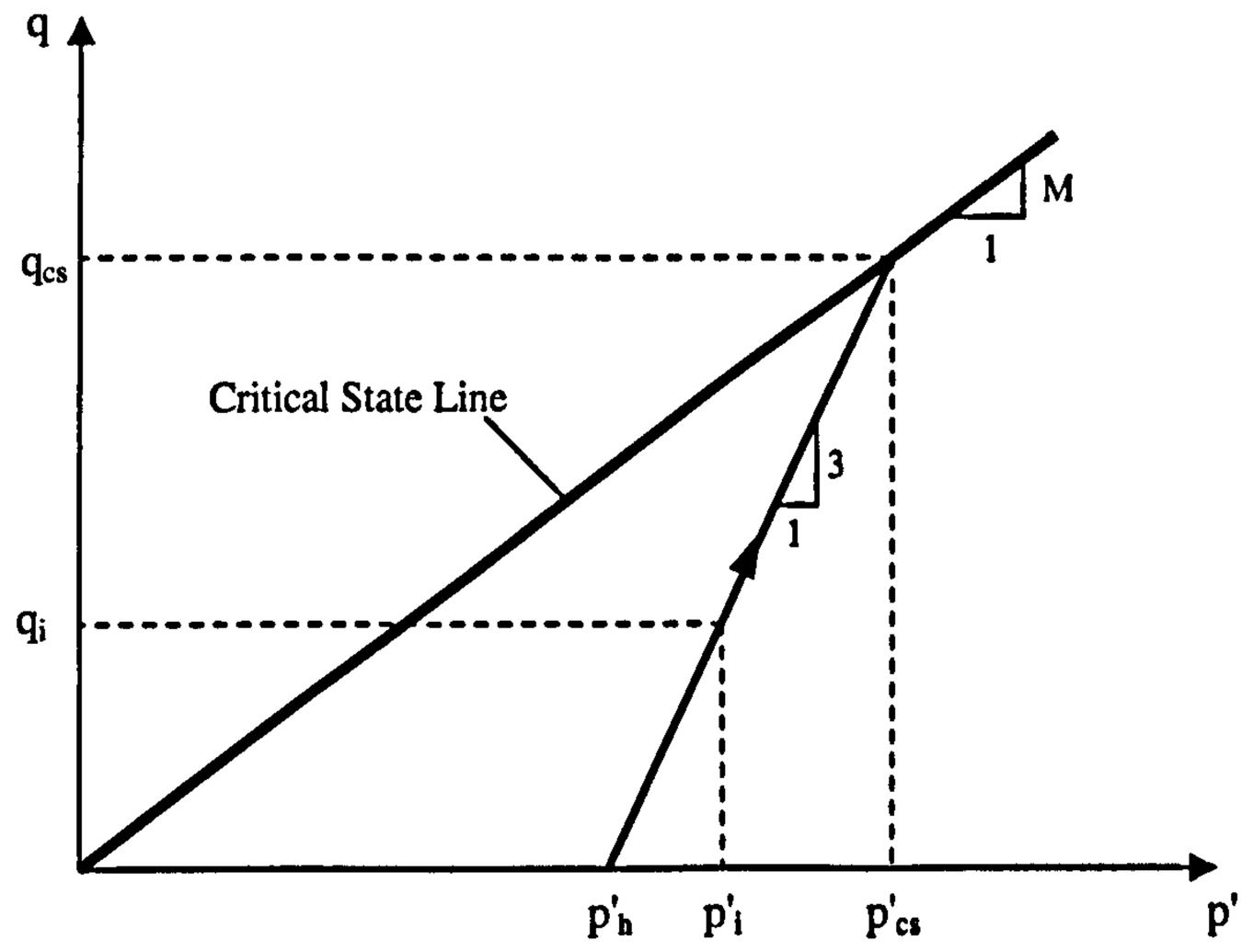

Figure 6-1 Stress path and critical state line of drained triaxial compression test

In the drained triaxial compression test, a cylindrical sample of soil is subjected to axial compression, while the radial total stress is maintained constant and no excess pore water pressures are allowed to develop. The initial stresses in the sample are given by p'_i and q_i. The stress path of the drained triaxial compression test is shown in Figure 6-1, which can be expressed as:

$$p' = \frac{q}{3} + p'_h \qquad \textit{Eq. 6-8}$$

$$\delta p' = \frac{1}{3}\delta q \qquad \textit{Eq. 6-9}$$

in which p'_h is the intercept of the stress path with the p' axis, as shown in Figure 6-1.

The analytical solutions given below include the values of volumetric strain ε_p and deviator strain ε_q (both elastic and plastic), associated with any current values of mean effective stress p'_c and deviator stress q_c. The critical state condition imposes limits on the values of p'_c and q_c. Stresses at critical state can be calculated from the intercept point of the stress path line and the critical state line, as shown in Figure 6-1:

$$q_{cs} = \frac{Mp'_h}{1-\frac{M}{3}} \qquad \textit{Eq. 6-10}$$

$$p'_{cs} = \frac{p'_h}{1-\frac{M}{3}} \qquad \textit{Eq. 6-11}$$

The elastic volumetric strain can be integrated from Eq. 2-28:

$$\varepsilon_p^e = \int_{p'_i}^{p'_c} \frac{\kappa}{v}\frac{dp'}{p'} = \frac{\kappa}{v}\ln\left(1+\frac{q_c-q_i}{3p'_i}\right) \qquad \textit{Eq. 6-12}$$

To calculate the elastic deviator strain, it is assumed that the shear modulus G is specified using a constant Poisson's ratio μ according to the discussion in section 2.4.3. Therefore, the elastic deviator strain can be integrated as:

$$\varepsilon_q^e = \int_{q_i}^{q_c} \frac{dq}{3G} = \frac{\kappa}{v}\frac{2(1+\mu)}{3(1-2\mu)}\ln\left(\frac{3p'_h+q_c}{3p'_h+q_i}\right) \qquad \textit{Eq. 6-13}$$

To predict the plastic strain (both volumetric and deviator strain), the initial yield stress (intersect between stress path and the initial yield surface) needs to be worked out because plastic straining only begins when the initial yield stress is reached. The position of the initial yield surface relative to the initial stress state depends on the overconsolidation ratio (*OCR*), which defines the initial value of p'_0 (i.e. p'_{0i}). The intersect point of the stress path and the initial yield surface can be obtained by solving the quadratic equation derived from Eq. 6-8 and 2-35 as below:

$$\frac{M^2+9}{9M^2}q^2 + \frac{2p'_h-p'_{0i}}{3}q + p'_h(p'_h-p'_{0i}) = 0 \qquad \textit{Eq. 6-14}$$

The initial yield deviator q_y is the positive root of the above equation:

$$q_y = \frac{-\frac{2p'_h - p'_{0i}}{\sqrt{3}} \pm \sqrt{\left(\frac{2p'_h - p'_{0i}}{3}\right)^2 - 4p'_h(p'_h - p'_{0i})\frac{M^2+9}{9M^2}}}{2\frac{M^2+9}{9M^2}} \qquad \textit{Eq. 6-15}$$

and the initial yield mean stress p'_y can be expressed as:

$$p'_y = \frac{q_y}{3} + p'_h \qquad \textit{Eq. 6-16}$$

The plastic volume strain can be calculated by substituting Eq. 2-36 and 6-8 into Eq. 2-40, and carrying out the integration from the initial yield stress to the current stress:

$$\varepsilon_p^p = \frac{\lambda-\kappa}{v}\int_{q_y}^{q_c}\left[-\frac{1}{3p'_h+q} + \frac{2(M^2+9)q+6M^2p'_h}{(M^2+9)q^2+6M^2p'_hq+9M^2p'^2_h}\right]dq$$

$$= \frac{\lambda-\kappa}{v}\left[-\ln(3p'_h+q)+\ln\left((M^2+9)q^2+6M^2p'_hq+9M^2p'^2_h\right)\right]_{q_y}^{q_c} \qquad \textit{Eq. 6-17}$$

The incremental plastic volumetric and deviator strains are related by Eq 2-38, which can be rewritten as follows (where Λ is the plastic scalar multiplier defined in section 2.4.1):

$$\delta\varepsilon_p^p = \Lambda\frac{\partial g}{\partial p'} = \Lambda(2p' - p'_0) \qquad \textit{Eq. 6-18}$$

$$\delta\varepsilon_q^p = \Lambda\frac{\partial g}{\partial q} = \Lambda\frac{2q}{M^2} \qquad \textit{Eq. 6-19}$$

Combining Eq. 6-18 with Eq. 2-35, 2-36 and 2-40 gives the following expression for the plastic scalar multiplier Λ:

$$\Lambda = \frac{\lambda-\kappa}{v}M^2\frac{2qp'\delta q + M^2p'^2q\delta p' - q^2\delta p'}{M^4p'^4 - q^4} \qquad \textit{Eq. 6-20}$$

Substituting the above equation into Eq. 6-18 and then removing the p' terms using the stress path equations Eq. 6-8 and Eq. 6-9, gives the following expression for the incremental plastic deviator strain:

$$\delta\varepsilon_q^p = \frac{\lambda-\kappa}{v}\left[\frac{-18p'_h}{(M^2+9)q^2+6M^2p'_hq+9M^2p'^2_h} + \frac{\frac{3}{M}}{3Mp'_h+(M+3)q} + \frac{\frac{3}{M}}{3Mp'_h+(M-3)q}\right]\delta q$$

Eq. 6-21

The plastic deviator strain for the current stress can be obtained by integrating the above equation from the initial yield stress to the current stress, which results in:

$$\varepsilon_q^p = \frac{\lambda-\kappa}{v}\left\{\begin{aligned}&-\frac{2}{M}\tan^{-1}\left[\frac{(M^2+9)q}{9Mp'_h}+\frac{M}{3}\right]+\frac{3}{M(M+3)}\ln\left(3Mp'_h+(M+3)q\right)\\&+\frac{3}{M(M-3)}\ln\left(3Mp'_h+(M-3)q\right)\end{aligned}\right\}_{q_y}^{q_e} \qquad \textit{Eq. 6-22}$$

An idealised drained triaxial compression test example, taken from Potts and Zdravkovic (1999), is considered to demonstrate the analytical solutions of the MCC model. A cylindrical sample is assumed to be isotropically normally consolidated to a mean effective stress of 200 kPa, with zero pore water pressure. The soil parameters used for the analysis, after transformation from ***J-p'*** plane to the ***q-p'*** plane, are listed in Table 6-1.

Table 6-1 Material properties for the MCC model

Overconsolidation ratio (***OCR***)	1.0
Specific volume at unit pressure on virgin consolidation line, ***N***	1.788
Slope of virgin consolidation line in ***v-lnp'*** plane, λ	0.066
Slope of swelling line in ***v-lnp'*** plane, κ	0.0077
Slope of critical state line in ***q-p'*** plane, ***M***	1.2
Poisson's ratio	0.3

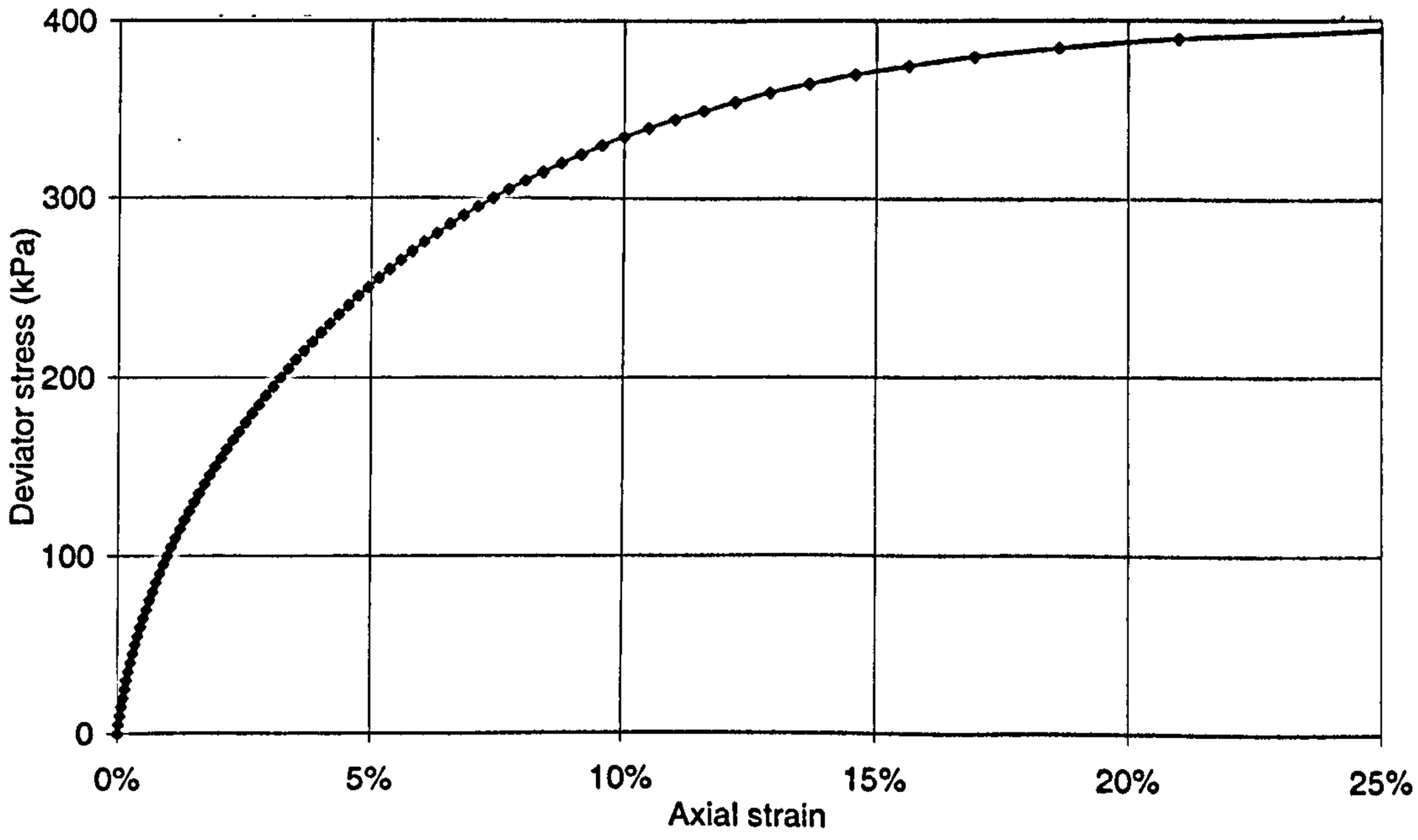

Figure 6-2 Analytical solutions of the MCC model: deviator stress vs. axial strain

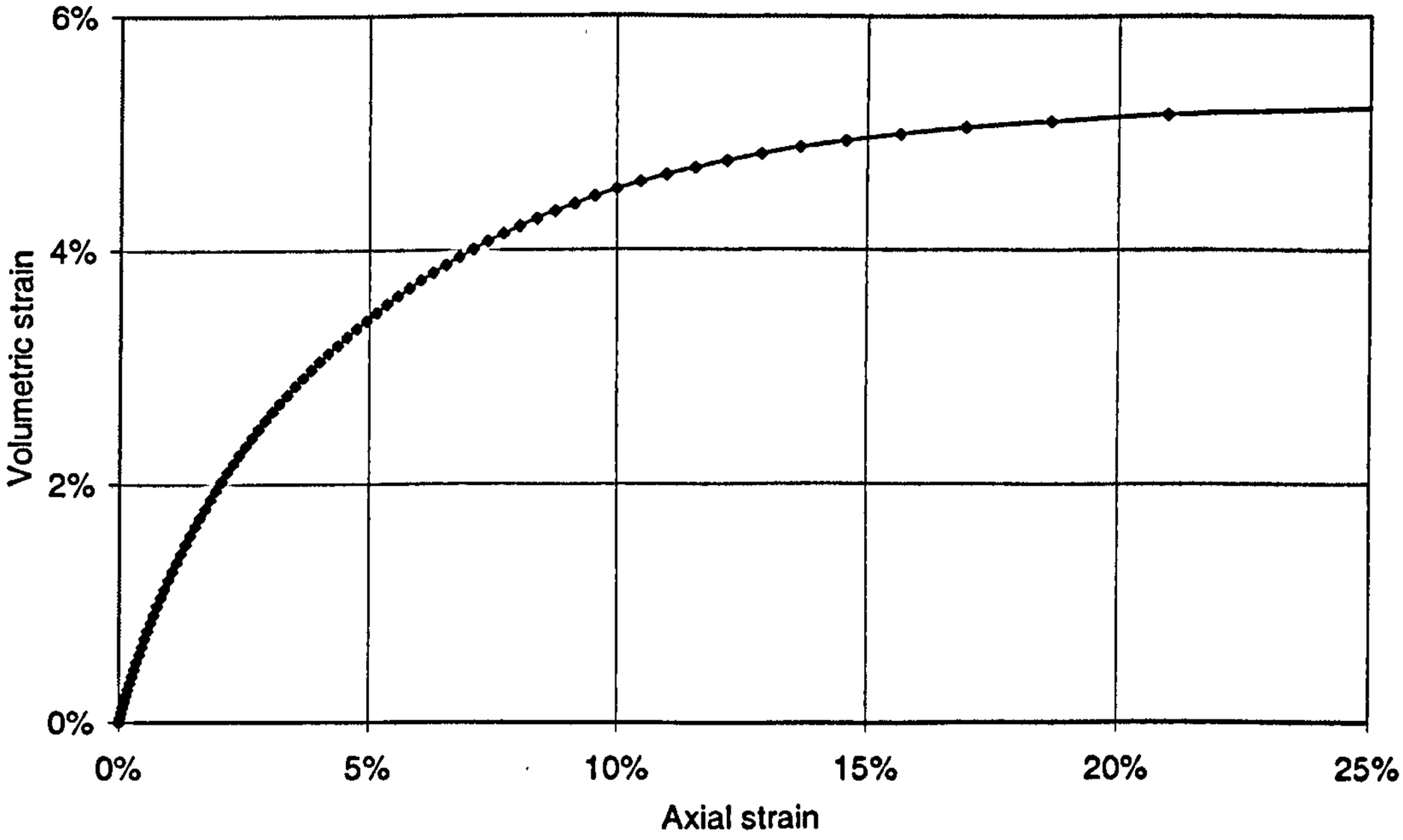

Figure 6-3 Analytical solutions of the MCC model: volumetric strain vs. axial strain

A spreadsheet calculation is applied to obtain the analytical solutions of the MCC model for the soil properties in Table 6-1. Axial stress is increased by 5 kPa until the deviator stress reaches its critical strength, while maintaining a constant radial stress and zero pore water pressure. The results are presented in Figure 6-2 and Figure 6-3 as plots of deviator stress and volumetric strain versus axial strain respectively, which are the same as those presented in Potts and Zdravkovic (1999). It can be seen that the critical state is reached at an axial strain of about 25%, while the deviator stress is about 400 kPa and the volumetric strain is 5.2%.

6.3.2 Combining MCC with CM

According to the CM proposed in Chapter 4, the volumetric strains of MSW under compression come from not only the movement of waste particles but also the compression of the compressible particles themselves. Only the reorganisation of waste particles causes shear strains, i.e. the plastic shear strain is coupled with the volumetric strain due to inter-voids compression if the MCC model is applied for waste material. Therefore, an additional volumetric strain due to the intra-voids compression needs to be calculated in addition to that due to the inter-voids compression, with only the latter coupled with the deviator stress in the MCC model. To calculate the volumetric strain in the drained triaxial compression test by the CM, the following assumptions are required:

1) To simplify the calculation and assessment of the contribution of the intra-voids compression, the volumetric strain caused by compressible particles is assumed to be plastic only, which means the slope of the intra-void ratio swelling line is zero;
2) The intra-voids compression occurs only in the axial direction in the drained triaxial compression test, which is consistent with the assumption that the volumetric strain due to compressible particles is not coupled with shear strain.

The incremental plastic volumetric strain induced by intra-voids compression can be obtained by:

$$\delta\varepsilon_p^f = \frac{\lambda_f}{v_f}\frac{\delta p'}{p'} \qquad \textit{Eq. 6-23}$$

in which v_f is the specific volume excluding the inter-void ratio e.

The same drained triaxial compression test on soil presented and used to demonstrate the MCC model (section 6.3.1) employed with the volumetric strain calculated from Eq. 6-23 to model waste compression behaviour. The additional required parameters for the CM are given in Table 6-2. The selected parameter values are close to those used in modelling the synthetic waste composition SW09 (a real waste composition simulation) in section 4.4.2, which mean the intra compression behaviour of this modelling is comparable to that of SW09.

Table 6-2 Additional material parameters for the MCC model combined with CM

Intra-void ratio at unit pressure on virgin consolidation line, f_1	10
Slope of virgin consolidation line in f-lnp' plane, λ_f	1.2

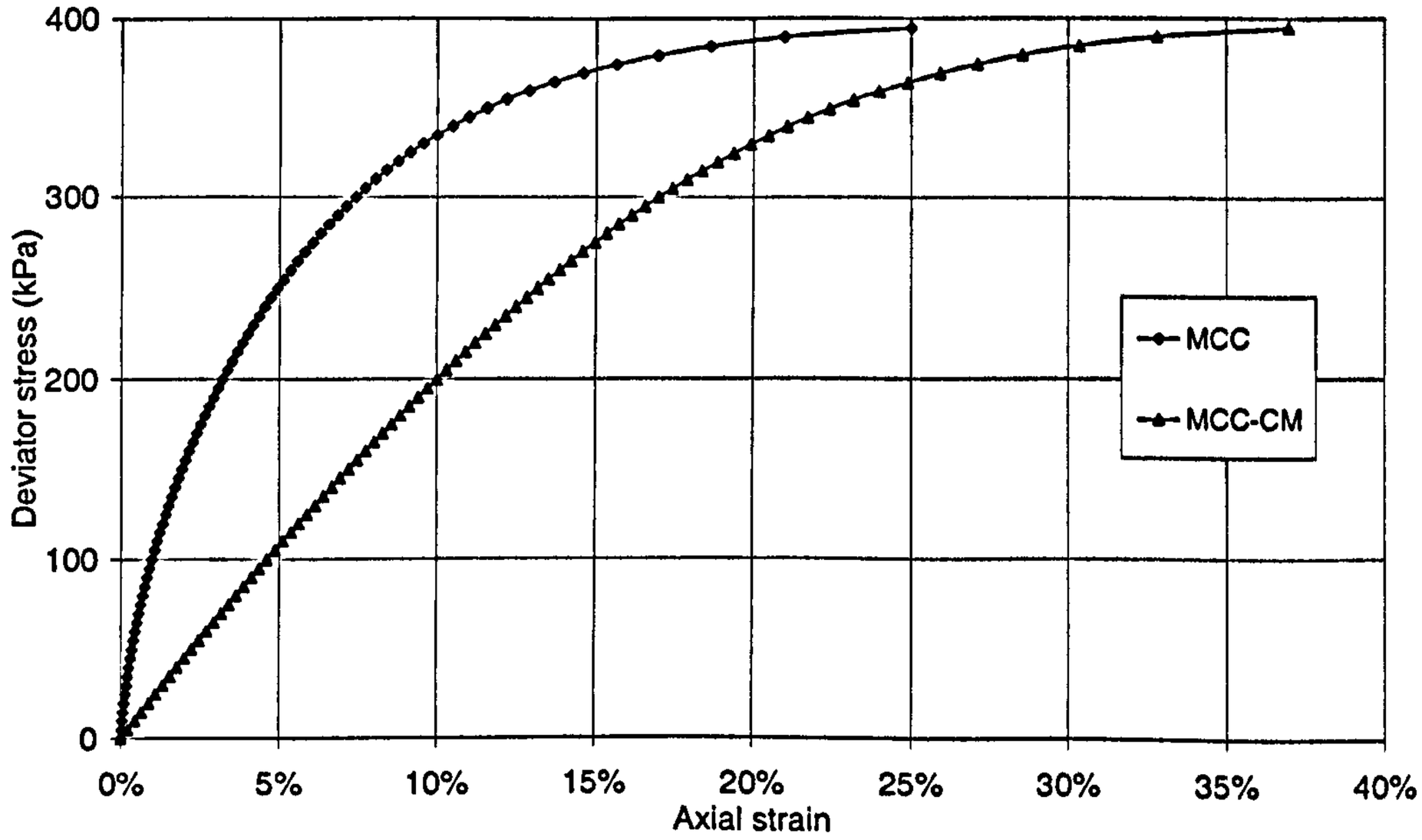

Figure 6-4 Analytical solutions for the MCC-CM model: deviator stress vs. axial strain

The results are presented in Figure 6-4 and Figure 6-5 together with the MCC model results for comparison. It should be noted that the axial strain and the volumetric strain (Eq. 6-23) values are added according the second assumption, therefore the critical state is reached at larger axial strain, as shown in Figure 6-4. It can also be seen that applying the CM does not increase the value of failure stress. Stiffness behaviour for the MCC model is obviously changed by applying the CM. The MCC-CM results show a lower stiffness than that for the MCC. This is consistent with the reported low waste stiffness behaviour in initial and intermediate strain ranges observed in the drained triaxial compression tests reviewed in section 2.2.2 (Figure 2-14). Meanwhile, it can be seen from Figure 6-5 that much more volume change can be obtained by using the MCC-CM to represent waste material than using the MCC model developed for soils.

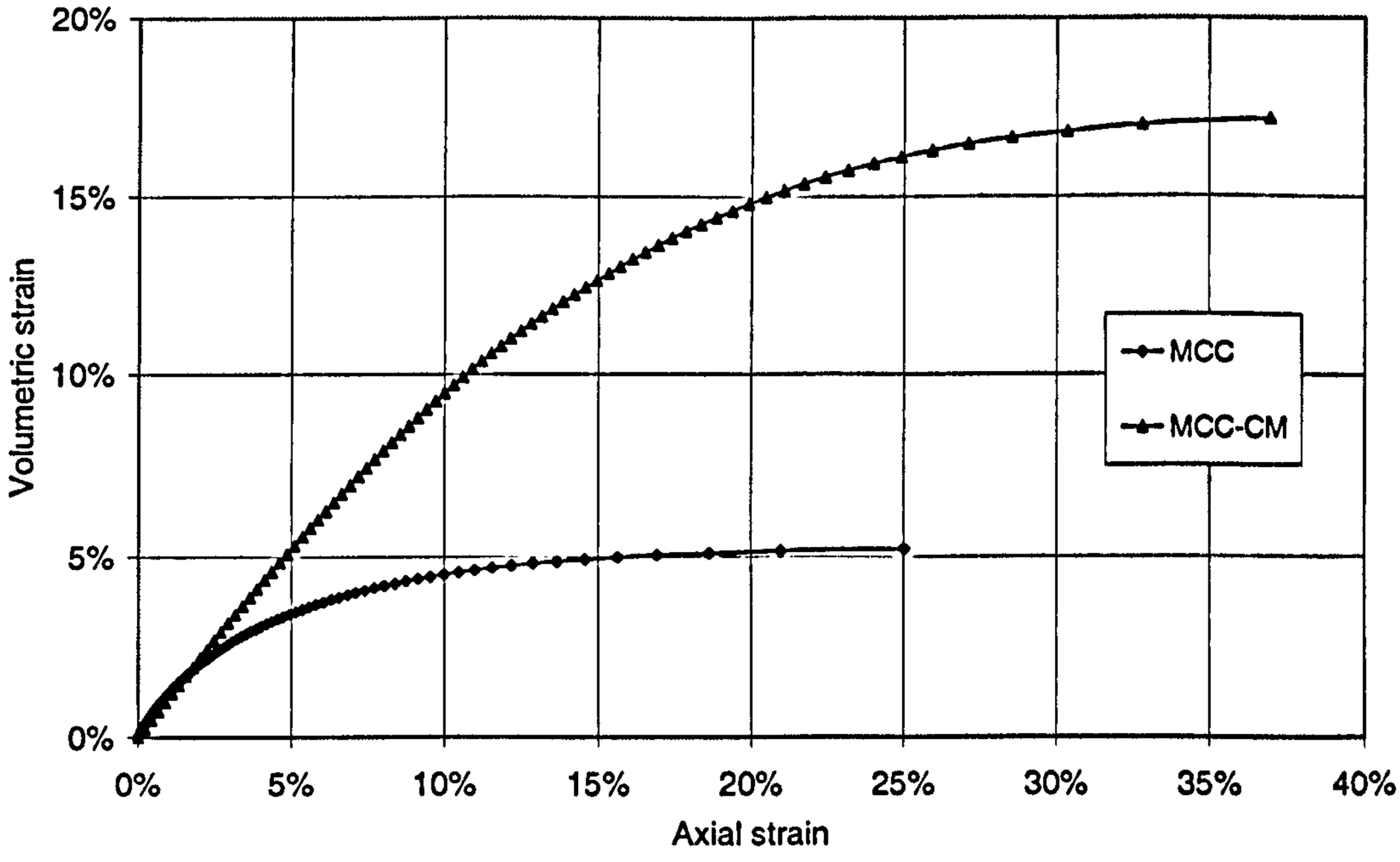

Figure 6-5 Analytical solutions for the MCC-CM model: volumetric strain vs. axial strain

Sensitivity analyses are carried out to show the influence of the compressibility of compressible particles on shear and volumetric behaviour of the combined MCC-CM model. A range of low to high particle compressible than the base model, i.e. different values of the slope of the intra-void ratio virgin compression line (λ_f), as shown in Table 6-3, are modelled and the results are presented in Figure 6-6 and Figure 6-7, together with the MCC model results for comparison. Label MCC-CM_B represents the base case which was presented in Figure 6-4 and Figure 6-5, MCC-CM_LC represents the lower compressibility case and MCC-CM_HC means the higher compressibility case. The results show that with higher values of λ_f, lower shear stiffnesses are obtained and more volumetric strains (and axial strains) can be reached.

Table 6-3 Parameters for the MCC-CM model sensitivity analysis

Model Case	Slope of virgin consolidation line in f-lnp' plane, λ_f
MCC-CM_LC	1.0
MCC-CM_HC	1.4

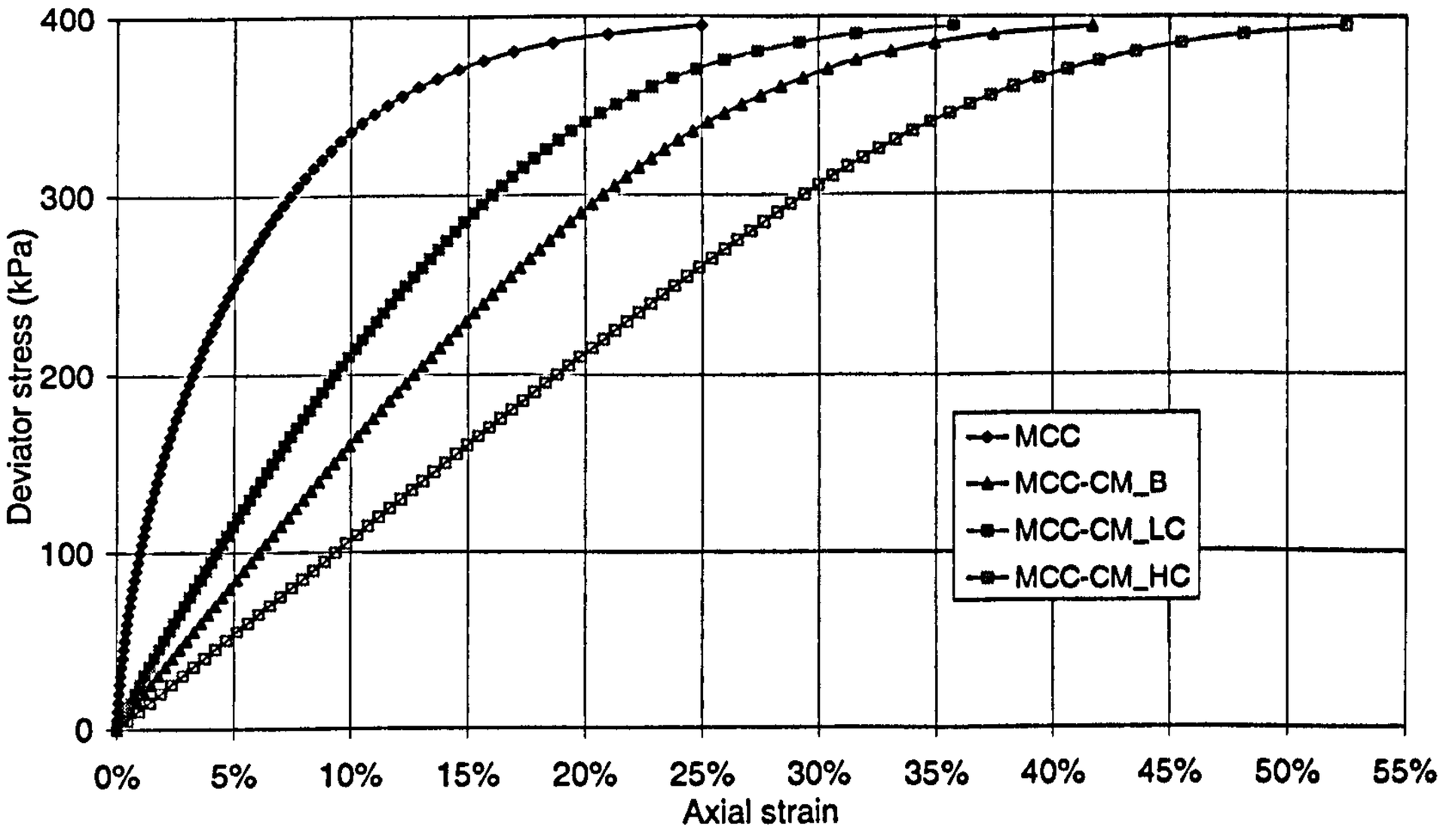

Figure 6-6 Deviator stresses vs. axial strains for MCC-CM model with lower and higher values of the slope of the intra-void ratio virgin compression line

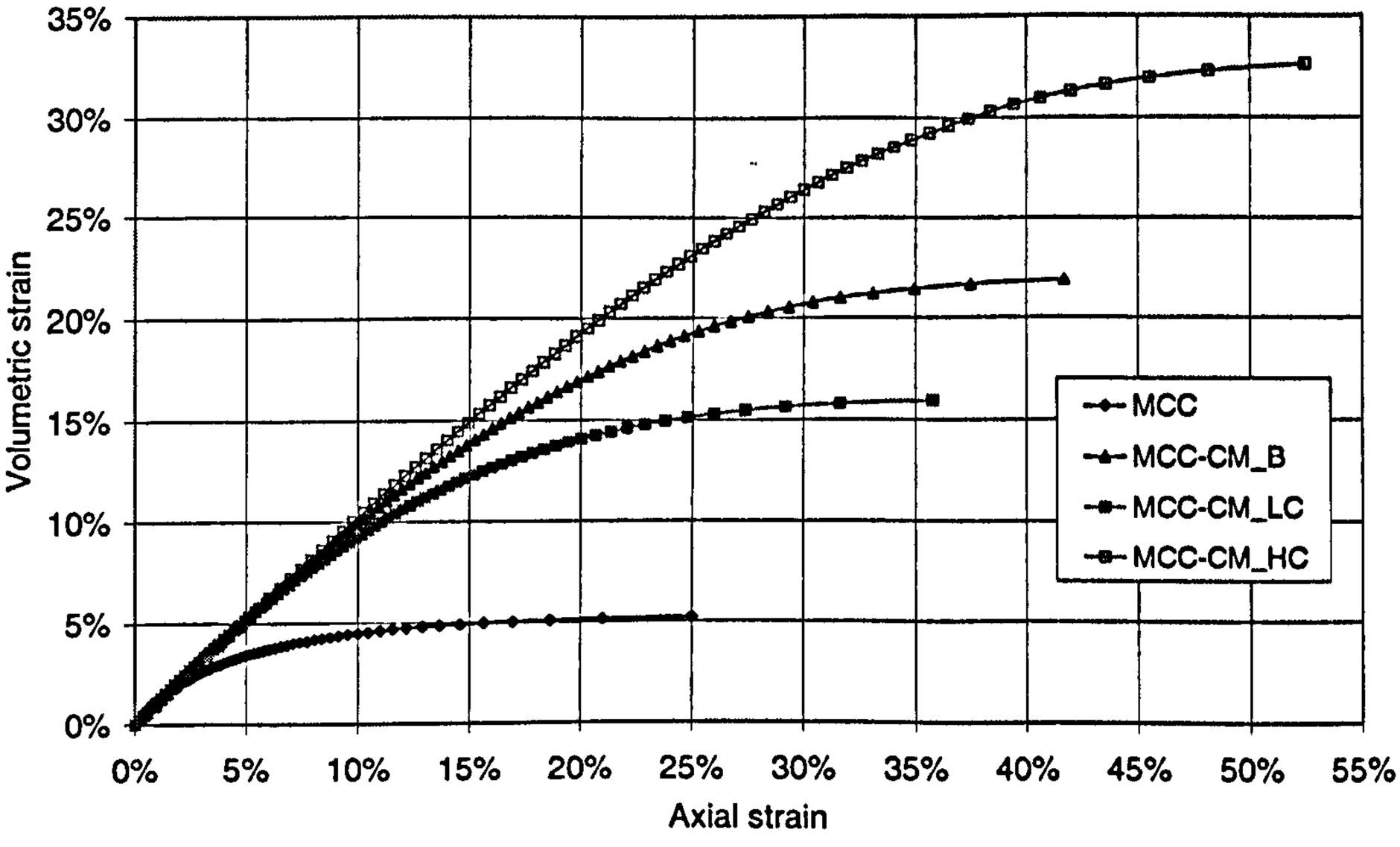

Figure 6-7 Volumetric strains vs. axial strains for MCC-CM model with lower and higher values of the slope of the intra-void ratio virgin compression line

6.3.3 Combining MCC with RM

Combining the MCC model with the RM can be performed in the finite element analysis though the linear mobilised tensile stiffness analysis (LMSTA) as discussed in section 5.4, which was listed in Figure 5-1 as one of the fibre reinforced soil model LMSTA-E-MCC (or LMSTA-P-MCC). The implementation of the finite element method will be explained in detail in Chapter 7. As the analytical results of the MCC model have been obtained for the drained triaxial compression boundary condition through a spreadsheet analysis, the combination with the RM can also be carried out though the same kind of analysis for this particular boundary value problem analytically. An additional confining stress provided by the fibres can be calculated by multiplying the radial strain of the triaxial sample with the equivalent mobilised tensile stiffness of the fibres defined in section 5.5.1 (assuming the linear elastic fibre material model is adopted). The equivalent tensile stiffness can be obtained from material properties of the fibres such as single fibre tensile stiffness, fibre volume content and fibre length, which were described in detail in section 5.5.1. To demonstrate the RM behaviour combined with the MCC model, an equivalent tensile stiffness value has been applied directly for presentation of the analytical solutions below. Determination of the equivalent tensile stiffness from fibre material properties for waste material will be discussed later in section 8.3. In the spreadsheet calculation, additional confining stress can be calculated from the radial strain accumulated over all the loading increments before the current step, by the following expression:

$$\sigma_f = K_{fe}\varepsilon_r \qquad \textit{Eq. 6-24}$$

in which K_{fe} is the equivalent tensile stiffness which can be obtained from Eq. 5-33, and ε_r is the radial strain of the triaxial sample.

Analytical solutions for the MCC-RM model are obtained through spreadsheet analysis again, in which the equivalent tensile stiffness for the sample is assumed as 500 kPa. For instance, assuming average Young's modulus for waste reinforcing particles is 1×10^5 kPa which is the same as the polyamide material discussed in section 5.5.1, fibre volume content ρ=1%, specimen radius R=100 mm, and average fibre length l=50 mm, the equivalent tensile stiffness can be obtained as around 500 kPa. More detailed information on how to obtain sensible parameter values from fibre material properties will be discussed in section 8.3. Results are presented in Figure 6-8 and Figure 6-9, together with the MCC model results for comparison. It can be seen that the MCC-RM model improves the shear strength with higher axial strain at the critical state compared with the MCC model curve, and higher shear stiffness is obtained in the large strain range. Volumetric strains are almost identical to those for the MCC model except that higher axial strain can be reached.

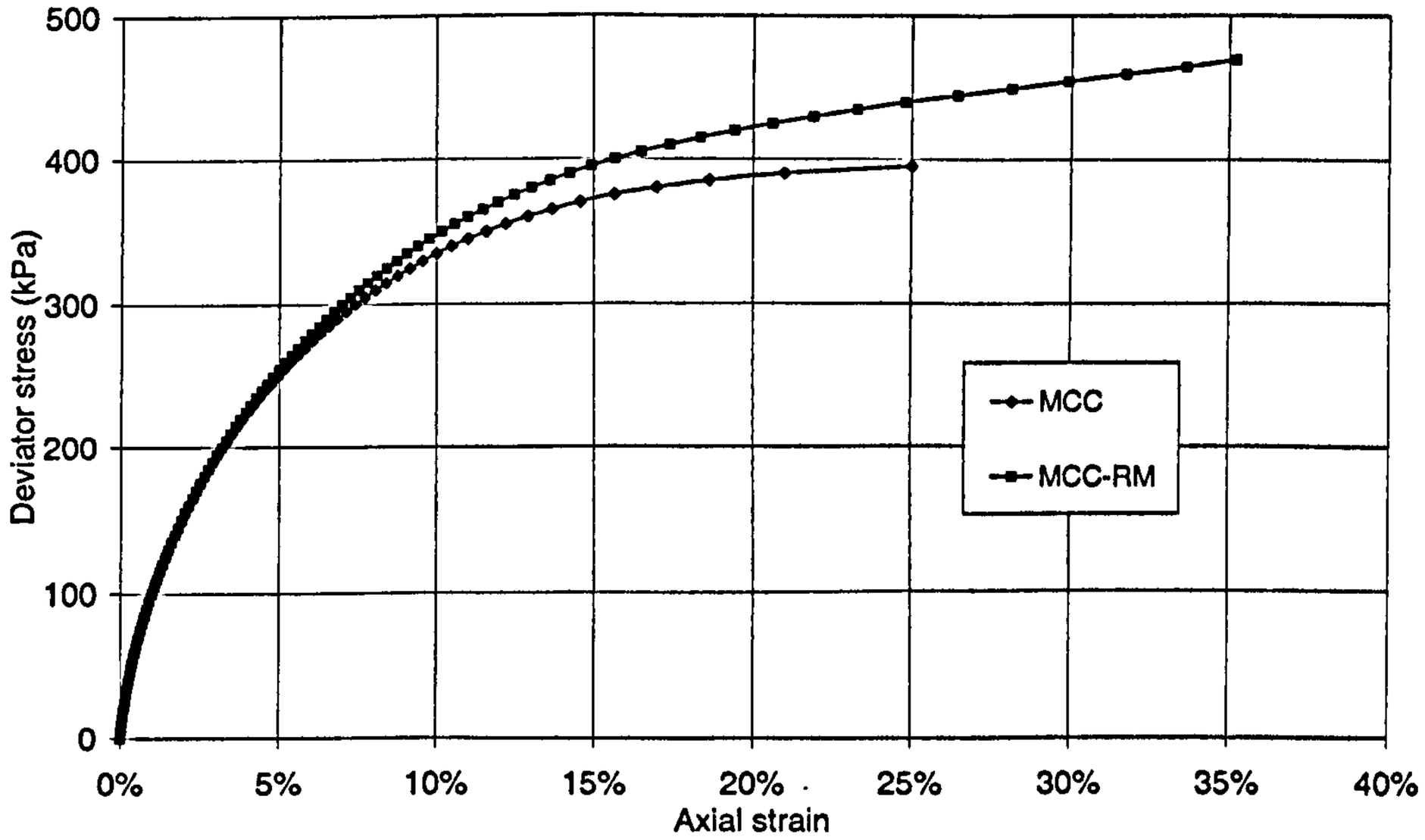

Figure 6-8 Analytical solutions for the MCC-RM model: deviator stress vs. axial strain

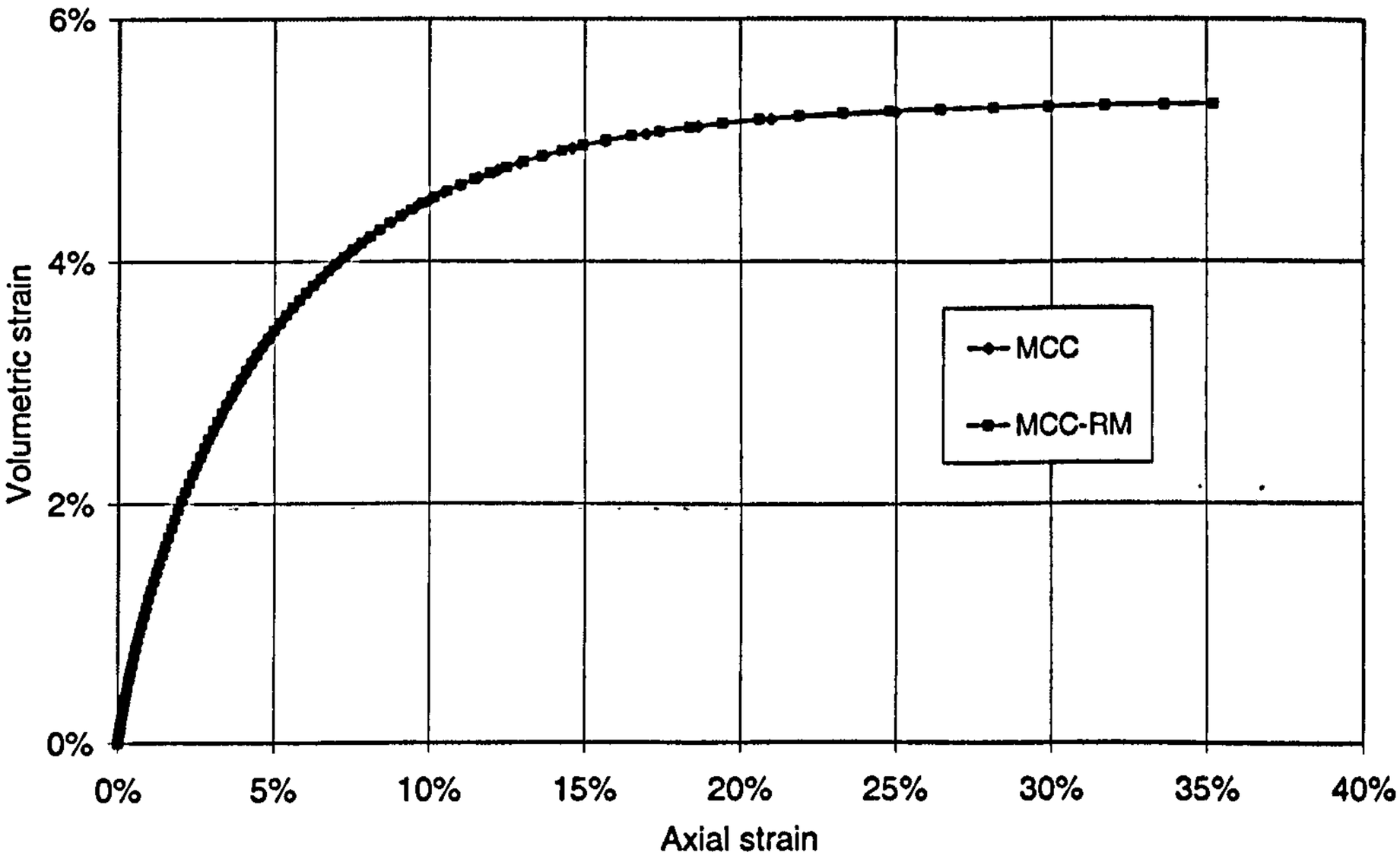

Figure 6-9 Analytical solutions for the MCC-RM model: volumetric strain vs. axial strain

Sensitivity analyses have been run for the MCC-RM model in terms of changing the value of the equivalent tensile stiffness. Lower (K_{fe}=250 kPa) and higher tensile stiffness (K_{fe}=1000 kPa) than the value assumed for the base model are adopted to perform the parametric study. Label MCC-RM_B is for the base model from which results were presented in Figure 6-8 and Figure 6-9, MCC-RM_LS represents the lower equivalent tensile stiffness value case and MCC-RM_HS means the higher stiffness value case. The results show that with higher values of the equivalent tensile stiffness, a higher peak shear strength is obtained and high shear stiffnesses values are

produced when the stress state is close to the critical state. The opposite is true for lower value of equivalent tensile stiffness. However, shear stiffnesses below 10% of the axial strain are almost the same for both cases. This is because the fibre tensile stresses are not mobilised under relative small radial strains. No obvious change in volumetric behaviour is produced for different tensile stiffness values.

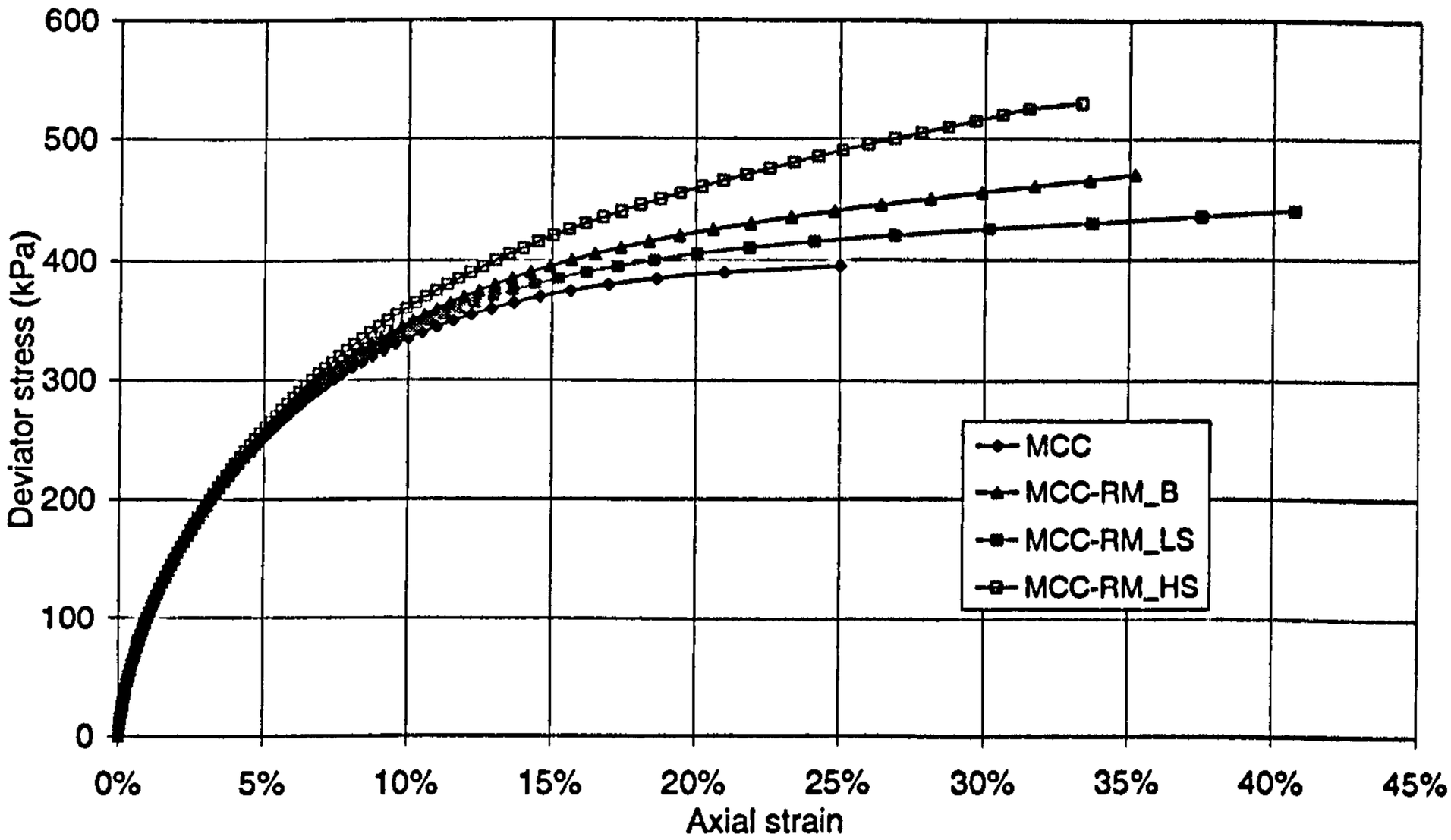

Figure 6-10 Deviator stresses vs. axial strains for MCC-RM model with lower and higher values of the equivalent tensile stiffness

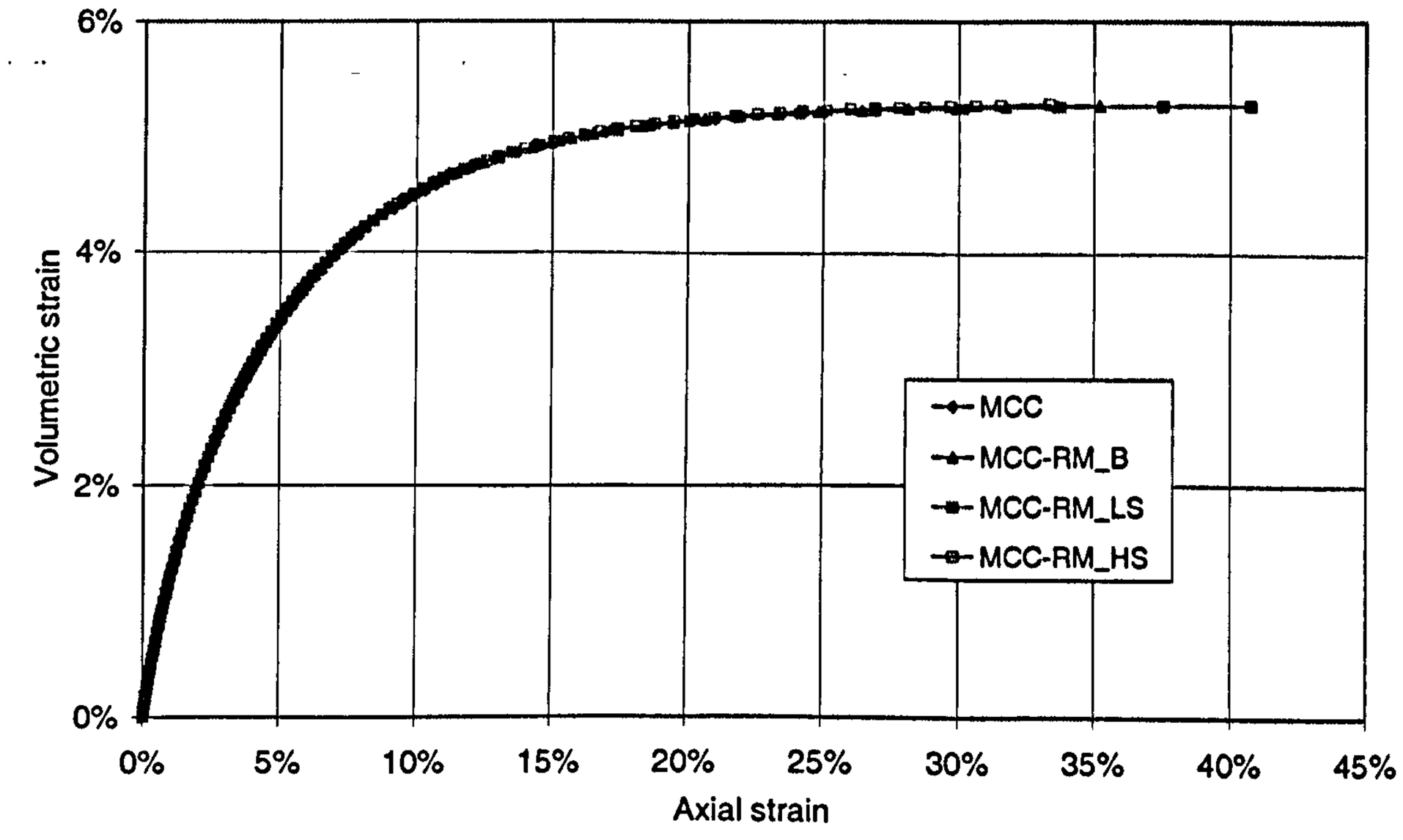

Figure 6-11 Volumetric strains vs. axial strains for MCC-RM model with lower and higher values of the equivalent tensile stiffness

6.3.4 MSW Constitutive Model

A constitutive model for MSW is produced by combining the MCC model with both CM and RM in the ways presented above. Analytical solutions for the MSW constitutive model are calculated and presented together with the MCC model results in Figure 6-12 and Figure 6-13.

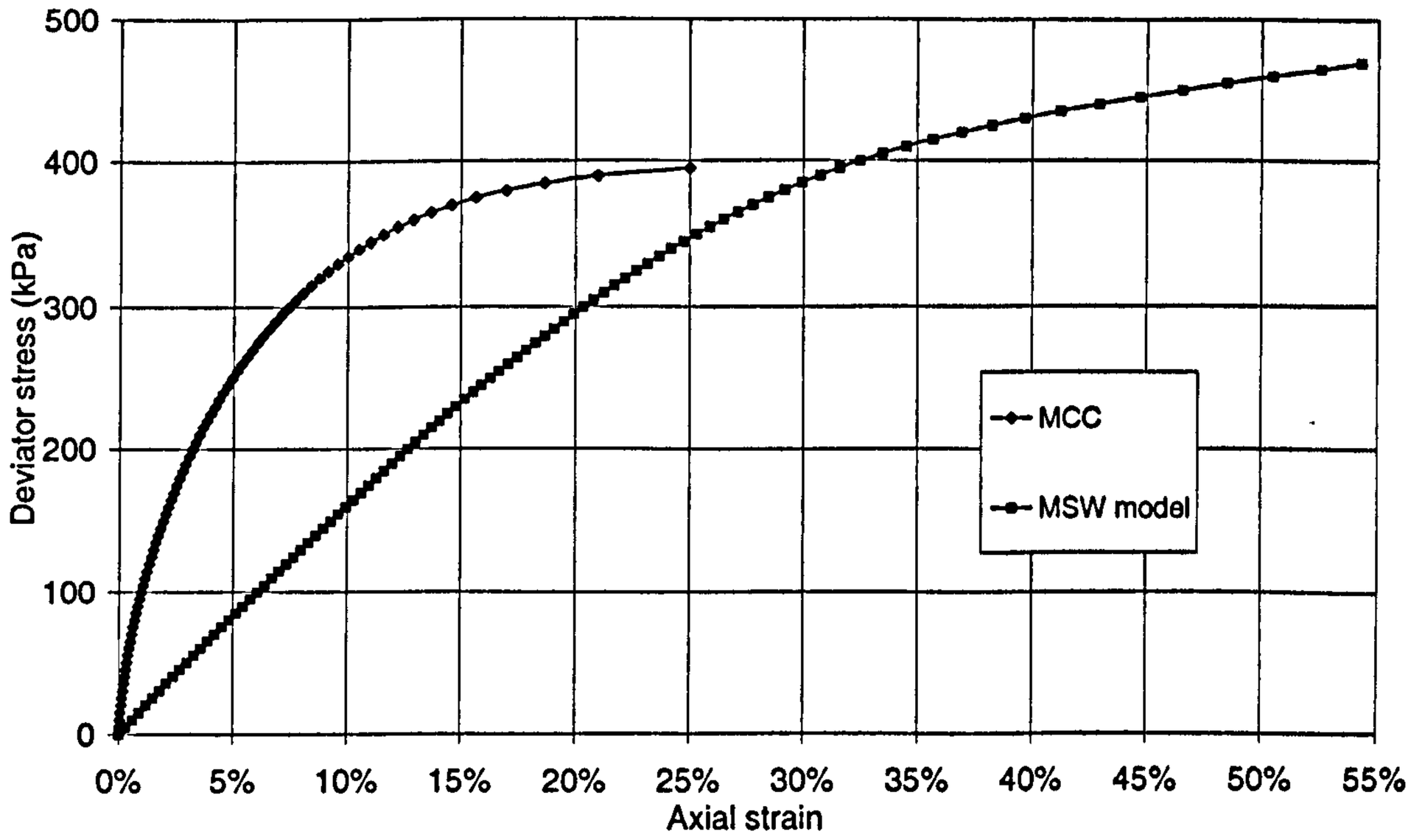

Figure 6-12 Analytical solutions for the MSW model: deviator stress vs. axial strain

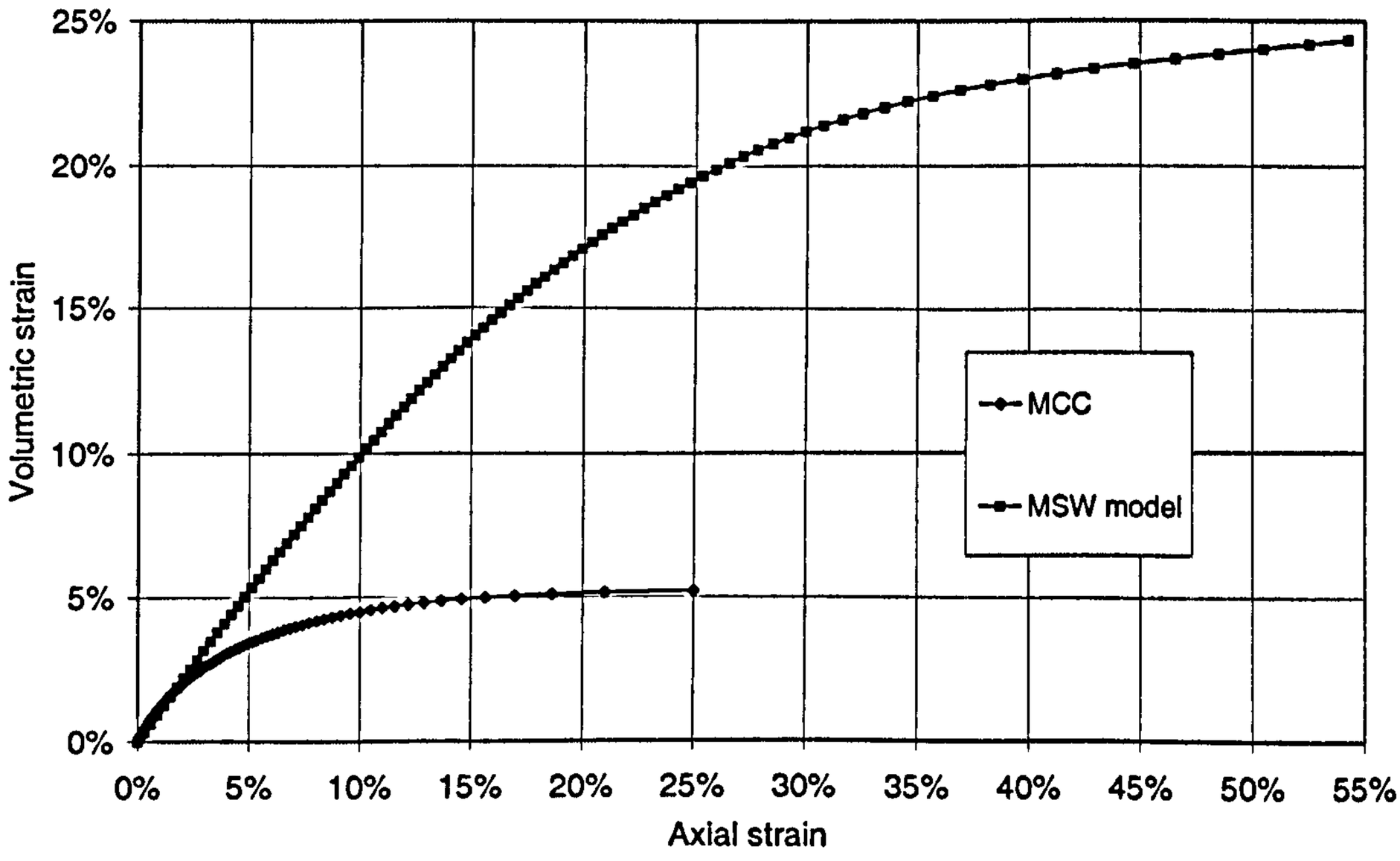

Figure 6-13 Analytical solutions for the MSW model: volumetric strain vs. axial strain

It can be seen from the results that the MSW model can reproduce the stiffness and volumetric behaviour of MSW material found in triaxial compression tests which are reviewed in section 2.2.2. Firstly, lower shear stiffness of MSW material in the initial and intermediate strain ranges can be reproduced by the MSW model, which cannot be reproduced by soil models. Secondly, higher peak strength and stiffness of the MSW material (compared to pure paste material without fibre material) can be modelled according to fibre material properties. Although critical state does still exist, shear stiffness does not deteriorate to zero like the MCC model for soil. This is due to the contribution of the fibre material. Finally, more volumetric strain can be generated before the critical state is reached by the MSW model, which cannot be simulated by using soil models.

6.3.5 Modelling MSW Triaxial Tests Using the MSW Model

Triaxial test results reported by Machado *et al.* (2002) have been modelled using the proposed MSW model in a spreadsheet analysis. A representative triaxial compression test which was presented in Figure 2-13 has been selected from Machado's shredded waste tests to validate the MSW model. Three different confining stress conditions, i.e. 100 kPa, 200 kPa and 400 kPa were modelled. Parameters needed for the modelling cannot be obtained directly from the tests because compressible particles were not recognised in Machado's paper. Moreover, the method used to measure void ratios of MSW samples in their confined compression tests was not recorded. Therefore, parameters are back analysed to reproduce the MSW behaviour observed in their tests. A summary of the input parameters are listed in Table 6-4.

Table 6-4 Material properties assumed for the MSW model

Overconsolidation ratio (***OCR***)	1.0
Specific volume (no intra void) at unit pressure on virgin consolidation line, N	1.5
Slope of virgin consolidation line in ***v-lnp'*** plane (no intra void), λ	0.07
Slope of swelling line in ***v-lnp'*** plane (no intra void), κ	0.0065
Slope of critical state line in ***q-p'*** plane, M	1.2
Poisson's ratio μ	0.3
Intra-void ratio at unit pressure on virgin consolidation line, f_1	10
Slope of virgin consolidation line in ***f-lnp'*** plane, λ_f	0.6
Equivalent tensile stiffness of fibre components, K_{fe} (kPa)	1000

Comparisons between the test and modelling results for different confining stresses (including deviator stress vs. axial strain and volumetric strain vs. axial strain) are shown in Figure 6-14 and Figure 6-15. It can be seen from Figure 6-14 that the model can reproduce the MSW stress-strain

behaviour under triaxial compression in the initial (0-10%) and intermediate (10%-20%) strain ranges which are defined in section 2.2.2 (though less well for the confining stress of 400 kPa). When the axial strains enter the large strain range which is more than 20%, the modelling curves keep turning downwards until the critical states are reached, at which the shear stiffness is not zero as the MCC model due to the combination of the reinforcing model. However, the testing curves keep turning upwards and no peak shear strengths are obtained at the end, which cannot be reproduced by the current MSW model. With the increasing normal stress, more and more compressible particles are compressed and some of them are changed to be the new reinforcing particles due to the shape changing, after which more reinforcing particles will be available. Meanwhile, more fibres can be mobilised with increasing strains so that the shear stiffness of the material can be increased. These two factors would contribute to the increasing stiffness behaviour observed in large strain range. Apparently the linear mobilised tensile stiffness analysis is not capable to model this behaviour. Non-linear mobilised tensile stiffness analysis discussed in section 5.2 is required to model this behaviour in a future work.

It can be seen from Figure 6-15 that the model can produce large volumetric strains (about 13% at critical states in this case) that the MCC model cannot normally do (will be shown later in this section). The predicted volumetric strains do not vary much under different confining stresses. This is a typical behaviour for critical state models, i.e. almost the same amounts of volumetric strain coupled with the shear strain are obtained at the critical states for different confining stresses. It should be noted that the volumetric strains presented in the triaxial test results do not include the volumetric strains from the consolidation stage (i.e. isotropic compression). Moreover, the volumetric strains caused by intra-void compression during the triaxial loading (after the consolidation stage) are almost the same as a constant λ_f value was define in the waste model. The volumetric strains for higher confining stresses are slightly larger than those for lower confining stresses in the modelling results because higher effective normal stresses p' are obtained for higher confining stresses at the critical states.

However, the Machado's triaxial test results showed a very different trend with larger volumetric strains obtained with lower confining stresses which indicates that the volume loss from compressible particles is confining stress dependent, as discussed in section 2.2.2. It can be explained that higher consolidation stresses in the consolidation stage compressed more compressible particles so that intra-voids become more difficult to be compressed at the shearing stage. The current MSW model cannot simulate this behaviour because linear relationship was assumed for intra-void ratio versus logarithm of the vertical stresses (i.e. a constant λ_f was assumed) and therefore this part of volumetric strains are not dependent on confining stress (it has been discussed in section 4.5). Therefore, a non-linear intra-voids compression model is required in the future work to model this waste volumetric behaviour.

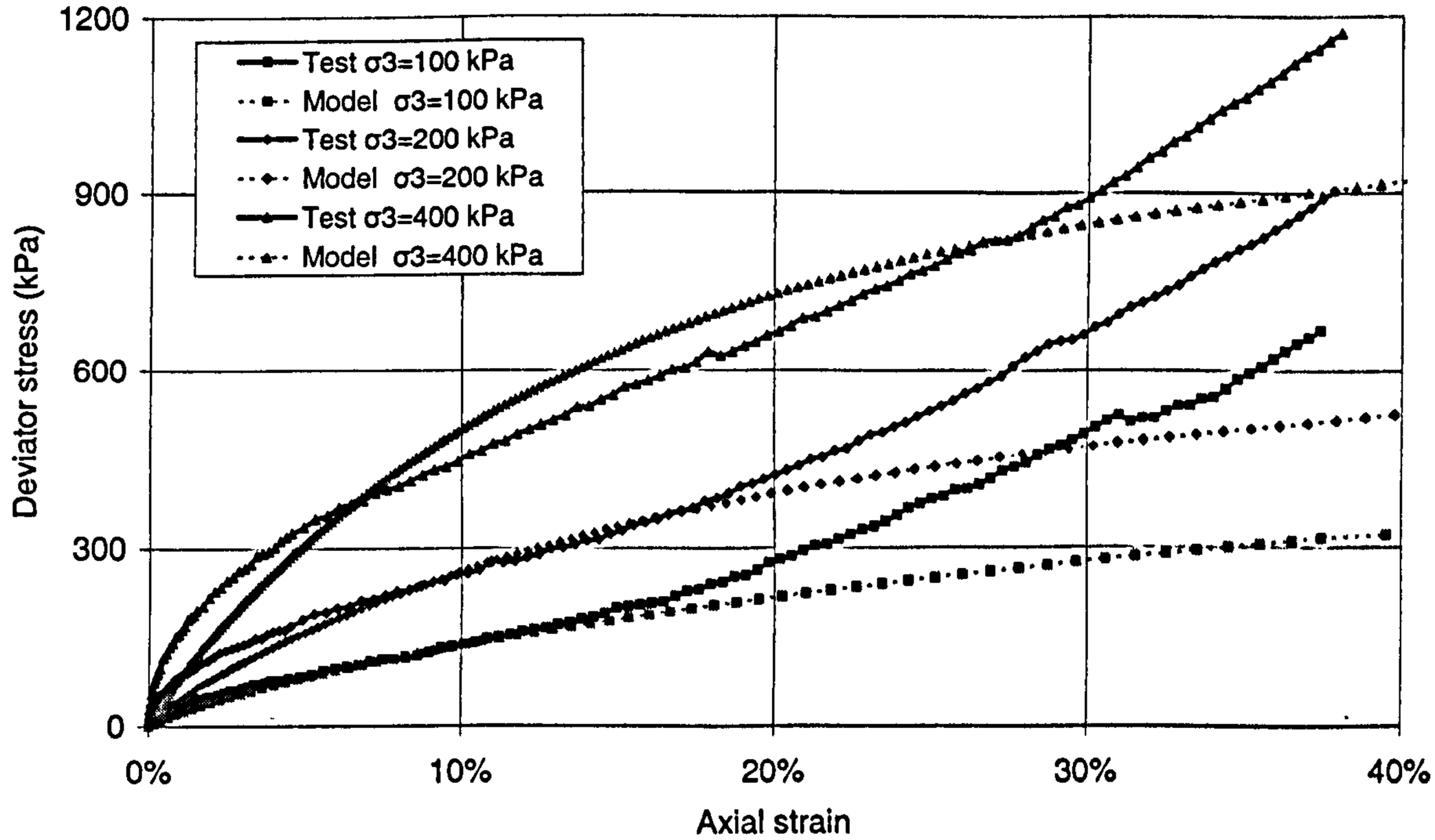

Figure 6-14 Comparison between test and modelling results under different confining stresses: deviator stress vs. axial strain

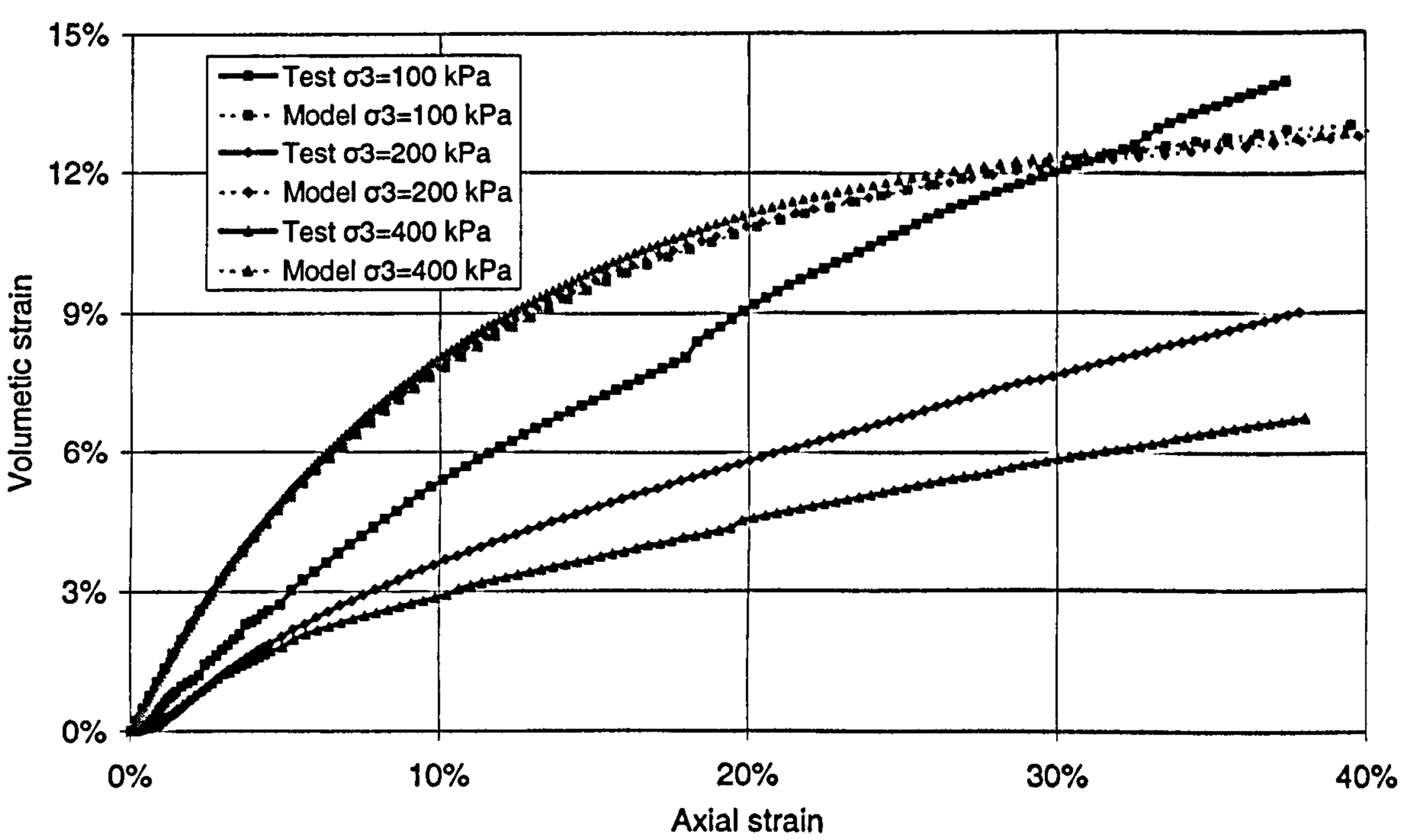

Figure 6-15 Comparison between test and modelling results under different confining stresses: volumetric strain vs. axial strain

To show the potential of the current MSW model in modelling the particular waste behaviour, changing values of the slope of virgin consolidation line in ***f-lnp'*** plane, λ_f, for different

consolidation stresses can be tried to predict different volumetric strains. Different values of λ_f shown in Table 6-5 have been applied for each confining stress and results are presented in Figure 6-16 and Figure 6-17. It can be seen from the figures that although only slightly changing shear behaviour, the model can predict different values of volumetric strains under different confining stresses. Although the model cannot reproduce the test curves, it demonstrates a capability to simulate the trend.

Table 6-5 Different values of λ_f for different confining stresses

Confining stresses (kPa)	Slope of virgin consolidation line in *f-lnp'* plane, λ_f
100	0.6
200	0.4
400	0.2

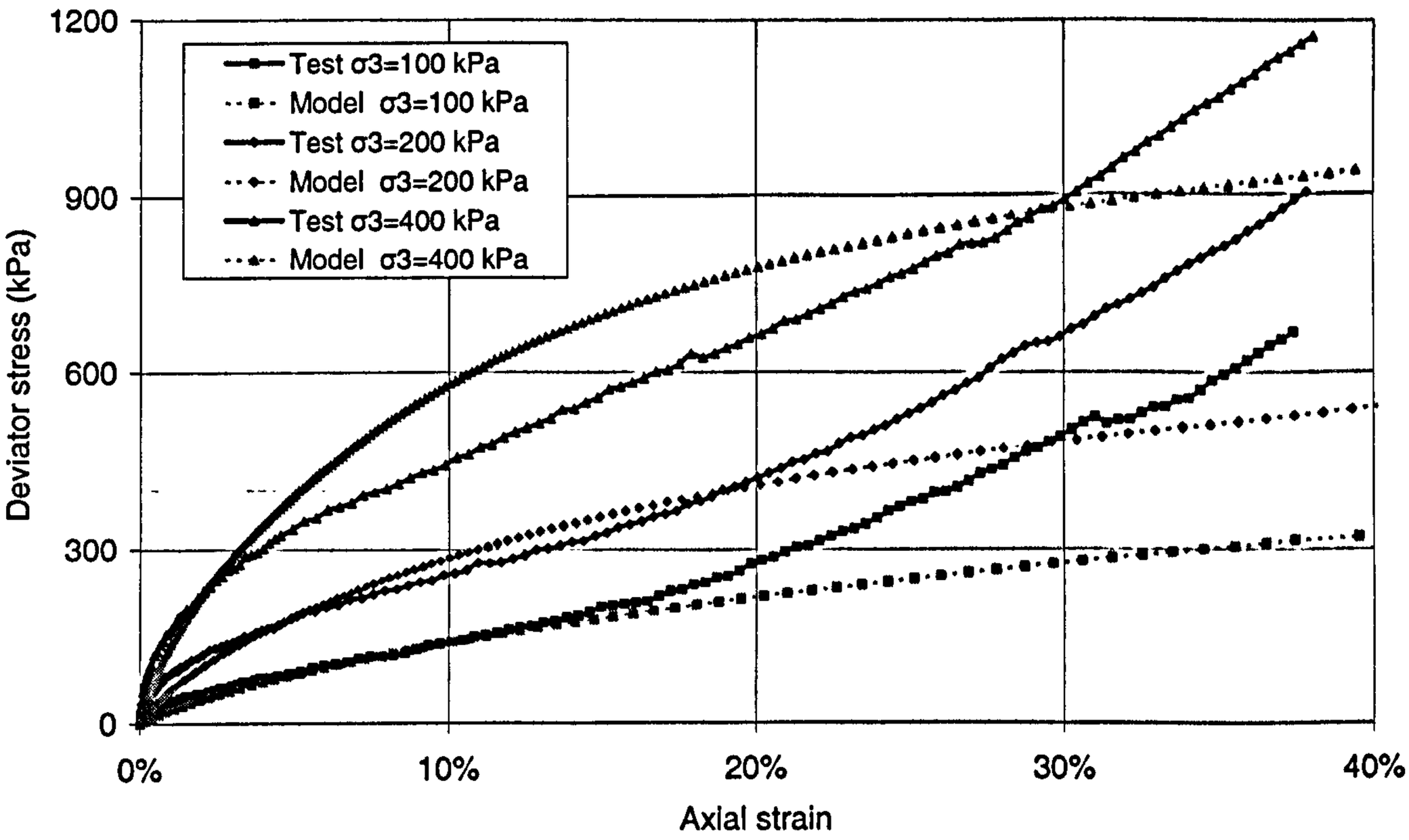

Figure 6-16 Improved model results considering confining stress dependent intra-voids compression: deviator stress vs. axial strain

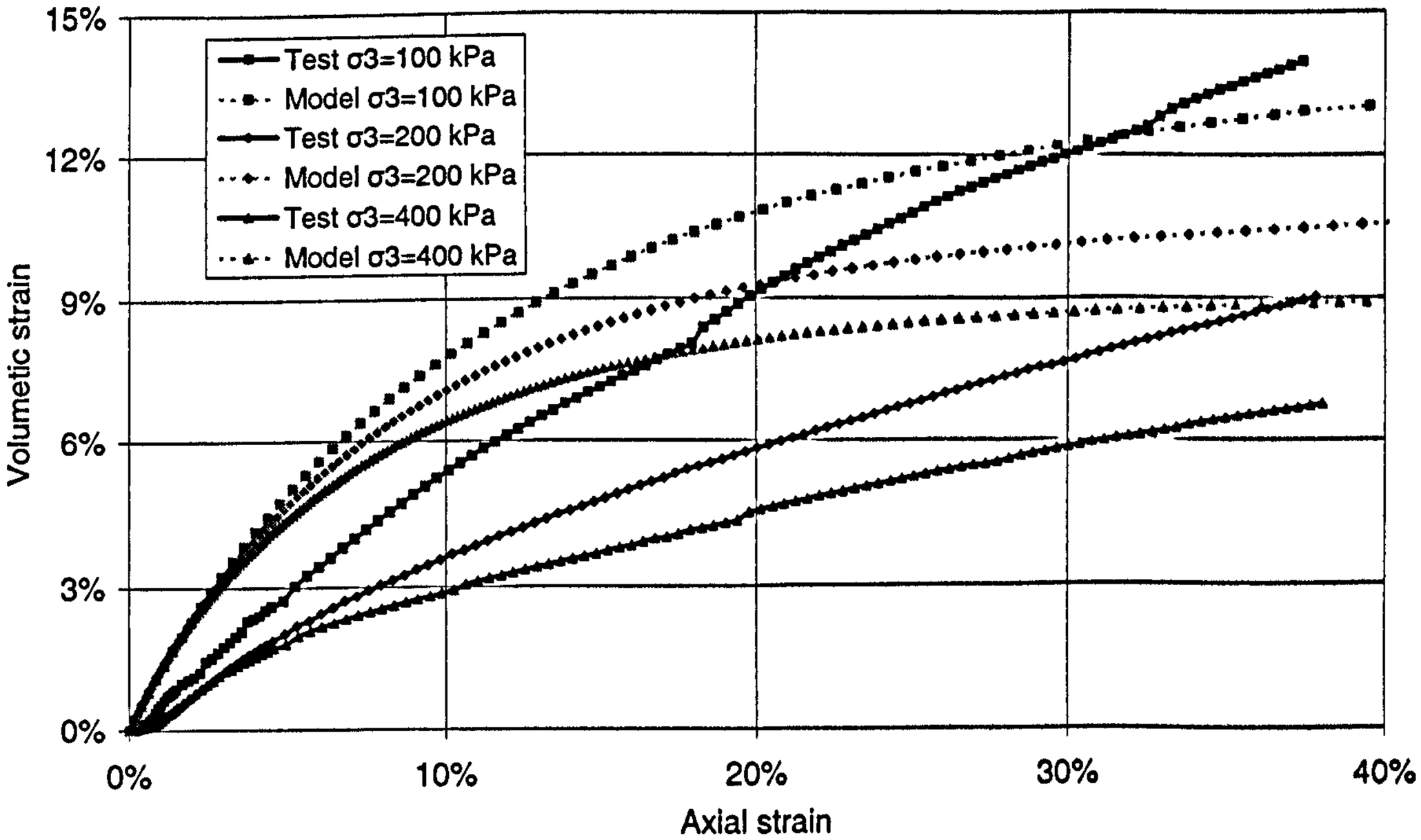

Figure 6-17 Improved model results considering confining stress dependent intra-voids compression: volumetric strain vs. axial strain

In order to understand the advantages of the proposed MSW model over the MCC model for modelling MSW mechanical behaviour shown in triaxial compression tests, the MCC modelling results using the same parameters in Table 6-4 are also presented together with the testing results in Figure 6-18 and Figure 6-19. It can be seen that the MCC model cannot reproduce the MSW stiffness behaviour when axial strain is less than 20% as the MSW model, and the predicted peak strengths of the material are also much lower than those predicted by the MSW model. On the other hand, the predicted volumetric strain values are almost the same for the three different consolidation stresses, and larger volumetric strains for lower consolidation stresses cannot be predicted.

To have larger volumetric strain, higher λ value indicating higher plastic compressibility is needed to produce more plastic strains (both shear strain and volumetric strain) in the MCC model. Figure 6-20 and Figure 6-21 show the relevant results assuming λ=0.11 comparing with initially λ=0.07. It can be seen that using higher plastic compressibility values larger volumetric strains can be obtained, but at the same time very large plastic shear strains are predicted. Up to 80% of axial strain is predicted in this case with very low shear stiffness in most of the strain range, indicating a very soft and plastic behaviour. This is one of the major disadvantages of using soil models to model waste behaviour in numerical modelling, which will be further discussed in section 8.6.

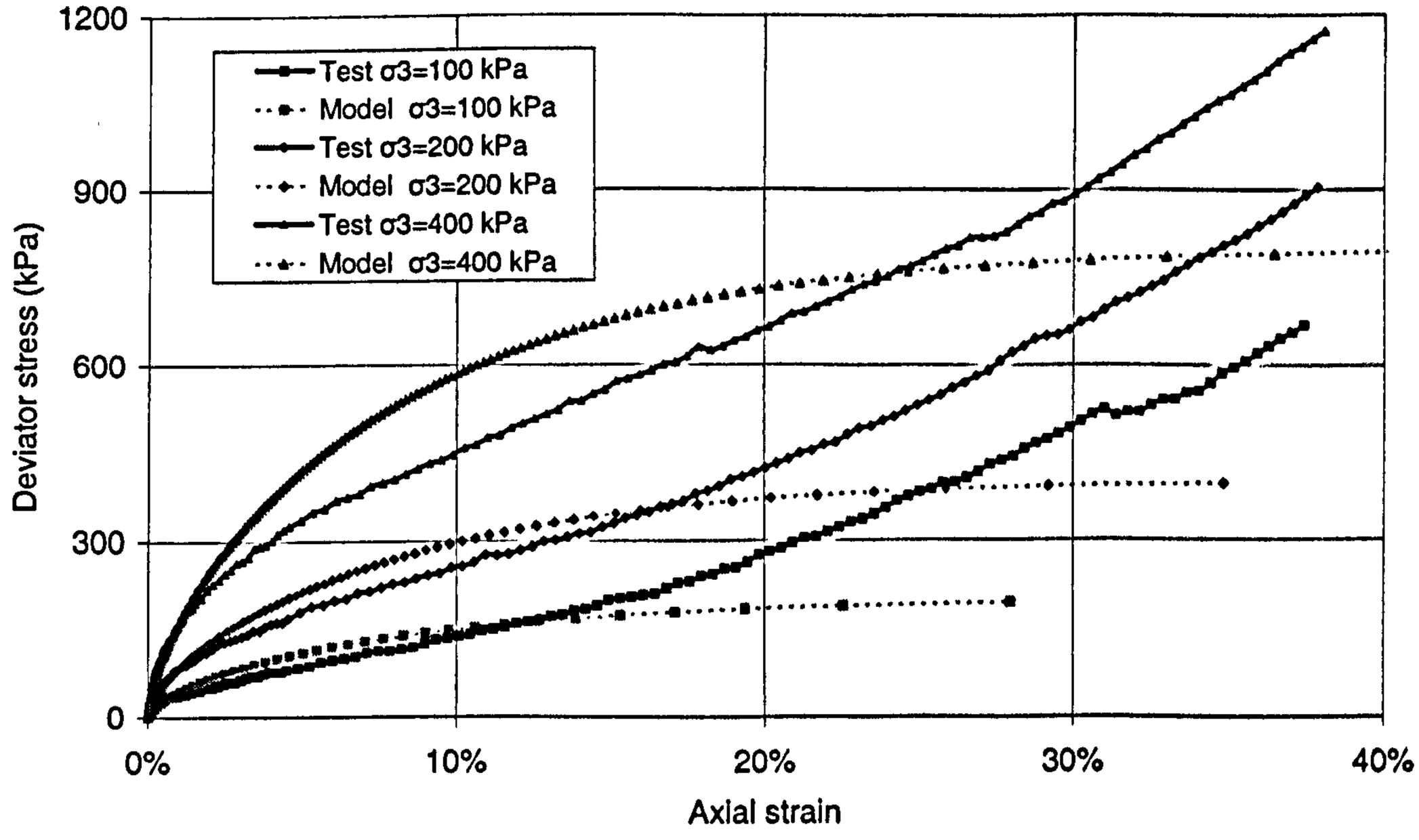

Figure 6-18 The MCC modelling results together with the testing results: deviator stress vs. axial strain

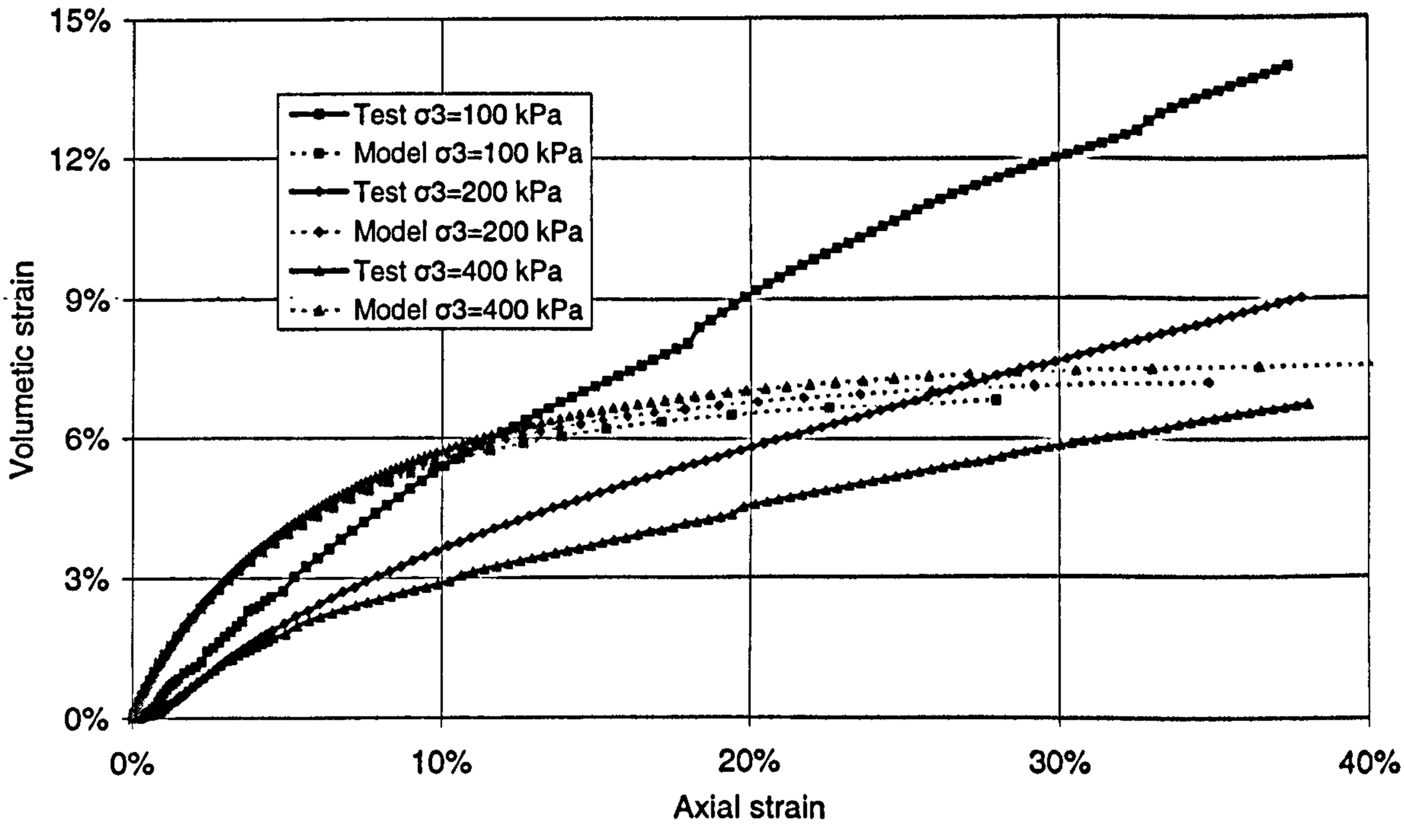

Figure 6-19 The MCC modelling results together with the testing results: volumetric strain vs. axial strain

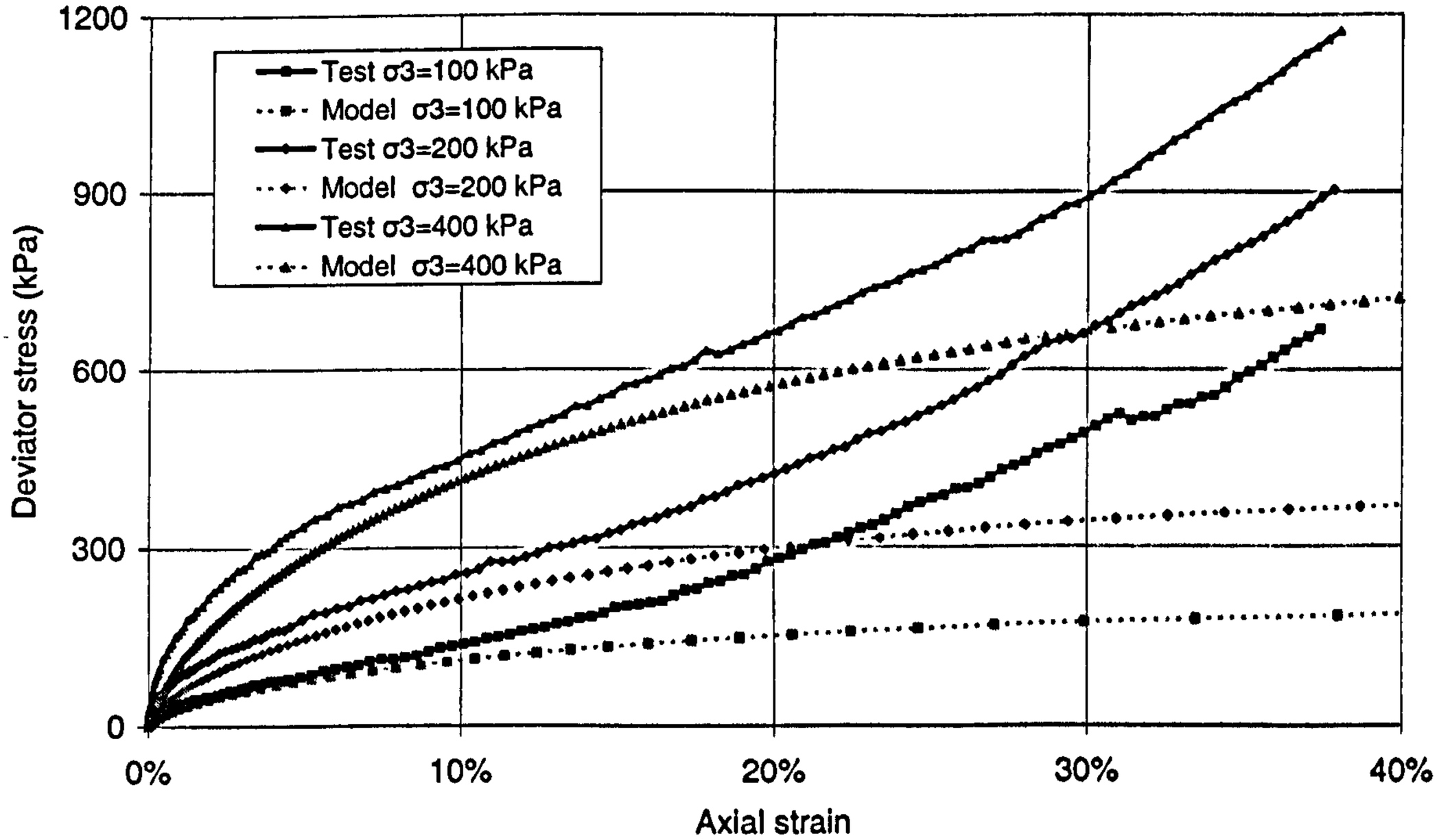

Figure 6-20 The MCC modelling results with higher λ value: deviator stress vs. axial strain

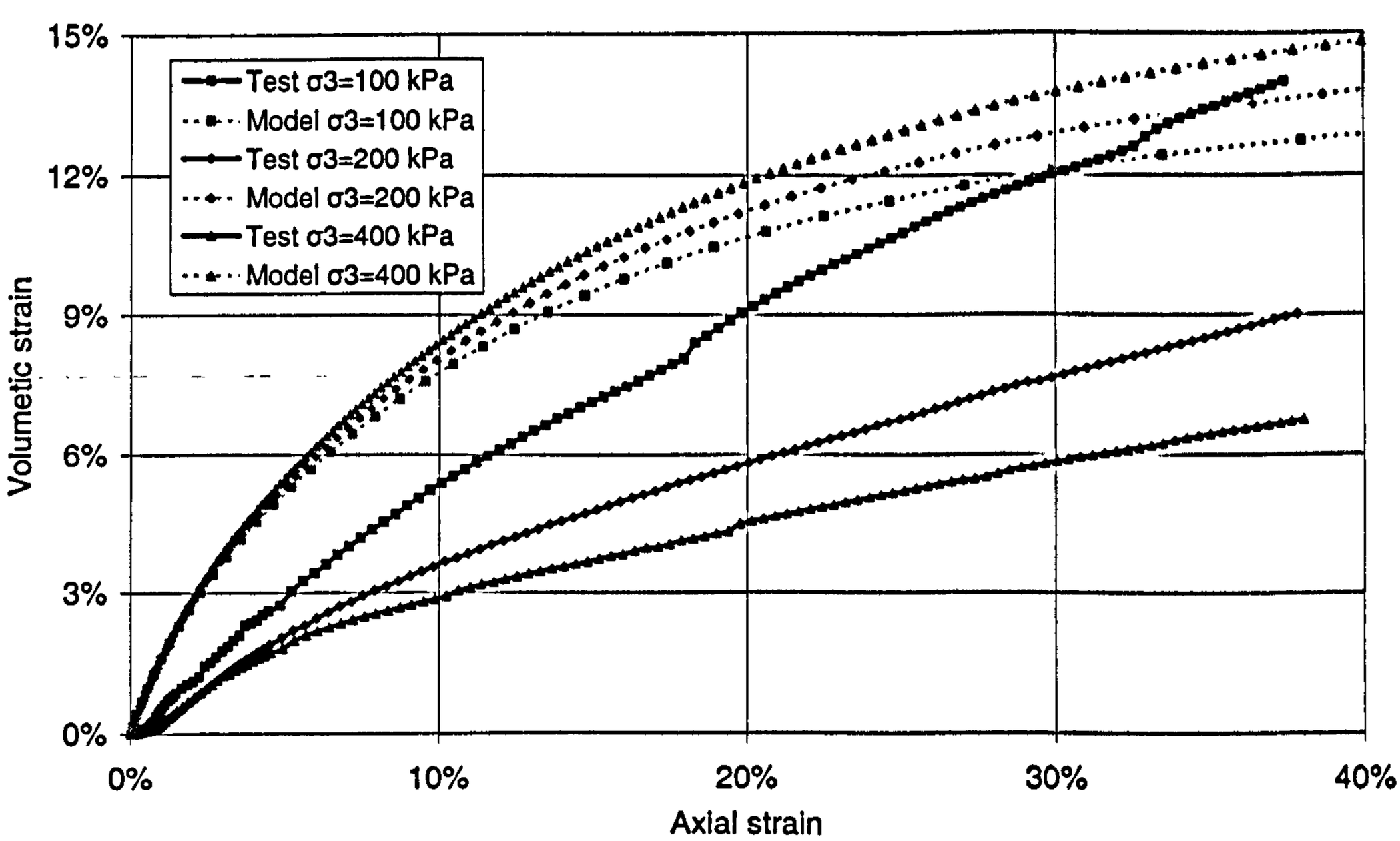

Figure 6-21 The MCC modelling results with higher λ value: volumetric strain vs. axial strain

6.4 Discussion and Summary

A constitutive model for MSW has been proposed by combining the Modified Cam-Clay model with the one-dimensional compression MSW model and the fibre reinforcing model. Initially, the general development of the model was discussed, in which general issues of how to combine the

models together were proposed and basic formulations were presented. Development of the MSW constitutive model for a specific boundary condition, i.e. the drained triaxial compression test, was then discussed. Analytical solutions for the MCC model under drained triaxial compression was derived in ***q-p'*** stress plane. The MCC model was combined with the CM and the RM respectively to demonstrate their capabilities in modelling the influences of compressible and reinforcing particles on the MSW mechanical behaviour. An MSW model including both the CM and the RM was developed and its behaviour was demonstrated, after which triaxial compression tests reported by Machado *et al.* (2002) was modelled using the proposed MSW model.

Although only one triaxial compression test was modelled (it represents typical MSW behaviour as shown in section 2.2.2), the MSW model showed its advantages in modelling MSW mechanical behaviour in the following aspects:

1) The MSW model can reproduce the stress-strain behaviour of MSW observed in triaxial compression tests in the initial and intermediate strain ranges. Shear stiffness values in these strain ranges is not as high as predicted by soil models and the stiffness degradation is also slower than soil models. This MSW behaviour is mainly dominated by the existence of compressible particles and can be simulated by the one-dimensional compression model;

2) Larger volume change can be predicted by the MSW model than soil models, without increasing plastic shear strain and sacrificing shear stiffness. It is one of the requirement of waste model applied in numerical modelling discussed in section 3.2.1 and 3.2.2;

3) The triaxial tests on waste demonstrated different MSW volumetric behaviour to soils i.e. with lower confining stresses more volumetric strains were obtained. It has been suggested that this behaviour can be attributed to the non-linear relationship between the intra-void ratio change and logarithm of the normal stress. This volumetric behaviour can be possibly modelled by applying confining stress dependent intra-voids compression parameters, though there is no such experimental data to determine the parameters at present.

However, the MSW model cannot reproduce the exact shapes and values obtained from the tests. For the deviator stress versus axial strain curves, increasing stiffness behaviour was observed in the large strain range. Transformation from compressible particles to reinforcing particles and more reinforcing particles are mobilised with larger strains are considered as the two main factors related to the increasing stiffness behaviour. Although the current MSW model cannot reproduce the observed stress-strain behaviour in the large strain range, it has the potential to model this aspect of behaviour by incorporating the non-linear mobilised tensile stress analysis in future work. It should be noted that the strain range boundary values are dependent on the waste composition, e.g. proportions of compressible and reinforcing particles. The MSW model has the

potential to model the influences of compressible and reinforcing particles by using appropriate parameter values which will be discussed Chapter 8.

For the volumetric strain versus axial strain curves, the model used was based on one-dimensional compression and this was applied to triaxial compression directly, which probably led to the gap between modelling and measured curves. In addition, a constant intra compression index (i.e. linear model) was used in the compression model, while higher consolidation stress makes the particles more difficult to be compressed (because more compressible particles have already been compressed) which indicates a non-linear relationship is required. However, currently no such experiment can quantify the non-linear relationship between the intra-void ratio change and logarithm of the normal stresses.

It should be noted that all the parameters adopted in the above modelling were back-analysed to provide a fit between the modelling results and testing curves, instead of measuring from tests (e.g. one-dimensional compression and triaxial compression tests). This was done as a completely different methodology was adopted for MSW modelling, and little useful information can be found in Machado *et al.* (2002) to determine the required parameters. In addition, no method has been developed to determine the parameters required for the compression model proposed in Chapter 4 and the reinforcing model in Chapter 5, which will be further discussed in Chapter 8.

CHAPTER

7

Finite Element Method Implementation

7.1 Introduction

In order to demonstrate in this chapter the applicability of applying the proposed MSW model into numerical modelling, the model will be incorporated into the finite element method. As discussed in section 3.5, the finite element programming method proposed by Smith and Griffith (1998) has been selected for including the MSW constitutive modelling. Firstly, general programming methods employed in the finite element method are introduced, particularly the non-linear finite element algorithms. Then, the LMTSA-E-MC (which was validated in Chapter 5) and LMTSA-P-MC are coded into the finite element method by combining the fibre model with the Mohr-Coulomb soil model. The Modified Cam-Clay model is coded into the program using non-linear finite element analysis techniques, after which the MSW model combining the Modified Cam-Clay model with the compression and fibre reinforcing models is implemented into the finite element method. It should be noted that all the programs are coded for the triaxial boundary condition, as the MSW model is currently restricted to triaxial compression, and also the finite element programs can be verified by the analytical solutions presented in Chapter 6.

7.2 Programming the Finite Element Method

Prior to the detailed programming of the proposed material model, several general issues about programming the finite element method will be discussed, i.e. the basic programming structure in FORTRAN 90, and finite element theory for non-linear materials.

7.2.1 Programming Structure in FORTRAN 90

Smith and Griffith (1998) programmed the finite element method in FORTRAN 90 with a strongly structured sense. A nested structure was seen for most of the subroutines and a representation method called "structure charts" (Lindsey, 1977) rather than flow charts was

adopted to describe the actions. The main features of these charts have been identified by Smith and Griffith (1998) as follows:

- **The Block**

Figure 7-1 shows a typical block structure, which is normally used for the outermost level of each structure chart. It can be seen that the indicated actions are to be performed sequentially within a block.

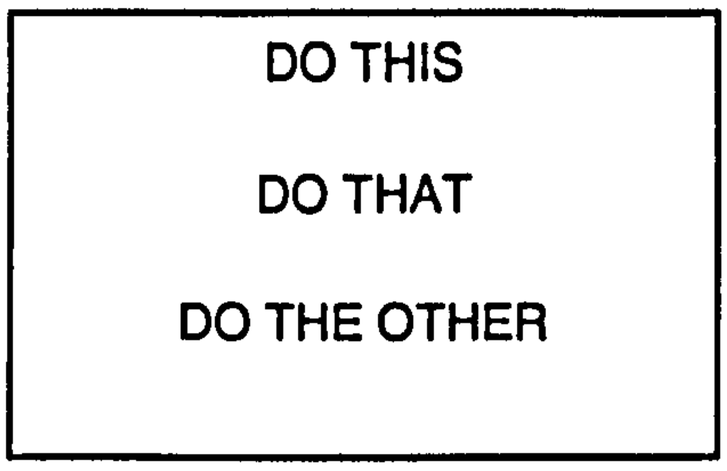

Figure 7-1 Structure charts: The block (Smith and Griffith, 1998)

- **The Choice**

Figure 7-2 shows a typical choice structure, in which the IF...THEN...ELSE, IF...THEN...END IF or SELECT CASE types of constructs are used.

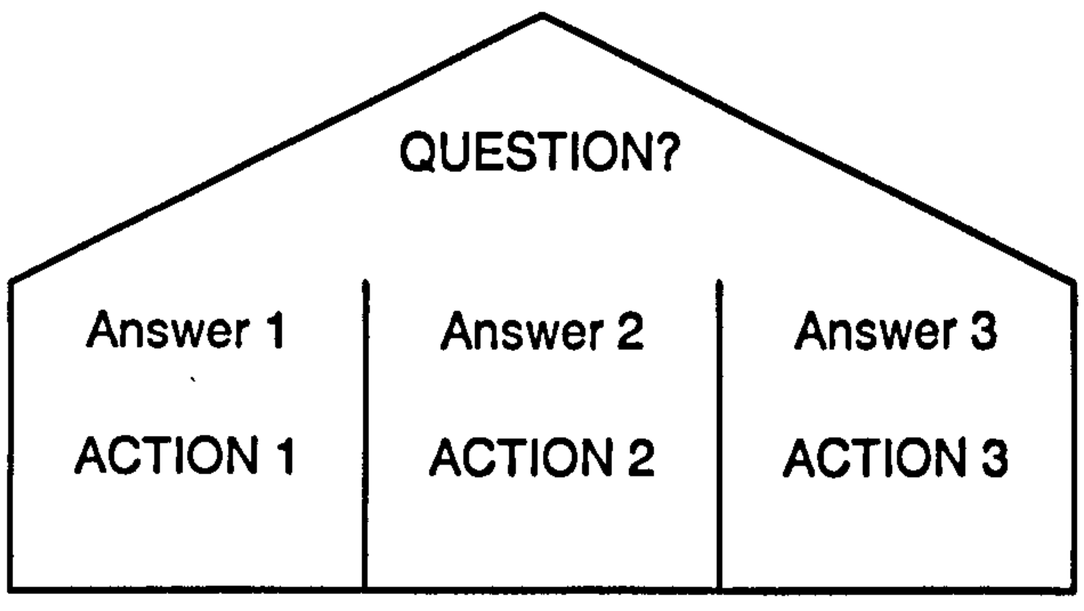

Figure 7-2 Structure charts: The choice (Smith and Griffith, 1998)

- **The Loop**

Figure 7-3 shows typical loops, in which various forms of loops are used, either for a fixed number of repetitions or "forever" (so-called because of the danger of the loop never being completed).

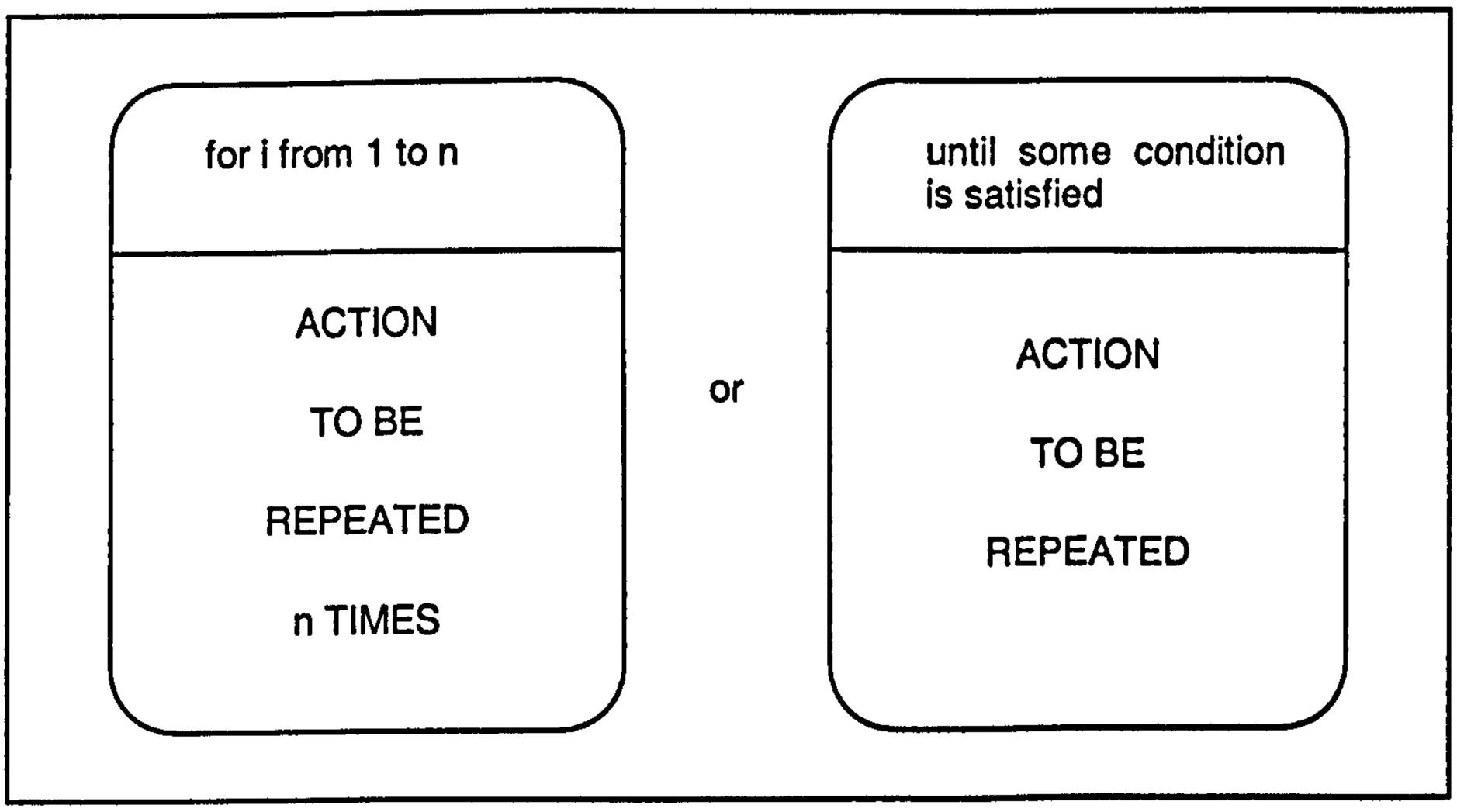

Figure 7-3 Structure charts: The loop (Smith and Griffith, 1998)

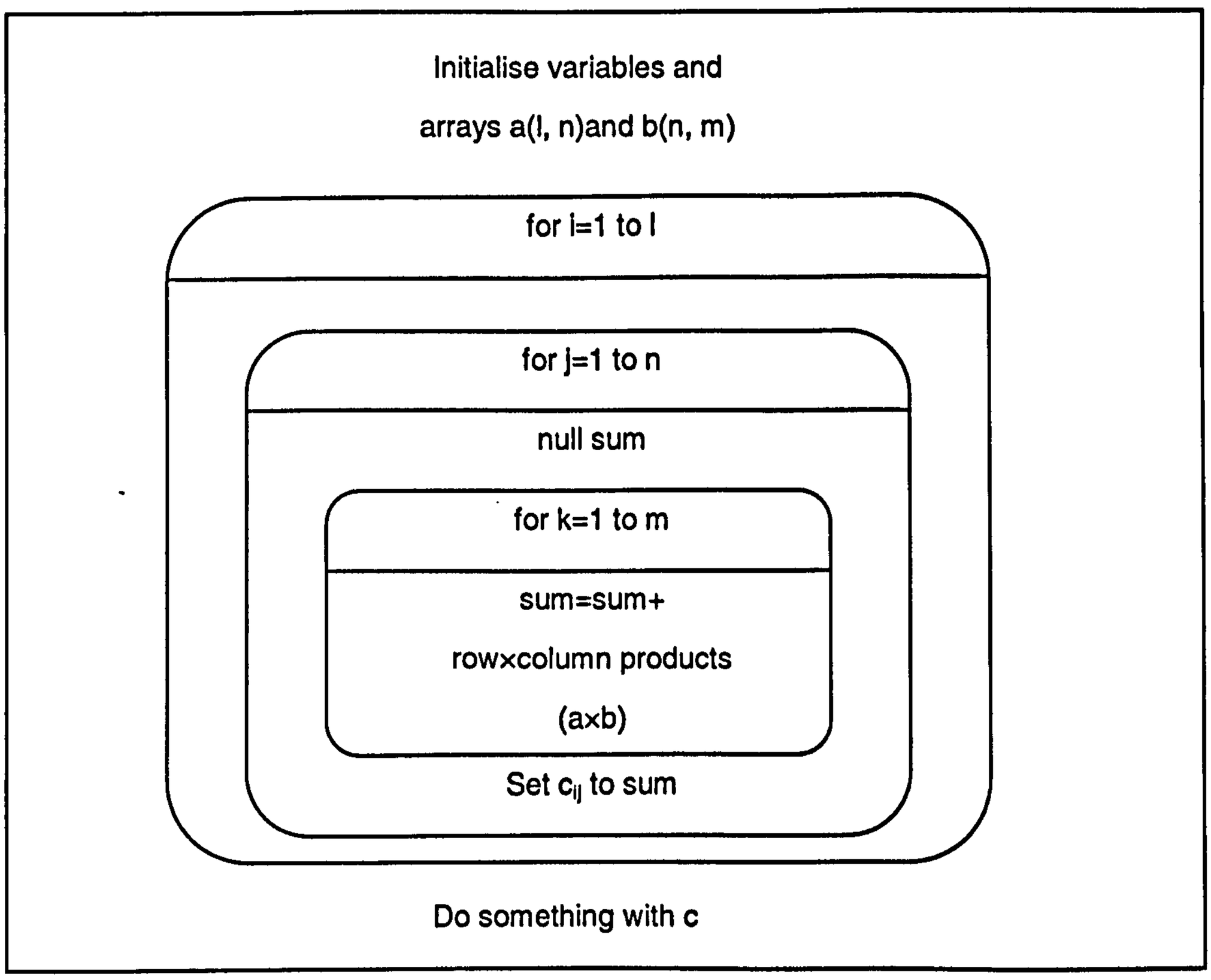

Figure 7-4 An example of structure charts: matrix multiplication (Smith and Griffith, 1998)

It should be noted that the structure charts notation discourages the use of GOTO statements which may result in confusions. Using the three types of structure discussed above, a matrix

multiplication program would be represented as shown in Figure 7-4, in which the nested nature of a typical program can be seen.

7.2.2 Non-Linear Finite Element Analysis

Non-linear finite element analysis is required when the non-linearity is raised by either material or geometry, or both of them. This section explains how the finite element method can be adapted to deal with the material non-linearity. When analysing a boundary value problem using the finite element method, four basic solution requirements need to be satisfied, which are equilibrium, compatibility, constitutive relationship and boundary conditions. Non-linearity introduced by the constitutive relationship (i.e. material non-linearity) causes the governing finite element equations to be reduced to the following incremental form (Owen and Hinton, 1980):

$$K_i \Delta u_i = \Delta P_i \qquad \textit{Eq. 7-1}$$

where K_i is the incremental global system stiffness matrix, Δu_i is the vector of incremental nodal displacements, ΔP_i is the vector of incremental nodal forces and i is the loading increment number. To obtain a solution for a boundary value problem, the change in boundary conditions (e.g. load size and type, construction and/or excavation) is applied in a series of increments and for each loading increment the above equation needs to be solved. The final solution can be reached by summing the results of all the loading increments. Due to the non-linearity of the material constitutive relationship, the incremental global stiffness matrix K_i is dependent on the current stress and strain levels and therefore is not constant, but varies over every increment. This variation has to be included in the analysis unless a very larger number of small loading increments are used. Thus, the solution of Eq. 7-1 is not straightforward and different solution strategies have been proposed. The objective of all such strategies is to find the solution of the equation as accurate as possible, ensuing satisfaction of the four basic requirements mentioned above. Potts and Zdravkovic (1999) summarised three popular solution strategies, which are the tangent stiffness, visco-plastic and the Modified Newton-Raphson scheme as follows:

➢ Tangent Stiffness Method

The tangent stiffness method, sometimes called the variable stiffness method, is the simplest solution strategy. It is the method implemented in the geotechnical finite element program CRISP (Britto and Gunn, 1987), which is widely used in engineering practice. In this approach, the incremental stiffness matrix K_i in Eq. 7-1 is assumed to be constant over each increment and is calculated using the current stress state at the beginning of each increment. This is equivalent to using many pieces of linear relationship to approximate the non-linear constitutive behaviour. In order to illustrate the application of this approach, a uniaxially loaded non-linear bar (i.e. one-

dimensional problem) is considered, as shown in Figure 7-5. When the bar is loaded, the true load displacement response has been shown in Figure 7-6, which represents the nonlinear behaviour of an elastic-hardening plastic material.

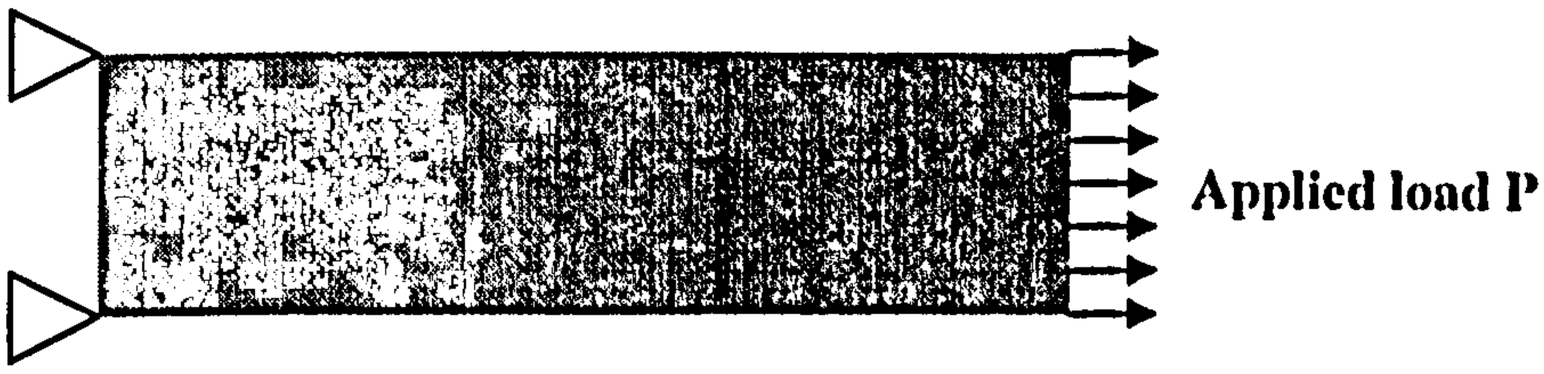

Figure 7-5 Uniaxial loading of a bar of non-linear material

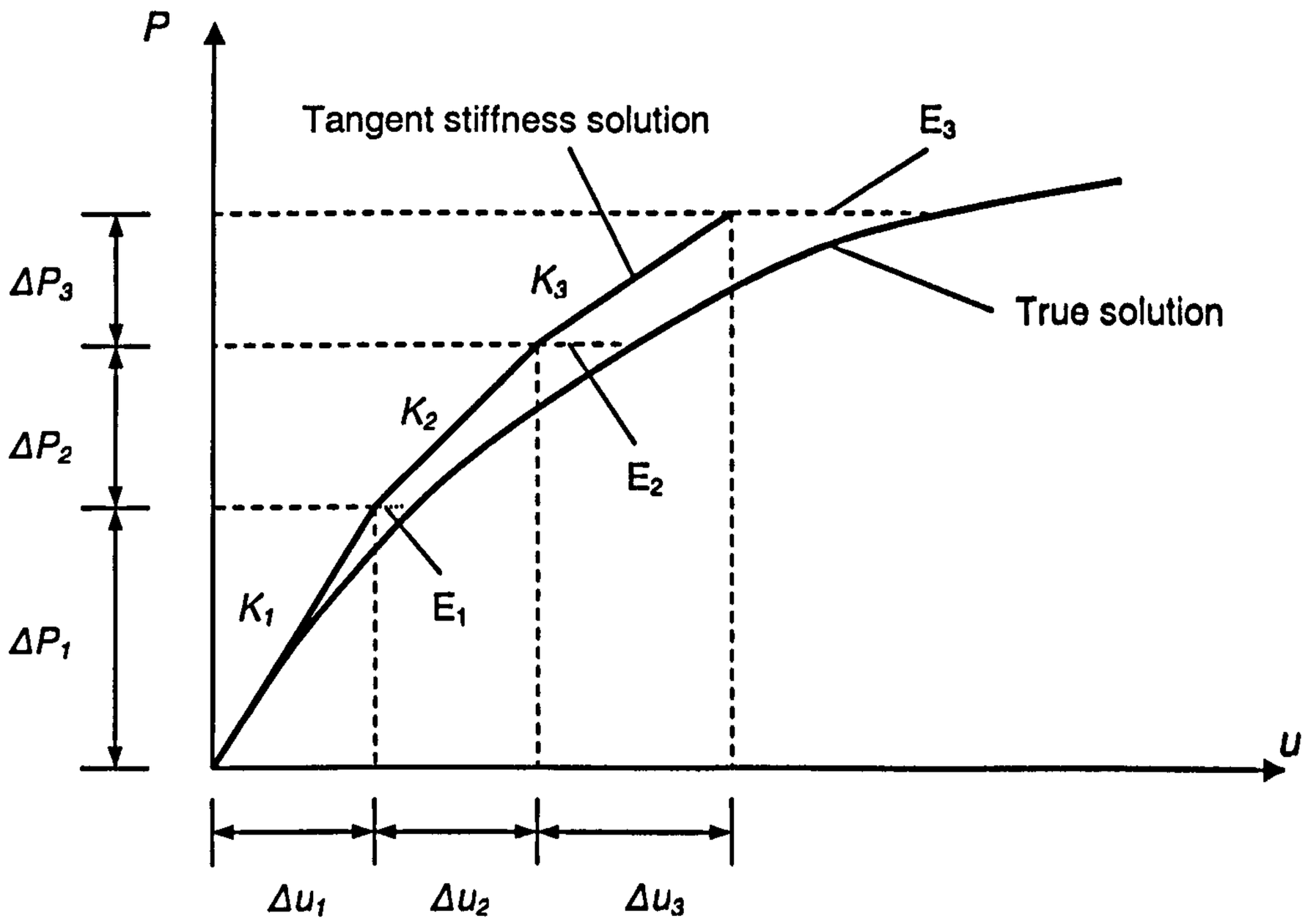

Figure 7-6 Application of the tangent stiffness algorithm to the uniaxial loading of a bar of a non-linear material (after Potts and Zdravkovic, 1999)

The applied load normally needs to split into a sequence of increments in the non-linear finite element analysis, including the tangent stiffness approach. Three loading increments have been shown in Figure 7-6, which are ΔP_1, ΔP_2 and ΔP_3. The analysis starts from the application of ΔP_1, at which the incremental global stiffness matrix K_1 for this increment is evaluated based on the unstressed stage of the bar, i.e. the initial tangent stiffness. For an elasto-plastic material, this stiffness matrix can be obtained using the elastic constitutive matrix D (see Eq. 5-7). After that, the incremental nodal displacement Δu_1 can then be calculated using Eq. 7-1. As the stiffness

matrix for this loading increment is assumed to be constant, a linear relationship between load and displacement has been predicted, from which an error E_1 between the true solution and the predicted solution has occurred at the end of the increment.

When the second increment of load is applied, the incremental global stiffness matrix K_2 is evaluated using the stresses and strain appropriate to the end of the first increment. The nodal displacement Δu_2 can be calculated from Eq. 7-1. Another linear relationship is predicted and this deviates further from the true solution. A similar procedure occurs when the third loading increment ΔP_3 is applied. The global stiffness K_3 is evaluated using the stresses and strains at the end of the second increment. Therefore, the load displacement curve again drifts further from the true solution with another linear prediction. It can be seen easily that the error at the end of each increment is accumulated from the errors for the previous increments, plus the error occurs at this increment due to the linear prediction. Thus, the accuracy of the tangent stiffness solution is extremely dependent on the size of the loading increments. It can be concluded from the simple example that many small solution increments are needed for the tangent stiffness method in order to obtain accurate solutions for strongly non-linear problems.

In addition, according to Potts and Zdravkovic (1999), the tangent stiffness method can give particularly inaccurate results when material behaviour changes from elastic to plastic or vice versa. The reason for this error is that the yield (and plastic potential) derivatives are evaluated in illegal stress, i.e. with stress values which do not satisfy the yield (or plastic potential function. This is mathematically wrong and leads to incorrect elasto-plastic constitutive matrices. Potts and Zdravkovic (1999) compared the tangent stiffness finite element analysis results with the analytical results for the one-dimensional compression program, using both the elastic-perfectly plastic Mohr-Coulomb model and the Modified Cam-Clay model. It was observed that the errors using the Modified Cam-Clay model are much greater than those for the Mohr-Coulomb model. The reason is that, for the Modified Cam-Clay model, the yield (and plastic potential) derivatives vary on the yield (or plastic potential) surface, while constant for the Mohr-Coulomb model. Moreover, for the strain hardening/softening models, once the analysis goes wrong, incorrect plastic strains and hardening/softening parameters will be calculated.

➢ Visco-Plastic Method

This method uses the equations of visco-plastic behaviour to calculate the behaviour of non-linear, elasto-plastic, and time independent materials (Owen and Hinton, 1980; Zienkiewicz and Cormeau, 1974). In this method, the material is allowed to sustain stresses outside the yield surface for finite periods. Overshoot of the yield criterion, as indicated by a positive value of the yield function f, is an integral part of the method and is actually used to drive the algorithm.

The simple example of a uniaxially loaded non-linear bar shown in Figure 7-5 is again used to illustrate the application of the visco-plastic method in the finite element method. The material is assumed to instantaneously behave linear elastically when a increment of load is applied. If the resulting stress state lies within the yield surface, i.e. the yield function f is negative, the incremental behaviour is elastic and therefore the calculated displacements are correct; if the resulting stress state violates the yield criterion, i.e. f is positive, the stress state can only be sustained momentarily and the visco-plastic strain occurs. The magnitude of the visco-plastic strain rate can be determined by the value of the yield function, which is a measure of the degree by which the current stress state exceeds the yield surface. The visco-plastic strains increase with time, causing the material to relax with a reduction in the yield function and hence the visco-plastic strain rate. A convergence criterion is needed to step forward in time until the visco-plastic strain rate is very small. Until then, the accumulated visco-plastic strain and the associated stress change are equal to the incremental plastic strain and stress change respectively. The above process can be explained in Figure 7-7.

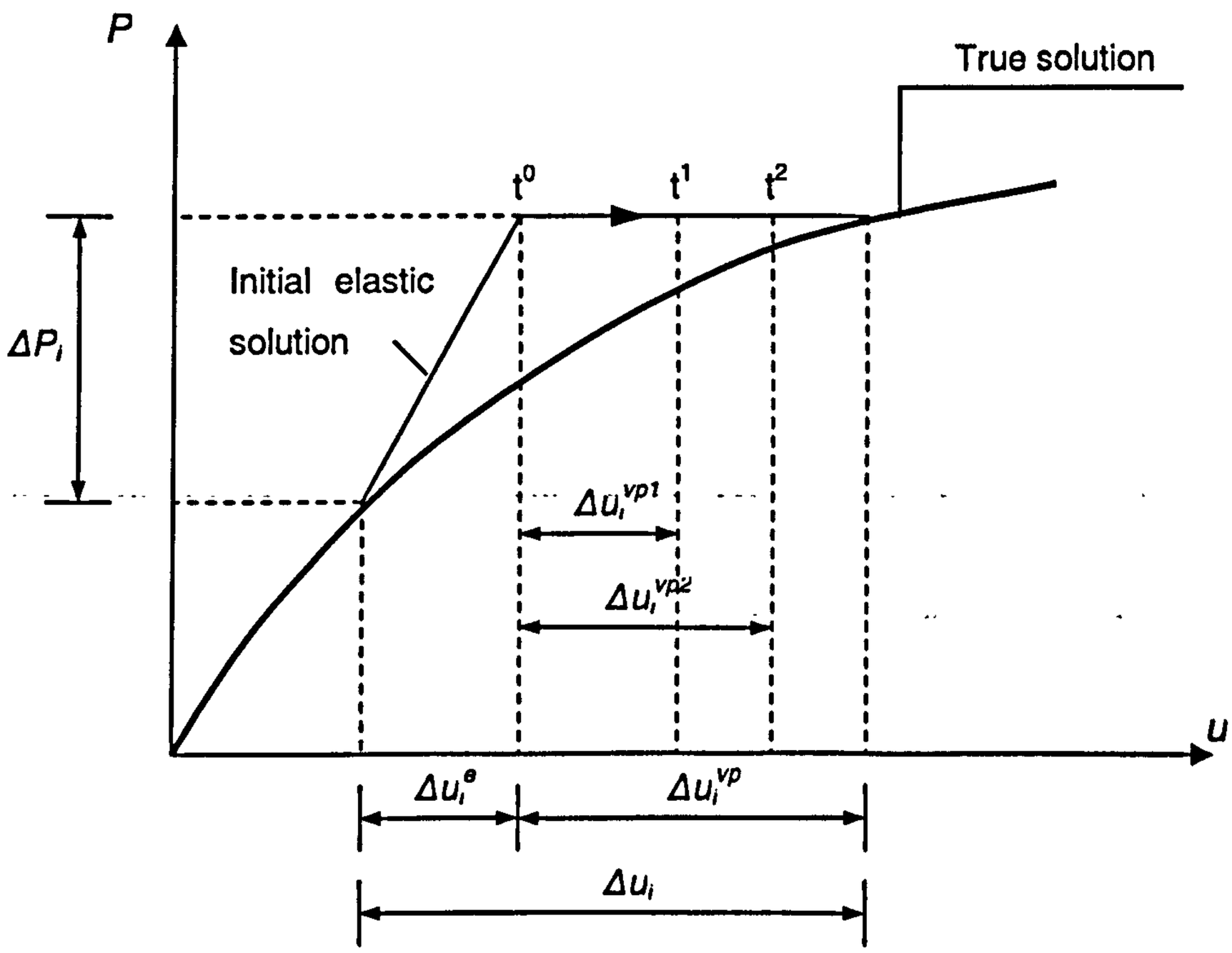

Figure 7-7 Application of the visco-plastic algorithm to the uniaxial loading of a bar of a non-linear material (after Potts and Zdravkovic, 1999)

The visco-plastic strain rate that is related to the amount by which yield has been violated can be expressed as:

$$\dot{\varepsilon}^{vp} = f\frac{\partial g}{\partial \sigma} \qquad \textit{Eq. 7-2}$$

in which f is the yield function and g is the plastic potential, which are the same if associate flow rule is adopted as discussed in section 2.4.1. Over a time step t to $t+\Delta t$ (i.e. the j^{th} iteration), the visco-plastic strain is given by:

$$\left(\delta\varepsilon^{vp}\right)^{j} = \int_{t}^{t+\Delta t}\dot{\varepsilon}^{vp}\,dt \qquad \textit{Eq. 7-3}$$

and for small time steps the above equation can be approximated to:

$$\left(\delta\varepsilon^{vp}\right)^{j} = \Delta t\cdot\dot{\varepsilon}^{vp} \qquad \textit{Eq. 7-4}$$

Therefore, the incremental visco-plastic strain can be obtained for the j^{th} iteration under the i^{th} loading increment by:

$$\left(\Delta\varepsilon^{vp}\right)^{j} = \left(\Delta\varepsilon^{vp}\right)^{j-1} + \Delta t\cdot\dot{\varepsilon}^{vp} \qquad \textit{Eq. 7-5}$$

The "time step" for unconditional numerical stability has been derived by Cormeau (1975) and depends on the assumed yield criterion. For the Mohr-Coulomb elastic-perfectly plastic soil model:

$$\Delta t = \frac{4(1+\mu)(1-2\mu)}{E\left(1-2\mu+\sin^{2}\phi\right)} \qquad \textit{Eq. 7-6}$$

It is necessary to calculate nodal forces equivalent to the change in incremental visco-plastic strains and add them to the increment global right had side vector. The elastic stress increment associated with the change in visco-plastic strains for the j^{th} iteration is given by:

$$\left(\delta\sigma^{vp}\right)^{j} = D\cdot\left(\delta\varepsilon^{vp}\right)^{j} = D\cdot\Delta t\left(\dot{\varepsilon}^{vp}\right)^{j} \qquad \textit{Eq. 7-7}$$

The incremental global right hand side load vector then becomes:

$$\left(\Delta P_i\right)^{j} = \left(\Delta P_i\right)^{j-1} + \sum_{elements}^{all}\int_{V} B^{T}D\cdot\Delta t\left(\dot{\varepsilon}^{vp}\right)^{j}dV \qquad \textit{Eq. 7-8}$$

in which B is the shape function matrix, D is the constitutive matrix in the finite element method, and V is the volume of the element.

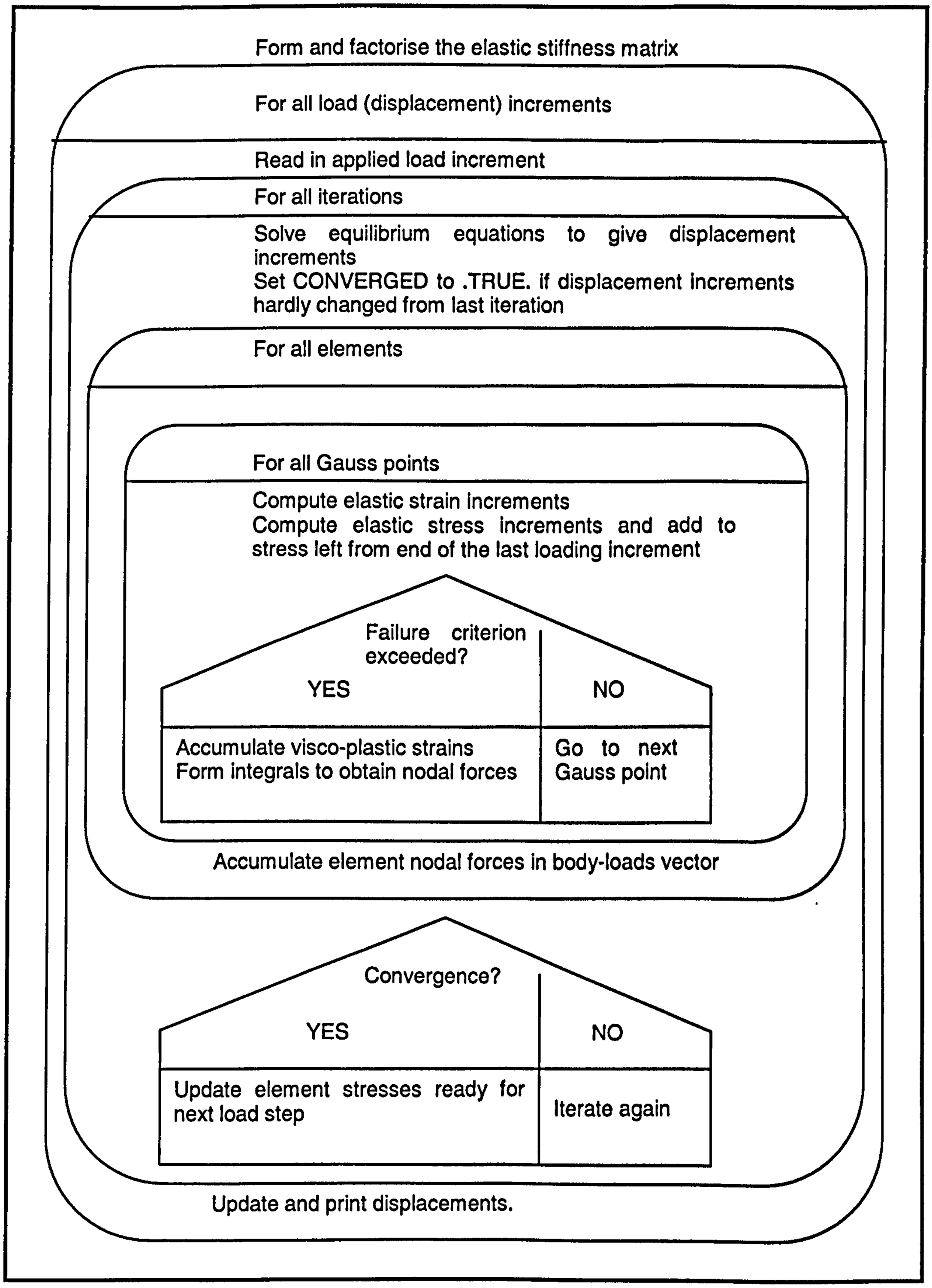

Figure 7-8 Structure chart for the visco-plastic method (Smith and Griffith, 1998)

This process is repeated at each "time step" iteration until no Gauss point stresses violates the yield criterion within a certain tolerance. The convergence criterion is based on a dimensionless

measure of the amount by which the displacement increment vector Δu_i^j changes from one iteration to the next. An outline of the visco-plastic method which comes after the stiffness matrix formation is given in the structure chart by Smith and Griffith (1998) in Figure 7-8. It should be noted that the structure chart is only for the elastic-perfectly plastic material models, e.g. the elastic-perfectly plastic Mohr-Coulomb model, rather than the elastic-hardening plastic materials.

Theoretically, the visco-plastic method can be applied for both the elastic-perfectly plastic and elastic-hardening plastic materials. In order to identify the errors of this method applied for different constitutive models, Potts and Zdravkovic (1999) programmed this algorithm in their finite element program for both elastic-perfectly plastic materials, such as Tresca and Mohr-Coulomb models, and the elastic-hardening plastic material, such as the Modified Cam-Clay model, and carried out the analysis for the one-dimensional loading problem. It was concluded from comparison of the results that, the visco-plastic algorithm works well for simple constitutive models of the Tresca and Mohr-Coulomb types, while it can involve severe errors for complex critical state constitutive models.

➢ Modified Newton-Raphson Method

It has been demonstrated that, for both the tangent stiffness method and the visco-plastic method, significant errors can arise when the constitutive behaviour is evaluated based upon illegal stress states, particularly for the elastic-hardening plastic material (e.g. the Modified Cam-Clay model). The Modified Newton-Raphson (MNR) algorithm which will be described in this section attempts to rectify this problem by only evaluating the constitutive behaviour in, or very near to, the legal stress states. The original Newton-Raphson method will be described prior to the modified method.

An iterative technique is used to solve Eq. 7-1 in the Newton-Raphson scheme, as shown in Figure 7-9 for the simple uniaxial loading problem. Two loading increments, ΔP_1 and ΔP_2 have been considered in the figure. The first iteration for the first increment is essentially the same as the tangent stiffness method. However, it is recognised that the solution is likely to be in error and the predicted incremental displacement Δu_1^1 are used to calculate the residual load EP_1^1 (which is a measure of the error in the analysis) by:

$$EP_1^1 = \Delta P_1 - K\Delta u_1^1 \qquad \textit{Eq. 7-9}$$

in which $K = K(u)$ is evaluated using the displacement at the end of this iteration. $K\Delta u_1^1$ is the true resisting force provided by the system in its current deformation state. In the elasto-plastic

analysis, the resisting forces can be calculated directly from element stresses, without generating a stiffness matrix in the process, which will be discussed in detail later in this section.

Once EP_1^1 is determined, Eq. 7-1 is then solved again with this residual load, from which the second iterative displacement Δu_1^2 can be obtained. Eq. 7-1 can be rewritten as:

$$(K_t)^j(\Delta u_t)^j = (EP_t)^{j-1} \qquad \textit{Eq. 7-10}$$

in which the superscript j is the iteration number and $(EP_1)^0 = \Delta P_1$. A new global stiffness matrix will be calculated at the beginning of each iteration, based on the latest estimate of the stresses and strains obtained from the previous iteration. The process is repeated until the residual load is smaller than the user-defined convergence criterion. The incremental displacements can be worked out by the sum of the iterative displacements. In principle, the iterative scheme ensures that for each solution increment the analysis satisfies all solution requirements.

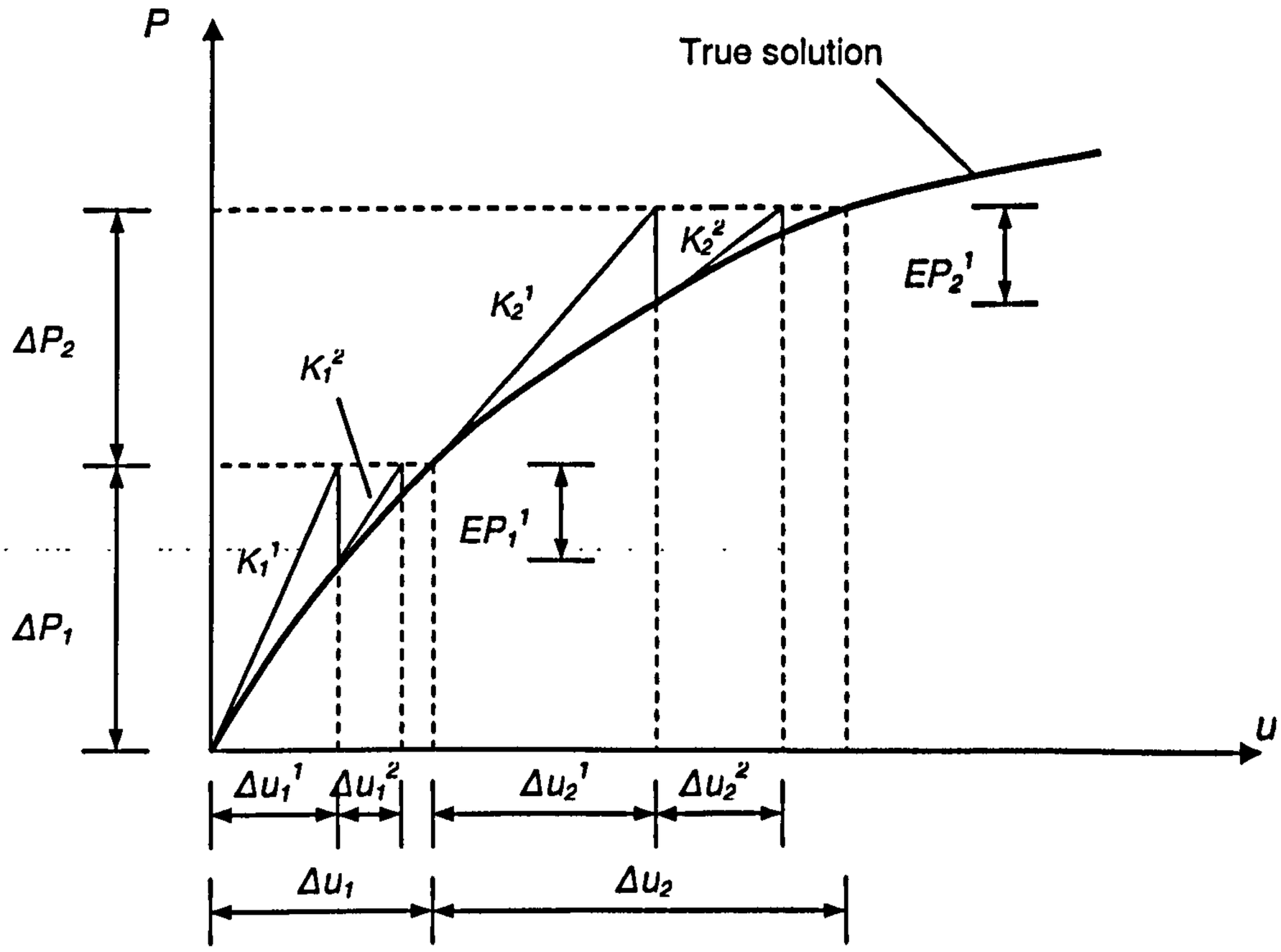

Figure 7-9 Application of the Newton-Raphson algorithm to the uniaxial loading of a bar of a non-linear material (after Owen and Hinton, 1980)

The process described above is called the Newton-Raphson method, in which the incremental global stiffness matrix K_t is recalculated and inverted for each iteration. In order to reduce the cost of computation, the MNR method is often adopted in many non-linear finite element programs, in which the stiffness matrix is only calculated and inverted at the beginning of the loading increment and used for all iterations within the increment. In some cases the initial elastic

stiffness is used throughout all the loading increments. Although the MNR method required more iterations than the original method, each iteration is accomplished more quickly, and the cost savings can be appreciable. The MNR scheme can be depicted in Figure 7-10 for the simple uniaxial loading problem. A structure chart of the MNR method is given in Figure 7-11.

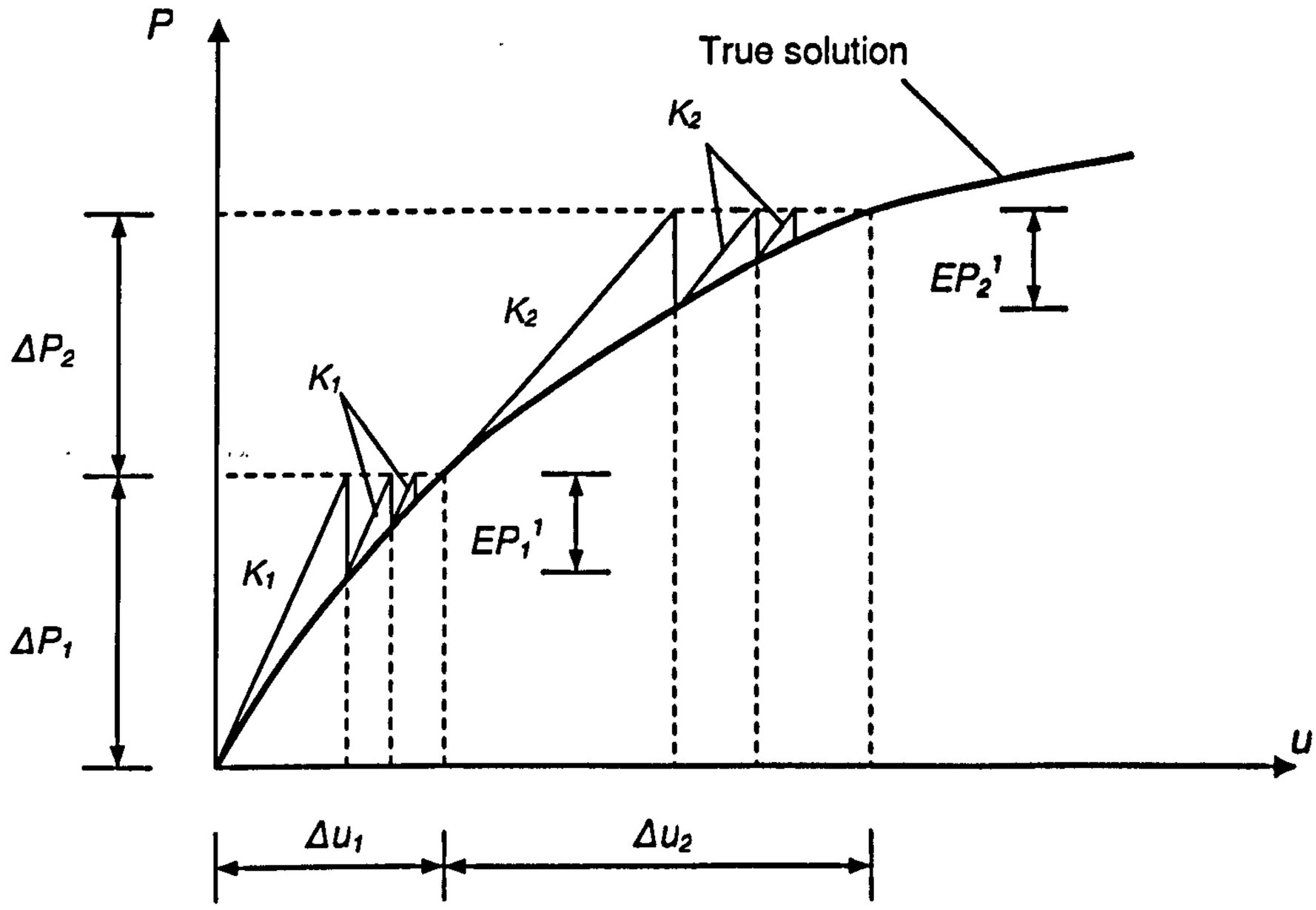

Figure 7-10 Application of the MNR algorithm to the uniaxial loading of a bar of a non-linear material (after Cook et al., 2002)

A very important step in this analysis process mentioned above is to determine the residual load vector at the end of each iteration. It can be calculated directly from the element stresses in the elasto-plastic finite element analysis. At the end of each iteration the current estimate of the incremental displacements is calculated and used to evaluate the incremental strains at each integration point for multi-dimensional problems. The constitutive model is then integrated along the incremental strain paths to obtain an estimate of the stress changes. These stress changes are added to the stresses at the beginning of the increment and used to evaluate consistent equivalent nodal forces. The difference between these nodal forces and the externally applied loads (from the boundary conditions) gives the residual load vector. Since the constitutive behaviour of the non-linear material changes over the loading increment (particularly for the elasto-plastic analysis), care must be taken when integrating the constitutive equations to obtain the stress change. Methods of performing this integration constitute the stress point algorithm (as highlighted in Figure 7-11) and both explicit and implicit approaches have been proposed and discussed in the literature. Potts and Zdravkovic (1999) reviewed two types of stress point algorithms which are

widely accepted in the non-linear finite element analysis, i.e. the substepping algorithm and the return algorithm.

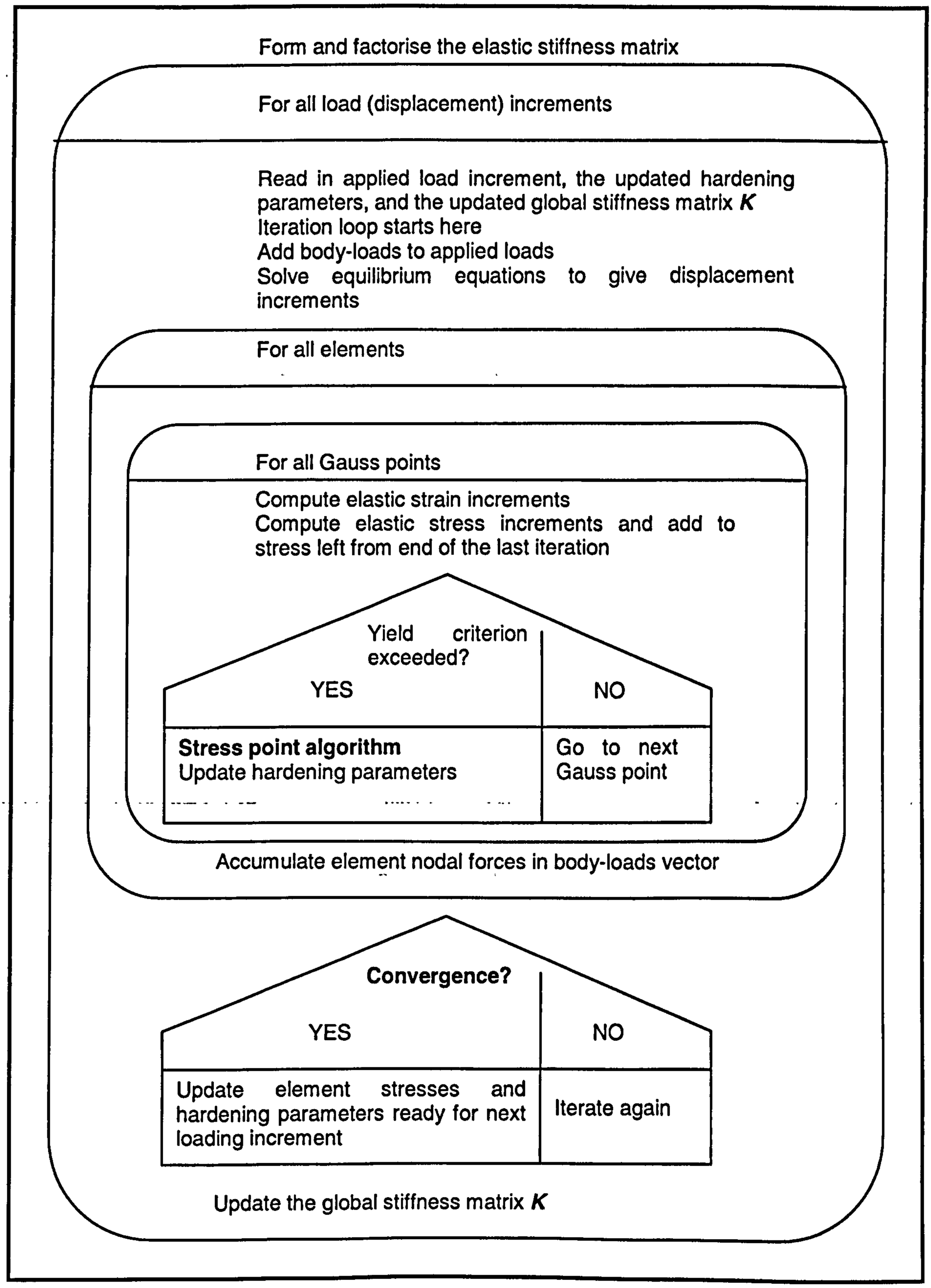

Figure 7-11 Structure chart for the MNR method

The schemes proposed by Wissman and Hauck (1983) and Sloan (1987) are examples of the substepping stress point algorithms, which are essentially explicit. In this method, the incremental strains are divided into a number of substeps. It is assumed that in each substep the strains are a proportion of the incremental strains. Thus, the ratio between the strain components is the same as that for the incremental strains, which means the strains are vary proportionally over the increment. For some boundary conditions, this assumption is correct and consequently the solutions are extremely accurate. However, generally it may not be true and an error can be introduced, the magnitude of which is dependent on the size of the solution increment (Potts and Zdravkovic, 1999). The substepping approach is illustrated in Figure 7-12(a).

The schemes proposed by Borja and Lee (1990) and Borja (1991) are examples of one-step return algorithms, which are essentially implicit. In this approach, the plastic strains over the increment are calculated from the stress conditions corresponding to the end of the increment. However, the stress conditions are not known, which leads to the implicit nature of this method. Most formulations involve some form of elastic predictor to give a first estimate of the stress changes, coupled with a sophisticated iterative sub-algorithm to transfer from this stress state back to the yield surface. The objective of the iterative sub-algorithm is to ensure that the constitutive behaviour is satisfied with the assumption that the plastic strains over the increment are based on the plastic potential at the end of the increment. The basic assumption of the return algorithm is that the plastic strains over the increment can be calculated from the stress state at the end of the increment. Potts and Zdravkovic (1999) pointed out that, this assumption is theoretically incorrect as the plastic response, particularly the plastic flow direction, is a function of the current stress state. If the plastic flow direction does not change over an increment, the return algorithm solution is accurate, while this is not the case for most of the problems and an error is introduced. The magnitude of any error is dependent on the size of the solution increment. The return algorithm approach is illustrated in Figure 7-12(b).

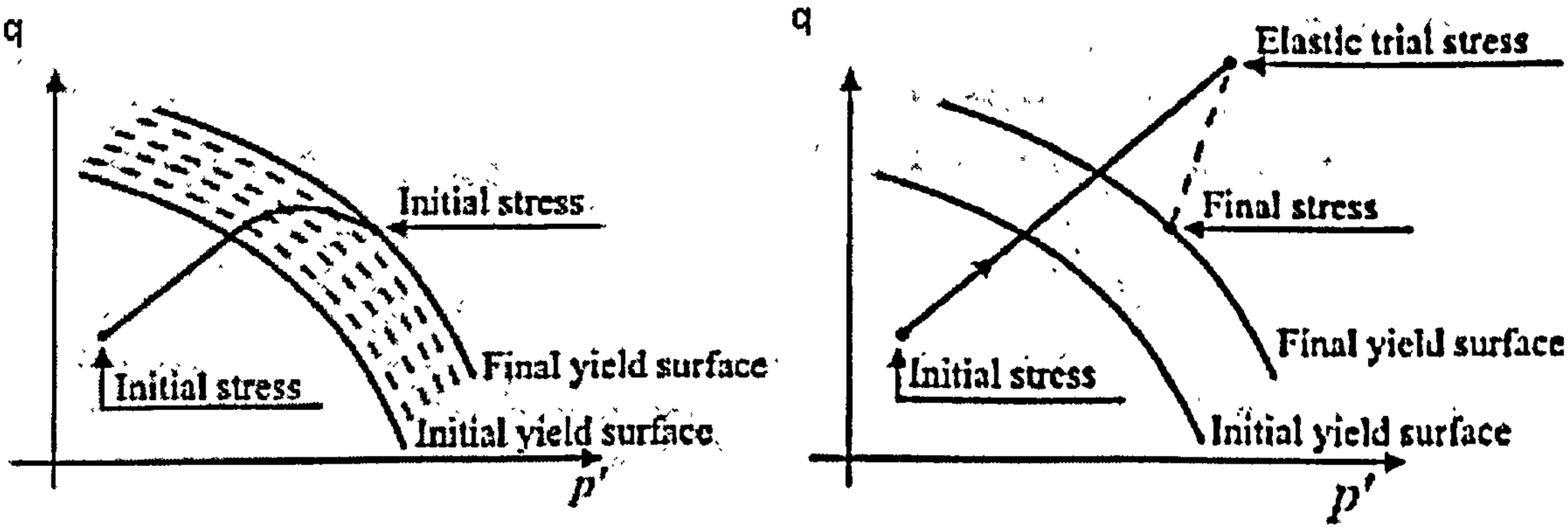

(a) *(b)*

Figure 7-12 Stress pointing algorithms. (a) Substepping approach; and (b) Return algorithm approach (Potts and Zdravkovic, 1999)

Potts and Zdravkovic (1999) performed a fundamental comparison of these two types of stress point algorithms and concluded that both algorithms give accurate results, but, of the two, the substepping algorithm is better. Another advantage of the substepping approach was identified; it is extremely robust and can easily deal with constitutive models in which two or more yield surfaces are active simultaneously and for which the elastic portion of the model is highly non-linear. The return algorithm is not common to any constitutive model. It involves some complicated mathematics to accommodate different constitutive models, which means considerable efforts are required to include a new or modified model. Therefore, the substepping approach proposed by Sloan (1987) will be adopted in this thesis when the MNR method is used. It will be described in section 7.2.3.

Another issue needing addressing in the MNR scheme is the convergence criterion at the end of each iteration, as highlighted in Figure 7-10. This usually involves setting limits to the size of both the iterative displacements $(\Delta u_i)^j$, and the residual loads $(EP_i)^j$. As both the quantities are vectors, it is normal to express their size in terms of the scalar norms through:

$$\left\|(\Delta u_i)^j\right\| = \sqrt{\left((\Delta u_i)^j\right)^T \cdot (\Delta u_i)^j} \qquad \textit{Eq. 7-11}$$

$$\left\|(EP_i)^j\right\| = \sqrt{\left((EP_i)^j\right)^T \cdot (EP_i)^j} \qquad \textit{Eq. 7-12}$$

The iterative displacement norm is usually compared with the norm of the incremental displacement $\|\Delta u_i\|$. It should be noted that the incremental displacement is the sum of the iterative displacements calculated for that increment so far. Similarly, the norm of the residual loads is compared to the norm of the incremental global right hand side load vector $\|\Delta P_i\|$. Potts and Zdravkovic (1999) suggested that the convergence criterion is usually set such that the iterative displacement norm is less than 1% of the incremental displacement norms, and the residual load norm is less than 1% to 2% of the incremental global right hand side load vector norm. Special attention has to be given to boundary value problems which only involve prescribed displacement boundary conditions, as the incremental right hand side load vector is zero. This will be discussed in Section 7.2.4.

7.2.3 Substepping Scheme

Sloan (1987) proposed two substepping schemes for integrating elasto-plastic stress-strain relations, which are designed for use in finite element plasticity calculations and solve for the stress increments assuming that the strain increments are known. Both methods are applicable to a

general type of constitutive law and control the error in the integration process by adjusting the size of each substep automatically. The first method is based on the well-known modified Euler scheme, whereas the second technique employs a high order Runge-Kutta formula. Since the modified Euler scheme is easier to implement and more widely used, it will be adopted in the thesis and will be described here for a general elastic-hardening plastic material model.

Firstly, it is necessary to find a solution to determine the initial yielding of the material. Under a certain loading increment, the strain increments at an integration point may be computed from strain-displacement relations according to:

$$\Delta\varepsilon = B\Delta u \qquad \textit{Eq. 7-13}$$

where B denotes the strain-displacement matrix and Δu is the vector of nodal displacement increments for the current loading increment (or iteration). Once the strains have been determined, the elastic stress increments may be calculated using Hook's law:

$$\Delta\sigma = D\Delta\varepsilon \qquad \textit{Eq. 7-14}$$

At any stage during the solution process the stress-strain behaviour at an integration point will either be 'elastic' or 'plastic'. If a point changes from an elastic to a plastic state, it is necessary to determine the portion of the stress increment that cause purely elastic deformation. Let σ_a denotes the stresses at the beginning of a load step such that

$$f(\sigma_a, \chi) = f_a < 0 \qquad \textit{Eq. 7-15}$$

where the hardening parameter χ remains constant while deformation takes place within the yield surface. By definition, plastic yielding must occur if

$$f(\sigma_a + \Delta\sigma, \chi) = f(\sigma_b, \chi) = f_b > 0 \qquad \textit{Eq. 7-16}$$

In order to determine the portion of the stress increment that lies within the yield surface, a scalar α needs to be found such that

$$f(\sigma, \chi) = 0 \qquad \textit{Eq. 7-17}$$

where

$$\sigma = \sigma_a + \alpha\Delta\sigma,\ 0 < \alpha < 1 \qquad \textit{Eq. 7-18}$$

A first guess for α may be obtained by a simple linear interpolation in f which gives

$$\alpha_1 = \frac{f_a}{f_a - f_b} \qquad \textit{Eq. 7-19}$$

This is theoretically correct if the yield function $f(\sigma, k)$ is a linear function of stress. However, this is rarely the case, and consequently a more refined estimated for α is required. An iteration scheme can be used to find the more accurate α value, which can be expressed as:

$$\alpha_{i+1} = \alpha_i - \frac{f(\sigma_i, \chi)}{f(\sigma_i, \chi) - f(\sigma_{i-1}, \chi)}(\alpha_i - \alpha_{i-1}) \qquad \textit{Eq. 7-20}$$

where the starting values are $\sigma_0=\sigma_a$, $\alpha_0=0$ and α_1 from Eq.7-19. The iteration process to find α is demonstrated by the structure charts, as shown in Figure 7-13.

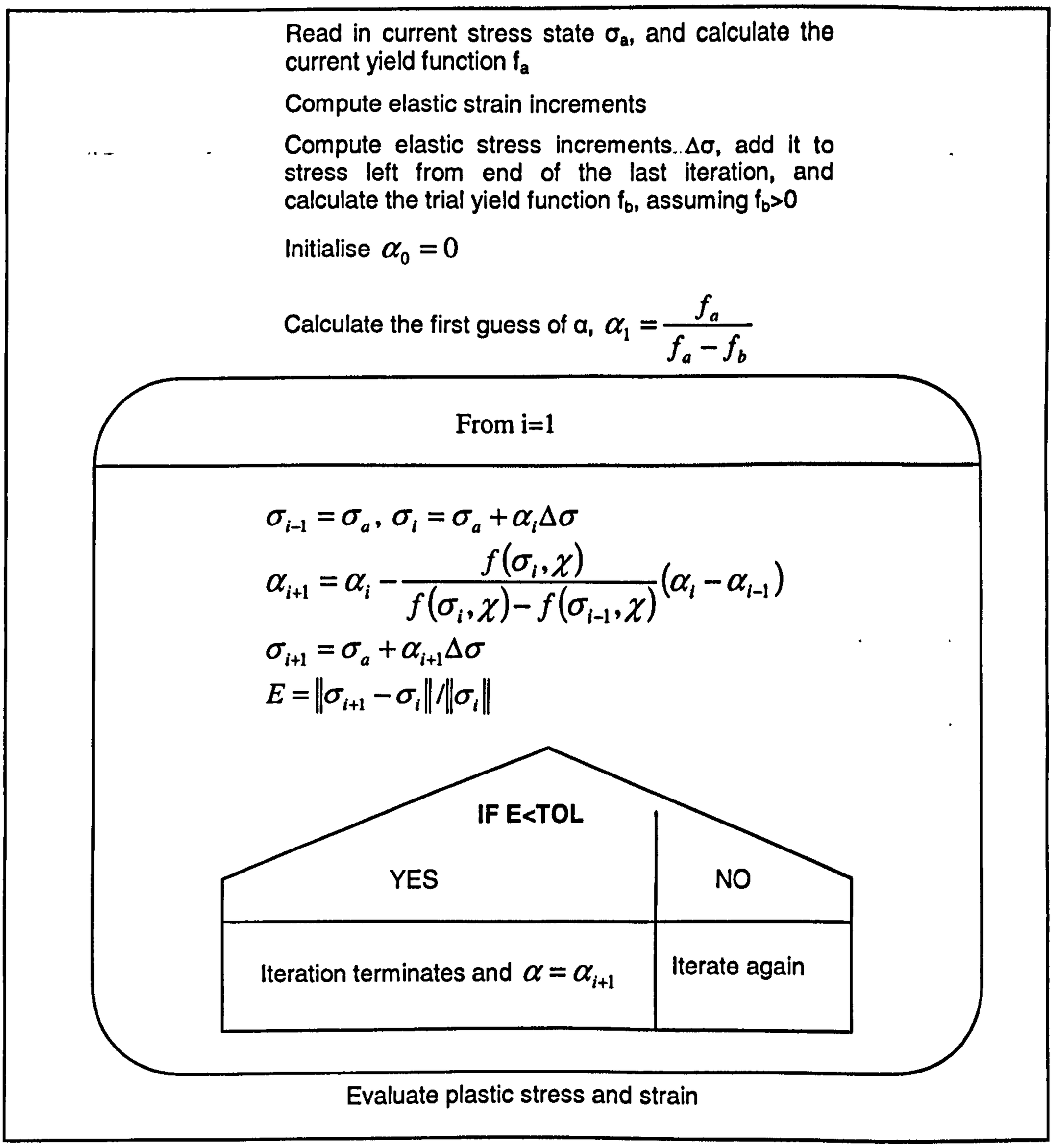

Figure 7-13 Structure chart for determining the plastic stress

Having determined α, the purely elastic portions of the stress and strain increments can be evaluated as:

$$\Delta\sigma^e = \alpha\Delta\sigma \qquad \textit{Eq. 7-21}$$

$$\Delta\varepsilon^e = \alpha\Delta\varepsilon \qquad \textit{Eq. 7-22}$$

The portion of the strain increment that remains, i.e. $(1-\alpha)\Delta\varepsilon$, is associated with elasto-plastic behaviour and it is therefore necessary to integrate the elasto-plastic constitutive matrix D^{ep} over this part of the strain increment. For most constitutive models this cannot be performed analytically and some form of approximation is required. In the substepping approach the strain increment $(1-\alpha)\Delta\varepsilon$ is split into smaller substeps and various simplifications introduced. The size of the substeps can be controlled by estimating the error involved in the simplifications. A modified Euler scheme with error control presented by Sloan (1987) will be adopted. The scheme involves splitting the strain step $(1-\alpha)\Delta\varepsilon$ into a series of smaller substeps, $\Delta T(1-\alpha)\Delta\varepsilon$ (where $0 < \Delta T \leq 1$), and using a modified Euler approximation for each such substep. The size of each substep is determined by estimating the error in the stress changes and comparing this with a user-defined tolerance, TOL. The modified Euler algorithm, which incorporates error control and a variable step size for each integration point, can be summarised as follows:

1) Initialising parameters:

$$\sigma = \sigma_0 + \Delta\sigma^e \qquad \textit{Eq. 7-23}$$

$$\Delta\varepsilon_s = (1-\alpha)\Delta\varepsilon \qquad \textit{Eq. 7-24}$$

$$T = 0 \qquad \textit{Eq. 7-25}$$

$$\Delta T = 1 \qquad \textit{Eq. 7-26}$$

in which T is the accumulate time step. The procedure begins by assuming that only one substep is needed, therefore, ΔT is set to unity initially.

2) Set the substep strain equal to:

$$\Delta\varepsilon_{ss} = \Delta T \cdot \Delta\varepsilon_s \qquad \textit{Eq. 7-27}$$

and calculate a first estimate of the associated stress and hardening/softening parameter changes using a first order Euler approximation:

$$\Delta\sigma_1 = D^{ep}(\sigma, \chi)\cdot\Delta\varepsilon_{ss} \qquad \textit{Eq. 7-28}$$

$$\Delta\varepsilon_1^p = \Lambda(\sigma, \chi, \Delta\varepsilon_{ss})\frac{\partial g(\sigma,\chi)}{\partial\sigma} \qquad \textit{Eq. 7-29}$$

$$\Delta\chi_1 = \Delta\chi\left(\Delta\varepsilon_1^p\right) \qquad \textit{Eq. 7-30}$$

in which χ is the hardening parameter.

3) Using the above results, the stresses and hardening/softening parameters at the end of the substep can be updated as $\sigma + \Delta\sigma_1$ and $\chi + \Delta\chi_1$ respectively. They are then used to calculate a second estimate for the changes in stress and hardening/softening parameters over the substep:

$$\Delta\sigma_2 = D^{ep}(\sigma + \Delta\sigma_1, \chi + \Delta\chi_1)\cdot\Delta\varepsilon_{ss} \qquad \textit{Eq. 7-31}$$

$$\Delta\tilde{\varepsilon}_2^p = \Lambda(\sigma + \Delta\sigma_1, \chi + \Delta\chi_1, \Delta\varepsilon_{ss})\frac{\partial g(\sigma + \Delta\sigma_1, \chi + \Delta\chi_1)}{\partial\sigma} \qquad \textit{Eq. 7-32}$$

$$\Delta\chi_2 = \Delta\chi\left(\Delta\varepsilon_2^p\right) \qquad \textit{Eq. 7-33}$$

4) It is now possible to obtain a more accurate modified Euler estimate of the changes in stress, plastic strain and hardening/softening parameters:

$$\Delta\sigma = \frac{1}{2}(\Delta\sigma_1 + \Delta\sigma_2) \qquad \textit{Eq. 7-34}$$

$$\Delta\varepsilon^p = \frac{1}{2}\left(\Delta\varepsilon_1^p + \Delta\varepsilon_2^p\right) \qquad \textit{Eq. 7-35}$$

$$\Delta\chi = \frac{1}{2}(\Delta\chi_1 + \Delta\chi_2) \qquad \textit{Eq. 7-36}$$

5) Computing an estimate of the local truncation error for the substep ΔT according to:

$$E = \frac{1}{2}(-\Delta\sigma_1 + \Delta\sigma_2) \qquad \textit{Eq. 7-37}$$

The relative error for the substep ΔT can be determined from:

$$R = \frac{\|E\|}{\|\sigma + \Delta\sigma\|} \qquad \textit{Eq. 7-38}$$

which can be checked against the user defined tolerance TOL. The typical range of TOL is 10^{-2} to 10^{-5} suggested by Sloan (1987).

6) If R>TOL, the error in stress is not acceptable and the time step needs to be refined, then go to step 7). Else, this substep is accepted so update the dimensionless time, the stresses, plastic strains and the hardening parameter according to:

$$T = T + \Delta T \qquad \textit{Eq. 7-39}$$

$$\sigma = \sigma + \Delta\sigma \qquad \textit{Eq. 7-40}$$

$$\varepsilon^p = \varepsilon^p + \Delta\varepsilon^p \qquad \textit{Eq. 7-41}$$

$$\chi = \chi + \Delta\chi \quad \textit{Eq. 7-42}$$

Then extrapolate to obtain the size of the next substep. A factor needs to be determined before this by:

$$q = \min\left\{0.8(TOL./R)^{1/2}, 2\right\} \qquad \textit{Eq. 7-43}$$

The new size of the next substep can be calculated by:

$$\Delta T_{new} = q\Delta T \qquad \textit{Eq. 7-44}$$

Before returning to step 2, check that the integration does not proceed beyond T=1 by setting:

$$\Delta T = \min\left\{\Delta T_{new}, 1 - T\right\} \qquad \textit{Eq. 7-45}$$

7) If this substep has failed (i.e. R>TOL in step 6)), extrapolate to obtain a smaller dimensionless time step. First compute

$$q = \max\left\{0.8(TOL/R)^{1/2}, 0.1\right\} \qquad \textit{Eq. 7-46}$$

The refined time step can be set as:

$$\Delta T = q\Delta T \qquad \textit{Eq. 7-47}$$

before returning to step 2.

8) The above procedure stops when T becomes equal to 1.0.

7.2.4 Prescribed Displacement

In most finite element calculations displacement boundary conditions are defined in order to restrict rigid body movements, to restrain part of the structure, or to apply the load. In triaxial compression test FEM modelling, prescribed displacement is normally adopted to apply the axial loading. Different methods can be used to include the prescribed displacement in FEM modelling.

Smith and Griffiths (1998) adopted the following method. For boundary conditions where the prescribed displacements are zero, the equation components associated with these nodes are not required in the solution and information is given to the assembly routine which prevents these components from ever being assembled into the final system. Therefore, only the non-zero nodal displacement values are solved (most of the FEM program do so). It can reduce the number of equations but the value of the reaction force cannot be found through this method. A variation of this condition occurs when known values of displacement are prescribed for some nodes in the system. A named penalty method is used in Smith and Griffiths' program to handle this condition, which is normally adopted in structural analysis. In this method, a 'large' number or 'penalty' term (where the method name comes from), say 10^{12}, is added to the leading diagonal of the stiffness matrix in the row in which the prescribed displacement is required. The term in the same row of the right hand side vector, i.e. the nodal force vector, is then set to the prescribed displacement value multiplied by the augmented stiffness coefficient. Compared with the 'large terms' on both side of the equation, the other terms are relatively small hence can be neglected in the calculation. For example, suppose the value of the displacement at node i is prescribed as δ in an FEM system. The unconstrained set of equations would be assembled and the term at i row and i column in the stiffness matrix augmented by adding 10^{12}. In the subsequent solution there would be an equation:

$$\left(K_{i,i}+10^{12}\right)\phi_i + small\_term = \left(K_{i,i}+10^{12}\right)\delta \qquad \textit{Eq. 7-48}$$

which would have the effect of making ϕ_i equal to δ. Clearly this procedure is only successful if indeed 'small terms' are small relative to 10^{12}. This method could also be used to enforce the boundary condition $\phi = 0$ and has some attractions due to simplicity of programming.

When the MNR method is used to perform the non-linear FEM analysis, the penalty method discussed above is not applicable to prescribe displacements. An iteration technique is applied in the MNR method, in which the residual force has to be calculated at the end of each iteration. Since the reaction force cannot be obtained by the penalty method, other solutions are required to consider the prescribed displacement. Owen and Hinton (1980) described a method by application to a particular problem. The method included the prescribed displacement values into the equations by modifying the process of the Gauss reduction that is used to solve the equations. Thus the reaction forces which are related to the prescribed displacements can be calculated from the known displacement values and the right hand side vectors. Subroutines for the Gauss reduction and back substitution processes have to be modified if this method is adopted. When applying the method, two key points that should be considered were addressed by Owen and Hinton (1980) as follows:

1) For the MNR solution algorithm considered, the processes are essentially accumulative with the value of the unknowns being totalled from the incremental values obtained for each iteration. Therefore, in order to maintain the fixed unknowns at their prescribed values, it is necessary to input the prescribed values into subroutines for the first iteration of a load increment and then prescribe zero values for all subsequent iterations. In this way the final displacements will equal the prescribed values on convergence of the solution.
2) When determining the residual forces in the MNR method, the contribution to the right hand side vector of the reactions at nodal points at which the value of the unknown is prescribed must be accounted for, since any reactions can be interpreted as additional applied loads necessary to maintain the prescribed value of the unknown. Therefore, the evaluated reactions must be added into the vector of applied nodal loads at every iteration.

Two types of convergence criteria are normally applied in the MNR solution scheme, the displacement criterion and load vector criterion discussed in Section 7.2.2. If the structure is to be loaded by prescribed displacement values, the load vector convergence criterion cannot be used because the incremental right hand side load vector is zero for the first iteration. Therefore, only the displacement convergence criterion is available in the prescribed displacement case.

7.3 Programming the Undrained Analysis for Mohr-Coulomb Material

The principle of incorporating the undrained analysis in the finite element method has been illustrated in Section 5.3. Smith and Griffiths (1998) produced an example of undrained analysis combined with the Mohr-Coulomb model in their finite element program. A conventional triaxial compression test (axisymmetric condition) on a undrained soil sample has been modelled. The visco-plastic method was applied to calculate the plastic strains in the program. The structure chart for this program has been given in Figure 7-15. The main program of the undrained analysis can be found in Smith and Griffiths (1998). Only one eight-node rectangle quadrilateral element was used in the finite element mesh, as shown in Figure 7-14.

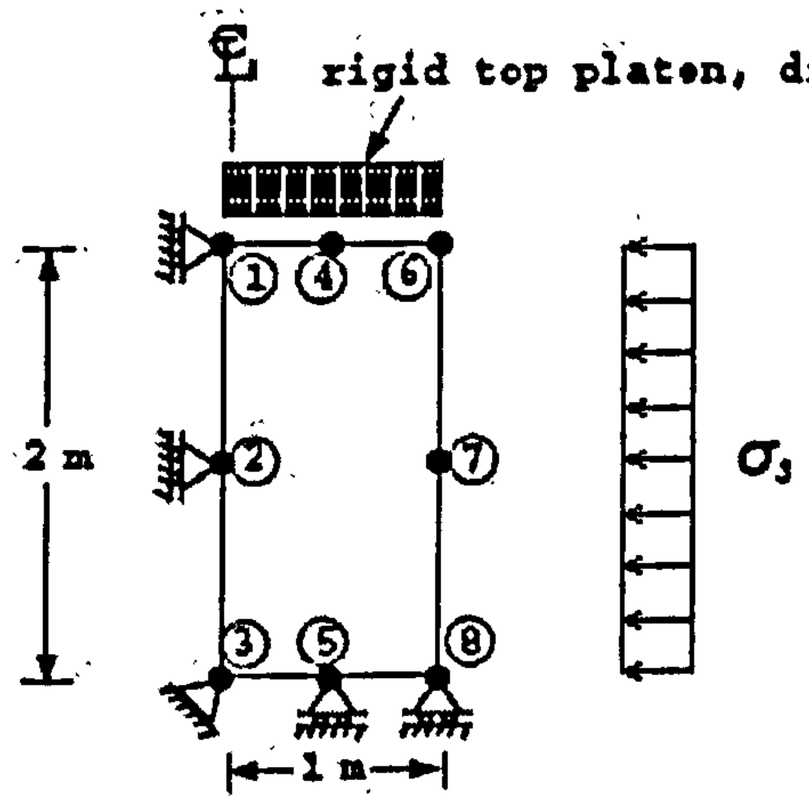

Figure 7-14 Finite element mesh for triaxial compression (Smith and Griffiths, 1998)

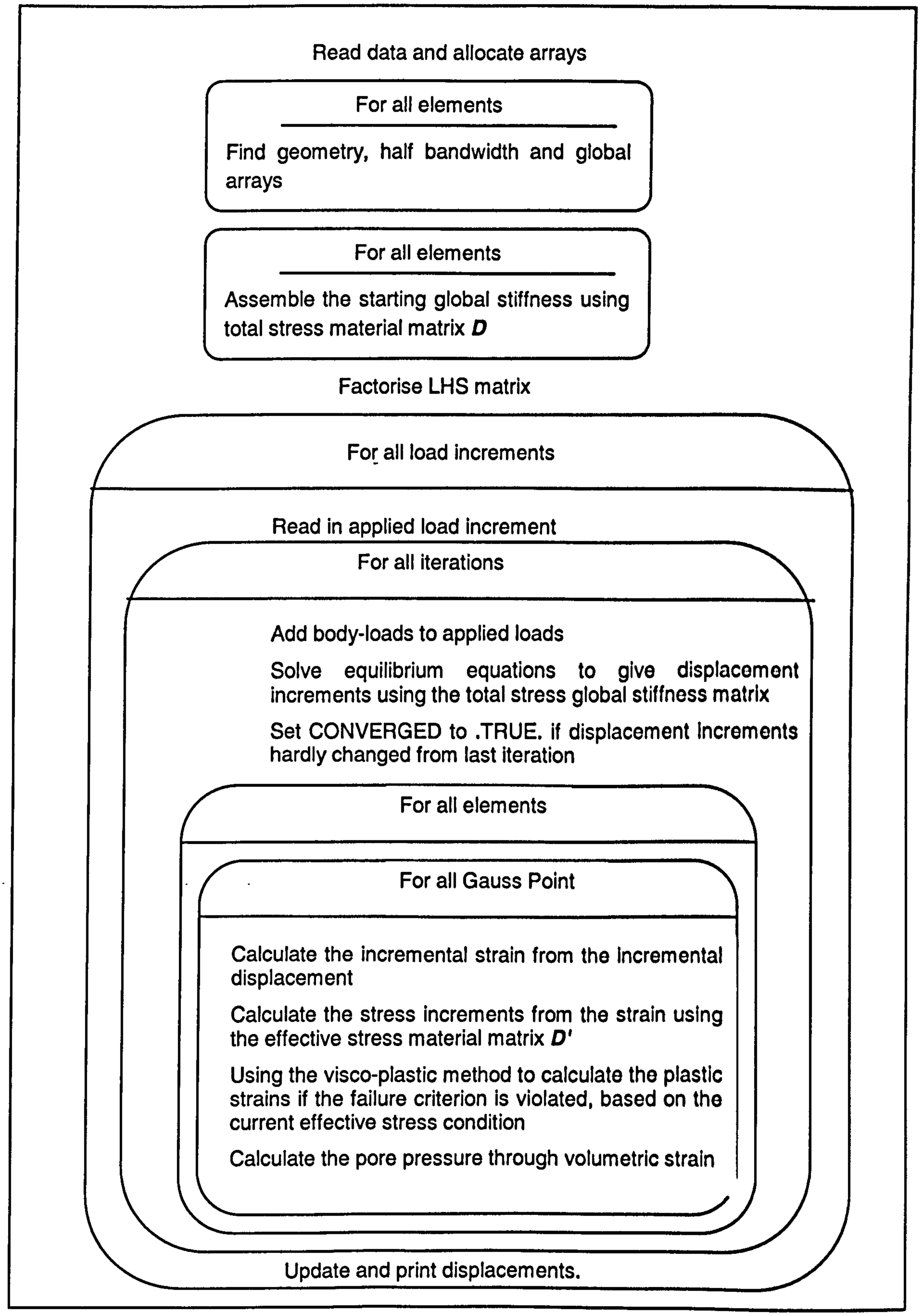

Figure 7-15 Structure chart for program of the undrained analysis for Mohr-Coulomb material

7.4 LMTSA Program with Mohr-Coulomb Model

It has been explained in section 5.2 that the principle of the mobilised tensile stress analysis came from the undrained analysis. Therefore, the program of the mobilised tensile stress analysis is similar to that of the undrained analysis. The effective stress material matrix $\boldsymbol{D'}$ for both analysis have the same expression, the only difference between the two analyses is the use of a different total stress material matrix $\boldsymbol{D}$, which can be obtained from Eq. 5-6 for the undrained analysis and Eq. 5-17 for the linear mobilised tensile stress analysis.

7.4.1 The LMTSA-E-MC Program

The LMTSA-E-MC is the simplest analysis considering linear elastic behaviour of the fibre (or fibre/paste interaction) and the Mohr-Coulomb model for the paste material. Thus, the LMTSA-E-MC program can easily be produced by modifying the formation of the total stress material matrix $\boldsymbol{D}$ in the program of the undrained analysis. The code of the LMTSA-E-MC can be found in Appendix A.

7.4.2 The LMTSA-P-MC Program

As discussed in section 5.2, the improvement of the LMTSA-P-MC comparing to the LMTSA-E-MC is in the constitutive relationship for the reinforcing components. The LMTSA-E-MC considers a linear elastic behaviour for the fibre material (or the interaction between fibres and paste), while the LMTSA-P-MC includes an elastic-perfectly plastic behaviour for fibre material (or the interaction). If an elastic-perfectly plastic behaviour is assumed for a single fibre, an almost elastic-perfectly plastic behaviour will be obtained for the equivalent tensile stress-strain relationship, as shown in Section 5.5.

In the LMTSA-E-MC program, equivalent tensile stress linearly increases with the tensile strain in the related direction without ultimate values being reached. In the LMTSA-P-MC program, an ultimate tensile strain value for fibres needs to be defined and checked against the macroscopic strain level in the related direction. As soon as the ultimate strain value is reached, the tensile stress provided by the fibres remain constant, which is the value multiplied by the equivalent tensile stiffness and the ultimate tensile strain. The LMTSA-P-MC program can be coded by modifying the LMTSA-E-MC program. The structure chart for the LMTSA-P-MC program has been given in Figure 7-16, and the code can be found in Appendix B.

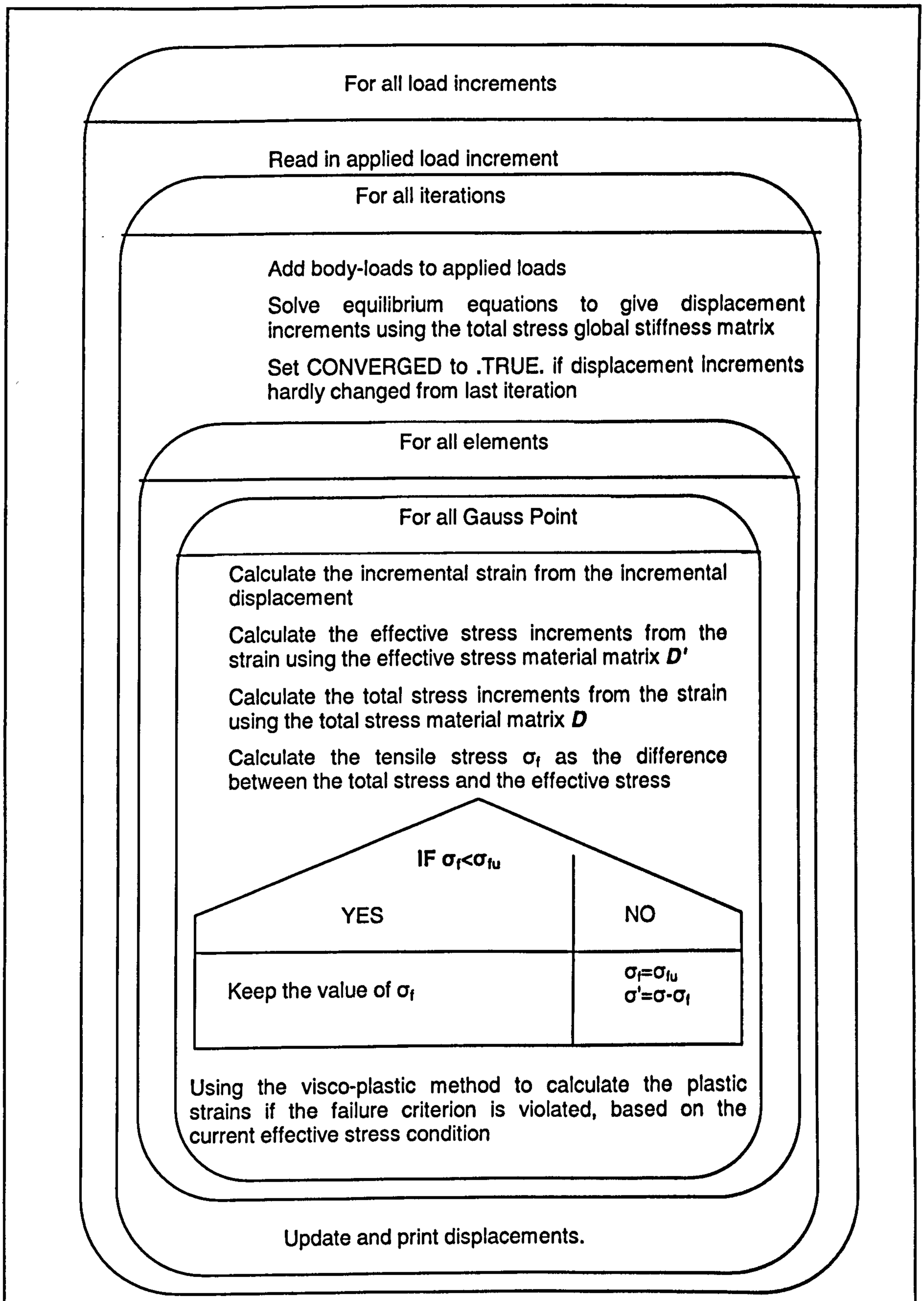

Figure 7-16 Structure chart for the LMTSA-P-MC program

7.5 Programming the Modified Cam-Clay Model

In Smith and Griffiths' finite element program (Smith and Griffiths, 1998), only elastic-perfectly plastic material models (i.e. Mohr-Coulomb model, Von Mises model) were included. The elastic-hardening plastic model, e.g. the MCC model needs to be coded into the existing finite element program, in which the non-linear finite element method and the substepping scheme introduced above will be included.

The MNR method is selected as the non-linear analysis algorithm because of its high accuracy. A boundary value problem of drained triaxial compression will be considered in the program so that it can be verified by the analytical solutions obtained in section 6.3.1. Triaxial loading is applied through prescribed displacements in the FEM program. Accordingly, some subroutines related to Gauss reduction and equation solving need to be reprogrammed. The structure chart of the MCC model program under drained triaxial compression is given in Figure 7-17, and the code is presented in Appendix C. Parameters for material properties are read into the program by using an input data file.

To ensure the program can predict the expected soil behaviour, it has been validated with the analytical results for the drained triaxial compression test presented in Chapter 6 which was taken from Potts and Zdravkovic (1999). The same finite element mesh as shown in Figure 7-14 was used. Figure 7-18 and Figure 7-19 show the comparison between FEM program and analytical results for the MCC model, together with the results produced by the geotechnical FEM software package Sage-CRISP (in which tangent stiffness method is adopted). It can be seen that the curve of deviator stress versus axial strain predicted by the Author's FEM program is very close but not identical to the analytical results, while the predicted volumetric strain curve is not that good compared with the analytical solution. Table 7-1 compares the analytical deviator stress and volumetric strain values when the critical state is reached, with those predicted by the Author's FEM program and Sage-CRISP. Although it can be seen that the Author's FEM program results are more accurate than the Sage-CRISP results, some unknown errors still exist in Author's FEM program which will be further discussed in Section 8.5.

Table 7-1 FEM and analytical results comparison for selected drained triaxial test

Analysis type	Deviator stress q (kPa)	Volumetric strain (%)
Analytical	395.0	5.22
FEM program	410.5 (3.9%)	3.69 (-29.3%)
Sage CRISP	747.4 (89.2%)	7.92 (51.7%)

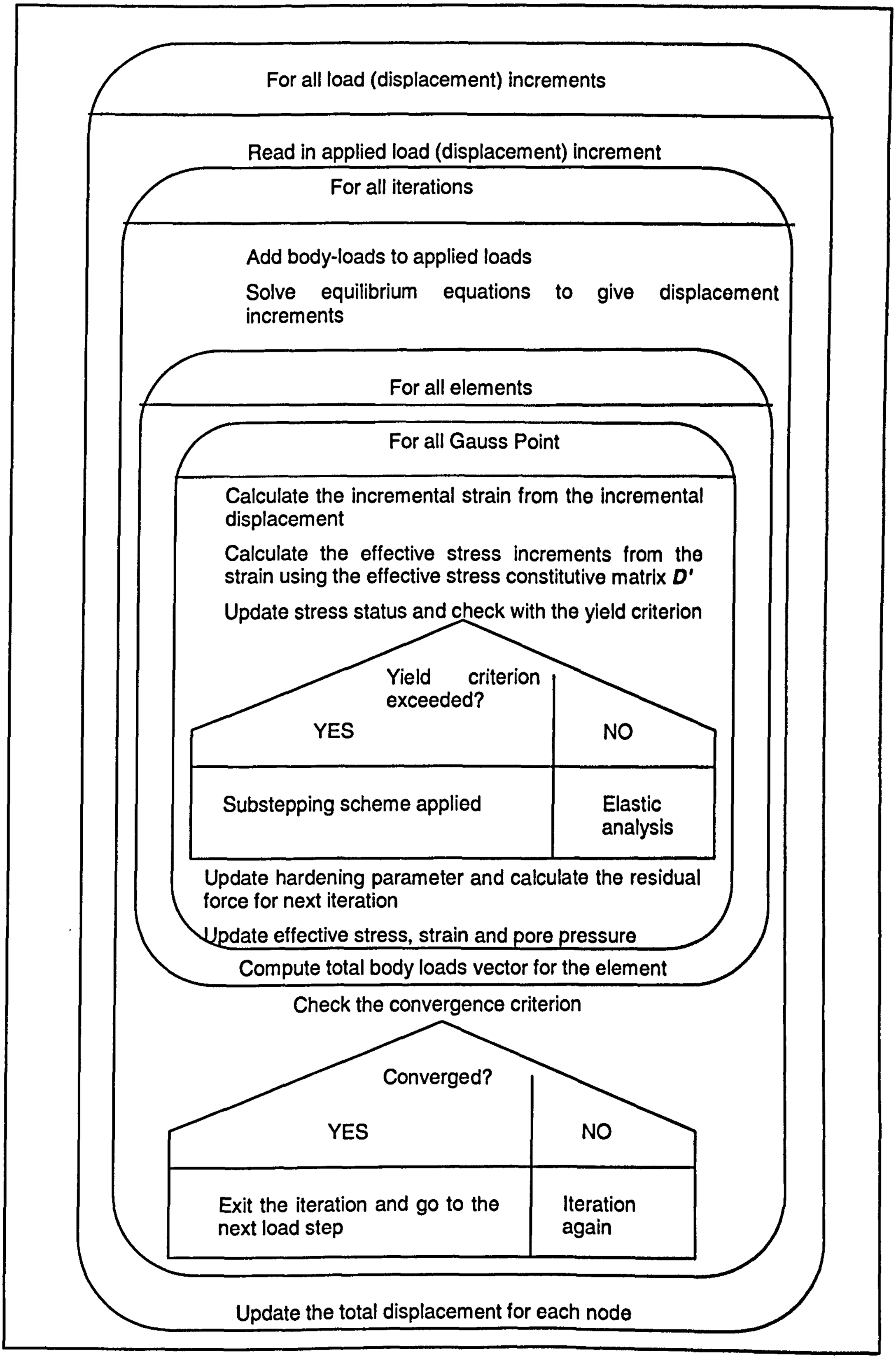

Figure 7-17 Structure chart for the MCC program

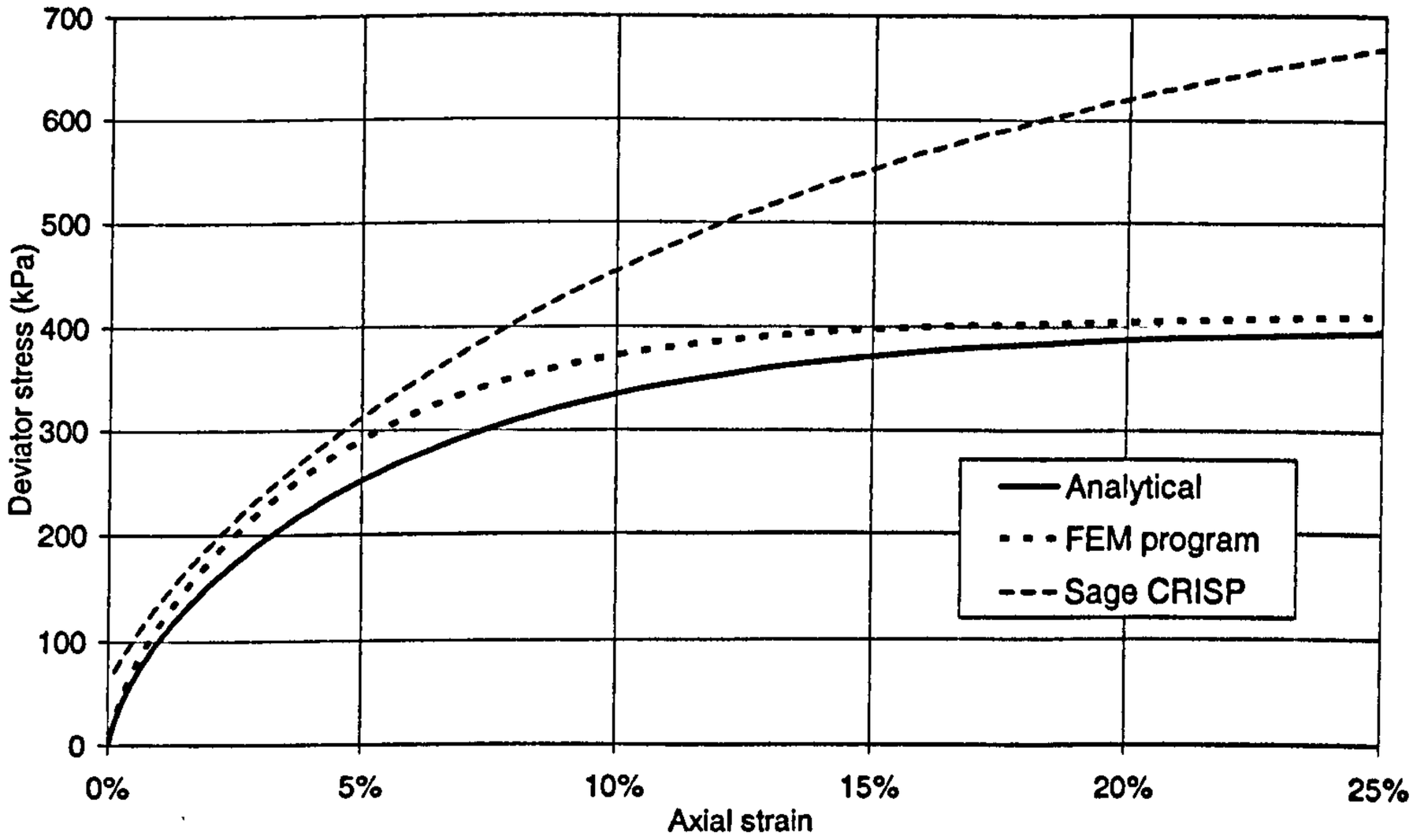

Figure 7-18 Comparison between FEM and analytical results: deviator stress vs. axial strain

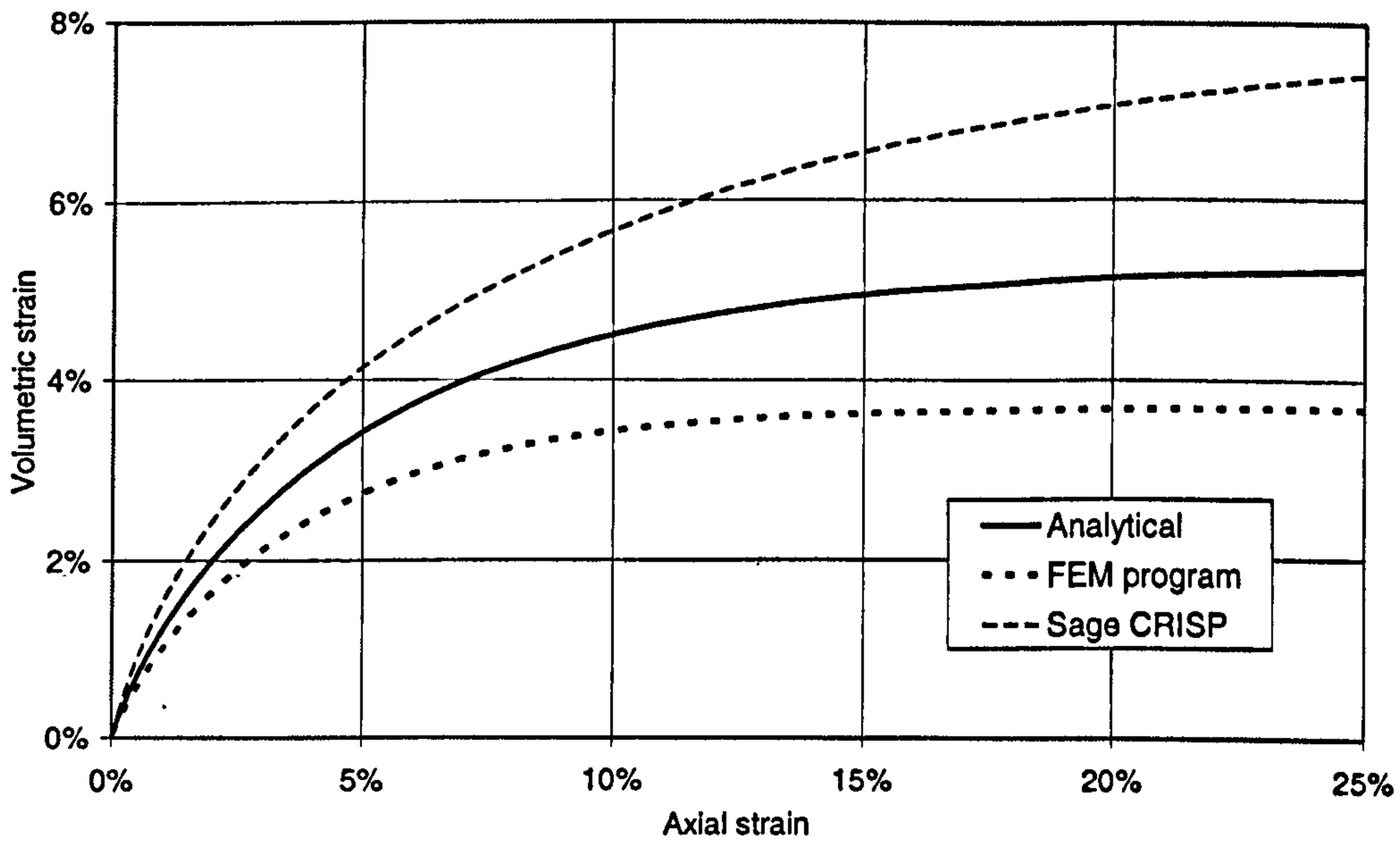

Figure 7-19 Comparison between FEM and analytical results: volumetric strain vs. axial strain

7.6 The MSW Constitutive Model Program

The MSW model program can be produced by incorporating the compression and the fibre material models into the MCC model program. For combining the fibre model with the MCC model, i.e. LMTSA-E-MCC, the same method as for the LMTSA-E-MC can be applied. For the compression model, an additional volumetric strain from intra-voids compression will be calculated and added to the axial strain according to the current normal stress. Currently this step is completely separate from the FEM calculation. To include the compression model in FEM modelling, more research needs to be done on compression mechanisms of waste material, which

should be the focus of future work to develop further a MSW constitutive. It will be further discussed in section 8.5. The code for MSW model program can be found in Appendix D.

The MSW model program has been applied to model the same material which is considered in section 6.3.4. The FEM modelling results are presented in Figure 7-20 and Figure 7-21 together with the analytical results of both the MCC model and the MSW model which have been presented in Chapter 6. The differences between the analytical and FEM modelling results are believed to be from the errors of the MCC model FEM program which has been noticed in section 7.5. Further discussion on the MSW model program will be given in Chapter 8.

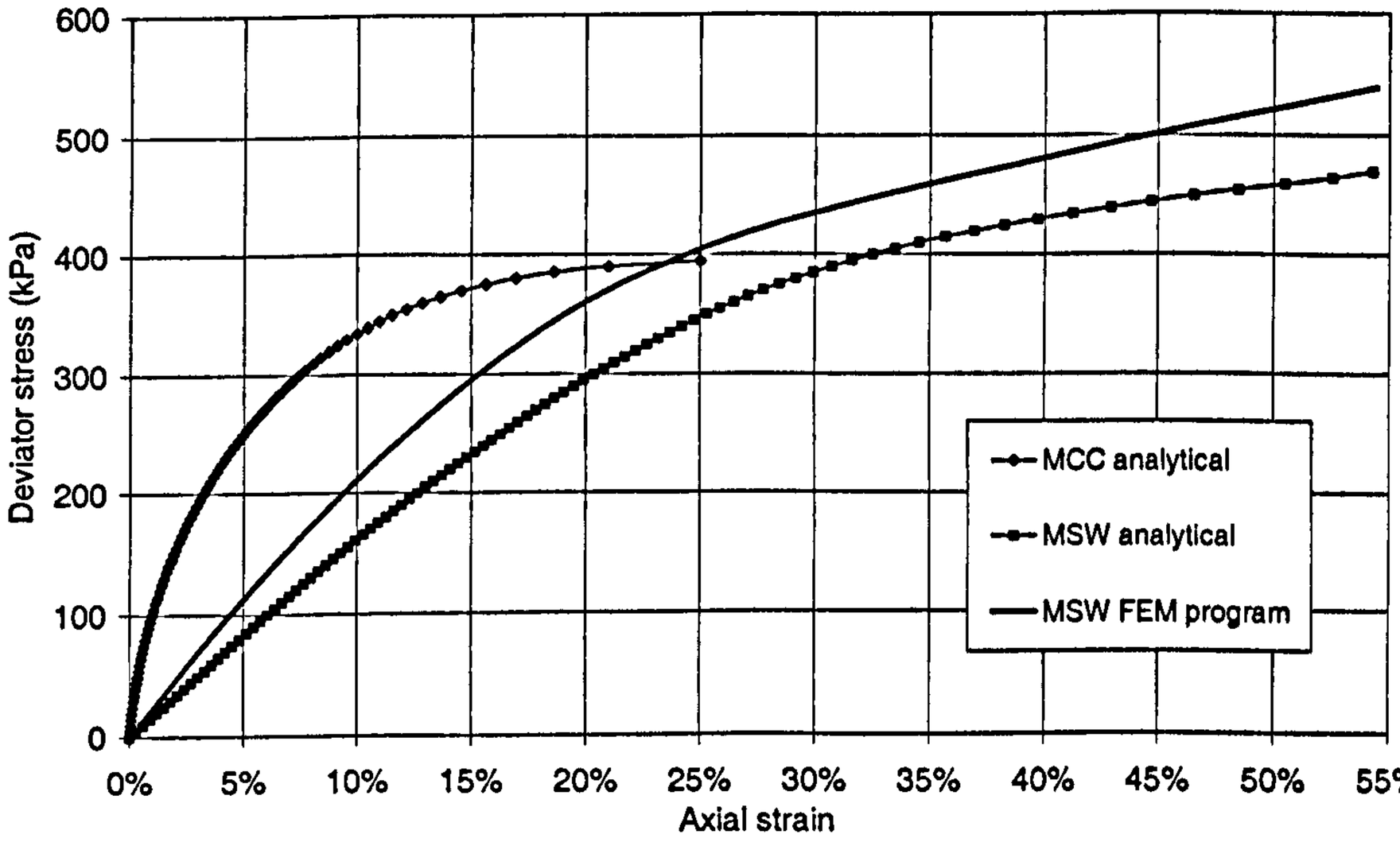

Figure 7-20 Comparison between MSW model analytical and FEM modelling results: deviator stress vs. axial strain

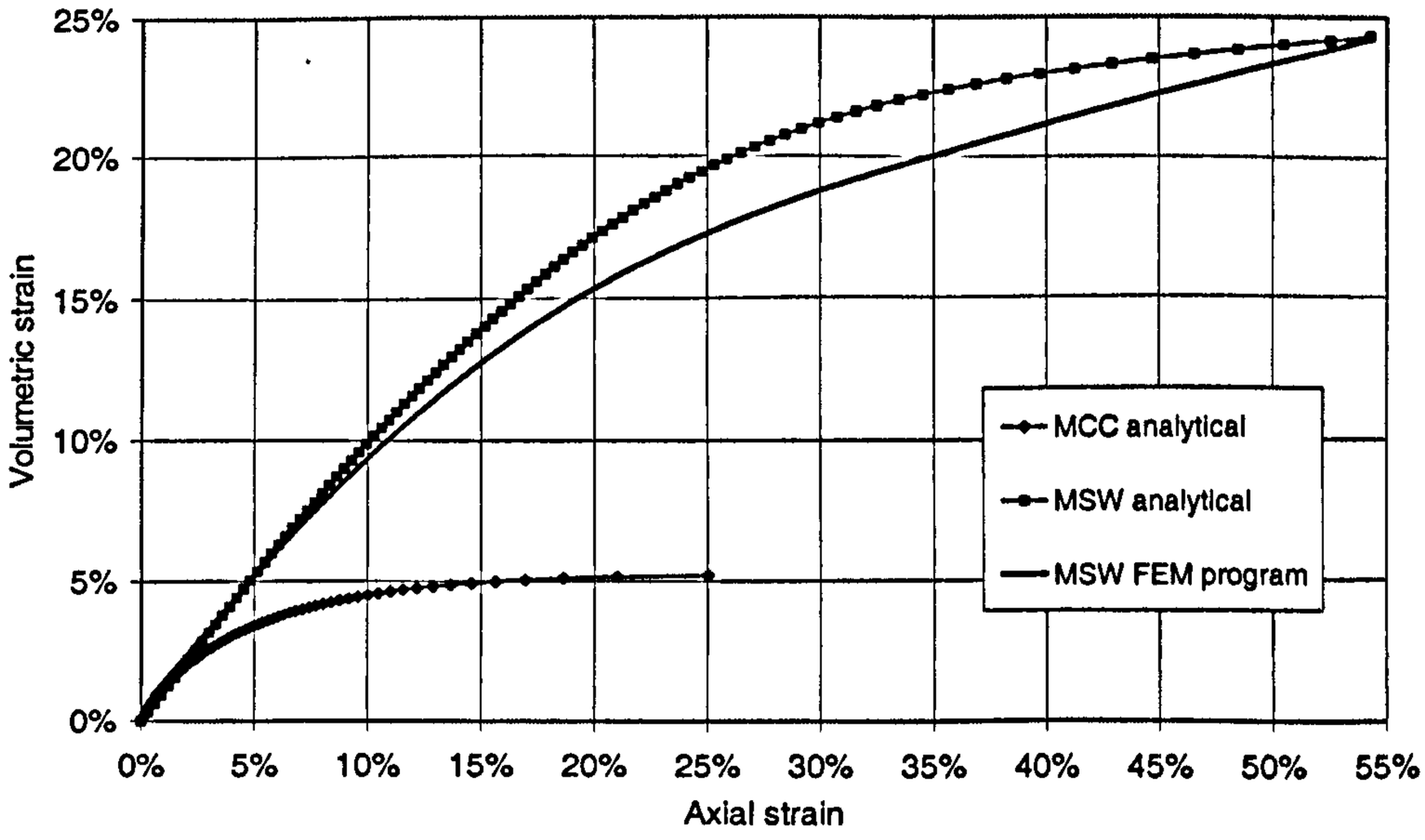

Figure 7-21 Comparison between MSW model analytical and FEM modelling results: volumetric strain vs. axial strain

7.7 Summary

The FEM programming techniques, particularly the non-linear solution schemes have been presented in this chapter. Relevant issues related to programming an elastic-hardening plastic material model into FEM, e.g. substepping scheme and prescribed displacement condition, were also discussed. The technique of including the LMSTA into the FEM process is similar to that in undrained analysis programming. An undrained analysis program for the Mohr-Coulomb material was introduced prior to coding of the programs for the LMSTA-E-MC and LMSTA-P-MC models. Finally, FEM programs for the MCC model and the MSW model were coded and applied to the drained triaxial compression tests that are presented in Chapter 6.

Most of the subroutines presented in Smith and Griffith (1998) can be directly used, but some of them have to be modified according to the different requirements, with three new subroutines created. Table 7-2 gives a list of programs and subroutines which were coded by the author. The subroutines have been presented in Appendix E.

Table 7-2 List of programs and subroutines

Program or Subroutine Name	Description
LMTSA-E-MC	Program for the randomly distributed fibre reinforced soil model, i.e. the linear mobilised tensile stress analysis combined with elastic fibre behaviour and the Mohr-Coulomb model. The program is modified from the undrained analysis for the Mohr-Coulomb elastic-perfectly plastic soil model.
LMTSA-P-MC	Program for the randomly distributed fibre reinforced soil model, i.e. the linear mobilised tensile stress analysis combined with elastic-perfectly plastic fibre behaviour and the Mohr-Coulomb soil material. The program is modified from the undrained analysis for the Mohr-Coulomb elastic-perfectly plastic soil model.
MCC_SUBSTEPPING	Program for the MCC model, using the MNR solution scheme and substepping stress point algorithm, loaded by prescribed displacement.
MCC_SUBSTEPPING_CM_RM	Program for the MSW model, i.e. the linear mobilised tensile stress analysis (elastic fibre behaviour) combined with the MCC model and the one-dimensional compression model.
GREDUC_DISP	Subroutine for the Gauss reduction calculation using prescribed displacement
BACKSUB_DISP	Subroutine for the back substitution calculation using prescribed displacement
MCCFLOW	Subroutine to calculate the first derivative of the yield function and the plastic potential function of the MCC model

As explained earlier in section 3.5 that a main program is needed for each material model, four main programs are listed in Table 7-2 for four constitutive models under triaxial compression loadings. Each program has its independent input/output stream and finite element analysis engine, while same subroutines (either produced by Smith and Griffith or listed in the table) are called wherever they are needed in the main program. For the input data, a data file needs to be provided and read at the beginning of the program. As soon as all the loading steps and iterations finish, a data file is produced automatically, in which all the information (including stress, strain and displacement etc) for every loading/iteration step and element/node are included. Graphic results like Figure 7-20 and 7-21 can then be produced using Microsoft Excel.

CHAPTER

8

Discussion

8.1 Introduction

In this chapter, the one-dimensional compression model, the randomly distributed fibre reinforcing model, the MSW constitutive model and the finite element method implementation are summarised and discussed. A numerical model to assess the interaction between the MSW body and the lining system is described to demonstrate the advantages of the proposed MSW constitutive model over soil models.

8.2 One-dimensional Compression Model

Compression behaviour is one of the most important components of MSW behaviour which has been a main research topic in waste mechanics study for decades. Both short-term and long-term compression behaviour should be studied for different concerns. When calculating the landfill settlement, the long-term compression behaviour including creep and degradation should also be considered, which is not covered in this thesis. When assessing the interaction between the waste body and the lining system, e.g. the down drag force on the lining system caused by adjacent waste vertical displacement during the staged construction process, the instant compression behaviour (i.e. the short-term compression behaviour) should be modelled, which is one of the main subjects of this thesis defined in Chapter 3. Moreover, compression behaviour is usually related to shear behaviour in constitutive modelling of soils and represents one of the essential components of an elasto-plastic constitutive model (i.e. flow rule), as discussed in section 2.4.1. Therefore, a compression model is required to model the MSW compression behaviour observed in MSW one-dimensional compression tests, and which can also be incorporated into a constitutive model for MSW.

Traditional methods in soil mechanics are widely accepted to study waste mechanical behaviour. In soil mechanics, soil material is treated as a particulate material in which all the particles are

incompressible. However, a large proportion of waste particles can be compressible according to the waste classification system proposed by Langer (2006), which means the traditional soil mechanics theories may not be appropriate. The influence of compressible components on waste behaviour, particularly the compression behaviour, has been recognised by several researchers, e.g. Powrie and Beaven (1999), and Langer (2006) by analysing their one-dimensional MSW compression test results. Powrie and Beaven (1999) measured solid and void volumes under different vertical pressures in their MSW compression tests. The relationship between void ratio and the logarithm of vertical pressure was then plotted and a non-linear relationship was noticed compared to a linear one for soils. Particle compression was attributed to this scenario in their paper but no further discussion was given. Langer (2006) included a compressible component in his waste classification system and performed a series of confined compression tests on synthetic waste samples which were composed of incompressible and compressible particles. Compressible particles, e.g. aluminium cans, were noticed to be compressed by investigating the components after compression and photos were taken during the compression process. Although contributions from compressible particles were recognised, traditional soil mechanics parameters were still applied to represent the waste compression behaviour.

A compressible model for MSW was proposed based on a case study of experimental data for a MSW compression sample reported in Powrie and Beaven (1999). After investigating their test data, it was found that the non-linear relationship between the tested void ratio values and the logarithm of vertical stress values came from the traditional definition of void ratio in soil mechanics. The void ratio is defined in soil mechanics as the ratio of the void volume to the solid volume, in which the solid volume is assumed to be a constant. It is obvious that the solid volume of waste material is not a constant due to the existence of the compressible particles, from which the non-linear relationship was obtained. The non-linear behaviour originates from definition of the void ratio rather than representing a real compression behaviour. It means using the traditional void ratio concept will result in a far more complicated situation when explaining the waste compression test data than that for soils. Therefore, the traditional definition of void ratio needs to be amended and more variables may be needed for waste materials to explain the compression behaviour in a simple way as in soil mechanics. An innovative phase relation for waste material was proposed based on the traditional phase relation used in soil mechanics theory prior to producing the compression model. Concepts of the inter and intra-void ratios were defined and a total potential incompressible volume was assumed to have a constant solid volume when the inter and intra-void ratios are calculated.

To have a simple relationship between void ratios and stress levels as in soils, linear relationships were assumed for both the inter and intra void ratios versus the logarithm of vertical effective stresses in the compression model. Since the total specific volume is a simple addition by the inter

and intra void ratios and an unity (Eq. 4-12), a linear relationship between the total volume change and the logarithm of vertical stresses will be obtained according to the assumption. This outcome is in accordance with most of MSW compression test results reported in the literature, in which the relationships between the vertical strains and the logarithm of vertical stresses are almost linear. Therefore, four parameters are needed to characterise the slope of the virgin compression and swelling lines for both inter and intra-void ratio changes, which are listed in Table 8-1. Two additional parameters are required if the full compression curve is to be modelled, i.e. the inter-void ratio and intra-void ratio values under unit pressure, characterising the initial points of both inter and intra-void ratios compression curves.

Table 8-1 Parameters for the compression model

Parameter description	Symbol
Compression index for inter-void ratio	$C_{C\text{-}Inter}$
Swelling index for inter-void ratio	$C_{S\text{-}Inter}$
Inter-void ratio under the unit pressure p'=1	e_1
Compression index for intra-void ratio	$C_{C\text{-}Intra}$
Swelling index for intra-void ratio	$C_{S\text{-}Intra}$
Intra-void ratio under the unit pressure p'=1	f_1

The model was then applied back into the compression data used in the case study and the results showed good agreements between the modelling curves and the test curves. Since it is difficult to determine the proportions of inter and intra voids compression from the test data, three different combinations are assumed and modelled. It is demonstrated that whatever the proportions of inter and intra voids in a waste sample, the compression model has a flexibility to reproduce the compression curves. The parameters needed in the model were directly back calculated from the test data.

The compression model was developed from a set of compression test data (DM3 from Powrie and Beaven, 1999) and calibrated with the same set of data. In order to show its ability to model more general waste compression data, the compression test results on synthetic waste samples reported by Langer (2006) were modelled by the compression model. The results showed good agreements between test data and modelling curves, except for the higher stress part for some samples. To model this behaviour, variable intra compression index values need to be applied for different stress levels due to the existence of some specific compressible particles in synthetic waste (perhaps also for real waste). This behaviour has been confirmed later in modelling MSW triaxial compression test results in section 6.3.5. Compared to Powrie and Beaven's test, even less

information was available to separate the inter and intra-void ratio changes. Again, the compression model has shown its flexibility for modelling different combinations of inter and intra-void ratio changes. However, most of the parameters in this modelling were simply assumed based on limited information to reproduce the final total compression and swelling lines.

It can be summarised from the two modelling cases that the final compression curves can be reproduced by the compression model with any combination of inter and intra-void ratio change behaviour. If only the instant settlement is of concern, it is not necessary to separate the inter and intra-voids compression behaviour in the compression model, i.e. traditional soil mechanics method is adequate to predict the final compression curve assuming a linear relationship is applicable for the full compression curve between vertical strains and the logarithm of vertical stresses. However, without the MSW compression model, it would be very difficult to interpret the compression test data with void ratio values obtained and defined by traditional soil mechanics method, e.g. the compression data from Powrie and Beaven (1999), though reliable void ratio values for MSW are extremely difficult to obtain from tests. More importantly, the model can calculate the volume loss from the compression of compressible particles which should not be coupled with its shear behaviour. The classical elasto-plastic theory for particulate material can then be applied to model the waste material with some modifications, which were discussed in Chapter 6.

To obtain the parameters for the compression model listed in Table 8-1 is a difficult task. Even values of the traditional compression index (C_c) for waste material, which is normally accepted to calculate the instant compression, are very difficult to determine though laboratory tests because the void ratio values are not as easy as for soil materials to obtain. Currently no standard test method is available for MSW void ratio determination, as its constituent particles are far more complicated than sand or clay (i.e. varying specific gravity) and is very hard to measure (partly due to the existence of compressible particles). Some literature presented the compression index values which were related to the initial void ratio e_0 (e.g. Sowers, 1973); some used the settlement coefficient (slope of the compression curve in terms of vertical strains versus the logarithm of vertical effective stresses) instead of the compression index to characterise the waste compression behaviour (e.g. Edil *et al.*, 1990); both of them avoided using compression index due to difficulties in determining the void ratio values. Although some literature published the compression data with void ratio values (e.g. Gabr and Valero, 1995; Machado *et al.*, 2002), detailed test methods were not given and qualities of the results are unknown, as discussed in section 2.2.1. Powrie and Beaven (1999) obtained some valuable void ratio values under different vertical effective pressures through the flushing and draining method discussed in Chapter 4, based on which the compression model was proposed. However, inter and intra-void ratio cannot be separated by using their test method so that three different cases were assumed and modelled.

A test method is required in future to determine the inter and intra-void ratio values and their change in behaviour under different vertical stresses. Photographic techniques applied in synthetic waste compression tests by Langer (2006) is a potential test method to investigate the proportions of inter and intra-voids compression. Typical parameter value ranges for different types of MSW, based on classification system proposed by Langer (2006), could be determined through this potential test method. For example, with higher content of compressible particles, high compression index for intra-void ratio will be obtained. All the compression model parameters listed in Table 8-1 are required for the MSW constitutive model produced in Chapter 6, which will be further discussed in section 8.4.

8.3 Fibre Reinforcing Model

In addition to compression behaviour, shear behaviour is another important mechanical behaviour of MSW which should be considered in the constitutive modelling of MSW. The compression model has revealed that existence of compressible particles can be used to help explain the waste shear behaviour, as existing modelling methods are deficient (discussed in section 8.2). Reinforcing components in waste material have been considered in the literature as the most influential factor controlling waste shear behaviour, e.g. Kölsh (1995), Machado *et al.* (2002), Krase and Dinkler (2005), and Langer (2006). Moreover, Machado *et al.* (2002), Krase and Dinkler (2005) proposed their constitutive models for MSW mainly considering the influence of the reinforcing particles on MSW shear behaviour, which have been discussed in section 2.3.1.

An innovative method was proposed in Chapter 5 to model the fibre reinforced soil behaviour, named linear mobilised tensile stiffness analysis (LMTSA), which can be simply implemented in the finite element method similar to undrained analysis for saturated soils. The idea of the method originated from the pore water pressure analysis (i.e. undrained analysis) for a saturated soil, in which pore water can sustain part of the compressive stress and only the effective stress is applied on soil particles. Fibres were assumed to be randomly and uniformly distributed in the matrix material, and then can provide a confining stress for the matrix material in the direction that the combined material tends to expand. For the boundary condition of conventional triaxial compression, fibres are only activated in the radial direction to provide an additional confining stress. Strain compatibility was assumed between fibres and the matrix material in the model. Both linear elastic and elastic-perfectly plastic properties were considered for the fibre material so that two types of analysis, i.e. LMTSA-E and LMTSA-P, were introduced.

A key parameter for the LMTSA, the equivalent mobilised tensile stiffness, was proposed and defined for both the LMTSA-E and LMTSA-P. Methods to obtain the equivalent mobilised tensile stiffness were introduced. Single fibre analysis was performed which was then integrated for the fibres in tension, assuming all the fibres have the same material properties. A technique to

separate the fibres in tension and compression was adopted from Michalowski and Cermark (2003). A reduction factor was used to calculate the equivalent tensile stiffness by reducing the tensile stiffness of a single fibre. It was found that the reduction factor was dependent on fibre content (volumetric) ρ, fibre length l, dilation angle of the matrix material ψ, the critical angle to distinguish fibres in tension from compression θ_0 (it is a function of ψ), and the radius of the triaxial compression specimen R for the axisymmetric boundary condition.

The LMTSA-E was combined with the Mohr-Coulomb elastic-perfectly plastic soil model to produce a fibre reinforced soil model LMTSA-E-MC. It was then validated against the fibre sand triaxial compression data reported by Michalowski and Cermark (2003). All parameters were directly taken from the test except for the tensile stiffness of a single fibre which was determined by back analysis (but it was very close to the value estimated from the fibre material). Two polyamide fibre reinforced fine sand samples that have different volumetric fibre content (0.5% and 2%) were modelled by the LMTSA-E-MC. Failure strengths of the two samples for different confining stresses under triaxial compression were predicted by the fibre soil model and compared with the test results and the modelling results predicted by the fibre sand model proposed by Michalowski and Cermark (2003). It has been shown that the LMTSA-E-MC can accurately predict the strength of polyamide fibre reinforced fine sand, in which most of the fibres did not fail in tension or bond failure did not occur between fibres and sand. The LMTSA-P-MC could be more accurate if such failures were allowed to take place, but further experiments are required to validate the model, as discussed in section 5.6.

The model was proposed for general randomly distributed fibre reinforced material, e.g. fibre reinforced sand or waste material, assuming the mechanisms of fibres affecting the overall shear behaviour are the same. The LMTSA-E-MC can only predict shear strength of the fibre reinforced sand but not the full stress-strain curve. To obtain this, a more advanced constitutive model than the Mohr-Coulomb model is required, which can reproduce the full stress-strain relationship for sand. This is then combined with the LMTSA-E or LMTSA-P models. Similarly, to have a full MSW constitutive model, a constitutive model which can predict the full stress-strain curve is required for the matrix to include the fibre reinforcing factor. The Modified Cam-Clay model was selected as the constitutive model for matrix model in waste material and was combined with the LMTSA-E to produce a constitutive model for MSW in Chapter 6.

A difficult task of applying the LMTSA to the MSW material is the determination of the parameters required for fibres and matrix material. When modelling the fibre reinforced sand, material properties of fibres and sand can be obtained separately from tests because they are mixed purposely. However, in waste material this is not the case, as reinforcing components and other components are difficult to equate with engineering properties and therefore parameters are

very difficult to determine. Moreover, some fibre material properties, e.g. fibre tensile stiffness and fibre length, must vary in waste material for all reinforcing particles, but only one value can be accepted by the model. A method to obtain average values for the parameter is required. For the volumetric fibre content, the waste classification system including reinforcing components proposed by Langer (2006) should be helpful in future work to obtain some typical fibre content values for different types of waste, and also the range of the average fibre material properties.

In addition, the current model is restricted to an axisymmetric model. It needs to be extended to a more general 3D stress space in future before it can be applied to practical problems. Since fibres can only be effective in the direction that the matrix material tends to expand, a smart method is needed to distinguish the strain type in every finite element, i.e. to tell if the strain is compressive or tensile, so that relative fibre contribution items can be determined and added into the material matrix before the stiffness matrix is formed in the finite element analysis.

8.4 MSW Constitutive Model

According to the constitutive model framework proposed for MSW in section 3.4.4, a model for MSW has been produced in Chapter 6 by combining a classic elasto-plastic soil model—the Modified Cam-Clay (MCC) model with the one-dimensional MSW compression and the fibre reinforcing models. A specific boundary condition and stress path, the conventional triaxial compression test, was selected to develop the model due to the current limitation of the fibre reinforced material model. Analytical solutions for the MSW constitutive model were derived and presented through a spreadsheet analysis to simulate reported MSW behaviour (shear behaviour and volumetric behaviour) from triaxial compression tests. The triaxial compression tests reported by Machado *et al.* (2002) were modelled and comparisons were carried out between the modelling and testing results.

Compared with Modified Cam-Clay (or the general critical state models), the MSW model can better reproduce the reported MSW behaviour from triaxial compression tests, not only by reproducing the stress-strain curves obtained from the tests, but also by explaining the observed behaviour with a more clear physical and mechanical meanings than the constitutive model proposed by Machado *et al.* (2002) that was discussed in section 2.3.1. More importantly, the MSW model has the potential to be improved to represent observed behaviour more accurately by improving its compression and reinforcing behaviour from linear to non-linear relationships in a future study. Since triaxial compression test results reported by Machado *et al.* (2002) are typical MSW triaxial test results compared with those reported by Jessberger and Kockel (1993) and Grisolia *et al.* (1995) as shown in section 2.2.2, it indicates that the MSW model can reproduce typical measured MSW stress-strain behaviour.

Table 8-2 Parameters for the MSW model

Sub-models	Parameter Description	Symbol	Determination Method
Modified Cam-Clay model	Slope of swelling line in *v-lnp'* plane (no intra void)	κ	Isotropic or one-dimensional compression tests removing compressible particles
	Slope of virgin consolidation line in *v-lnp'* plane (no intra void)	λ	Isotropic or one-dimensional compression tests removing compressible particles
	Specific volume (no intra void) at unit pressure on virgin consolidation line	N	Isotropic or one-dimensional compression tests removing compressible particles
	Poisson's ratio	μ	Estimated from material properties removing compressible and reinforcing particles
	Slope of critical state line in *q-p'* plane	M	Triaxial compression or direct shear test removing compressible and reinforcing particles
Compression Model	Slope of virgin consolidation line in *f-lnp'* plane	λ_f	Isotropic or one-dimensional compression tests for only compressible particles
	Slope of swelling line in *f-lnp'* plane	κ_f	Isotropic or one-dimensional compression tests for only compressible particles
	Intra-void ratio under the unit pressure $p'=1$	f_1	Isotropic or one-dimensional compression tests for only compressible particles
Fibre Reinforcing Model	Tensile stiffness for each single fibre (kPa)	K_f	Tension test for reinforcing particles
	Fibre volume content	ρ	Waste sorting analysis
	Fibre length (m)	l	Waste sorting analysis
	Radius of triaxial compression specimen (m)	R	Triaxial compression cell size

Parameters needed for the MSW model are parameters used in the three individual components, i.e. the Modified Cam-Clay , the one-dimensional compression and the fibre reinforced material models. Determination of parameters for the compression and fibre reinforced material models has been discussed in section 8.2 and 8.3, in which more experimental methods were recommended to be used. For the five parameters needed in the Modified Cam-Clay model, theoretically they can also be determined through the experimental methods which can remove the influences of compressible and reinforcing particles. All the parameters for the MSW model have been listed in Table 8-2, together with the suggested determination methods. It can be seen that the most important and difficult step in the determination methods is to remove the influences of the other particles which should not be included in the sub-model behaviour. A waste sorting

analysis is suggested to separate the different types of particles, which can be carried out based on the waste classification system developed by Langer (2006).

It can be seen from the table that twelve parameters are required for the MSW model formulated in the axisymmetric stress space, in which five are for the Modified Cam-Clay model, three are for the compression model and four are for the fibre reinforcing model. If the general 3D stress state is used in future, only the parameters for the fibre reinforcing model require modification. It should be noted that the slope of the swelling line in the ***f-lnp'*** plane used in the compression model κ_f was set as zero in this study to simplify the model indicating all intra-voids compression are plastic, so that elastic compression behaviour is only dependent on the inter-voids compression, which can be calculated in the Modified Cam-Clay model. Accordingly, the Poisson's ratio defining the relationship between the elastic volumetric strain and the elastic shear strain is currently only dependent on the inter-voids compression. In addition, since the associated flow rule was assumed for the Modified Cam-Clay model, the dilation angle of the matrix material used in the fibre reinforced material model ψ is not an independent parameter, i.e. it has the same value as the friction angle ϕ which is dependent on the slope of the critical state line M under the triaxial compression boundary condition, which has already been give in Eq. 2-19.

8.5 Finite Element Implementation

The MSW constitutive model was produced in order to be incorporated into practical numerical analyses of practical waste slope stability analysis and waste/barrier interaction modelling problems. Although only the triaxial compression boundary value problem was considered for the current MSW model, it was necessary to incorporate the MSW model into the finite element analysis for the specific boundary condition to show its feasibility for being included in numerical modelling, which has been performed in Chapter 7.

The programming structure in FORTRAN 90 and non-linear elasto-plastic finite element solution schemes were presented and discussed. In addition, two specific issues related to non-linear analysis, i.e. substepping scheme and prescribed displacement were also discussed in detail. Two fibre reinforced soil models combining the LMTSA with the Mohr-Coulomb elastic-perfectly plastic soil model considering different constitutive relations for fibre material (i.e. the LMTSA-E-MC and the LMTSA-P-MC) were programmed for the drained triaxial compression boundary condition according to the principal of the LMTSA proposed in section 5.4. The LMTSA-E-MC program has already been used in section 5.6 to perform the validation against the fibre sand triaxial compression test results.

Since the MSW model consists of three components (i.e. the Modified Cam-Clay model, the one-dimensional compression and the fibre reinforcing models), each component of the model should

be considered and incorporated into the finite element program. Initially, the Modified Cam-Clay model was coded into the finite element method, in which non-linear solution techniques were used. The FEM model results have been presented and compared with the analytical solutions. The stress-strain curve predicted by the FEM model contrasts well with the analytical curve, but the predicted volumetric strain values are less than the analytical results. The error can arise due to the use of only one eight-node quadrilateral element; a larger number of elements and higher order element would improve this. In addition, when applying the substepping algorithm, yield surface drift may occur from which the error cumulates (Potts and Gens, 1985). It can be corrected but was not included in the finite element program developed in section 7.5, which may lead to the observed error. The results from Sage-Crisp in both graphs differ from the closed-form solution. This may be due to the nonlinear algorithm used being the tangent stiffness method and not enough increments included.

The fibre reinforcing model can be combined with the Modified Cam-Clay model through the LMTSA program that is designed for the finite element analysis in section 5.4. This is one of the fibre reinforcing models LMTSA-E-MCC presented in Figure 5-1. For the compression model, since no method is currently available to quantify the inter and intra-voids compression, and only the one-dimensional model is developed, a simplified method has been used to calculate the volumetric strain caused by intra-voids compression according to the present normal stress values, which is completely separate from the finite element method process. The method can only be used to model the triaxial compression test with very simple stress status and stress path. For the general 3D stress space, the intra-voids compression cannot be simply calculated so that it has to be included in the finite element analysis process as part of future work. In addition, a general 3D compression model considering particle compression is required for this model. By modelling triaxial compression tests and comparing results with the analytical results, it is confirmed that the MSW model can be implemented in the finite element method and used to predict expected behaviour.

Currently the FEM program for the MSW model is only designed for the specific boundary condition and stress path—the conventional drained triaxial compression. This is because the MSW model was proposed under this specific boundary condition due to the limitation of the current fibre reinforced material model, i.e. the LMTSA is currently restricted to triaxial compression. To have a more general FEM program including the MSW model, the LMTSA should be extended to the general stress space in the future. In addition, the compression model is restricted to the one-dimensional case, which needs to be extended to 3D condition in future. Therefore, more studies on waste compression mechanisms (e.g. isotropic compression tests) are required and relevant finite element implementation issues need further development.

8.6 MSW Model Application

The current constitutive model for MSW has been proposed to simulate the volumetric and shear behaviour observed in element tests on MSW samples. As introduced in Chapter 1, the motivation behind the constitutive modelling of MSW has originated from the application of numerical modelling techniques for assessment of stability and integrity of steep (and/or shallow) slope lining systems in landfills. Therefore, the next step would be applying the constitutive model for MSW to practical modelling of landfill structures which have behaviour dependent on the waste behaviour. However, at present this cannot be carried out due to the model limitations discussed above (i.e. boundary conditions), but possible advantages of using the MSW model over using soil models can be discussed by virtually applying the MSW model in numerical modelling.

In Chapter 3, three typical numerical modelling cases related to waste behaviour, i.e. modelling of horizontal MSW support, MSW settlement and MSW slope stability, were discussed and requirements of a MSW constitutive model were proposed through the discussion. It should be noted that the long-term settlement related to creep and degradation is not included in the proposed MSW model so that long-term MSW settlement cannot be modelled at present. Therefore, only the instant MSW settlement is modelled to exert a downdrag force on the lining system in this study. Jones and Dixon (2005), Fowmes *et al.* (2006), and Sia (2007) performed numerical modelling for both shallow and steep slope lining systems and demonstrated the importance of evaluating the correct instant waste settlement to the integrity of the liner.

A typical steep slope lining system used in UK landfills, as sketched in Figure 8-1 (a), is considered as one of the examples to demonstrate the significance of modelling appropriate waste behaviour in numerical modelling. Only three lifts of waste are drawn in the graph to typify the staged construction. In reality 3 m to 5 m is allowed for each lift of the waste, therefore for a typical 30 m high landfill 6 to 10 lifts are needed. A mineral layer is required by the European Community Landfill Directive (1999) as the geological barrier (clay is adopted in this case as shown in the figure), on which a multi-layer geo-composite liner (composite geomembrane liner with geotextile) is placed. As shown in Figure 1-1 (a), waste horizontal support is important for stability and integrity of this type of lining system. As discussed in section 3.2.1, a major task of the numerical modelling for this type of steep slope lining system is to accurately evaluate the horizontal (or nearly horizontal) support from the waste body. In addition, downdrag forces caused by the instant waste settlement during stage construction (earlier waste lifts will be compressed by later ones) also need to be evaluated as they can result in generation of post peak strengths at liner interfaces and result in disruption to protection and drainage layer. For modelling the shallow slope lining system, the instant waste settlement plays an more significant role than the lateral waste support, in which waste compression behaviour needs to be evaluated accurately. Only the steep slope case is given here to show the waste/barrier interaction.

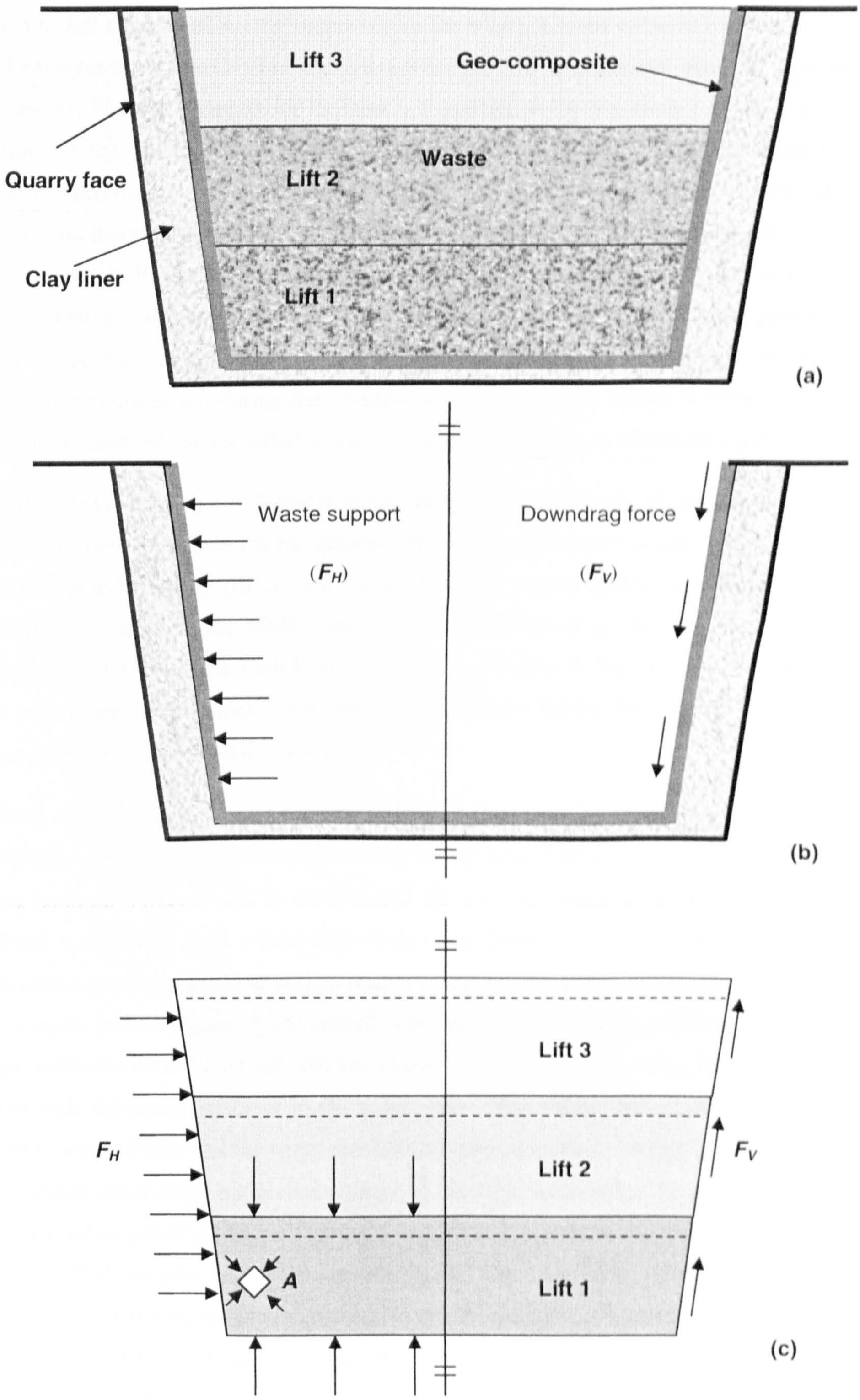

Figure 8-1 Waste/barrier interaction analysis for a typical steep slope lining system

In steep slope lining systems, as the mineral liner is normally not self-supported, i.e. it cannot stand to full height without the support from the waste, it tends to move towards the waste body and generate the interaction between them when the in-situ horizontal waste stress is insufficient to support. The waste support for the liner is simplified as the horizontal pressure F_H, as shown in Figure 8-1 (b), and the waste body is pressed by the liner with the same amount of force but in opposite direction, as shown in Figure 8-1 (c). Meanwhile, the waste body settles due to self-weight and therefore downdrag force along the lining system is generated, which is simplified as F_V as shown in Figure 8-1 (b). In addition, for the bottom waste lift as shown in Figure 8-1 (c), the successive waste lifts induce vertical loads while the underlying subgrade applies a resisting force to the base of the waste. It appears that the waste body in this type of landfill mainly experience compression during the construction period, which means to some extent the waste behaviour observed and modelled in triaxial compression test can inform the analysis.

Disadvantages of using a soil model in the numerical analysis will be investigated initially. The Modified Cam-Clay model (or the general critical state soil model) is again selected here as it is a classic elastic-hardening plastic soil model which is widely applied in geotechnical numerical modelling. In addition, the MSW model was proposed based on the Modified Cam-Clay model and both model behaviour have been compared in Chapter 6. Elastic or elastic-perfectly plastic soil models are not considered because real waste must be an elasto-plastic material with non-linear stiffness as discussed in section 2.2.

Typical shear stress-strain curve of the Modified Cam-Clay has been shown in Figure 6-2 and comparison between the Modified Cam-Clay model behaviour and the MSW test results has been given in Figure 6-18. It can be noticed that for a typical Modified Cam-Clay model, its shear stiffness is relatively high in the initial strain range (from 0 to 10% defined in section 2.2.2) but deteriorates gradually until the critical state is reached. The typical MSW triaxial compression test stress-strain curves (Figure 2-14) started with relatively low shear stiffness in the initial strain range, remained almost constant stiffness in the intermediate strain range (from 10% to 20%), and ended with increasing stiffness in the large strain range. Therefore, if the Modified Cam-Clay model is adopted to model the waste material, the predicted waste support would be overestimated in the initial strain range but underestimated in the large strain range. In addition, less volumetric strain would be predicted in the Modified Cam-Clay as shown in Figure 6-19, which means less instant MSW settlement would be predicted. The downdrag force would therefore be underestimated and therefore unconservative design would be obtained. Larger volumetric strain can be obtained in the Modified Cam-Clay model by using higher plastic compressibility λ, as shown in Figure 6-21. However, shear behaviour is also affected by this change as shown in Figure 6-20, i.e. a much softer and more plastic material is obtained and therefore waste support is very much underestimated in this case.

From the above discussion, it is apparent that there are disadvantages of using the Modified Cam-Clay model to simulate real MSW stiffness behaviour and its consequences, and more importantly an irreconcilable contradiction between shear behaviour and volumetric behaviour has been identified. This contradiction is originated from the basic assumption of the critical state soil models—it is assumed that shear strain and volumetric strain are coupled. It is also based on another basic assumption of the classical soil mechanics theory, that is, all soil particles are assumed to be incompressible. Thus, volume change can be coupled with shear behaviour, i.e. most of the volume change is from the rearrangement of soil particles along the shear band. However, this basic assumption for soil mechanics theory seems not to be applicable for waste mechanics because a significant proportion of waste particles are compressible and can deform.

The proposed MSW model has included the influences of compressible particles to solve the contradiction by only coupling the volumetric strain to particle rearrangement (i.e. the shear strain). The volumetric strain due to compressible particles is calculated separately and distributed to one or more directions as compressive strains. Currently only a one-dimensional compression model has been produced and all the calculated volumetric strain due to compressible particles is distributed to only the axial direction in modelling triaxial compression tests. In the virtual numerical modelling case shown in Figure 8-1 (c), greater horizontal strain would be obtained by considering compressible particles than that predicted by the Modified Cam-Clay under the same incremental horizontal stress, which means lower stiffness would be estimated for the waste body in a specific strain range, as shown in Figure 6-14. This means more realistic waste support conditions can be estimated using the MSW model than using the Modified Cam-Clay model. In addition, the MSW model has shown its capability in predicting larger volumetric strain without a big reduction of stiffness, as shown in Figure 6-16 and Figure 6-17. Therefore, the MSW settlement will not be underestimated and an appropriate degree of downdrag force can be applied at the same time.

It has been suggested in section 2.2.2 that the MSW stress-strain behaviour in the initial strain range observed from triaxial compression tests is actually dominated by its compression behaviour (i.e. compressible particles) rather than the shear behaviour that is normally assumed for soil material (particles are all assumed as incompressible). However, information obtained from MSW triaxial compression tests dose not reflect the real shear behaviour of MSW because the axial strain not only includes shear strain (it is only the shear strain for soil) but also compressive strain due to compressible particles. To evaluate the waste support to the lining system in numerical modelling, pure shear behaviour information is probably not of concern in the initial strain range, as compressible particles are playing a significant role in this strain range before reinforcing particles dominate. In the large strain range when the reinforcing particles start to dominate the shear behaviour, the current MSW model seems unable to simulate the increasing

stiffness, but it has the potential to include this aspect of behaviour by incorporating the non-linear mobilised tensile stress analysis, as discussed in section 6.3.5.

The pure shear behaviour is probably of interest for another numerical modelling case, i.e. modelling of MSW slope stability. A temporary waste slope has been sketched in Figure 8-2. For this type of boundary value problem, MSW behaviour observed from triaxial compression test is probably not applicable because material is not under similar compressive stress conditions and therefore compressible particles do not dominate the behaviour. Direct shear test may be the better test method to obtain more appropriate shear strength and stress-strain behaviour of MSW. Reinforcing particles must be considered carefully in this case because they dominate the MSW shear behaviour. Strain compatibility was assumed in the fibre reinforced material model proposed in Chapter 5. Interaction between these particles and the matrix material needs further consideration because normal stresses are much lower in this type of case than those in triaxial compression tests. For example, the constitutive model proposed by Krase and Dinkler (2005) that considered more complicated interaction between fibre reinforcement and the matrix phase may be more suitable for assessing MSW slope stability.

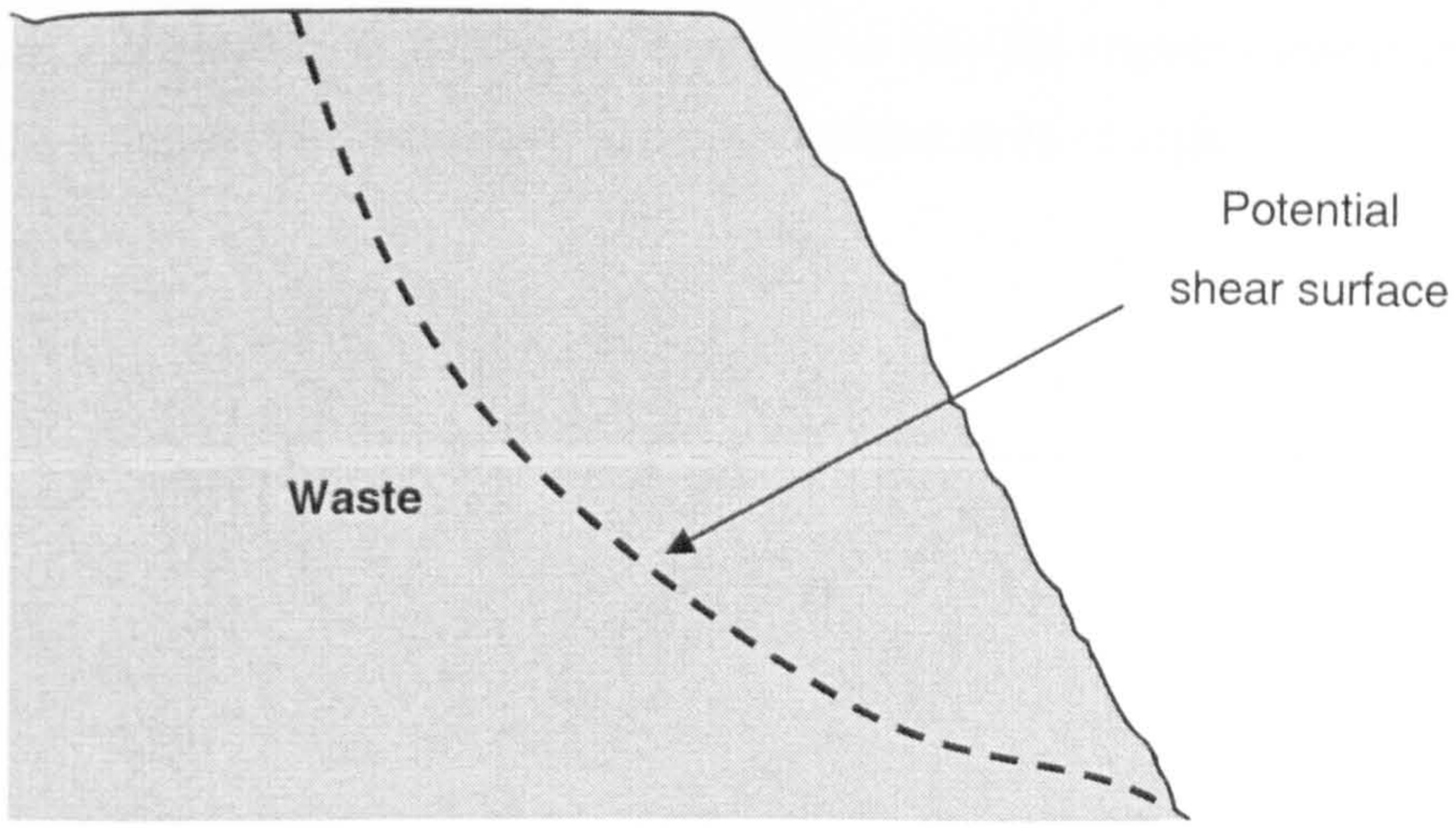

Figure 8-2 Waste slope stability analysis

In order to apply the MSW model into real problems, more studies need to be done in the future. First of all, the current constitutive model for MSW needs to be generalised from the axisymmetric boundary condition to the general stress space. Since the Modified Cam-Clay can already be used in general stress condition, only the compression and reinforcing models need the generalisation. For the compression model, since the current model is for one-dimensional compression, it needs to be extended to three-dimensional compression model by including the compression of compressible particles in different directions. For the reinforcing model,

contribution of the mobilised tensile stresses of fibres needs to be extended to three-dimensional stress space from the current axisymmetric condition.

As soon as the MSW model is generalised to the three-dimensional stress space, it can then be incorporated into a more general finite element analysis program. To model a real problem regarding interaction between lining system and waste body in landfill, the finite element program should cover many aspects such as adaptive finite element mesh, material interface, stage construction etc. In addition, appropriate pre-processor and post-processor are also needed to help user to build the model and process the results easily.

Once the finite element program reaches its commercial usable level, a real landfill lining system interacted with waste can be modelled and further validation of the MSW model can be done. For example, in-situ experimental data of liner behaviour observed at Burntstump landfill by Dixon *et al.* (2004) can be modelled by the finite element program. Meanwhile, more sensitivity analysis can be carried out refine the parameters used in the model, which will help to improve the model itself and also its application. Links between proportions of compressible/reinforcing particles and related parameters might be able to established through these analysis.

Eventually, the proposed constitutive model for MSW can be applied to numerical modelling of the waste/barrier interaction in landfill engineering, to help the engineer assess the stability and integrity of the lining system, and hence be more confident in the design.

CHAPTER

9

Conclusions and Recommendations for Future Work

9.1 Conclusions

To assess the stability and structural integrity of lining systems in landfills, numerical modelling techniques have been suggested as the most appropriate approach to simulate the interactions between MSW body and lining systems. An appropriate constitutive model for MSW is therefore required to be included in numerical modelling.

Key aspects of MSW behaviour have been identified by reviewing the MSW behaviour reported in the literature. For the compression behaviour observed in one-dimensional compression tests, influences of compressible particles on MSW compression curves and reinforcing particles on in situ horizontal stress have been recognised. For the stress-strain behaviour observed in triaxial compression tests, compressible and reinforcing particles appear to dominate within different strain ranges. The review of constitutive modelling of MSW has suggested an appropriate level of integration strategy to consider the influence of reinforcing particles, which should not only have a reasonable physical and mechanical explanation, but also require an appropriate and achievable number of parameters.

Requirements of an appropriate constitutive model for MSW have been suggested from the numerical modelling experience related to MSW. Five aspects of MSW behaviour have been identified to be included in the constitutive model, i.e. instant compression, creep and degradation, in situ horizontal stress, shear strength and non-linear stress-strain behaviour. A framework to develop a constitutive model for MSW has been proposed, in which a compression model is used to consider the influences of compressible particles, a fibre reinforcing model is used to consider the influences of reinforcing particles, and an elasto-plastic soil model is used to consider soil-like behaviour.

A one-dimensional MSW compression model has been developed to include the influences of compressible particles on MSW compression behaviour. An innovative phase relationship has been created for material containing compressible particles to model voids between and voids within particles separately. Linear relationships between void ratios (including inter and intra) and logarithm of vertical stress have been obtained for the compression test results, while the non-linear behaviour identified in the literature review result from adopting the traditional definition of void ratio from soil mechanics theory. Results from modelling of compression tests on both real and synthetic waste samples have shown that the compression model can reproduce the compression curve by using different proportions of inter and intra compression mechanisms.

An innovative method has been developed to include the influences of reinforcing particles on the MSW shear strength and stress-strain behaviour. Linear mobilised tensile stiffness analysis (LMTSA) has been proposed and applied to develop the fibre reinforcing model, which can be executed in the finite element analysis. A fibre reinforced soil model LMTSA-E-MC has been produced by assuming a linear elastic model for the fibre phase combined with an elastic-perfectly plastic Mohr-Coulomb model for the matrix phase. It has been applied to model a fibre reinforced sand triaxial compression test and the results have shown that the model can predict the measured improved shear strength values under a range of confining stresses.

A constitutive model for MSW has been developed by combining the Modified Cam-Clay with the one-dimensional MSW compression and the fibre reinforcing models. The compression and reinforcing models have been combined with the Modified Cam-Clay to demonstrate their influence on stress-strain behaviour within different strain ranges, which are consistent with the observed MSW stress-strain behaviour dominated by compressible and reinforcing particles within different strain ranges. Typical MSW triaxial compression tests have been modelled and the results have shown that the MSW model can reproduce the stress-strain behaviour in the initial and intermediate strain ranges. The current model cannot simulate the stress-strain behaviour in the lager strain range but it could be improved by incorporating non-linear tensile stiffness behaviour.

The constitutive model for MSW has been coded into a non-linear elasto-plastic finite element method program. Comparisons between the finite element analysis results and the analytical solutions have been performed and good agreements have been obtained. Since the current MSW model is developed only for the axisymmetric stress condition, a virtual model application has been carried out to demonstrate its advantages over soil constitutive models. Two main aspects of waste/barrier interaction related to MSW behaviour, i.e. horizontal support and vertical settlement, have been investigated and it has been shown that the MSW model can predict the interaction more appropriately than the soil constitutive models.

9.2 Recommendations for Future Work

Future work is required to include long-term MSW behaviour into the constitutive model for MSW. Creep and degradation have been identified as one of the key aspects of MSW behaviour which should be considered for assessment of long-term waste/barrier interaction. In addition, long-term shear behaviour related to degradation should be included in the MSW constitutive model. The influence of water on MSW mechanical behaviour should also be incorporated into the MSW model, e.g. water could soften some types of particles such as paper which results in reduction of the shear strength and alteration of stress-strain behaviour.

The compression model was developed for one-dimensional cases in this study, therefore a more general compression model is required to be developed in the 3D stress space in the future work. Isotropic compression test on MSW samples, rather than one-dimensional compression test, should be carried out to investigate the 3D compression behaviour of MSW. In addition, an experimental technique is required to determine the proportions of inter and intra-voids compression during compression. For instance, photographic techniques can be applied in synthetic waste compression to investigate the component compression behaviour. Typical parameter value ranges should be suggested according to the different proportion of compressible particles and their compression behaviour. A further validation of the compression model is required since only one MSW compression test measured the void ratio values and was modelled.

The fibre reinforcing model was developed in the axisymmetric stress condition, thus it should be extended into 3D general stress space in a future study. Since fibres can only be effective in the direction that the matrix material tends to expand, a method should be developed to distinguish the strain directions in every finite element so that relative fibre contribution items can be determined and added into the material matrix before the stiffness matrix is formed in the finite element analysis. Also, strain compatibility between matrix and fibre phases was assumed for the current model, therefore a more realistic and advanced interaction behaviour should be developed in the future. Non-linear mobilised tensile stress analysis is possibly required to model this interaction. The fibre reinforced soil model LMTSA-P-MC needs to be further validated using more experimental data on fibre reinforced soil samples in which fibre rupture or bond failure will occur. For the determination of parameters for use in modelling MSW reinforcing behaviour, an averaging technique is required since only one value for each fibre parameter can be accepted by the reinforcing model.

The constitutive model for MSW needs to be improved in the future according to the extensions of the compression and reinforcing models respectively discussed above. In addition, as the model cannot reproduce the stress-strain behaviour in the large strain range, it needs further improvement to cover this aspect of behaviour. Therefore, further studies on possible particle type

transformation (from compressible particles to reinforcing particles) and mobilisation of more reinforcing particles should be performed. Compression behaviour of MSW should be further investigated to include different intra-void ratio change parameters for different consolidation stress levels. Although parameter determination methods have been suggested, significantly more studies are required to remove the influences of the other types of particles when parameters related to one specific type of particle are investigated through experimental methods. A waste sorting analysis should be carried out based on the classification system developed by Langer (2006).

The finite element method implementation is for the axisymmetric stress condition so that the extension to the general 3D stress space should also be included in future work. Finite element modelling results of the Modified Cam-Clay can be improved by using higher order elements and/or correcting the yield drifting. Implementation of the compression and reinforcing models in the finite element method needs further improvement. The finite element program for the MSW model should be improved to solve real problems and back analysis can be done to further validate the model in the future. Hopefully it can be applied to real engineering evaluation of stability and integrity of the lining system in a near future.

This thesis has made a contribution to the understanding of constitutive modelling of MSW and new ideas of including MSW behaviour *dominated by* compressible and reinforcing particles in MSW modelling. It is emphasised that this work is the first step *of developing a constitutive* model for MSW which can be applied to practical numerical modelling involving MSW behaviour. It is anticipated that future research will result in a better understanding of MSW mechanical behaviour and hence development of more comprehensive constitutive models for MSW.

References

AL-KHAFAJI, A. W. N. and ANDERSLAND, O. B., 1981. Compressibility and Strength of Decomposing Fibre. *Geotechique,* 31(4), 497-508.

ANDERSLAND, O. B., KHATTAK, A. S. and AL-KHAFAJI, A. W. N., 1981. Effect of Organic Material on Soil Strength. *In:* Yong, R. N. and Townsend, F. C., eds. *Laboratory shear strength of soil,* American Society for Testing and Materials, pp. 226-242.

BEDFORD, A. and DRUMHELLER, D. S., 1983. Recent Advances: Thoeries of Immiscible and Structured Mixtures. *International Journal of Engineering Science,* 21(8), 863-960.

BIOT, M. A., 1941. General Theory of Three-Dimensional Consolidation. *Journal of Applied Physics,* 12, 155-164.

BORJA, R. I., 1991. Cam Clay Plasticity, Part II: Implicit Integration of Constitutive Equations Based on Nonlinear Elastic Stress Prediction. *Computer Methods in Applied Mechanics and Engineering,* 88, 225-240.

BORJA, R. I. and LEE, S. R., 1990. Cam Clay Plasticity, Part I: Implicity Integration of Constitutive Relations. *Computer Methods in Applied Mechanics and Engineering,* 78, 49-72.

BRITTO, A. M. and GUNN, M. J., 1987. *Critical State Soil Mechanics Via Finite Elements.* Chichester: Ellis Horwood.

COOK, R. D., MALKUS, D. S., PLESHA, M. E. and WITT, R. J., 2001. *Concepts and Applications of Finite Element Analysis. 4th edn.* New York, NY: Wiley.

CORMEAU, I. C., 1975. Numerical Stability in Quasi-Static Elasto-Viscoplasticity. *International Journal for Numerical Methods in Engineering,* 9(1), 109-127.

COUSSY, O., DORMIEUX, L. and DETOURNAY, E., 1988. From Mixture Theory to Biot's Approach for Porous Media. *International Journal of Solids Structures,* 35, 4619-4635.

COWLAND, J. W., TANG, K. Y. and GABAY, J., 1993. Density and Strength Properties of Hong Kong Refuse. *In: Proc. Sardinia 1993, Fourth International Symposium on Landfill,* S. Margherita di Pula, Cagliari, Italy.

DI PRISCO, C. and NOVA, R., 1993. A Constitutive Model for Soil Reinforced by Continuous Threads. *Geotextiles and Geomembranes,* 12, 161-178.

DIXON, N. and JONES, D. R. V., 2005. Engineering Properties of Municipal Solid Waste. *Geotextiles and Geomembranes,* 23, 205-233.

DIXON, N., NG' AMBI, S. and JONES, D. R. V., 2004. Structural Performance of a Steep Slope Landfill Lining System. *Proceedings of the Institution of Civil Engineering: Geotechnical Engineering,* 157(3), 115-126.

DIXON, N., WHITTLE, R. W., JONES, D. R. V. and NG'AMBI, S., 2006. Pressuremeter Tests in Municipal Solid Waste Measurement of Shear Stiffness. *Geotechique,* 56(3), 211-222.

DRUCKER, D. C., GIBSON, R. E. and HENKEL, D. J., 1957. Soil Mechanics and Work Hardening Theories of Plasticity. *Trans. ASCE,* 122, 338-346.

EDIL, T. B., RANGUETTE, V. J. and WUELLNER, W. W., 1990. Settlement of Municipal Refuse. *In:* Landva, A. O. and Knowles, G. D., eds. *Geotechnics of Waste Fill - Theory and Practise, ASTM*, Philadelphia, USA, pp. 225-239.

EUROPEAN COMMUNITY, 1999. Council Directive of 26 April 1999 on the Landfill of Waste (1999/31/EC). *Official Journal of the European Communities*; Council of the European Community L182(1).

FASSETT, J. B., LEONARDS, G. A. and REPETTO, P. C., 1994. Geotechnical Properties of Msw and Their Use in Landfill Design. *In: WasteTech '94 - Landfill Technology Conference*, January 13-14, Charleston, South Carolina, USA.

FOWMES, G., ZHANG, B., DIXON, N., EL-HAMALAWI, A. and JONES, D. R. V., 2005. Modelling Waste/Barrier Interaction. *In: Proceedings of International Workshop on Hydro-Physico-Mechanics of Landfills*, Grenoble, France.

GIROUD, J. P., 1994. Mathematical Model of Geomembrane Stress-Strain Curves with a Yield Peak. *Geotextiles and Geomembranes,* 13, 1-22.

GOTTELAND, P., GACHET, C., and VUILLEMIN, M., 2001. Mechanical Study of Municipal Solid Waste Landfill. *In: Proc. Sardinia 2001, 8th International Waste Management and Landfill Symposium*, S. Margherita di Pula, Cagliari, Italy., 425-433.

GOTTELAND, P., GOURC, J. P., ABOURA, A. and THOMAS, S., 2000. On Site Determination of Geomechanical Characteristics of Waste. *In: International Conference on Geotechnical and Geological Engineering*, Melbourne, Australia.

GRISOLIA, M., NAPOLEONI, Q., SIRINI, P. and TANCREDI, G., 1991. Geotechnial Behaviour of Sanitary Landfill Based on Laboratory and in Situ Tests. *In: XV Conference di Geotecnica di Torino*, Torino, Italy.

GRISOLIA, M., NAPOLEONI, Q. and TANCREDI, G., 1995. The Use of Triaxial Test for the Mechanical Characterisation of MSW. *In: Proc. Sardinia 1995, Fifth International Symposium on Landfill*, S. Margherita di Pula, Cagliari, Italy, pp. 703-710.

GUTIERREZ, 2003. Mixture Theory Characterization and Modeling of Soil Mixtures. *In: PROCEEDINGS of the First Japan-U.S. Workshop on Testing, Modeling, and Simulation in Geomechanics*, June 27-29, MIT Endicott House, Boston, USA: ASCE Geotechnical Special Publication, pp. 600-616.

JESSBERGER, H. L. and KOCKEL, R., 1993. Determination and Assessment of the Mechanical Properties of Waste Materials. *In: Proc. Sardinia 1993, Fourth International Symposium on Landfill*, S. Margherita di Pula, Cagliari, Italy, pp. 167-177.

JESSBERGER, H. L., SYLWASSCHY, O. and KOCKEL, R., 1995. Investigation of Waste-Body-Behaviour and Waste-Structure-Interaction. *In: Proc. Sardinia 1995, Fifth International Waste Management and Landfill Symposium*, S. Margherita di Pula, Cagliari, Italy, pp. 731-743.

JONES, D. R. V. and DIXON, N., 2003. *Stability of Landfill Lining Systems: Report No. 1: Literature Review.* R&D Technical Report P1-385, Environmental Agency, UK.

JONES, D. R. V. and DIXON, N., 2005. Landfill Lining Stability and Integrity: The Role of Waste Settlement. *Geotextiles and Geomembranes,* 23(27-53).

KAVAZANJIAN, E., 2001. Mechanical Properties of MSW. *In: Proc. Sardinia 2001, Eighth International Waste Management and Landfill Symposium*, S. Margherita di Pula, Cagliari, Italy, pp. 415-424.

KAVAZANJIAN, E., MATASOVIC, N. and BACHUS, R. C., 1999. Large-Diameter Static and Cyclic Laboratory Testing of Municipal Solid Waste. *In: Proceedings Sardinia 99, Seventh International Waste Management and Landfill Symposium*, S. Margherita di Pula, Cagliari, Italy.

KOERNER, R. M. and SOONG, 2000. Leachate in Landfills: The Stability Issues. *Geotextiles and Geomembranes,* 18, 293-309.

KÖLSCH, F., 1993. The Bearing Behaviour of Domestic Waste and Related Consequences for Stability. *In: Proc. Sardinia 1993, Fourth International Symposium on Landfill*, S. Margherita di Pula, Cagliari, Italy, pp. 1393-1410.

KÖLSCH, F., 1995. Material Values for Some Mechanical Properties of Domestic Waste. *In: Proc. Sardinia 1995, Fifth International Symposium on Landfill*, S. Margherita di Pula, Cagliari, Italy.

KRASE, V. and DINKLER, D., 2005. Constitutive Modelling of Mechanical Behaviour of Municiple Solid Waste. *In: Proc. Sardinia 2005, Tenth International Waste Management and Landfill Symposium*, S. Margherita di Pula, Cagliari, Italy.

LANDVA, A. O. and CLARK, J. I., 1990. Geotechnics of Waste Fill - Theory and Practice. *In:* Landva, A. O. and Knowles, G. D., eds. *Geotechnics of Waste Fill - Theory and Practise, ASTM*, Philadelphia, USA, pp. 225-239.

LANDVA, A. O., VALSANGKAR, A. J. and PELKEY, S. G., 2000. Lateral Earth Pressure at Rest and Compressibility of Municipal Solid Waste. *Canadian Geotechnical Journal,* 37, 1157-1165.

LANGER, U., 2006. *Shear and Compression Behaviour of Undegraded Municipal Solid Waste.* Ph.D. Thesis, Loughborough University, Loughborough, UK.

LINDSEY, 1977. Structure Charts: A Structure Alternative to Flow Charts. *SIGPLAN Notices,* 12(11), 36.

LING, H. I., LESCHCHNSKY, D., MOHRI, I. and KAWABATA, T., 1998. Estimation of Municipal Solid Waste Landfill Settlement. *Journal of Geotechnical and Geoenvironmental Engineering, ASCE,* 124(1), 21-28.

MACDOUGALL, J. R. and HAY, J., 2005. Hydro-Bio-Mechanical Modelling of Landfilled Waste: Formulation and Testing. *In: Proceedings of International Workshop on Hydro-Physico-Mechanics of Landfills*, Grenoble, France.

MACHADO, S. L., CARVALHO, M. F. and VILAR, O. M., 2002. Constitutive Model for Municipal Solid Waste. *Journal of Geotechnical and Geoenvironmental Engineering, ASCE,* 128(11), 940-951.

MARQUES, A. C. M., FILZ, G. M. and VILAR, O. M., 2003. Composite Compressibility Model for Municipal Solid Waste. *Journal of Geotechnical and Geoenvironmental Engineering, ASCE,* 129(4), 372-378.

MCDOUGALL, J. R. and PYRAH, I. C., 2004. Phase Relations for Decomposable Soils. *Geotechique,* 54(7), 487-494.

MCDOUGALL, J. R., PYRAH, I. C., YUEN, S. T. S., MONTEIRO, V. E. D., MELO, M. C. and JUCA, J. F. T., 2004. Decomposition and Settlement in Landfill Waste and Other Soil-Like Material. *Submitted to Geotechnique*).

MICHALOWSKI and CERMAK, 2003. Triaxial Compression of Sand Reinforced with Fibers. *Journal of Geotechnical and Geoenvironmental Engineering, ASCE,* 129(2), 125-136.

MITCHELL, J. K. and SOGA, K., 2005. *Fundamentals of Soil Behavior.* Hoboken, NJ: John Wiley & Sons.

MUIR WOOD, D., 2005. *Geotechnical Modelling.* London: Spon Press.

NALOR, D. J., 1974. Stresses in Nearly Incompressible Materials by Finite Elements with Application to the Calculation of Excess Pore Pressures. *International Journal for Numerical Methods in Engineering,* 8, 443-460.

OWEN, D. R. J. and HINTON, E., 1980. *Finite Elements in Plasticity :Theory and Practice.* Pineridge P.

POTTS, D. M. and GENS, A., 1985. A Critical Assessment of Methods of Correcting for Drift from the Yield Surface in Elasto-Plastic Finite Element Analysis. *International Journal for Numerical and Analytical Methods in Geomechanics,* 9, 149-159.

POTTS, D. M. and ZDRAVKOVIC, L., 1999. *Finite Element Analysis in Geotechnical Engineering: Theory.* London: Thomas Telford.

POWRIE, W. and BEAVEN, R. P., 1999. Hydraulic Properties of Household Waste and Implicatios for Landfills. *Proceedings of the Institution of Civil Engineering: Geotechnical Engineering,* 137, 235-247.

QIAN, X., KOERNER, R. M. and GRAY, D. H., 2002. *Geotechnical Aspects of Landfill Design and Construction.* Upper Saddle River, NJ: Prentice Hall.

ROSCOE, K. H. and BURLAND, J. B., 1968. On the Generalised Stress-Strain Behaviour of 'Wet' Clay. *In: Engineering Plasticity,* Cambridge: Cambridge University Press, pp. 535-609.

ROSCOE, K. H. and SCHOFIELD, A. N., 1963. Mechanical Behaviour of an Idealised 'Wet' Clay. *In: Proc of 2nd European Conference on SMFE,* Wiesbaden, pp. 47-54.

ROSCOE, K. H., SCHOFIELD, A. N. and WROTH, C. P., 1958. On the Yielding of Soils. *Geotechique,* 8, 22-52.

SCHOFIELD, A. N. and WROTH, C. P., 1968. *Critical State Soil Mechanics.* London: McGraw-Hill.

SCOTT, R., 1985. Plasticity and Constitutive Relations in Soil Mechanics. *Journal of Geotechnical Engineering, ASCE,* 111(5), 563-605.

SIA, A., 2007. *Landfill Engineering Design: A probabilistic Approach.* Ph.D. Thesis, Loughborough University, Loughborough, UK.

SINGH, S. and MURPHY, B. J., 1990. Evaluation the Stability of Sanitary Landfills. *In:* Landva, A. O. and Knowles, G. D., eds. *Geotechnics of Waste Fill - Theory and Practise, ASTM,* Philadelphia, USA, pp. 240-258.

SLOAN, S. W., 1987. Substepping Schemes for the Numerical Integration of Elastoplastic Stress-Strain Relations. *International Journal for Numerical Methods in Engineering,* 24, 893-911.

SMITH, I. M. and GRIFFITHS, D. V., 1998. *Programming the Finite Element Method. 3rd edn.* Chichester: Wiley.

SOWERS, G. F., 1968. Foundation Problems in Sanitary Land Fills. *Journal of Sanitary Engineering Division, ASCE,* 94(1), 103-116.

SOWERS, G. F., 1973. Settlement of Waste Disposal Fills. *In: Proceedings of 8th International Conference on Soil Mechanics and Foundation Engineering,* Moscow, pp. 207-210.

STALLEBRASS, S. E. and TAYLOR, R. N., 1997. The Development and Evaluation of a Constitutive Model for the Prediction of Ground Movements in Overconsolidated Clay. *Geotechique,* 47(2), 235-254.

TAYLOR, D. W., 1948. *Fundamentals of Soil Mechanics.* Chapman and Hall.

THOMAS, S., ABOURA, A., GOURC, J. P., GOTTELAND, P., BILLARD, H., DELINEAU, T., GISBERT, T., OUYRY, J. F. and VUILLEMIN, M., 1999. An in Situ Waste Mechanical Experimentation on a French Landfill. *In: Proceedings Sardinia 99, Seventh International Waste Management and Landfill Symposium,* S. Margherita di Pula, Cagliari, Italy, pp. 445-452.

TRUESDELL, C. A. and TOUPIN, R., 1960. The Non-Linear Field Theories of Mechanics. *In:* Flugge, S., ed. *Encyclopedia of Physics* Vol. 3, Berlin: Springer-Verlag, pp. 226-793.

VAN IMPE, W. F. and BOUAZZA, A., 1996. Geotechnical Properties of MSW. *In: Proceedings of 2nd International Congress on Environment Geotechnics,* ISSMFE & Japanese Geotechnical Society.

WARDWELL, R. E. and NELSON, J. D., 1981. Settlement of Sludge Landfills with Fibre Decomposition. *In: Proceedings of 10th International Conference on Soil Mechanics and Foundation Engineering.*

WHITTLE, A. J., 1987. *A Constitutive Model for Overconsolidated Clays with Application to the Cyclic Loading of Friction Piles.* Ph.D. Thesis, Massachusetts Institute of Technology.

WHITTLE, R. W., 1999. Using Non-Linear Elasticity to Obtain the Engineering Properties of Clay: A New Solution for the Self-Boring Pressuremeter Test. *Ground Engineering,* 32(5), 30-34.

WISSMAN, J. W. and HAUCK, C., 1983. Efficient Elasto-Plastic Finite Element Analysis with Higher Order Stress Point Algorithms. *Computers and Structures,* 17, 89-95.

WOOD, D. M., 1990. *Soil Behaviour and Critical State Soil Mechanics.* Cambridge: Cambridge University Press.

WOODS, R. and RAHIM, A., 2001. *Sage-Crisp Technical Reference Manual: For Use with Sage-Crisp Version 4.*

ZIENKIEWICZ, O. C. and CORMEAU, I. C., 1974. Visco-Plasticity, Plasticity and Creep in Elastic Solids - a Unified Numerical Solution Approach. *International Journal for Numerical Methods in Engineering,* 8, 821-845.

ZYTYNSKI, M., RANDOLPH, M., NOVA, R. and WROTH, C. P., 1978. On Modelling the Unloading–Reloading Behaviour of Soils. *International Journal for Numerical and Analytical Methods in Geomechanics,* 2, 87-93.

List of Publications

Conference papers:

FOWMES, G., ZHANG, B., DIXON, N., EL-HAMALAWI, A. and JONES, D. R. V., 2005. Modelling Waste/Barrier Interaction. *In: Proceedings of International Workshop on Hydro-Physico-Mechanics of Landfills*, Grenoble, France.

DIXON, N., ZHANG, B. and EL-HAMALAWI A., 2005. Constitutive Modelling of MSW. *Proceedings Sardinia 2005, Tenth International Waste Management and Landfill Symposium*, Cagliari, Italy.

DIXON, N., ZHANG, B., FOWMES, G.J., SIA, A., LANGER, U., EL-HAMALAWI, A. and JONES, D.R.V., 2006. Landfill Engineering: Waste Mechanics and Design Practice. *Proc. Asian-European Sustainable Urban Development Conference*, Chongqing, China.

FOWMES, G.J., SIA, A., ZHANG, B., DIXON, N and JONES, D.R.V., 2007. Numerical analysis of the stability and integrity of multilayer landfill lining system. *Proc GEE07: 7th Japanese-Korean-French Seminar "Geo-Environmental Engineering"*. Grenoble, France, May 22-24th 2007. pp69-74.

Journal Papers:

ZHANG, B., DIXON, N. and EL-HAMALAWI A., 2007. A One-dimensional Compression Model for MSW. *Proceedings of ICE: Waste and Resource Management.* In preparation.

ZHANG, B., EL-HAMALAWI A. and DIXON, N., 2007. Constitutive Modelling of Municipal Solid Waste. *International Journal for Numerical and Analytical Methods in Geomechanics.* In preparation.

Appendix

Appendix A

```
    Program LMTSA-E-MC
!-----------------------------------------------------------------------
!      program of drained axisymmetric linear mobilised tensile stress
!      analysis of an elastic-plastic (Mohr-Coulomb) solid
!      using 8-node quadrilateral elements; viscoplastic strain method
!-----------------------------------------------------------------------
 use new_library    ;   use  geometry_lib  ;       implicit none
 integer::nels,nxe,nye,neq,nband,nn,nr,nip,nodof=2,nod=8,nst=4,ndof,          &
          i,j,k,iel,iters,limit,incs,iy,ndim=2,loaded_nodes
 logical::converged       ; character (len=15) :: element='quadrilateral'
 real::e,v,det,phi,c,psi,dt,f,dsbar,dq1,dq2,dq3,lode_theta,                   &
         sigm,pi,snph,bulk,cons,presc,ptot,radius,tol
!------------------------------ dynamic arrays----------------------------
 real    ,allocatable :: kv(:),loads(:),points(:,:),bdylds(:),totd(:),       &
                         evpt(:,:,:),oldis(:),width(:),depth(:),stress(:),   &
                         dee(:,:),coord(:,:),jac(:,:),weights(:),storkv(:),  &
                         der(:,:),deriv(:,:),bee(:,:),km(:,:),eld(:),eps(:), &
                         sigma(:),bload(:),eload(:),erate(:),g_coord(:,:),   &
                         evp(:),devp(:),m1(:,:),m2(:,:),m3(:,:),flow(:,:),   &
                         tensor(:,:,:),etensor(:,:,:),tensile(:,:),fun(:)
 integer, allocatable :: nf(:,:) , g(:), no(:) ,num(:), g_num(:,:) ,g_g(:,:)
!-----------------------------input and initialisation----------------------
  open (10,file='input.dat',status=    'old',action='read')
  open (11,file='output.res',status='replace',action='write')
  read (10,*) phi,c,psi,e,v,bulk,cons,     nels,nxe,nye,nn,nip
  ndof=nod*nodof
  allocate (nf(nodof,nn), points(nip,ndim),weights(nip),g_coord(ndim,nn),     &
            width(nxe+1),depth(nye+1),num(nod),evpt(nst,nip,nels),            &
            coord(nod,ndim),g_g(ndof,nels),tensor(nst,nip,nels),fun(nod),     &
            etensor(nst,nip,nels),dee(nst,nst),tensile(nip,nels),stress(nst), &
            jac(ndim,ndim),der(ndim,nod),deriv(ndim,nod),g_num(nod,nels),     &
            bee(nst,ndof),km(ndof,ndof),eld(ndof),eps(nst),sigma(nst),        &
            bload(ndof),eload(ndof),erate(nst),evp(nst),devp(nst),g(ndof),    &
            m1(nst,nst),m2(nst,nst),m3(nst,nst),flow(nst,nst))
  nf=1; read (10,*) nr ; if(nr>0) read(10,*)(k,nf(:,k),i=1,nr)
  call formnf(nf); neq=maxval(nf);read(10,*) width , depth
!------------ loop the elements to find nband and set up global arrays -------
     nband = 0
       elements_1:   do iel = 1 , nels
                       call geometry_8qyv(iel,nye,width,depth,coord,num)
                       call num_to_g(num,nf,g) ;    g_num(:,iel)=num
                       g_coord(: , num )=transpose(coord); g_g( : , iel ) = g
                       if (nband<bandwidth(g)) nband = bandwidth(g)
       end do elements_1
!    write(11,'(a)') "Global coordinates "
!    do k=1,nn;write(11,'(a,i5,a,2e12.4)')"Node",k,"     ",g_coord(:,k);end do
!    write(11,'(a)') "Global node numbers "
!    do k = 1 , nels; write(11,'(a,i5,a,8i5)')                                &
!                              "Element ",k,"         ",g_num(:,k); end do
!   write(11,'(a,i5,a,i5)')          &
!            "The system has ",neq," equations and the half-bandwidth is",nband
allocate(kv(neq*(nband+1)),loads(0:neq),bdylds(0:neq),oldis(0:neq),totd(0:neq))
          kv=0.0; oldis=0.0; totd=0.0 ; tensor = 0.0; etensor = 0.0
  call deemat(dee,e,v); call sample(element,points,weights)
!------------------ equivalent tensile shear stiffness is "bulk" -------------
  dee(1,1)=dee(1,1)+bulk;dee(4,4)=dee(4,4)+bulk
  pi = acos( -1. ); snph = sin(phi*pi/180.)
  dt = 4.*(1.+ v)*(1.-2.*v)/(e*(1.-2.*v+snph*snph))
!---------- element stiffness integration and assembly & initial conditions----
 elements_2: do iel = 1 , nels
                num = g_num(: ,iel ) ; coord = transpose (g_coord(: ,num ))
                g = g_g( : ,iel )    ;      km=0.0
             gauss_pts_1:  do i =1 , nip    ; call shape_fun(fun,points,i)
               call shape_der (der,points,i);  jac = matmul(der,coord)
               det = determinant(jac)  ;   call invert(jac)
               deriv=matmul(jac,der);call bmataxi(bee,radius,coord,deriv,fun)
             km=km+matmul(matmul(transpose(bee),dee),bee)*det*weights(i)*radius
               tensor(1:2,i,iel)=cons; tensor(4,i,iel)=cons
             end do gauss_pts_1
```

```
   call formkv (kv,km,g,neq)
 end do elements_2
!--------------- prescribe displacements and factorise l.h.s. --------------
      read(10,*) loaded_nodes ; allocate(no(loaded_nodes),storkv(loaded_nodes))
          read(10,*)no , presc  , incs , tol , limit
          do i=1,loaded_nodes
             kv(nf(2,no(i)))=kv(nf(2,no(i)))+1.e20 ; storkv(i)=kv(nf(2,no(i)))
          end do                ;      call banred(kv,neq)
write(11,'(/A)')"step    displ       tensile       p           q       iters"
!--------------------displacement increment loop--------------------------------
    call deemat(dee,e,v)
   load_increments: do iy=1,incs
    ptot = presc * iy
!   write(11,'(/,a,i5)') 'Load increment',iy ;  iters=0;  bdylds=.0;  evpt=.0
!---------------------------   iteration loop  -------------------------------
   iterations: do
    iters=iters+1;  loads = .0
     do i=1,loaded_nodes;loads(nf(2,no(i)))=storkv(i)*presc; end do
     loads = loads + bdylds  ;  call bacsub(kv,loads)
!-----------------------  check convergence ------------------------------
      call checon(loads,oldis,tol,converged)
      if(iters==1)converged=.false.
!----------------------- go round the Gauss Points ---------------------------
      elements_3: do iel = 1 , nels
       bload=.0
       num = g_num( : , iel ) ; coord = transpose( g_coord( : , num ))
       g = g_g( : , iel )     ; eld = loads ( g )
       gauss_points_2 : do i = 1 , nip
          call shape_fun(fun,points,i)
          call shape_der ( der,points,i); jac=matmul(der,coord)
          det = determinant(jac)  ;  call invert(jac)
          deriv = matmul(jac,der) ;  call bmataxi (bee,radius,coord,deriv,fun)
          eps=matmul(bee,eld); det = det * radius;  eps=eps-evpt(:,i,iel)
          sigma=matmul(dee,eps)  ;    stress=sigma+tensor(: , i , iel)
          call invar(stress,sigm,dsbar,lode_theta)
!--------------------  check whether yield is violated ----------------------
          call mocouf (phi, c , sigm, dsbar , lode_theta , f )
          if(f>=.0) then
           call mocouq(psi,dsbar,lode_theta,dq1,dq2,dq3)
           call formm(stress,m1,m2,m3)
           flow=f*(m1*dq1+m2*dq2+m3*dq3)      ;   erate=matmul(flow,stress)
           evp=erate*dt; evpt(:,i,iel)=evpt(:,i,iel)+evp;devp=matmul(dee,evp)
           eload=matmul(devp,bee)     ; bload=bload+eload*det*weights(i)
          end if
         if(converged.or.iters==limit)  then
!----------------   update stresses and calculate tensile stress  -------------
          tensor(:,i,iel)=stress
          etensor(:,i,iel)=etensor(:,i,iel)+eps+evpt(:,i,iel)
          tensile(i,iel)=etensor(1,i,iel)*bulk
        end if
    end do gauss_points_2
!         compute the total bodyloads vector
    bdylds( g ) = bdylds( g ) + bload      ; bdylds(0) = .0
  end do elements_3
  if(converged.or.iters==limit)exit
end do iterations
  totd = totd + loads
  write(11,'(a,e12.4)') "     Displacement" , ptot
  write(11,'(a,3e14.6)')                &
      "Effective normal stresses",tensor(1,1,1),tensor(2,1,1),tensor(4,1,1)
  write(11,'(a,4e12.4)')                &
      "Normal tensile stress",tensile(1,1),tensile(2,1),tensile(3,1),tensile(4,1)
  write(11,'(a,i5,a)') "It took",iters,"  iterations to converge"
  write(11,'(I4,4E12.4,I5)')iy,totd(nf(2,no(1))),tensile(4,1),sigm,dsbar,iters
  if(iters==limit)stop
  if(f>=.0)stop
end do load_increments
end Program LMTSA-E-MC
```

Appendix B

```
    Program  LMTSA-P-MC
!-----------------------------------------------------------------------
!      program of LMTSA-P-MC axisymmetric linear mobilised tensile stress
!      analysis of an elastic-plastic (Mohr-Coulomb) solid
!      using 8-node quadrilateral elements; viscoplastic strain method
!-----------------------------------------------------------------------
 use new_library    ;   use  geometry_lib  ;       implicit none
 integer::nels,nxe,nye,neq,nband,nn,nr,nip,nodof=2,nod=8,nst=4,ndof,          &
          i,j,k,iel,iters,limit,incs,iy,ndim=2,loaded_nodes
 logical::converged       ; character (len=15) :: element='quadrilateral'
 real::e,v,det,phi,c,psi,dt,f,dsbar,dq1,dq2,dq3,lode_theta,                   &
          sigm,pi,snph,bulk,cons,epstu,tensile_u,presc,ptot,radius,tol

!------------------------------ dynamic arrays---------------------------------
 real    ,allocatable :: kv(:),loads(:),points(:,:),bdylds(:),totd(:),       &
                         evpt(:,:,:),oldis(:),width(:),depth(:),stress(:),   &
                         dee(:,:),dee_t(:,:),coord(:,:),jac(:,:),weights(:), &
                         der(:,:),deriv(:,:),bee(:,:),km(:,:),eld(:),eps(:), &
                         sigma(:),bload(:),eload(:),erate(:),g_coord(:,:),   &
                         evp(:),devp(:),m1(:,:),m2(:,:),m3(:,:),flow(:,:),   &
                         tensor(:,:,:),tensor_eff(:,:,:),etensor(:,:,:),     &
                         tensile(:,:),fun(:),stress_eff(:),storkv(:)
 integer, allocatable :: nf(:,:) , g(:), no(:) ,num(:), g_num(:,:) ,g_g(:,:)
!-----------------------------input and initialisation-------------------------
  open (10,file='input.dat',status=    'old',action='read')
  open (11,file='output.res',status='replace',action='write')
  read (10,*) phi,c,psi,e,v,bulk,cons,epstu,     nels,nxe,nye,nn,nip
  ndof=nod*nodof
  allocate (nf(nodof,nn), points(nip,ndim),weights(nip),g_coord(ndim,nn),     &
            width(nxe+1),depth(nye+1),num(nod),evpt(nst,nip,nels),            &
            coord(nod,ndim),g_g(ndof,nels),tensor(nst,nip,nels),dee(nst,nst), &
            tensor_eff(nst,nip,nels),fun(nod),etensor(nst,nip,nels),          &
            dee_t(nst,nst),tensile(nip,nels),stress(nst),stress_eff(nst),     &
            jac(ndim,ndim),der(ndim,nod),deriv(ndim,nod),g_num(nod,nels),     &
            bee(nst,ndof),km(ndof,ndof),eld(ndof),eps(nst),sigma(nst),        &
            bload(ndof),eload(ndof),erate(nst),evp(nst),devp(nst),g(ndof),    &
            m1(nst,nst),m2(nst,nst),m3(nst,nst),flow(nst,nst))
  nf=1; read (10,*) nr ; if(nr>0) read(10,*)(k,nf(:,k),i=1,nr)
  call formnf(nf); neq=maxval(nf);read(10,*) width , depth
!------------ loop the elements to find nband and set up global arrays --------
     nband = 0
       elements_1:    do iel = 1 , nels
                        call geometry_8qyv(iel,nye,width,depth,coord,num)
                        call num_to_g(num,nf,g) ;     g_num(:,iel)=num
                        g_coord(: , num )=transpose(coord); g_g( : , iel ) = g
                        if (nband<bandwidth(g)) nband = bandwidth(g)
       end do elements_1
!     write(11,'(a)') "Global coordinates "
!     do k=1,nn;write(11,'(a,i5,a,2e12.4)')"Node",k,"      ",g_coord(:,k);end do
!    write(11,'(a)') "Global node numbers "
!     do k = 1 , nels; write(11,'(a,i5,a,8i5)')                                &
!                                "Element ",k,"         ",g_num(:,k); end do
!    write(11,'(a,i5,a,i5)')          &
!            "The system has ",neq,"  equations and the half-bandwidth is",nband
allocate(kv(neq*(nband+1)),loads(0:neq),bdylds(0:neq),oldis(0:neq),totd(0:neq))
           kv=0.0; oldis=0.0; totd=0.0 ; tensor = 0.0; etensor = 0.0
  call deemat(dee,e,v); call sample(element,points,weights)
!------------------ equivalent tensile shear stiffness is "bulk" -------------
  dee_t=dee; dee_t(1,1)=dee_t(1,1)+bulk;dee_t(4,4)=dee_t(4,4)+bulk
  pi = acos( -1. ); snph = sin(phi*pi/180.)
  dt = 4.*(1.+ v)*(1.-2.*v)/(e*(1.-2.*v+snph*snph))
!---------- element stiffness integration and assembly & initial conditions----
 elements_2: do iel = 1 , nels
                num = g_num(: ,iel ) ; coord = transpose (g_coord(: ,num ))
                g = g_g( : ,iel )    ;       km=0.0
             gauss_pts_1:  do i =1 , nip    ; call shape_fun(fun,points,i)
               call shape_der (der,points,i);  jac = matmul(der,coord)
               det = determinant(jac) ';   call invert(jac)
               deriv=matmul(jac,der);call bmataxi(bee,radius,coord,deriv,fun)
```

```
                km=km+matmul(matmul(transpose(bee),dee_t),bee)*det*weights(i)*radius
                  tensor(1:2,i,iel)=cons; tensor(4,i,iel)=cons
                  tensor_eff(1:2,i,iel)=cons; tensor_eff(4,i,iel)=cons
                end do gauss_pts_1
    call formkv (kv,km,g,neq)
  end do elements_2
!---------------- prescribe displacements and factorise l.h.s. ---------------
       read(10,*) loaded_nodes ; allocate(no(loaded_nodes),storkv(loaded_nodes))
           read(10,*)no , presc  , incs , tol , limit
           do i=1,loaded_nodes
              kv(nf(2,no(i)))=kv(nf(2,no(i)))+1.e20 ; storkv(i)=kv(nf(2,no(i)))
           end do                 ;      call banred(kv,neq)
write(11,'(/A)')"step    displ       tensile       p           q       iters"
!--------------------displacement increment loop--------------------------------
!     call deemat(dee,e,v)
    load_increments: do iy=1,incs
     ptot = presc * iy
!     write(11,'(/,a,i5)') 'Load increment',iy ;  iters=0;  bdylds=.0;  evpt=.0
!--------------------------  iteration loop  ---------------------------------
    iterations: do
     iters=iters+1;  loads = .0
      do i=1,loaded_nodes;loads(nf(2,no(i)))=storkv(i)*presc; end do
      loads = loads + bdylds  ;  call bacsub(kv,loads)
!-----------------------  check convergence ---------------------------------
       call checon(loads,oldis,tol,converged)
       if(iters==1)converged=.false.
!---------------------- go round the Gauss Points ----------------------------
       elements_3: do iel = 1 , nels
        bload=.0
        num = g_num( : , iel ) ; coord = transpose( g_coord( : , num ))
        g = g_g( : , iel )      ; eld = loads ( g )
        gauss_points_2 : do i = 1 , nip
           call shape_fun(fun,points,i)
           call shape_der ( der,points,i); jac=matmul(der,coord)
           det = determinant(jac)  ;  call invert(jac)
           deriv = matmul(jac,der) ;  call bmataxi (bee,radius,coord,deriv,fun)
           eps=matmul(bee,eld); det = det * radius;  eps=eps-evpt(:,i,iel)
           sigma=matmul(dee_t,eps)  ;    stress=sigma+tensor(: , i , iel)
           sigma=matmul(dee,eps);        stress_eff=sigma+tensor_eff(:,i,iel)
           tensile(i,iel)=stress(1)-stress_eff(1)
           if (tensile(i,iel)>=epstu*bulk) then
              tensile(i,iel)=epstu*bulk
              stress_eff(1)=stress(1)-tensile(i,iel)
              stress_eff(4)=stress(4)-tensile(i,iel)
           endif
           call invar(stress_eff,sigm,dsbar,lode_theta)
!--------------------  check whether yield is violated ----------------------
           call mocouf (phi, c , sigm, dsbar , lode_theta , f )
           if(f>=.0) then
            call mocouq(psi,dsbar,lode_theta,dq1,dq2,dq3)
            call formm(stress_eff,m1,m2,m3)
            flow=f*(m1*dq1+m2*dq2+m3*dq3)     ;   erate=matmul(flow,stress_eff)
            evp=erate*dt; evpt(:,i,iel)=evpt(:,i,iel)+evp;devp=matmul(dee,evp)
            eload=matmul(devp,bee)    ; bload=bload+eload*det*weights(i)
           end if
         if(converged.or.iters==limit)  then
!---------------   update stresses and calculate tensile stress  ------------
           tensor(:,i,iel)=stress
           tensor_eff(:,i,iel)=stress_eff
           etensor(:,i,iel)=etensor(:,i,iel)+eps+evpt(:,i,iel)
         end if
      end do gauss_points_2
!------------------   compute the total bodyloads vector  ---------------------
      bdylds( g ) = bdylds( g ) + bload      ; bdylds(0) = .0
    end do elements_3
    if(converged.or.iters==limit)exit
   end do iterations
    totd = totd + loads
     write(11,'(a,3e14.6)')            &
```

```
          "Effective normal stresses",tensor(1,1,1),tensor(2,1,1),tensor(4,1,1)
     write(11,'(a,1e12.4)') "     Yield function", f
   write(11,'(I3,4E12.4,I5)')iy,totd(nf(2,no(1))),tensile(4,1),sigm,dsbar,iters
  if(iters==limit)stop
  if(f>=.0)stop
end do load_increments
end Program LMTSA-P-MC
```

Appendix C

```
    Program Mcc_Substepping
!-----------------------------------------------------------------------
!      Program axisymmetric 'drained' strain of an elasto-plastic
!      (Modified Cam-Clay) solid using 8-node quadrilateral elements;
!      using MNR method and substepping stress point algorithm
!-----------------------------------------------------------------------
 use new_library    ;   use  geometry_lib  ;       implicit none
 integer::nels,nxe,nye,neq,nband,nn,nr,nip,nodof=2,nod=8,nst=4,ndof,          &
          i,j,k,iel,iters,limit,incs,iy,ndim=2,loaded_nodes,iters_fnew
 logical::converged       ; character (len=15) :: element='quadrilateral'
 real::kappa,lambda,am,mu,volume,en,det,fnew,ff,fstiff,dlam,dslam,dsbar,      &
           lode_theta,sigm,top,bot,tload,tloads,bulk,cons,presc,ptot,pcs,     &
           radius,residual,tol,fftol,ltol,gk,bk,hard,epsvp,pye,pcn,           &
           alpha_value,error,delta_t,accum_t,accum_temp,beta,sstol,ff0,       &
           scalar_temp1,scalar_temp2,temp,scalar_xdisp,scalar_tdisp,pcn1,pcn2,&
           scalar_sigma1,scalar_sigma2,ef1,lambda_f,volume_t,epsv_f,epsvp1,epsvp2
!------------------------------ dynamic arrays---------------------------------
 real    ,allocatable :: kv(:,:),loads(:),points(:,:),bdylds(:),totd(:),     &
                         oldis(:),width(:),depth(:),stress(:),tensor(:,:,:), &
                         dee(:,:),dep(:,:),coord(:,:),jac(:,:),weights(:),   &
                         der(:,:),deriv(:,:),bee(:,:),km(:,:),eld(:),eps(:), &
                         sigma(:),bload(:),eload(:),elso(:),g_coord(:,:),    &
                         ddylds(:),dl(:,:),mccfl(:),mccfl2(:,:),kv_bak(:,:), &
                         dload(:),caflow(:),dsigma(:),ress(:),rmat(:,:),     &
                         acatc(:,:),qmat(:,:),qinva(:),daatd(:,:),mccflq(:), &
                         mccfla(:),mcctemp(:,:),etensor(:,:,:),qinvr(:),     &
                         pore(:,:),fun(:),pc(:,:),sigma1(:),epsp(:),alpha(:),&
                         stress1(:),sigma2(:),temp1(:),temp2(:),deps(:),     &
                         epsp1(:),epsp2(:),val(:,:),qinc(:),bakloads(:),     &
                         dsigma_elastic(:),tdisp(:),dee_t(:,:),xdisp(:),     &
                         epse(:),react(:),disp(:),fixed(:),treac(:),         &
                         stress_t(:),tensor_t(:,:,:),stress2(:),epsv(:,:)
 integer, allocatable :: nf(:,:),g(:),no(:),num(:), g_num(:,:),g_g(:,:),ifpre(:)
!---------------------------input and initialisation-------------------------
  open (10,file='input.dat',status=    'old',action='read')
  open (11,file='output.res',status='replace',action='write')
  open (12,file='km.res',status='replace',action='write')
  read (10,*) kappa,lambda,am,mu,en,ef1,lambda_f,bulk,cons,pye,nels,nxe,nye,nn,nip
  ndof=nod*nodof
  allocate (nf(nodof,nn), points(nip,ndim),weights(nip),g_coord(ndim,nn),     &
            width(nxe+1),depth(nye+1),num(nod),mcctemp(1,nst),epse(nst),      &
            coord(nod,ndim),g_g(ndof,nels),tensor(nst,nip,nels),fun(nod),     &
            etensor(nst,nip,nels),dee(nst,nst),pore(nip,nels),stress(nst),    &
            jac(ndim,ndim),der(ndim,nod),deriv(ndim,nod),g_num(nod,nels),     &
            bee(nst,ndof),km(ndof,ndof),eld(ndof),eps(nst),sigma(nst),        &
            bload(ndof),eload(ndof),elso(nst),mccfl(nst),mccfl2(nst,nst),     &
            dload(ndof),g(ndof),qinva(nst),qinvr(nst),dl(nip,nels),ress(nst), &
            caflow(nst),dsigma(nst),rmat(nst,nst),acatc(nst,nst),sigma1(nst), &
            qmat(nst,nst),daatd(nst,nst),mccflq(nst),mccfla(nst),pc(nip,nels),&
            epsp(nst),stress1(nst),sigma2(nst),temp1(nst),temp2(nst),         &
            deps(nst),epsp1(nst),epsp2(nst),dsigma_elastic(nst),dep(nst,nst), &
            dee_t(nst,nst),stress_t(nst),tensor_t(nst,nip,nels),stress2(nst), &
            epsv(nip,nels))
  nf=1; read (10,*) nr ; if(nr>0) read(10,*)(k,nf(:,k),i=1,nr)
  call formnf(nf); neq=maxval(nf);read(10,*) width , depth
!------------ loop the elements to find nband and set up global arrays --------
     nband = 0
       elements_1:    do iel = 1 , nels
                      call geometry_8qyv(iel,nye,width,depth,coord,num)
                      call num_to_g(num,nf,g) ;     g_num(:,iel)=num
                      g_coord(: , num )=transpose(coord); g_g( : , iel ) = g
                      if (nband<bandwidth(g)) nband = bandwidth(g)
       end do elements_1
!    write(11,'(a)') "Global coordinates "
!    do k=1,nn;write(11,'(a,i5,a,2e12.4)')"Node",k,"       ",g_coord(:,k);end do
!    write(11,'(a)') "Global node numbers "
!    do k = 1 , nels; write(11,'(a,i5,a,8i5)')                                &
!                                "Element ",k,"         ",g_num(:,k); end do
!  write(11,'(a,i5,a,i5)')           &
```

```
!           "The system has ",neq," equations and the half-bandwidth is",nband
  allocate(kv(neq,neq),kv_bak(neq,neq),loads(0:neq),fixed(0:neq),xdisp(0:neq),&
           react(0:neq),bakloads(0:neq),bdylds(0:neq),oldis(0:neq),totd(0:neq)&
           ,ddylds(0:neq),tdisp(0:neq),treac(0:neq),ifpre(0:neq),disp(0:neq))
   kv=0.0; oldis=0.0; totd=0.0
!---------------------- shape elastic stiffnes matrix -------------------------
   pcs=0.5*pye; volume=en-lambda*log(-cons)
   volume_t=volume+ef1-lambda_f*log(-cons)
   bk=-volume*cons/kappa; gk=1.5*(1.-2.*mu)*bk/(1.+mu)
   call deemat_kg(dee,bk,gk); call sample(element,points,weights)
   tensor=0.0; dl=0.0;etensor=0.0;epsv=0.0
!---------- element stiffness integration and assembly & initial conditions----
 elements_2: do iel = 1 , nels
               num = g_num(: ,iel ) ; coord = transpose (g_coord(: ,num ))
               g = g_g( : ,iel )    ;       km=0.0
             gauss_pts_1:  do i =1 , nip    ; call shape_fun(fun,points,i)
               call shape_der (der,points,i);  jac = matmul(der,coord)
               det = determinant(jac)  ;   call invert(jac)
               deriv=matmul(jac,der);call bmataxi(bee,radius,coord,deriv,fun)
             km=km+matmul(matmul(transpose(bee),dee_t),bee)*det*weights(i)*radius
               tensor(1:2,i,iel)=cons; tensor(4,i,iel)=cons; pc(i,iel)=pye
             end do gauss_pts_1
   call formkv_disp(kv,km,g,neq)
 end do elements_2
 kv_bak=kv
!--------------- prescribe displacements and factorise l.h.s. ---------------
      read(10,*) loaded_nodes ; allocate(no(loaded_nodes))
      read(10,*) no,presc,incs,fftol,sstol,limit
      write(11,'(/A)')"step    displ   epsv_f    vol    p     q    iters"
      totd=0.0; dl=0.0;ptot=0.0
!-------------------displacement increment loop--------------------------------
   load_increments: do iy=1,incs
     ptot = presc * iy
     iters=0;  bdylds=.0;loads=.0; fixed=0.0; tdisp=0.0; treac=0.0
     ifpre=0;  xdisp=0.0;react=0.0; disp=0.0
     do i=1,loaded_nodes; fixed(nf(2,no(i)))=presc; ifpre(nf(2,no(i)))=1;end do
     ddylds=0.0
!--------------------------  iteration loop  ---------------------------------
   plastic_iters: do
    iters=iters+1
    write(*,'(A,F8.4,A,I4)')"load",ptot,  "iteration",iters
    if (iters/=1) fixed=0.0
    if (iters/=1) loads=0.0
     loads = loads + bdylds + treac
     kv=kv_bak
     call greduc_disp(kv,loads,fixed,neq,ifpre)
     call bacsub_disp(kv,loads,fixed,xdisp,react,ifpre)
     disp=disp+xdisp
     if (iters/=1) tdisp=tdisp+xdisp
     treac=treac+react
     bdylds=.0
     kv=0.0
!------------------------go round the elements-------------------------------
       elements_4: do iel = 1 , nels
       bload=.0; dload=.0
       num = g_num( : , iel ) ; coord = transpose( g_coord( : , num ))
       g = g_g( : , iel )     ;    eld = xdisp ( g ); km=0.0
!----------------------- go round the Gauss points ---------------------------
      gauss_points_3 : do i = 1 , nip
         elso=.0; call shape_fun(fun,points,i)
         call shape_der ( der,points,i); jac=matmul(der,coord)
         det = determinant(jac)  ;  call invert(jac)
         deriv = matmul(jac,der) ;  call bmataxi (bee,radius,coord,deriv,fun)
         eps=matmul(bee,eld)
!---------------------update initial stress status-------------------------------
         stress=tensor(: , i ,  iel)
         call invar(stress,sigm,dsbar,lode_theta)
!--------------------------update specific volume-------------------------------
         pcs=0.5*pc(i,iel)
```

```
          volume=en-lambda*log(-sigm)
          ff0=dsbar*dsbar/(am*am)-sigm*(pc(i,iel)-sigm)
!-------------------------predict stress with elastic D-------------------------
          sigma=matmul(dee,eps);    stress=tensor(:,i,iel)+sigma
          call invar(stress,sigm,dsbar,lode_theta)
!-------------------------substepping if ff>0-----------------------------------
          ff=dsbar*dsbar/(am*am)-sigm*(pc(i,iel)-sigm)
          fstiff=ff
          if(ff>0.0) then
!-----------------------------determine alpha---------------------------------
          j=2; allocate (alpha(0:1000)); alpha(1)=0.0; alpha(2)=1.0
          alpha_iterations: do
             j=j+1
             alpha(j)=alpha(j-1)-ff*((alpha(j-1)-alpha(j-2))/(ff-ff0))
             write(12,'(a,4e14.6/)') "ff0 ff",ff0,ff
             ff0=ff
             call scalar(stress,scalar_sigma1)
             stress=tensor(:,i,iel)+alpha(j)*sigma
             call scalar(stress,scalar_sigma2)
             call invar(stress,sigm,dsbar,lode_theta)
             ff=dsbar*dsbar/(am*am)-sigm*(pc(i,iel)-sigm)
             if(abs((scalar_sigma2-scalar_sigma1)/scalar_sigma1)<=fftol)exit
          end do alpha_iterations
          alpha_value=alpha(j)
          deallocate (alpha)
          stress=tensor(:,i,iel)+alpha_value*sigma
          epse=alpha_value*eps
          call invar(stress,sigm,dsbar,lode_theta)
!-----------------------------substepping loop--------------------------------
          delta_t=1.0; accum_t=0.0; epsp=0.0; epsvp=0.0
          substepping: do
            iterate_on_delta_t: do
             sigma1=0.0; sigma2=0.0;deps=0.0;dsigma=0.0
             pcn=pc(i,iel)
             deps=delta_t*(1.0-alpha_value)*eps
!-----------------calculate the first estimate sigma1-------------------------
             call invar(stress,sigm,dsbar,lode_theta)
             call mccflow(stress,pcn,am,mccfl)
             caflow=matmul(dee,mccfl)
             bot=dot_product(mccfl,caflow)
             hard=volume*pcn*sigm*(2*sigm-pcn)/(lambda-kappa)
             bot=bot+hard
             call formaa(mccfl,dee,daatd)
             dep=dee-daatd/bot
             sigma1=matmul(dep ,deps)
!---------------------update hardening parameter----------------------------
             stress1=stress+sigma1
             call invar(stress1,sigm,dsbar,lode_theta)
             dsigma_elastic=matmul(dee,deps)
             temp=dot_product(mccfl,dsigma_elastic)
             dlam=temp/bot
             epsp1=mccfl*dlam
             epsvp1=dlam*(2*sigm-pcn)
             pcn1=pcn*exp(abs(volume*epsvp1/(lambda-kappa)))
!--------------------calculate the second estimate sigma2-----------------------
             call mccflow(stress1,pcn1,am,mccfl)
             caflow=matmul(dee,mccfl)
             bot=dot_product(mccfl,caflow)
             hard=volume*pcn1*sigm*(2*sigm-pcn1)/(lambda-kappa)
             bot=bot+hard
             call formaa(mccfl,dee,daatd)
             dep=dee-daatd/bot
             sigma2=matmul(dep ,deps)
!-----------check local error and calculate new delta_t if necessary----------
             stress2=stress+sigma2
             call invar(stress2,sigm,dsbar,lode_theta)
             temp=dot_product(mccfl,dsigma_elastic)
             dlam=temp/bot
             epsp2=mccfl*dlam
```

```
              epsvp2=dlam*(2*sigm-pcn1)
              pcn2=pcn1*exp(abs(volume*epsvp2/(lambda-kappa)))
              pcn=(pcn1+pcn2)/2
              temp1=(sigma2-sigma1)/2
              dsigma=(sigma1+sigma2)/2
              temp2=stress+dsigma
              call scalar(temp1,scalar_temp1)
              call scalar(temp2,scalar_temp2)
              error=scalar_temp1/scalar_temp2
              if (error<sstol) exit iterate_on_delta_t
              beta=0.8*sqrt(sstol/error)
              if (beta<0.1) beta=0.1
              if (beta>2.0) beta=2.0
              delta_t=beta*delta_t
            end do iterate_on_delta_t
!-------------------------update stress status-----------------------------
              stress=stress+dsigma
              epsp=epsp+(epsp1+epsp2)/2
              epsvp=epsvp+(epsvp1+epsvp2)/2
              call invar(stress,sigm,dsbar,lode_theta)
              call mccflow(stress,pcn,am,mccfl)
              caflow=matmul(dee,mccfl)
              bot=dot_product(mccfl,caflow)
              hard=volume*pcn*sigm*(2*sigm-pcn)/(lambda-kappa)
              bot=bot+hard
              call formaa(mccfl,dee,daatd)
              dep=dee-daatd/bot
!-----------------update hardening parameter and accum_t-------------------
              pc(i,iel)=pcn
              accum_t=accum_t+delta_t
              if (accum_t==1.0) exit
              delta_t=MIN(delta_t,1.0-accum_t)
              end do substepping
            end if
!-----------------------elastic analysis if ff<0-----------------------------
            if(fstiff<.0) call deemat_kg(dee,bk,gk)
!-----------------calculate the residual force for next iteration----------
            elso=tensor(:,i,iel)+sigma-stress
            eload=matmul(elso,bee)
            bload=bload+eload*det*weights(i)*radius
!--------------------update stress and strain for Gauss point---------------
            tensor(:,i,iel)=stress
            etensor(:,i,iel)=etensor(:,i,iel)+eps
            epsv(i,iel)=etensor(1,i,iel)+etensor(2,i,iel)+etensor(4,i,iel)
            eload=matmul(stress,bee); dload=dload+eload*det*weights(i)*radius
            km=km+matmul(matmul(transpose(bee),dep),bee)*det*weights(i)*radius
      end do gauss_points_3
!----------------  compute the total bodyloads vector  --------------------
      bdylds( g ) = bdylds( g ) + bload      ; bdylds(0) = .0
      ddylds( g ) = ddylds( g ) + bload      ; ddylds(0) = .0
      call formkv_disp(kv,km,g,neq)
      kv_bak=kv
    end do elements_4
    call scalar(bdylds,tload)
    call scalar(ddylds,tloads)
    call scalar(xdisp,scalar_xdisp)
    call scalar(tdisp,scalar_tdisp)
    if(iters==1) then; converged=.false.
!       elseif(tload<0.01*tloads) then; converged=.true.
        elseif(scalar_xdisp<0.005*scalar_tdisp) then; converged=.true.
    endif
    if(converged.or.iters==limit)exit
   end do plastic_iters
    totd = totd + disp
    write(11,'(I3,5E12.4,I5)')iy,totd(nf(2,1)),epsv_f,epsv(4,1),sigm,dsbar,iters
   if(iters==limit)stop
  end do load_increments
  end Program Mcc_Substepping
```

Appendix D

```
    Program Mcc_Substepping_CM_FM
!-----------------------------------------------------------------------
!      Program axisymmetric 'drained' strain of an elasto-plastic
!      (Modified Cam-Clay) solid combined with CM and FM for MSW
!      using 8-node quadrilateral elements;
!      using MNR method and substepping stress point algorithm
!-----------------------------------------------------------------------
 use new_library    ;   use  geometry_lib  ;       implicit none
 integer::nels,nxe,nye,neq,nband,nn,nr,nip,nodof=2,nod=8,nst=4,ndof,        &
          i,j,k,iel,iters,limit,incs,iy,ndim=2,loaded_nodes,iters_fnew
 logical::converged       ; character (len=15) :: element='quadrilateral'
 real::kappa,lambda,am,mu,volume,en,det,fnew,ff,fstiff,dlam,dslam,dsbar,    &
          lode_theta,sigm,top,bot,tload,tloads,bulk,cons,presc,ptot,pcs,    &
          radius,residual,tol,fftol,ltol,gk,bk,hard,epsvp,pye,pcn,          &
          alpha_value,error,delta_t,accum_t,accum_temp,beta,sstol,ff0,      &
          scalar_temp1,scalar_temp2,temp,scalar_xdisp,scalar_tdisp,pcn1,pcn2,&
          scalar_sigma1,scalar_sigma2,ef1,lambda_f,volume_t,epsv_f,epsvp1,epsvp2
!------------------------------ dynamic arrays----------------------------
 real    ,allocatable :: kv(:,:),loads(:),points(:,:),bdylds(:),totd(:),    &
                         oldis(:),width(:),depth(:),stress(:),tensor(:,:,:),&
                         dee(:,:),dep(:,:),coord(:,:),jac(:,:),weights(:),  &
                         der(:,:),deriv(:,:),bee(:,:),km(:,:),eld(:),eps(:),&
                         sigma(:),bload(:),eload(:),elso(:),g_coord(:,:),   &
                         ddylds(:),dl(:,:),mccfl(:),mccfl2(:,:),kv_bak(:,:),&
                         dload(:),caflow(:),dsigma(:),ress(:),rmat(:,:),    &
                         acatc(:,:),qmat(:,:),qinva(:),daatd(:,:),mccflq(:),&
                         mccfla(:),mcctemp(:,:),etensor(:,:,:),qinvr(:),    &
                         pore(:,:),fun(:),pc(:,:),sigma1(:),epsp(:),alpha(:),&
                         stress1(:),sigma2(:),temp1(:),temp2(:),deps(:),    &
                         epsp1(:),epsp2(:),val(:,:),qinc(:),bakloads(:),    &
                         dsigma_elastic(:),tdisp(:),dee_t(:,:),xdisp(:),    &
                         epse(:),react(:),disp(:),fixed(:),treac(:),        &
                         stress_t(:),tensor_t(:,:,:),stress2(:),epsv(:,:)
 integer, allocatable :: nf(:,:),g(:),no(:),num(:), g_num(:,:),g_g(:,:),ifpre(:)
!-----------------------------input and initialisation----------------------
  open (10,file='mcc.dat',status=    'old',action='read')
  open (11,file='mcc.res',status='replace',action='write')
  open (12,file='km.res',status='replace',action='write')
  read (10,*) kappa,lambda,am,mu,en,ef1,lambda_f,bulk,cons,pye,nels,nxe,nye,nn,nip
  ndof=nod*nodof
  allocate (nf(nodof,nn), points(nip,ndim),weights(nip),g_coord(ndim,nn),   &
            width(nxe+1),depth(nye+1),num(nod),mcctemp(1,nst),epse(nst),    &
            coord(nod,ndim),g_g(ndof,nels),tensor(nst,nip,nels),fun(nod),   &
            etensor(nst,nip,nels),dee(nst,nst),pore(nip,nels),stress(nst),  &
            jac(ndim,ndim),der(ndim,nod),deriv(ndim,nod),g_num(nod,nels),   &
            bee(nst,ndof),km(ndof,ndof),eld(ndof),eps(nst),sigma(nst),      &
            bload(ndof),eload(ndof),elso(nst),mccfl(nst),mccfl2(nst,nst),   &
            dload(ndof),g(ndof),qinva(nst),qinvr(nst),dl(nip,nels),ress(nst),&
            caflow(nst),dsigma(nst),rmat(nst,nst),acatc(nst,nst),sigma1(nst),&
            qmat(nst,nst),daatd(nst,nst),mccflq(nst),mccfla(nst),pc(nip,nels),&
            epsp(nst),stress1(nst),sigma2(nst),temp1(nst),temp2(nst),       &
            deps(nst),epsp1(nst),epsp2(nst),dsigma_elastic(nst),dep(nst,nst),&
            dee_t(nst,nst),stress_t(nst),tensor_t(nst,nip,nels),stress2(nst),&
            epsv(nip,nels))
  nf=1; read (10,*) nr ; if(nr>0) read(10,*)(k,nf(:,k),i=1,nr)
  call formnf(nf); neq=maxval(nf);read(10,*) width , depth
!------------ loop the elements to find nband and set up global arrays -------
     nband = 0
       elements_1:   do iel = 1 , nels
                       call geometry_8qyv(iel,nye,width,depth,coord,num)
                       call num_to_g(num,nf,g) ;    g_num(:,iel)=num
                       g_coord(: , num )=transpose(coord); g_g( : , iel ) = g
                       if (nband<bandwidth(g)) nband = bandwidth(g)
       end do elements_1
!     write(11,'(a)') "Global coordinates "
!     do k=1,nn;write(11,'(a,i5,a,2e12.4)')"Node",k,"       ",g_coord(:,k);end do
!     write(11,'(a)') "Global node numbers "
!     do k = 1 , nels; write(11,'(a,i5,a,8i5)')                              &
!                              "Element ",k,"        ",g_num(:,k); end do
```

```
!  write(11,'(a,i5,a,i5)')          &
!           "The system has ",neq," equations and the half-bandwidth is",nband
  allocate(kv(neq,neq),kv_bak(neq,neq),loads(0:neq),fixed(0:neq),xdisp(0:neq),&
           react(0:neq),bakloads(0:neq),bdylds(0:neq),oldis(0:neq),totd(0:neq)&
           ,ddylds(0:neq),tdisp(0:neq),treac(0:neq),ifpre(0:neq),disp(0:neq))
   kv=0.0; oldis=0.0; totd=0.0
!---------------------- shape elastic stiffnes matrix -----------------------
   pcs=0.5*pye; volume=en-lambda*log(-cons)
   volume_t=volume+ef1-lambda_f*log(-cons)
   bk=-volume*cons/kappa; gk=1.5*(1.-2.*mu)*bk/(1.+mu)
   call deemat_kg(dee,bk,gk); call sample(element,points,weights)
   tensor=0.0; dl=0.0;etensor=0.0;epsv=0.0
!------------------- fluid bulk or tensile modulus is "bulk" ------------------
   dee_t=dee; dee_t(1,1)=dee(1,1)+bulk;dee_t(4,4)=dee(4,4)+bulk
!---------- element stiffness integration and assembly & initial conditions----
 elements_2: do iel = 1 , nels
               num = g_num(: ,iel ) ; coord = transpose (g_coord(: ,num ))
               g = g_g( : ,iel )    ;       km=0.0
             gauss_pts_1:  do i =1 , nip    ; call shape_fun(fun,points,i)
               call shape_der (der,points,i);  jac = matmul(der,coord)
               det = determinant(jac)  ;   call invert(jac)
               deriv=matmul(jac,der);call bmataxi(bee,radius,coord,deriv,fun)
             km=km+matmul(matmul(transpose(bee),dee_t),bee)*det*weights(i)*radius
               tensor(1:2,i,iel)=cons; tensor(4,i,iel)=cons; pc(i,iel)=pye
             end do gauss_pts_1
   call formkv_disp(kv,km,g,neq)
 end do elements_2
 kv_bak=kv
!--------------- prescribe displacements and factorise l.h.s. --------------
      read(10,*) loaded_nodes ; allocate(no(loaded_nodes))
      read(10,*) no,presc,incs,fftol,sstol,limit
      write(11,'(/A)')"step    displ   epsv_f    vol     p      q    iters"
      totd=0.0; dl=0.0;ptot=0.0
!-------------------displacement increment loop--------------------------------
   load_increments: do iy=1,incs
     ptot = presc * iy
      iters=0;  bdylds=.0;loads=.0; fixed=0.0; tdisp=0.0; treac=0.0
      ifpre=0;  xdisp=0.0;react=0.0; disp=0.0
      do i=1,loaded_nodes; fixed(nf(2,no(i)))=presc; ifpre(nf(2,no(i)))=1;end do
      ddylds=0.0
!--------------------------   iteration loop  -------------------------------
   plastic_iters: do
    iters=iters+1
    write(*,'(A,F8.4,A,I4)')"load",ptot,  "iteration",iters
    if (iters/=1) fixed=0.0
    if (iters/=1) loads=0.0
     loads = loads + bdylds + treac
     kv=kv_bak
     call greduc_disp(kv,loads,fixed,neq,ifpre)
     call bacsub_disp(kv,loads,fixed,xdisp,react,ifpre)
     disp=disp+xdisp
     if (iters/=1) tdisp=tdisp+xdisp
     treac=treac+react
     bdylds=.0
     kv=0.0
!-----------------------go round the elements--------------------------------
       elements_4: do iel = 1 , nels
      bload=.0; dload=.0
      num = g_num( : , iel ) ; coord = transpose( g_coord( : , num ))
      g = g_g( : , iel )     ;    eld = xdisp ( g ); km=0.0
!---------------------- go round the Gauss points ---------------------------
      gauss_points_3 : do i = 1 , nip
         elso=.0; call shape_fun(fun,points,i)
         call shape_der ( der,points,i); jac=matmul(der,coord)
         det = determinant(jac)  ;  call invert(jac)
         deriv = matmul(jac,der) ;  call bmataxi (bee,radius,coord,deriv,fun)
         eps=matmul(bee,eld)
!---------------------update initial stress status-------------------------------
         stress=tensor(: , i ,  iel)
```

```
          call invar(stress,sigm,dsbar,lode_theta)
!-------------------------update specific volume-------------------------------
          pcs=0.5*pc(i,iel)
          volume=en-lambda*log(-sigm)
          ff0=dsbar*dsbar/(am*am)-sigm*(pc(i,iel)-sigm)
!------------------------predict stress with elastic D-----------------------
          sigma=matmul(dee_t ,eps); stress_t=tensor_t(:,i,iel)+sigma
          sigma=matmul(dee,eps);    stress=tensor(:,i,iel)+sigma
          pore(i,iel)=stress_t(1)-stress(1)
          call invar(stress,sigm,dsbar,lode_theta)
!-------------------------substepping if ff>0----------------------------------
          ff=dsbar*dsbar/(am*am)-sigm*(pc(i,iel)-sigm)
          fstiff=ff
          if(ff>0.0) then
!-------------------------------determine alpha----------------------------------
          j=2; allocate (alpha(0:1000)); alpha(1)=0.0; alpha(2)=1.0
           alpha_iterations: do
              j=j+1
              alpha(j)=alpha(j-1)-ff*((alpha(j-1)-alpha(j-2))/(ff-ff0))
              write(12,'(a,4e14.6/)') "ff0 ff",ff0,ff
              ff0=ff
              call scalar(stress,scalar_sigma1)
              stress=tensor(:,i,iel)+alpha(j)*sigma
              call scalar(stress,scalar_sigma2)
              call invar(stress,sigm,dsbar,lode_theta)
              ff=dsbar*dsbar/(am*am)-sigm*(pc(i,iel)-sigm)
              if(abs((scalar_sigma2-scalar_sigma1)/scalar_sigma1)<=fftol)exit
          end do alpha_iterations
          alpha_value=alpha(j)
          deallocate (alpha)
          stress=tensor(:,i,iel)+alpha_value*sigma
          epse=alpha_value*eps
          call invar(stress,sigm,dsbar,lode_theta)
!-----------------------------substepping loop-------------------------------
          delta_t=1.0; accum_t=0.0; epsp=0.0; epsvp=0.0
          substepping: do
         iterate_on_delta_t: do
           sigma1=0.0; sigma2=0.0;deps=0.0;dsigma=0.0
           pcn=pc(i,iel)
           deps=delta_t*(1.0-alpha_value)*eps
!-----------------calculate the first estimate sigma1-------------------------
           call invar(stress,sigm,dsbar,lode_theta)
           call mccflow(stress,pcn,am,mccfl)
           caflow=matmul(dee,mccfl)
           bot=dot_product(mccfl,caflow)
           hard=volume*pcn*sigm*(2*sigm-pcn)/(lambda-kappa)
           bot=bot+hard
           call formaa(mccfl,dee,daatd)
           dep=dee-daatd/bot
           sigma1=matmul(dep ,deps)
!--------------------update hardening parameter-----------------------------
           stress1=stress+sigma1
           call invar(stress1,sigm,dsbar,lode_theta)
           dsigma_elastic=matmul(dee,deps)
           temp=dot_product(mccfl,dsigma_elastic)
           dlam=temp/bot
           epsp1=mccfl*dlam
           epsvp1=dlam*(2*sigm-pcn)
           pcn1=pcn*exp(abs(volume*epsvp1/(lambda-kappa)))
!--------------------calculate the second estimate sigma2----------------------
           call mccflow(stress1,pcn1,am,mccfl)
           caflow=matmul(dee,mccfl)
           bot=dot_product(mccfl,caflow)
           hard=volume*pcn1*sigm*(2*sigm-pcn1)/(lambda-kappa)
           bot=bot+hard
           call formaa(mccfl,dee,daatd)
           dep=dee-daatd/bot
           sigma2=matmul(dep ,deps)
!-----------check local error and calculate new delta_t if necessary----------
```

```
            stress2=stress+sigma2
            call invar(stress2,sigm,dsbar,lode_theta)
            temp=dot_product(mccfl,dsigma_elastic)
            dlam=temp/bot
            epsp2=mccfl*dlam
            epsvp2=dlam*(2*sigm-pcn1)
            pcn2=pcn1*exp(abs(volume*epsvp2/(lambda-kappa)))
            pcn=(pcn1+pcn2)/2
            temp1=(sigma2-sigma1)/2
            dsigma=(sigma1+sigma2)/2
            temp2=stress+dsigma
            call scalar(temp1,scalar_temp1)
            call scalar(temp2,scalar_temp2)
            error=scalar_temp1/scalar_temp2
            if (error<sstol) exit iterate_on_delta_t
            beta=0.8*sqrt(sstol/error)
             if (beta<0.1) beta=0.1
             if (beta>2.0) beta=2.0
             delta_t=beta*delta_t
            end do iterate_on_delta_t
!-----------------------------update stress status-------------------------------
            stress=stress+dsigma
            epsp=epsp+(epsp1+epsp2)/2
            epsvp=epsvp+(epsvp1+epsvp2)/2
            call invar(stress,sigm,dsbar,lode_theta)
            call mccflow(stress,pcn,am,mccfl)
            caflow=matmul(dee,mccfl)
            bot=dot_product(mccfl,caflow)
            hard=volume*pcn*sigm*(2*sigm-pcn)/(lambda-kappa)
            bot=bot+hard
            call formaa(mccfl,dee,daatd)
            dep=dee-daatd/bot
!------------------update hardening parameter and accum_t-------------------
            pc(i,iel)=pcn
            accum_t=accum_t+delta_t
            if (accum_t==1.0) exit
              delta_t=MIN(delta_t,1.0-accum_t)
              end do substepping
            end if
!----------------------elastic analysis if ff<0-----------------------------
            if(fstiff<.0) call deemat_kg(dee,bk,gk)
!------------------calculate the residual force for next iteration----------
            elso=tensor(:,i,iel)+sigma-stress
            eload=matmul(elso,bee)
            bload=bload+eload*det*weights(i)*radius
!--------------------calculate particle compression-------------------------
            epsv_f=lambda_f*log(sigm/cons)/volume_t
!--------------------update stress and strain for Gauss point---------------
            tensor(:,i,iel)=stress
            tensor_t(1,i,iel)=tensor(1,i,iel)+pore(i,iel)
            tensor_t(4,i,iel)=tensor(1,i,iel)+pore(i,iel)
            tensor_t(2:3,i,iel)=tensor(2:3,i,iel)
            etensor(:,i,iel)=etensor(:,i,iel)+eps
            epsv(i,iel)=etensor(1,i,iel)+etensor(2,i,iel)+etensor(4,i,iel)
            eload=matmul(stress,bee); dload=dload+eload*det*weights(i)*radius
            km=km+matmul(matmul(transpose(bee),dep),bee)*det*weights(i)*radius
      end do gauss_points_3
!----------------  compute the total bodyloads vector  ---------------------
      bdylds( g ) = bdylds( g ) + bload      ; bdylds(0) = .0
      ddylds( g ) = ddylds( g ) + bload      ; ddylds(0) = .0
      call formkv_disp(kv,km,g,neq)
      kv_bak=kv
    end do elements_4
    call scalar(bdylds,tload)
    call scalar(ddylds,tloads)
    call scalar(xdisp,scalar_xdisp)
    call scalar(tdisp,scalar_tdisp)
    if(iters==1) then; converged=.false.
!       elseif(tload<0.01*tloads) then; converged=.true.
```

```
        elseif(scalar_xdisp<0.005*scalar_tdisp) then; converged=.true.
      endif
      if(converged.or.iters==limit)exit
    end do plastic_iters
    totd=totd+disp
    write(11,'(I3,5E12.4,I5)')iy,totd(nf(2,1)),epsv_f,epsv(4,1),sigm,dsbar,iters
    if(iters==limit)stop
  end do load_increments
  end Program Mcc_Substepping_CM_FM
```

Appendix E

```
Subroutine greduc_disp(bk,loads,fixed,n,ifpre)
!gaussian reduction on a vector for prescribed displacement
implicit none
real,intent(in out)::bk(:,:),loads(0:);real,intent(in)::fixed(0:)
integer,intent(in)::n,ifpre(0:)
integer::i,i1,i11,kbl,j,ij,nkb,m,ni,nj,iw ; real::sum
       do i=1,n
          if (ifpre(i)/=0) then
            do j=i,n
               loads(j)=loads(j)-bk(j,i)*fixed(i)
               bk(j,i)=0.0
            end do
!write(12,'(a,16e14.6/)') "loads1",loads
          else
            i1=i+1
            do j=i1,n
               loads(j)=loads(j)-bk(j,i)*loads(i)/bk(i,i)
               bk(j,:)=bk(j,:)-bk(j,i)*bk(i,:)/bk(i,i)
            end do
!write(12,'(a,16e14.6/)') "loads2",loads
!write(12,'(4e14.6/)') bk
          end if
        end do
return
end subroutine greduc_disp

Subroutine bacsub_disp(bk,loads,fixed,xdisp,react,ifpre)
!performs complete gaussian backsubstitution for prescribed displacement
implicit none
real,intent(in)::bk(:,:),loads(0:),fixed(0:)
real,intent(out)::xdisp(0:),react(0:)
integer,intent(in)::ifpre(0:)
integer::nkb,k,i,jn,jj,i1,n,iw;real::resid
   n = ubound(loads,1)
   do jj=1,n
      i=n-jj+1;resid=loads(i);i1=i+1
      if (i1-n>0)i1=n
      do k=i1,n
           if (i==n) exit
           resid=resid-bk(i,k)*xdisp(k)
      end do
      if(ifpre(i)==0.0)  xdisp(i)=resid/bk(i,i)
      if(ifpre(i)/=0.0)  xdisp(i)=fixed(i)
      if(ifpre(i)/=0.0)  react(i)=-resid
   end do
return
end subroutine bacsub_disp

Subroutine mccflow(stress,pc,m,mccfl)
!Forms the 1st derivatives of the yield function
implicit none
real,intent(in)::stress(:),pc,m; real,intent(out)::mccfl(:)
real::sigm; sigm=(stress(1)+stress(2)+stress(4))/3.
mccfl(1)=(2.*sigm-pc)/3.+3.*(stress(1)-sigm)/(m*m)
mccfl(2)=(2.*sigm-pc)/3.+3.*(stress(2)-sigm)/(m*m)
mccfl(3)=3.*stress(3)/(m*m)
mccfl(4)=(2.*sigm-pc)/3.+3.*(stress(4)-sigm)/(m*m)
return
end subroutine mccflow
```